UC San Diego

UC San Diego Electronic Theses and Dissertations

Title

Assessment of durability of carbon/epoxy composite materials after exposure to elevated temperatures and immersion in seawater for navy vessel applications

Permalink

https://escholarship.org/uc/item/1368n7hh

Author

Hong, SoonKook

Publication Date

2010

Peer reviewed|Thesis/dissertation

eScholarship.org Powered by the California Digital Library
University of California

UNIVERSITY OF CALIFORNIA, SAN DIEGO

Assessment of Durability of Carbon/Epoxy Composite Materials after Exposure to Elevated Temperatures and Immersion in Seawater for Navy Vessel Applications

A Dissertation submitted in partial satisfaction of the

Requirements for the degree of Doctor of Philosophy

in

Materials Science and Engineering

by

SoonKook Hong

Committee in charge:

Professor Vistasp M. Karbhari, Co-Chair
Professor Sungho Jin, Co-Chair
Professor Daniel Tatakovski
Professor Lubarda Vlado
Professor Qiao Yu

2010

Copyright

SoonKook Hong, 2010

All rights reserved.

The Dissertation of SoonKook Hong is approved, and it is acceptable in quality and form for publication on microfilm and electronically:

Co-Chair

Co-Chair

University of California, San Diego

2010

To my wife, EunJung

and my son, DongHo

Never underestimate your power to change yourself;

Never overestimate your power to change others.

- H. Jackson Brown, Jr.

TABLE OF CONTENTS

LIST OF SYMBOLS

A	Rate constant
A	Initial cross sectional area
$A_{c,f,m}$	Area of composite, fiber, and matrix, respectively
a_T	Shift factor
b	Width of the specimen tested
C_p	Specific heat of the composite material
D	Maximum deflection of the center of the beam
D	Fickian coefficient of diffusion
D_{corr}	Diffusion coefficient multiplied by a correction factor
E	Activation energy
E	Elastic modulus
E'	Storage Modulus
E''	Loss modulus
E_d	Decomposition activation energy
E_f	Elastic modulus of fiber
E_i	Initial modulus
E_m	Elastic modulus of matrix
E_M	Modulus of the polymer in the rubbery state
E_t	Modulus at time t
f	Frequency applied for DMTA test
$F_{c,f,m}$	Uniaxial load in composite, fiber, and matrix, respectively
F^{tu}	Ultimate tensile strength
G_{12}	Shear modulus
G_f	Nominal carbon fiber modulus (22 GPa)
G_m	Nominal epoxy modulus (1.308 GPa)
h	Enthalpy of the solid phase
h	Thickness of the specimen tested

h_g	Enthalpy of the volatile gas
k_x	Thermal conductivity of the composite material in the through-thickness direction
L	Support span
l	Length of the specimen
L_g	Extensometer gage length
M_∞	Weight gain after equilibrium
M_e	Final mass after decomposition
M_i	Initial mass
n	Order of reaction
n	Sample size
P(S)	Probability of survival
P_i	Load at the i^{th} instant
P^{max}	Maximum load prior to failure
Q_i	Heat of decomposition
Q_P	Heat of pyrolysis
R	Universal gas constant (8.3143J/mol^{o}K)
s	Sample standard deviation
t	Quantile of the t-distribution
T_g	Glass transition temperature
T_{ref}	Reference temperature
T_S	Surrounding temperature
T_s	Surface temperature
V_f	Fiber volume fraction
W_i	Initial weight of the specimen (prior to immersion)
W_t	Weight of the specimen after time t
α	Degree of decomposition
α	Shape parameter
β	Constant heating rate

β	Scale parameter
Γ	Gamma function
δ	Phase angle
δ_i	Increase in gauge length at the i^{th} instant
$\Delta\tau_{12}$	Difference in applied shear strength between two shear strain points
$\Delta\Upsilon_{12}$	Difference of two strain points
ε_f	Emissivity of the surrounding
ε_f	strain of fiber
ε_i	Tensile strain at the i^{th} instant
ε_m	Strain of matrix
ε_s	Emissivity of the surface
ε_{xx}	Longitudinal normal strain
ε_{yy}	Lateral normal strain
μ	Mean value
ρ	Density of the composite material
σ	Stepan-Boltzman constant
$\sigma_{11,}\sigma_{22}$	Normal stresses in the lamina coordinate system
$\sigma_{c,f,m}$	Stress of composite, fiber, and matrix, respectively
σ_i	Tensile strength at the i^{th} instant
σ_i	Initial strength
σ_t	Strength at time t
σ_{xx}	Applied tensile stress
τ_{12}	Shear strength
τ_{xy}	Induced shear strength
Υ_{12}	Sher strain
$\dot{q}$	Heat flow
$\overline{X}$	Sample mean

LIST OF FIGURES

LIST OF TABLES

ACKNOWLEDGEMENT

First of all, I must acknowledge Professor Vistasp M. Karbhari. He was my good advisor and mentor throughout my graduate studies and researches. His support and instruction have encouraged me to complete my research goals.

I must also acknowledge the support of Professor SungHo Jin whose generous support enabled the completion of these studies. He was good instructor to solve problems as a co-advisor.

I want to express a deep gratitude to Professor Minsoo Kim in Seoul National University and Professor YoungJoo Ko, Joono Seo in Korea Naval Academy for their good directions.

Thanks must be given to my lab members, Dr. Guijun Xian, Dr. Stephanie Laura Svetlik, Dr. Anna Goodman, Dr. Griffin Brungraber, Dr. Hyunjung Yang, Dr. Seungdae Kim and Sungjun Jin. I want to dedicate this dissertation to my friends; Dr SungSik Hur, Don Phillippi, Chulmin Choi, Hyungbo Sim, Jimyoun Moon, Kyungtae Kim, Dongwon Kim, Taewan Kim and Hyuck Son. These individuals provided much needed support and were always willing to lend themselves to assisting me with various issues.

I would also like to acknowledge the support of the Republic of South Korea Navy and Naval Academy which helped me to have an opportunity for advancing my ability.

Finally, I am grateful to my family in Korea who give the motivation for life.

VITA

1994	Bachelor, Naval Academy, Korea
1994-1997	Bachelor, Seoul National University, Korea
1997-2003	Facilities engineering officer, Korea
2003-2005	Master of Engineering, Seoul National University, Korea
2005-2006	Facilities engineering officer /Researcher, Naval Academy , Korea
2006-2010	Graduate Research Assistant, University of California, San Diego
2010	Doctor of Philosophy, University of California, San Diego

ABSTRACT OF THE DISSERTATION

Assessment of Durability of Carbon/Epoxy Composite Materials after Exposure to Elevated Temperatures and Immersion in Seawater for Navy Vessel Applications

by

SoonKook Hong

Doctor of Philosophy in Materials Science and Engineering

University of California, San Diego, 2010

Professor Vistasp M. Karbhari, Co-Chair

Professor Sungho Jin, Co-Chair

Carbon Fiber-Reinforced Polymer (CFRP) composites with epoxy matrices offer many advantages over conventional materials in terms of high strength-to-weight and high stiffness-to-weight ratios, design flexibility, corrosion resistance, and electromagnetic shielding for naval vessels in marine environments. However, the risk of fire and related structural degradation represent a challenge to the structural assessment of high performance composite structures. The accurate assessment of the

deterioration and degradation of a composite structure subjected to elevated temperatures is vital in the planning for maintenance of mission critical components.

In this research, carbon/epoxy composite materials have been thermally aged at nine (9) different temperatures for up to 72 hours of ageing time. In order to determine the residual mechanical properties of the specimens exposed to elevated temperatures, tensile, flexure, off-axis shear, and short beam shear tests were conducted in accordance with ASTM test procedures. In addition, the viscoelastic behavior and dynamic properties of these composites at varying ageing times and temperatures were found using Dynamic Mechanical Thermal Analysis (DMTA) and Differential Scanning Calorimetry (DSC). ThermoGravimetric Analysis (TGA) was performed to analyze the characteristics of thermal decomposition and Scanning Electron Microscopy (SEM) images were taken to investigate failure mechanisms such as interfacial debonding, delamination, and fiber fracture.

Since polymer composite used in marine environments can easily be exposed to moisture related to high relative humidity and immersion, degradation mechanisms related to moisture were investigated on specimens immersed in seawater and deionized water for 72 weeks after exposure to selected regimes of elevated temperature using gravimetric analysis, SEM and short beam shear test.

Finally, well-established prediction models such as Arrhenius rate model, Time-Temperature Superposition model and Weibull statistical strength model were used with experimental data to estimate characteristic associated with long-term service life.

1 Introduction

1.1 Introduction

Fiber-Reinforced Polymer (FRP) composites offer inherent advantages over traditional materials with regard to high strength-to-weight and stiffness-to-weight ratios, design flexibility, corrosion resistance, low maintenance and enhanced service life. Carbon/epoxy composite materials are particularly useful because they exhibit better mechanical properties than other FRP composites as well as provide the ability for electromagnetic shielding for stealth purpose. Due to these advantages, carbon/epoxy composites are a preferred materials choice for navy vessels of higher performance. Navy vessels require adequate performance and resistance over high temperature because fires on ships can be started by any number of causes such as electrical faults, ignition of flammable gases or liquids and weapon strikes. The risk of fire, and of fire-related structural degradation and failure, presents a significant challenge to the safe design and accurate structural assessment of composite structures. An accurate assessment of deterioration of a composite structure subjected to fire as represented in this study by exposure to elevated temperature is dependent on the accurate characterization of the time dependent residual mechanical characteristics of composite system as well as its viscoelastic properties.

When composite materials are generally exposed to high temperatures (200~ 300^{o}C), pyrolysis caused by chemical reactions with oxygen starts to occur from the surface and the resin component degrades to form gaseous products. In addition, the polymer matrix and organic fibers are thermally decomposed yielding volatile gases,

solid carbonaceous char and airborne soot particles (smoke) via a series of chemical reaction mechanisms. Polymer composites lose not only molecular weight but also mechanical characteristics by thermal decomposition. Molecular weight is reduced by mechanisms of random chain scission, chain-end scission and chain stripping within polymer structures. Therefore, when composite materials are thermally aged for periods of time, there is a need for the investigation of how much degradation and deterioration occurs after exposure as functions of time and temperature.

FRP composite materials are used in a variety of navy applications based on their stiffness, strength, reduced weight, and corrosion-free capabilities. Additional properties such as fire and ballistics resistance, signature reduction, and enhanced communications make them attractive for integrated structures. The use of FRP composite materials is rapidly spreading in naval applications with inherent advantages. Currently, the all-composite naval ships fabricated of carbon and glass fiber composites are being used in both Europe and the United State.

If the naval vessels made by composite materials are operating in the sea, the various forms of loading caused by rolling-pitching and their combination can be applied for ships. Since degradation and deterioration of the mechanical properties of composite materials in a fire and at elevated temperature can seriously compromise structural integrity, and cause rapid creep, buckling, collapse or some other failure mode, the composite materials degraded and deteriorated by heat must be evaluated in terms of the retention of mechanical properties to investigate whether the intrinsic functions of the material can be accomplished. In order to develop the experimental data for residual properties after exposure to elevated temperatures, tension, off-axis shear, flexure and

short beam shear test were carried out according to ASTM test procedures.

Polymers show the viscoelastic behavior in the presence of heat with the resin used in composite materials experiencing the change of a diversity of properties as a function of time and temperature. Thus, the severe drop of mechanical properties seen after exposure to elevated temperature is mainly attributed to the degradation of the resin than the fiber. For this reason, thermal analysis must be performed on polymeric composite materials. Dynamic Mechanical Thermal Analysis (DMTA), Differential Scanning Calorimetry (DSC) and Thermo-Gravimetric Analyses (TGA) were conduted on specimens exposed to elevated temperatures. DMTA measurements over a range of temperatures provide valuable insight into the structure, morphology and viscoelastic behavior of polymer materials while DSC is mainly used to investigate the thermal transitions of the polymer. TGA is a powerful and simple tool to estimate the thermophysical and thermomechanical properties exposed to a controlled temperature.

The environmental conditions likely to be faced in such applications include water, humidity, moisture and seawater can result in the ingress of moisture into FRP composites. Exposure to moisture is known to cause plasticization, hydrolysis and further deterioration of the resin over time and hence it is necessary to study the moisture uptake and resulting kinetics. While general investigations regarding moisture uptake are focused on the specimens of FRP composites cured in ambient temperature, this study is concentrated on the immersion effects of specimens after exposure to elevated temperature because the use of naval vessels fabricated from composite materials exposed to the various heat sources must be estimated in terms of operating life. This estimation can be an important criterion to evaluate how long naval vessels of

FRP composites can be allowed to operate after exposure to high temperatures. Degradation mechanisms related to moisture were investigated on specimens immersed in seawater and deionized water for 72 weeks using gravimetric analysis, SEM and short beam shear.

It is very important that predictive degradation models are used to evaluate functions for desired periods of time without failure and severe degradation, in specified environments. Based on the experimental data determined through mechanical tests, predictions of longer-term response can be obtained using well-established models such as the Arrhenius rate model, Time-Temperature Superposition (TTSP) model and Weibull statistical strength model.

This study contributes to the establishment of design factors and criteria to estimate and evaluate the performance of FRP composites exposed to elevated temperatures and immersed in seawater using the experimental data obtained throughout various tests and analysis.

1.2 Motivation

Significant research related to assessments of FRP composite materials after exposure to elevated temperature has been conducted as the applications of FRP composites were rapidly increased. Such research related to materials such as prepreg based autoclave cured composites been mainly focused on aerospace.

However, of late, there has been an increased interest in the development and application of composites to both primary and secondary structures as well as machinery components in naval ships and submarines. This interest in FRP composites is derived from increased requirements for corrosion-free, lightweight, stealth, and affordable low-cost alternative to metallic components used conventionally.

Naval vessels made from FRP composites are exposed to various loading conditions by rolling-pitching waves, high temperatures due to fires and UV light as well as moisture ingress from relative humidity and immersion. In particular, a significant technical issue that has limited the use of composite materials in naval ships and submarines is their combustible nature and the resulting issues of residual performance after periods of exposure to elevated temperatures.

Therefore, mechanical and thermal analysis must be carried out on composite specimens exposed to both elevated temperatures and marine conditions for the safe design and accurate assessment of naval vessels and components.

1.3 Research Objectives

The main objectives and goals for this research can be summarized as follows.

- Development of a fundamental understanding of time-and temperature-dependent behavior of wet layup based carbon/epoxy composite materials exposed to elevated temperatures for certain time
- Verification of residual post-cure effects on specimens cured at ambient temperatures and fabricated by manual wet layup process
- Morphological analysis of failure mechanism such as debonding between fibers and matrix, pull-out of fibers and delamination between layers using SEM
- Correlation between experimental data obtained through mechanical tests
- Thermal analysis to assess how much polymer-based composites are degraded or deteriorated by temperature and time
- Correlation of parameters such as glass transition temperature, decomposition temperature, loss tangent (tan δ), activation energy, etc determined from thermal analysis and mechanical property retention
- Verification of effects of immersion, failure mechanisms and mechanical properties on specimens immersed in seawater and deionized water
- Comparison of predictions obtained by use of established model and experimental data
- Categorization of property retention as a function of temperature, time, weight loss and weight gain due to immersion

1.4 Overview of Research

This research is focused on the assessment of durability of carbon/epoxy composite materials after exposure to elevated temperatures and immersion in seawater for navy vessel applications. For assessments, mechanical tests and thermal analysis were conducted on specimens exposed to various regimes of elevated temperature and exposure to aqueous environments. In addition, immersion characteristics were investigated using gravimetric analysis, SEM and short beam shear test. Previous researches and theories relevant to FRP composites are introduced in chapter 2. Material specifications, experimental conditions and test procedures are explained in chapter 3. Chapter 4 and chapter 5 deal with mechanical characterization and thermal analysis on specimens exposed to controlled conditions, respectively. The experimental results from immersion in seawater and deionized water for 72 weeks are presented in chapter 6. Predictions from 3 models are detailed in chapter 7.

2 Literature reviews

2.1 Fire Safety of FRP Composite Materials in Naval Applications

During past years, there has been development and application of composites for both primary and secondary load-bearing structures of Naval vessels. FRP composite materials are already being used in diverse areas such as deckhouse, mast, piping, valves, pumps and heat exchangers, ventilation ducts, etc. This interest in FRP composite materials is driven by fleet needs to reduce maintenance, save weight, increase covertness and provide affordable alternatives to metallic components with lower life cycle costs[1].

The use of structural composites inside naval submarines is now covered by MIL-STD-2031 (SH), which includes fire and toxicity test methods such as flame spread index (FSI), specific optical density, heat release rate and ignitability, oxygen-temperature index, combustion gas generation, long-term outgassing, etc and qualification procedure for composite materials systems used in hull, machinery, and structural applications[2]. This military standard involves test methods and requirements for flammability characteristics. The following two guiding criteria were established for the use of composite systems abroad US Navy vessels[3].

1. "The composite system will not be the fire source, i.e. it will be sufficiently fire resistant not to support spontaneous combustion."
2. "Secondary ignition of the composite system will be delayed until the crew can respond to the primary fire source; i.e. the composite system will not result in rapid spreading of the fire"

2.2 Thermal Decomposition of FRP Composite Materials in Fire

2.2.1 Introduction

A major concern of FRP composite materials is poor performance in fire. In case FRP composite materials are used in naval environments, especially in naval vessels, it can be exposed to be more dangerous because fires on ships can easily be started by any number of causes such as electrical faults, ignition of flammable gases or liquids and weapon strikes.

Therefore, it should be noted that thermal decomposition mechanisms in elevated temperatures caused by fire must be investigated because the behavior of composite materials in fire is dominated by the chemical process.

2.2.2 Description of Mechanisms of Thermal Degradation

When a heat flux caused by fire is applied to FRP composite materials, the change of initial temperature is dependent on the rate of heat conduction into the materials and the boundary conditions. If the heat flux is applied, the surface of FRP composite materials first reaches high temperature. This change of temperature can be caused chemical reactions (pyrolysis) and gaseous products are formed by degradation of polymer component[4]. In addition, chemical reaction can result in distortion, buckling or failure of FRP composite materials. In the process of decomposition on polymer matrix and fibers, volatile gases, char and smoke can be produced by chemical reaction mechanisms. The loss of molecular weight in polymers is attributed to the

fracture mechanisms of polymer structures such as random chain scission, chain-end scission and chain stripping.

2.2.2.1 Processes of Combustion in Composites

Polymer composites exposed to high temperatures experience self-sustained combustion in air and oxygen[5]. Burning polymer composites have a highly complex combustion system. The combustion in polymer composite system occurs as combined events[6] such as heating of the polymer, decomposition, ignition, and combustion. As mentioned in previous chapter, the decomposition process for most polymers produces solid carbonaceous char and gaseous volatiles. The chemical composition and amount of the volatiles is dependent on the polymer matrix, oxygen content and temperature, although the majority of the gases are flammable polymers. Combustion of the volatiles occurs in the solid and intermittent zones of a turbulent flame.

2.2.2.2 Epoxy Resin

Epoxy resins are characterized by the presence of epoxide groups prior to cure, and they may also contain aliphatic, aromatic or heterocyclic structures in the backbone. Epoxy resin is superior to any other polymer resins in terms of the long service time and good physical properties compared to other thermosets. Like other thermoset resins, epoxy resins can be rendered fire-retardant either by incorporating fire-retardant additives or by copolymerization with reactive fire retardants.

Three mechanisms for the oxidation of epoxies were suggested by many

researches[7], [8]. Any of these mechanisms leads to the formation of carbonyl groups which further decompose and result in chain splitting.

The thermal stability of epoxy resins and their flammability depend on the structure of the monomer, the structure of the curing agent and the crosslink density.

2.2.2.3 Carbon Fibers

The structures and properties of carbon fibers are dependent on the raw material used and the process conditions of manufacture. When carbon fibers are exposed to directly to fire, their surface can be oxidized..

Severe oxidation causes carbon fibers to lose weight due to the evolution of CO or CO_2 gases. However, slight oxidation may cause carbon fibers to gain weight slightly due to the formation of chemical bonds to various Compared to polymer matrix, reinforcing carbon fibers are generally more stable at elevated temperatures considered[9]. Thermal degradation was quantified by the amount of weight loss measured, while surface morphology changes by temperatures were monitored as attempt to investigate related physical and surface changes to the decreases in mechanical performance as a function of ageing.

In addition, trace impurities within carbon fiber act as a catalyst to the oxidation process, and this can cause thinning of the fiber. However, it should be noted that in most types of fiber the extent of oxidation is small because most carbon fibers within a composite are surrounded by char.

2.2.3 Review of Analytical Models for Effects of Fire

In order to predict the thermal response of composite materials by fire, many models were suggested. However, thermal response mechanisms on composite materials are very complicated because many considerations were included in the process of reactions. In this section, mathematical models suggested by many researchers who studied on mathematical models for fire response will be introduced.

1) One-dimensional equation on composite materials

Assuming that heat conduction is applied to composite material in through-thickness direction, the one-dimensional equation including heat of pyrolysis determined from the theoretical mass loss rate can be expressed as Equation (2.1)[10].

$$\rho C_p \frac{\partial T}{\partial t} = \frac{\partial}{\partial x}\left[k_x \frac{\partial T}{\partial x} \right] + \frac{\partial m}{\partial x} Q_p \qquad (2.1)$$

Where:

T = The temperature

t = time

x = the distance below the hot surface

ρ and C_p = the density and specific heat of the composite material

k_x = the thermal conductivity of the composite material in the through-thickness direction

2) Decomposition reaction model

To develop more precise model, new model were suggested after adding the diffusion of decomposition gases into Equation (2.4)[4]. The decomposition reactions

are modeled using single or multiple-order kinetic rate theory as shown in Equation (2.2).

$$\rho C_p \frac{\partial T}{\partial t} = k \frac{\partial^2 T}{\partial x^2} + \frac{\partial k}{\partial x}\frac{\partial T}{\partial x} - \dot{m}_g C_{pg} - \frac{\partial \rho}{\partial t}(Q_i + h - h_g) \qquad (2.2)$$

Where:

Q_i = The heat of decomposition

h = Enthalpy of the solid phase

h_g = Enthalpy of the volatile gas

Equation (2.2) is including the effect of heat conduction, the internal convection of thermal energy and rate of heat generation The rate of chemical reaction may be described using an Arrhenius rate expression of the form shown in Equation (2.6) assuming no expansion of the materials[4].

$$\frac{\partial \rho}{\partial t} = -A\left[\frac{(\rho - \rho_f)}{\rho_0}\right]^n e^{(-E/RT)} \qquad (2.3)$$

Where:

A = The rate constant

E = Activation energy

n = Oder of the reaction

R = The gas constant

2.3 Effects of Seawater on FRP Composites

This research is focused on FRP composites operating in marine environments which exists surrounding seawater. There are so many considerations to assess the FRP composite materials used in the marine environmental conditions such as immersion, salinity, UV, corrosion, cycling (thaw-freeze), and so on. However, this research is extremely concentrated on seawater immersion effect which is important in operating naval vessels.

2.3.1 Seawater Properties

The composition of seawater is very complex consisting of more than seventy trace elements and biological organisms, which have shown to cause some degradation. The main composition of seawater is summarized as shown in Table 2-1.

Table 2-1: Composition of seawater

Element	Symbol	Weight %
Chloride	Cl	55.04
Sulphate	SO_4	7.68
Calcium	Ca	1.16
Sodium	Na	30.61
Magnesium	Mg	3.69
Potassium	K	1.10

Seawater is composed mostly of water (H_2O). In fact it is about 96.5 wt% water. The salinity of sea water (usually 3.5%) is made up by all the dissolved salts. Interestingly, their proportions are always the same, which can be understood if salinity differences are caused by either evaporating fresh water or adding fresh water from

rivers. Freezing and thawing also matter. Seawater properties are as follows:

1) Density: Any substance dissolved in a liquid has the effect of increasing the density of that liquid. The greater the amount of solute, the greater the effect.
2) Freezing point: Because the salt is spread on frozen path, the freezing point is depressed. Salts also lower the temperature at which water reaches its maximum density.
3) Boiling point: the salts have the effect of making the water molecules cluster and become more orders, thus harder to pull apart and evaporate. Therefore, boiling point is elevated.
4) Conductivity: If an electromagnetic field is applied to seawater, the ions will migrate, producing an electric current.

Table 2-2 shows comparison of seawater and pure water properties.

Table 2-2: Comparison of seawater and pure water properties

Property	Seawater (35%)	Pure water
Density (g/cm3), 25℃	1.02412	1.0029
Specific conductivity (1/Ωcm), 25℃	0.0532	-
Viscosity (millipoise), 25℃	9.02	8.90
Freezing point (℃)	-1.91	0.00
Temperature of maximum density (℃)	-3.25	3.98
Specific heat (J/g℃), 17.5℃	3.898	4.182

2.3.2 Seawater Effect on Mechanical Properties

In this section, seawater effects on mechanical properties of FRP composite materials will be introduced from literatures which previous researchers have been studied. Many researches were focused on mechanical properties after immersing in deionized, distilled and tap water. Even though some researches on seawater immersion are available, studies in actual marine environments are lack because it is too difficult to test.

Accordingly, similarities and correlation factors between laboratory and real-site evaluation result need to be developed for real analyzing.

2.3.2.1 Tension

There are a lot of researches related to carbon- and glass-fiber composites immersed in saline conditions. In this section, the effects exposed to various environments will be introduced from summarizing of many studies toward tensile strength and modulus.

T.S Grant et al.[11] investigated the effect of immersion in seawater on transverse tensile properties of three graphite/epoxy composite materials. The transverse tensile strength was found to be reduced by 17% in one of the systems with essentially no change in the other two systems studied. The 17% decrease in transverse tensile strength was associated with degradation of the interfacial strength. Also they found that little difference was found in the behavior of composite immersed in distilled water and in seawater at ambient pressure or seawater at 20.7 MPa pressure. Leif A. Carlsson

et al.[12] accomplished tests using carbon/bismaleimide-epoxy, E-glass/epoxy, E-glass/polyphenylsulfide and carbon-epoxy for immersion more than 4000 hrs in distilled water and natural seawater at room temperature and 35°C. Transverse modulus, E_2 was not significantly changed after water absorption except for E-glass/polyphenylsulfide that lost about 60% of its dry modulus, despite of its low water absorption. The substantial reduction of E_2 was attributed to extensive fiber/matrix debonding induced by water. Also, all composites experienced large reduction in transverse tensile strength due to water absorption. The maximum reduction took placed in E-glass/polyphenylsulfide with 85% decrease of its dry strength. An E-glass/carbon/epoxy interlayer hybrid composite has been aged by immersion in simulated seawater for varying lengths of time and then tested in transverse tension by C.A Wood et al.[13]. From transverse tests, they showed that tension properties were proportional to water uptake and then dropped rapidly after moisture saturation. Failure mechanism was verified using an environmental SEM. Resin-rich areas were found to be sources of failure initiation where debonding occurred. E-glass/Vinylester composites were fabricated using wet layup with the application of a vacuum throughout the cure to investigate tensile properties in various environmental conditions such as 23℃ and 55% RH, synthetic sea water and real seawater by Lixin Wu et al.[14]. Exposure to all conditions resulted in a decrease in tensile strength and the absolute difference in response between the various exposures. The maximum reduction in tensile strength after 12 months of exposure was in sea water at a level of 13.5%, whereas the minimum, 8.26%, was recorded for the case of cycling in sea water. After immersion in sea water, the surfaces of all the specimens showed discoloration with the initiation of blistering at

areas where fibers were close to the surface, suggesting both effect of salts of the fiber-matrix integrity and the existence of osmotic processes.

2.3.2.2 Flexure

The flexural test measures the force required to bend a beam under three point or four point loading conditions. The data is often used to select materials for parts that will support loads without flexing. Flexural modulus is used as an indication of a material's stiffness when flexed. E.P. Gellert and D.M. Turley[15] performed flexural test using the polyester, phenolic and vinylester glass-fiber reinforced polymer materials immersed in 30℃ seawater either unloaded or loaded at 20% of the maximum strain at flexural failure ($0.2\varepsilon_f$) to examine the effects of loading on flexural property. Flexural strength continued to degrade for the unloaded polyester and vinylester GPRs as water uptake continued toward saturation, where strength losses between 15% and 21% occurred. The unloaded phenolic lost 25% of initial strength at saturation. For ageing, loading affected the strength of only phenolic GRP with strength loss advancing from 25 to 36% loss from the initial strength. Wayne C. Tucker and Richard Brown[16] generated all data on the vinlyester/graphite composite material immersed in natural filtered seawater in tubs in the laboratory at 1 atmosphere of pressure and in natural filtered seawater pressurized to a depth of 2000feet of seawater. The flexural strength and stiffness of the composite material were decreased by the high pressure exposure. In contrast, atmospheric seawater exposure did not produce any strength decrease. Both the enhanced moisture uptake and the strength decrease at high pressure exposure were

thought to be due to mechanical damage induced by the increased pressure. In 5% and 10% salt solution, the flexural properties (strength and modulus) of pultruded glass-fiber reinforced vinylester matrix composite coupons were measured for the 90^{o} specimens as-received and after ageing by K.Liao et al.[17]. Ageing in water and salt solutions resulted in degraded flexural and tensile properties of pultruded E-glass fiber reinforced vinylester matrix composite. Salt concentration did not seem to affect flexural properties in a noticeable way. However, in terms of flexural strength, reductions were larger than those subjected to distilled water.

2.3.2.3 Other Mechanical Properties

Beside tensile and flexural test after exposure to seawater, a wide variety of tests with regard to seawater effects were accomplished because marine composite materials are increasingly using in diverse applications. These tests are including impact, fracture, fatigue, and compression test. The effects of seawater immersion on the impact resistance of two glass/epoxy composites were characterized using instrumented impact test data obtained from penetration tests by Larry H. Strait et al.[18]. Two composite materials experienced substantial reductions in peak load and energy absorbed at peak load as result of moisture-induced degradation of the fibers and fiber/matrix interface. The results of this study indicate that moisture-induced degradation can significantly reduce the impact resistance of glass fiber reinforced epoxy composites. In order to examine the interlaminar fracture toughness, the glass/polyester and glass/vinyl ester composites panels were immersed in a large tank containing natural seawater with a

salinity content of about 2.9% and temperature of 30℃ for more than two years by A. Kootsookos and A.P Moritz[19]. This study reported that the mode I interlarminar fracture toughness of the composites was not affected significantly by seawater immersion, although the flexural stiffness and strength decreased with increasing amounts of water absorption. K.Y.Rhee et al.[20] conducted the compressive fracture tests of fully seawater-absorbed carbon/epoxy composites under normal atmospheric pressure and under three levels of hydrostatic pressure conditions using a high pressure tension-compression apparatus which can produce 700 MPa of hydrostatic pressure. Fracture characteristics of seawater of seawater-absorbed carbon/epoxy composites were significantly influenced by hydrostatic pressure. Compliance decreasesed but fracture load and fracture toughness increased with increasing hydrostatic pressure. McBagonluri et al.[21] accomplished tension-tension fatigue on E-glass/vinylester immersed in synthetic seawater. To simulate the environmental fatigue, a fluid cell was used for testing of specimens. It was found that immersion in seawater slightly improved the fatigue performance, in which degradation is attributed to a fiber-dominated process.

2.4 Naval/Marine Applications of FRP Composites

2.4.1 Introduction

FRP composite materials are being used in a variety of navy applications based on their stiffness, strength, reduced weight, and corrosion-free capabilities. Until recently, the use of composite materials for military applications was limited to

aerospace and US air force for high-performance applications. Currently, applications of composite materials in the U.S Navy are widely broaden into sonar bow domes, windows, hulls and so on. Moreover, there is a resurgence of interest for the use of composites in military applications including naval vessels, army combat vehicles, and unmanned vehicles. The all-composite naval ships are currently operating to perform multifunctional operation with the benefit for composite materials. Therefore, in following section, all-composite naval vessels will be introduced.

2.4.2 Surface ships

In early, use of composite materials was constrained to the construction of small patrol boats and landing craft in displacement due to relatively poor fabrication quality and low stiffness of the hulls. However, as fabrication technique and mechanical properties were improved, composite materials can be applied to larger patrol boat, minecountermeasure vessels, and corvettes.

Skjold (Figure 2-1) is the Royal Norwegian Navy's first fast patrol craft/littoral combat ship of the *Skjold*-class and is currently being evaluated by the US Navy. The ship is based on a catamaran hull where lift fans blow air into an air cushion between the hulls. The structure is built with FRP sandwich using uniaxial glass fiber and carbon laminates with vinyl-ester or polyester resin. Polyvinyl chloride (PVC) core material is used in main structural elements below main deck and polymethacrylimide (PMI) core material is used elsewhere and for the complete superstructure. The total length of *Skjold* is approximately 157 feet at a displacement of 260 tons[22].

Figure 2-1: Skjold class patrol boat built with FRP sandwich

The Swedish Navy is operating the Visby-class corvette (Figure 2-2) from 2000. Visby class is designed to be a multi-purpose vessel with capabilities for surveillance, combat, mine laying, and anti-submarine warfare operations[23]. The visby corvette is built from sandwich composite panels having face skins of hybrid carbon- and glass fiber polymer laminate covering a poly (vinyl chloride) foam core. With carbon-reinforced composite, Visby class can get the benefit of adequate electromagnetic shielding.

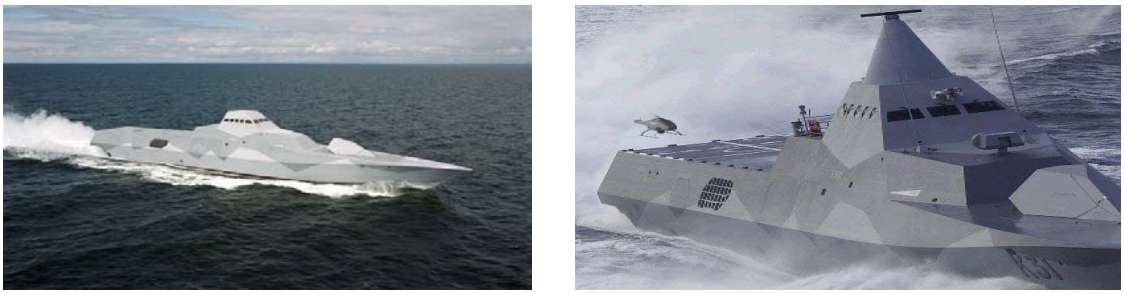

Figure 2-2: Visby corvette having hybrid carbon- and glass fiber polymer laminate

The M80 Stiletto (Figure 2-3) is a prototype naval ship manufactured to meet specific requirements of the Pentagon's Office of Force Transformation. M80 Stiletto represents the next generation of military vessels. It is built with new carbon-fiber

materials and has a networked architecture. It is unique for its hull design, speed, ride quality, payload capability and provision for unmanned vehicle support. The M80 Stiletto is a twin-M-hull vessel. It is 88ft in length with a 40ft beam, providing a rectangular deck area. When fully loaded, the vessel's draught is 3ft. The M80 Stiletto can reach speeds of 50kt to 60kt. The vessel is built on the advanced M-hull technology. Its carbon-fiber body ensures reduced weight and increased stiffness.

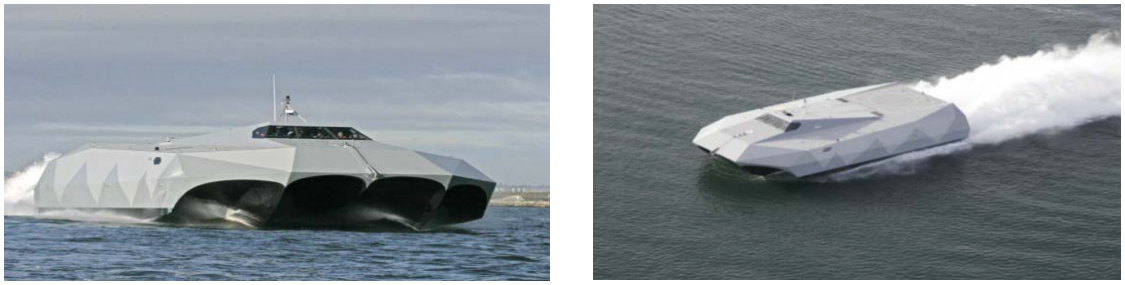

Figure 2-3: M80 Stiletto built with new carbon-fiber materials

2.4.3 Submarines

Several navies have used composites with outstanding success in a diverse range of submarine structures for nearly 50 years. Various submarine structures are made of composite materials, including sails, fins, mast strouds, casings over the upper pressure hull and bow sonar domes on nuclear submarine and combatant submarines by US Navy, Royal Navy and French Navy. In addition, periscope fairings have been built of FRP. These autoclave-cured parts are precision machined to meet the tight tolerances required of the periscope bearing system. The fairings are all glass, with a recent switch from polyester to epoxy resins.

The defense evaluation and research agency (UK) has investigated the feasibility

of lining the outside wall of the steel pressure hull with a sandwich composite material[24]. Covering the steel hull with composite cladding increased the overall buckling strength, lower fatigue strains, reduce corrosion and lower the acoustic, magnetic and electric signatures.

Composites are being used increasingly in submarine masts for communications and electronic surveillance as well as in non-hull penetrating masts. Masts made of composites have a number of advantages over those made of steel, including lighter weight and no corrosion. Composites allow moulding into complex shape without the need for machining, and the incorporation of radar absorbing materials over the entire length of the mast[25].

3 Materials and Test Methods

3.1 Material Specification

The carbon/epoxy composites were comprised of Tyfo S Epoxy and Tyfo SCH-41 reinforcing fabric supplied by FYFE Co. Composite panels comprising of two layers as shown in Figure 3-1 were fabricated using a mannual wet layup process with cure under ambient conditions. Tests were conducted after a minimum of 7 days cure. The fiber content was approximately 60% by weight. The fabric reinforcement was consisted of a primarily unidirectional fabric of 644 g/m^2 areal weight.

The fibers had a nominal tensile strength, modulus and density of 3.79 GPa, 230 GPa, 1.74g/cm^3, respectively. The resin system was a two-component epoxy with a viscosity of 600-700 cps at 25℃. After curing and then after 72 hours of post cure at 60℃, the glass transition temperature, tensile strength, modulus and elongation are specified as 82℃, 72.4 MPa, 3.18 GPa, and 5.0% , respectively.

All mechanical tests, except for the off-axis shear test, were performed using unidirectional 2 layer panels, while 0/90 panels were used for the off-axis shear test. Because composite panels were fabricated in the field, they were uniformly preconditioned at 23℃ and 30% relative humidity (RH), in a humidity chamber to set a uniform baseline.

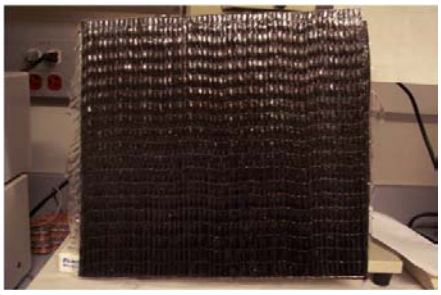

(a)

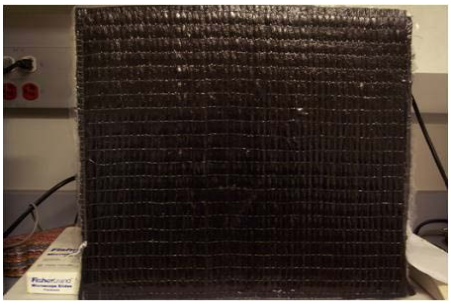

(b)

Figure 3-1: (a) Unidirectional panel and (b) 0/90^{o} panel

3.2 Environmental Conditions

3.2.1 Mechanical Properties and Thermal Analyses

After cutting composites panels with a tile saw, all specimens for mechanical properties and thermal analyses were stored in a humidity chamber (Figure 3-2 (a)) to ensure an initial condition for 2 weeks. Carbon/epoxy composite specimens were exposed thermally to ambient, 66, 93, 121, 149, 177, 204, 232, and 260℃ under ageing times of 1, 2, 4, 8, 16, 24, 48, and 72 hrs. Test specimens were kept in an oven (Figure 3-2 (b)) until they reached a set time and temperature, and then they were removed to ambient conditions for testing.

(a) (b)

Figure 3-2: (a) Humidity chamber for initial condition and (b) Oven for environmental conditions

The number of test specimens and sizes are listed in Table 3-1.

Table 3-1: Test specimens for mechanical properties and thermal analysis

Test	Specimens No	Size (mm)
Tension	temp case(9)×time case(8)×no. of test(5)+0 hour(5)=365	254×12.7×3
Off-axis shear	temp case(9)×time case(8)×no. of test(3)+0 hour(3)=219	228×12.7×3
Flexure	temp case(9)×time case(8)×no. of test(5)+0 hour(5)=365	70×12.7×3
SBS	temp case(9)×time case(8)×no. of test(5)+0 hour(5)=365	18×6×3
DMTA	temp case(9)×time case(8)×no. of test(2)+0 hour(2)=146	8.8×34×3
DSC	temp case(9)×time case(8)×no. of test(1)+0 hour(1)=146	10 ~ 15mg
TGA	temp case(9)×time case(8)×no. of test(2)+0 hour(2)=146	10 ~ 20mg
Weight Loss	temp case(9)×time case(8)×no. of test(3)+0 hour(3)=219	8.8×34×3
SEM	temp case(1)×time case(8)×no. of test[4]=32	
Total	2,003	

3.2.2 Immersion Tests

After the simulation of exposure to high temperatures such as those caused by fire in naval vessels, the characterization of mechanical properties and thermal analyses were accomplished at the various conditions to investigate how much degradation occurred in thermally aged specimens. Accurate evaluations are necessary to assess whether composite materials degraded by fire can operate at the required level of

functionality in seawater. Therefore, the specimens aged thermally at each temperatures were immersed in seawater under ambient temperature for up to 72 weeks. Simultaneously, test specimens were immersed in deionized (DI) water in the same conditions to provide a base-line comparison. Seawater from La Jolla shores was used and was periodically changed in the water bath. Figure 3-3 shows the specimens for water uptake tests and SBS tests

Moisture uptake tests were performed using gravimetric analysis. Test specimens were taken out from water bath to weigh the mass, periodically. In the case of short beam shear tests, tests were conducted after immersion in seawater and DI water under specified conditions (exposure to Ambient, 66, 93, 121, 149, 177, 204, 260℃ for 8 hr and exposure to 232℃ for 1, 2, 4, 8, 16, 24, 48 and 72hr). In addition, SEM images were taken to investigate internal fracture mechanisms caused by the exposure. The number of test specimens regarding water uptake, SBS test and SEM are summarized in Table: 3-2.

(a) (b)

Figure 3-3: (a) Test specimens for water uptake tests and (b) Test specimens for SBS tests immersed in seawater and DI water.

Table: 3-2: Test specimens for immersion tests

Test	Specimens No	Size (mm)
Water Uptake	Seawater (73) + DI water (73) = 143	25.4×25.4×3
SBS	16(temp)×8(ageing)×2(case)×5(Set) = 1,280	18×12.7×3
SEM	Some of SBS specimens	
Total	1,423	

3.3 Test Procedures

The main key to obtain more accurate data depends on how erroneous factors can be eliminated. Another key is to reduce outliers from the tests set. Therefore, experiments were carried out in following sequence.

1) Test specimens were cut with a tile saw into ASTM recommend dimensions from carbon/epoxy composite panels. Water was used as a liquid coolant to prevent material damage caused by the build-up of heat while test specimens were cut.
2) Test specimens were sanded to make edges of specimens smooth after cutting. Sanding can reduce the error factors caused by cutting.
3) Test specimens were carefully marked using a labeling metallic pen to prevent marking from disappearing during heat and chemical reactions from exposure.
4) To set initial baseline conditions, test specimens were kept in a humidity chamber at ambient conditions of 23℃ and 30% RH for 2 weeks.

5) The initialized test specimens were put in the oven to pre-specified environmental conditions. When the required time at fixed temperatures was reached, test specimens were removed to ambient conditions.
6) After cooling of test specimens, to ambient levels, they were tested immediately.
7) Based on collected data, data analysis was carried out in accordance with MIL-HDBK-1F introduced in following section.

3.4 Data Statistics

It should be noted that wet layup composite materials have significant scatter because they are made manually and hence there is a need to check for outliers. An outlier is an observation that is much lower or much higher than most other observation in a data set. Often outliers are erroneous values, due to operator error, incorrect setting of environmental conditions during testing, or due to a defective test specimen[26].

The Maximum Normed Residual (MNR) method is used in this study for quantitative screening for outliers.

$$\text{MNR}=\frac{\max\left|x_i-\bar{x}\right|}{s}, \quad i=1,2,3.....n \tag{3.1}$$

where $\bar{x}$ is sample mean, and s is sample deviation.

The value of MNR is compared to the critical value for the sample size n. These critical values are calculated from Equation (3.2).

$$C=\frac{n-1}{\sqrt{n}}\sqrt{\frac{t^2}{n-2+t^2}} \tag{3.2}$$

If MNR is smaller than the critical value, then no outliers are detected in the sample. In addition, if an outlier is detected, this value is omitted from the calculations and the MNR procedure is applied again. This process is repeated until no outliers are detected.

3.5 Test Methods

Composite materials were characterized through a series of tests including tensile, off-axis shear, flexure, short beam shear, DMTA, DSC, TGA and moisture uptake.

3.5.1 Tension

Tensile tests are important because they are the main characterizing element that defines the in-plane strength and modulus of composites[27]. The purpose of a tensile test is to determine the ultimate tensile strength and tensile modulus of composite materials. Tensile data on unidirectional composites are often used as one of the key factors in materials selection and in laminated design.

The tensile tests on the carbon/epoxy composites were performed in accordance with ASTM D3039M[27]. Test specimens were cut to dimensions of 254 mm in length and 12.7 mm in width with the length being parallel to the fiber direction as shown in Figure 3-4 (a). For tensile tests, an Instron model 8801(Figure 3-4 (b)) was used. This enables tensile testing to be conducted with hydraulic grips. To prevent test specimens from slippage, sand paper at the ends of the specimens were used to provide additional frictional force. In this research, the gauge length was 155 mm, and the specimen was

loaded in tension at a rate of 1.27 mm/min. An extensometer having a 25.4 mm gauge length was used to measure strains. When a level of 0.3% strain was reached the extensometer was removed from test equipment so as to not have damage from subsequent fiber rupture and brooming. In addition, tensile chord modulus can be obtained from the slope of the stress-strain curve.

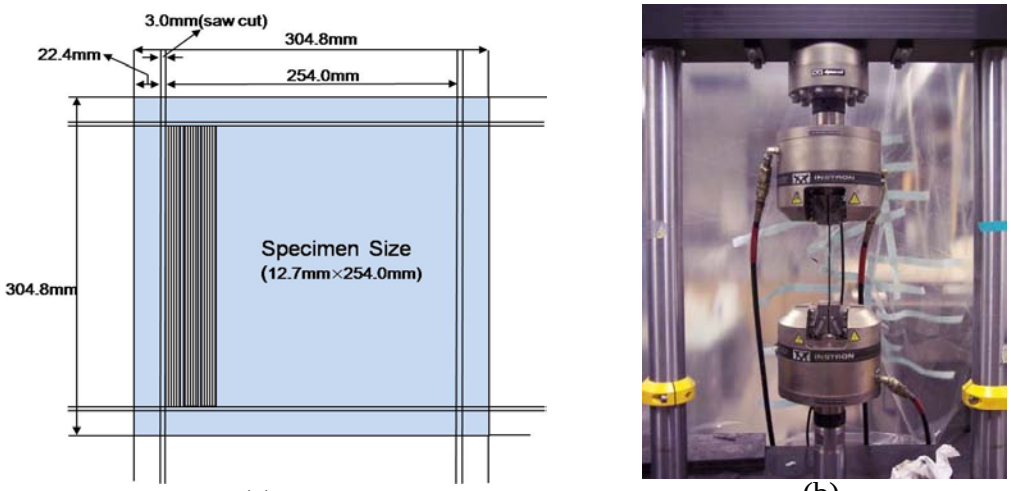

(a) (b)

Figure 3-4: (a) Test specimens for tensile test and (b) Grip of the tensile test machine (Instron 8801)

3.5.2 Off-Axis Shear

The off-axis shear test is used to determine the in-plane shear response of polymer matrix composite materials. In these tests shear distortion occurs entirely in the plane of the composites materials. The shear strength and the shear modulus can be determined from off-axis shear test.

There are many variations of the off-axis shear test such as the uniaxial tension of a 10^{o} off-axis laminate[28], V-notch beam shear[29], torsion tube tests[30], rail shear

tests[31] and uniaxial tension of a ± 45^{o} specimen[32]. In this study, off-axis shear characteristics were determined by uniaxial tension of a ± 45^{o} coupon. Off-axis shear test were carried out following ASTM D3518 with the same Instron 8801 as tension test.

Test specimens for off-axis shear test were cut to dimensions of 228.6 mm in length and 12.7 mm in width in the 45^{o} direction from 0/90^{o} carbon/epoxy panels as illustrated in Figure 3-5 (a). Sand papers at the ends of the specimens were also used to provide additional gripping force similar to that used in the tension test. The gauge length was 140 mm because the length of off-axis test specimens is smaller than that of tension test. The test procedures follow those of the unidirectional tensile test in accordance with ASTM D-3039M. When a strain level of 0.3% was attained the extensometer was removed from test equipment.

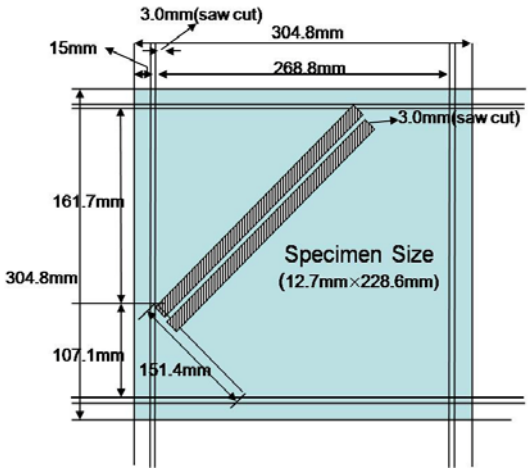

(a)

(b)

Figure 3-5: (a) Test specimens for Off-axis shear test and (b) Off-axis test Machine (Instron 8801)

3.5.3 Flexure

Flexure tests monitor the behavior of materials in simple beam loading.

Specimens are supported as a simple beam, with the load applied at midpoint, and thus ultimate stress and strain can be calculated. The three point bending flexural test measures bend or fracture strength, modulus of rupture, yield strength, modulus of elasticity in bending, flexural stress, flexural strain, and flexural stress strain materials response. Flexural strength represents the highest stress experienced within the material at its point of rupture.

Flexure tests are popular because of the simplicity of both specimen preparation and testing. Gripping of the specimen, the need for end tabs, obtaining a pure stress state and avoiding buckling are usually nonissues when conducting a flexure test[33]. In general, flexure tests are applicable to quality control and materials selection where comparative rather than absolute values are required.

The flexural tests for the carbon/epoxy composite specimens were conducted in accordance with ASTM D790[34]. For flexure test, specimens from carbon/epoxy composite panels were cut to the dimension of 12.7 mm in width and 70 mm in length as illustrated in Figure 3-6 (a). Specimens were placed on two supports and were loaded by means of a loading nose midway between the supports. The test span was 48 mm in keeping with the ASTM suggested for support span-to-depth ratio of 16:1 (the average depth of the specimens was 3 mm on 2 layers). Using Instron 5583, flexure test was carried out. As shown in Figure 3-6 (b), flexural test fixture which comprised of 2 supports and 1 load nose was used in this test. The load was applied to the specimens at a crosshead speed of 2 mm/min. The center deflection was determined throughout measurements of the vertical movement of the loading nose.

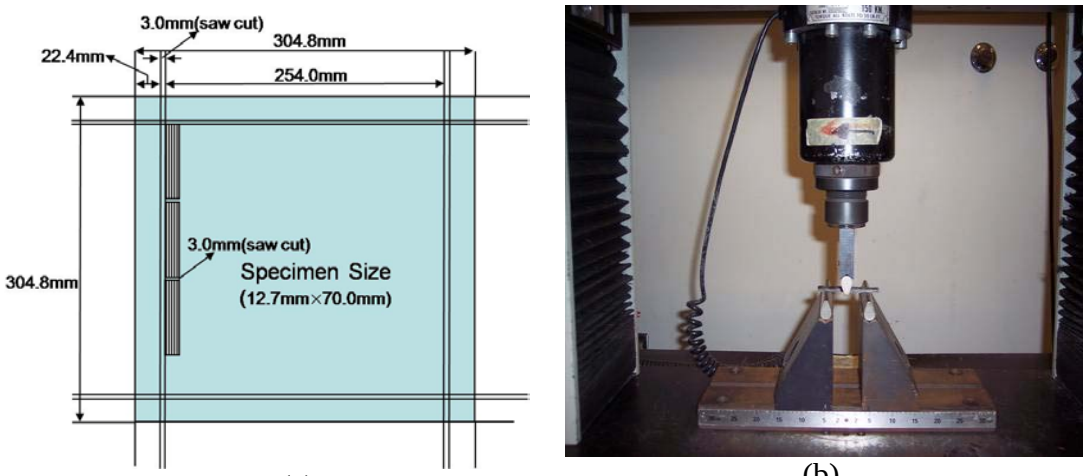

(a) (b)

Figure 3-6: (a) Test specimens for flexure test and (b) Flexure test fixture and Instron 5583

3.5.4 Short Beam Shear

Test methods available for the determination of interlaminar shear include short beam shear, four-point shear[35], double notch shear[36] and v-notch beam shear[37]. The short beam shear test was applied to determine the interlaminar shear strength in this research.

The short beam shear tests were accomplished following ASTM D2344[38] using specimens which were cut to dimension of 6 mm in width and 18 mm in length (Figure 3-7 (a)), using test fixture, and an Instron 5583 equipment (Figure 3-7 (b)). According to ASTM, the following geometries are recommended:

Specimen length = thickness ×6

Specimen width = thickness ×2

The test span in this case was 14 mm. A cross head speed of 1 mm/min was applied for all tests and the load was applied until failure of the specimens was attained.

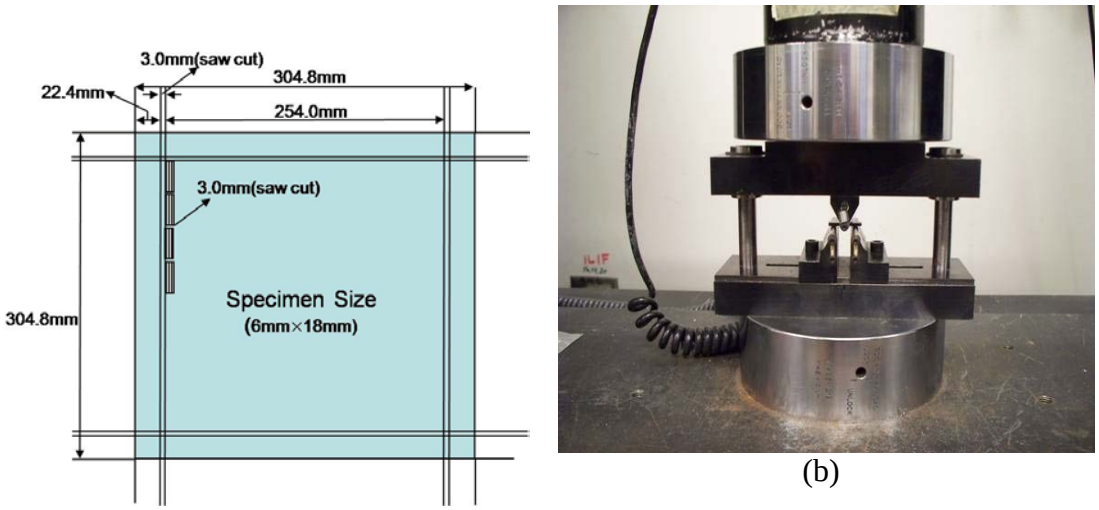

(a) (b)

Figure 3-7: (a) Test specimens for SBS and (b) SBS test fixture and Instron 5583

3.5.5 Dynamic Mechanical Thermal Analysis (DMTA)

Dynamic Mechanical Thermal Analysis (DMTA) examines the behavior of visco-elastic materials according to temperature and frequency dependent behavior. A small strain (deformation) is imposed on the material by application of a stress. The amount of strain resulting from the applied stress enables the collection of information about the modulus of the materials, its stiffness and damping properties.

In visco-elastic behavior, an imposed stress or strain gives a response which is somewhat retarded by the viscous component of the material, its fluid-like behavior, and yet because the material has substance, solid-like behavior, there is also an elastic response. DMTA separates these two responses into separate moduli values: Elastic or Storage (denoted by E') and Loss Modulus (denoted by E"). The storage modulus, represents the elastic component of the visco-elastic behavior in-phase with the imposed deformation ($\tau = \tau_o \cos\delta$), while the loss modulus, the viscous damping component, is out

of phase with the input signal ($\tau = \tau_o \sin\delta$). The overall lag of the system from the input signal is a phase angle, δ. The tangent of the phase angle, tan delta, is the ratio of loss modulus to storage modulus ($\tan\delta = E''/E'$) and is a valuable indicator of the relative damping ability of the material.

Glass transition temperature, T_g, can be determined with significant levels of sensitivity through DTMA by monitoring changes in the storage modulus, E', loss modulus, E", or the loss tangent, tan δ, as a function of temperature[39]. In general T_g, also changes based on the frequency used in testing and the rate of heating used. An increase in the heating rate is known to shift T_g to a higher temperatures[40] and an increase in test frequency for a constant heating rate also increases T_g[41]. Multi-frequency studies have been shown previously to be powerful tools for the determination of activation energy of glass transition and to follow crystallization and structural changes[42].

DMTA tests were performed in accordance with ASTM D5418[43] using the single cantilever frame fixture. The specimens for DMTA were cut to dimension of 8.8 mm in width and 34 mm in length as illustrated in Figure 3-8 (a). Multi-frequency DMTA tests were carried out on the specimens in longitudinal and transverse direction at 0.3, 1, 3, 10 and 30 Hz, with a heating rate of 2℃/min and an imposed strain of 0.01%. DMTA test equipment was a Rheometric Scientific dynamic mechanical thermal analyzer as shown in Figure 3-8 (b).

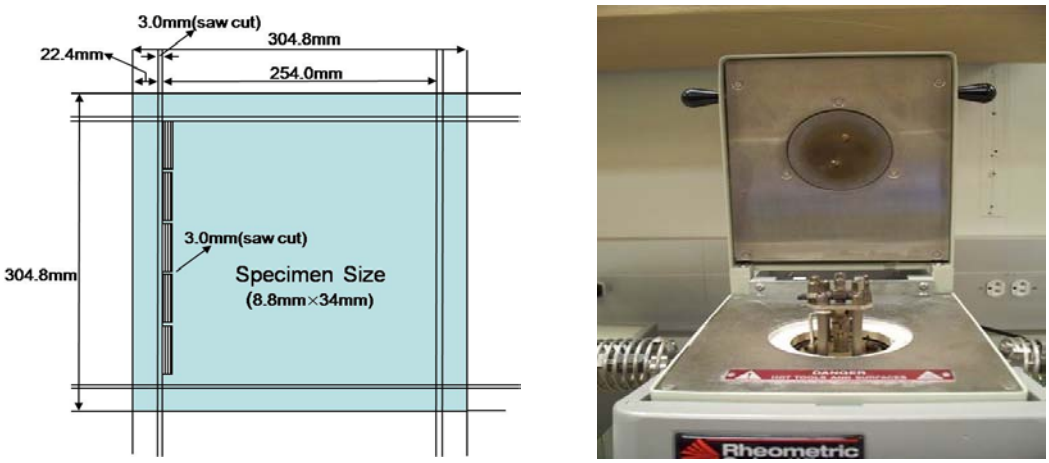

(a) (b)

Figure 3-8: (a) Test specimens for DMTA and (b) DMTA test fixture and Rheometric Scientific dynamic mechanical thermal analyzer

3.5.6 Differential Scanning Calorimetry (DSC)

Differential Scanning Calorimetry (DSC) measures the temperatures and heat flows related to transition in materials as a function of time and temperature in a controlled atmosphere. DSC tests provide quantitative and qualitative information about physical and chemical changes that include endothermic or exothermic process, or changes in heat capacity through the measurement of absorption or release of energy. In a DSC experiment the difference in energy input to a sample and a reference material is measured while the sample and reference are subjected to a controlled temperature program as shown in Figure 3-9 (a). DSC requires two pans equipped with thermocouples in addition to a programmable furnace, recorder, and gas controller.

In the case of polymer or polymer composite materials, glass transition temperature (T_g) is very useful aspect which can be obtained from DSC. If output DSC

data shifts upward suddenly at a certain temperature, this means more heat flow is needed to balance the temperature. This shows an increase in the heat capacity of sample. Namely, this happens because the polymer has just gone through the glass transition. Polymers have a higher heat capacity above the glass transition temperature than they do below it.

DSC tests were conducted following ASTM D 3418[44] using samples which were obtained from carbon/epoxy panels and DSC equipment by Rheometric Scientific corporation (Figure 3-9 (b)). Test samples were compressed by crimping for efficient heat transfer between the pan and the sample. Test samples of 10~15mg were heated at a ramp rate of 10℃/min from an initial temperature of 0℃ to final temperature of 160℃ in a controlled atmosphere flowing N_2 at 10 ml/min. For cooling down until 0℃, liquid nitrogen gas was utilized.

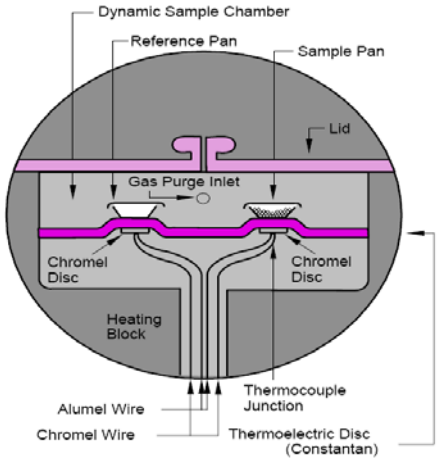

(a)

(b)

Figure 3-9: (a) Schematic of DSC and (b) Rheometric Scientific DSC SP equipment

3.5.7 Thermogravimetric Analysis

Thermogravimetric Analysis (TGA) is a thermal analysis technique used to measure changes in the mass of a sample as a function of temperature and/or time. TGA is commonly used to determine polymer degradation temperatures, residual solvent levels, absorbed moisture content, and the amount of inorganic (noncombustible) filler in polymer or composite material compositions.

The volatilization of residual solvent is typically associated with the initial weight loss process in a TGA heating run. In some cases, absorbed moisture may also be liberated over this same temperature range. After the initial solvent (or moisture) weight loss process, TGA profiles typically plateau to some constant weight level until the polymer degradation temperature range is reached. Detailed and precise factors of the thermal stability based on the initial decomposition temperature (IDT), temperature of maximum rate of weight loss (T_{max}), integral procedure decomposition temperature (IPDT), decomposition temperature range, and activation energy (E_a) of the decomposition reactions are readily determined by TGA[45].

Pyrolysis occurs through a many-stepped mechanism, where the temperature ranges for each step overlap, resulting in irregular weight-temperature curves that may be difficult to analyze. The sample weight drops slowly as pyrolysis begins, then drops precipitously over a narrow temperature range and finally turns back to a zero slope as the reactant is exhausted. The shape of the curve is determined by the kinetic parameters of the pyrolysis, such as reaction order, frequency factor, and energy of activation[46].

TGA tests were performed in accordance with ASTM E 1131[47] using samples which were cut from carbon/epoxy panels and were tested on a Mettler Toledo

TGA/SDTA851^{e} model (Figure 3-10 (a)). Samples having 10 ~ 20 mg mass were placed into a TGA sample crucible (Figure 3-10 (b)) which was attached to a sensitive microbalance assembly. The sample holder portion of the TGA balance assembly was subsequently placed into a high temperature furnace (Figure 3-10 (c)). The balance assembly measures the initial sample weight at room temperature and then continuously monitors changes in sample weight (losses or gains) as heat is applied to the sample. Samples were heated 25℃/750℃ with the heating rate of 10℃/min in flow of nitrogen environment (25 ml/min).

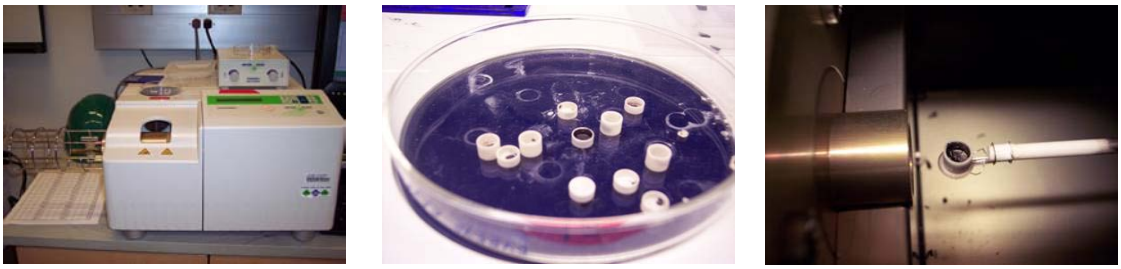

(a) (b) (c)

Figure 3-10: (a) Mettler Toledo TGA/SDTA851^{e} equipment, (b) Crucible and (c) Furnace for TGA tests

3.5.8 Moisture Uptake

For measuring the moisture uptake of the specimens immersed in sea water and de-ionized (DI) water, all samples exposed to elevated temperatures were removed from each immersion environment and kept at room temperature until measuring. All unidirectional specimens were cut to dimensions of 25.4 mm by 25.4 mm for gravimetric measurement. Wet samples from immersion environments were wiped for dryness with a paper towel prior to weighing. Weight measurements were undertaken

using a Sartorius Analytical Balance with a resolution of 10^{-5} grams. Weights were recorded when the LCD display of the balance kept a stable value for 5 seconds to ensure the consistency in test method. After measurement of weight, all samples were returned to the original environment for further exposure.

4 Mechanical Characterization

Degradation and deterioration of the mechanical properties of composite materials in a fire or at elevated temperature can seriously compromise structural integrity, and cause rapid creep, buckling, collapse or some other mechanisms of failure. The residual mechanical properties of thermally degraded composites following fire are very important factors in the design of the various applications used in the environments where fire can easily takes place. After a fire is extinguished, it is important to know the residual properties of an exposed composite at room temperature in order to determine the mechanical integrity and safety of the fire-damaged structure.

4.1 Tensile Testing

4.1.1 Introduction

Tensile tests in the fiber direction are important because tensile strength and modulus are the main mechanical properties that define the in-plane fiber characteristics of the composite materials. Although the tensile properties of unidirectional composites measured in the fiber direction can be considered to be fiber dominated it must be remembered that the wet layup process intrinsically results in the formation of a relatively high percentage of voids as well as significantly greater levels of variation and non-uniformity than prepreg based autoclave composites[48]. When carbon/epoxy composite materials are applied for naval vessels, composite materials can be subjected to tensile stress caused by rolling and pitching waves.

4.1.2 Data Reduction

In-plane tensile strength and modulus were determined from a standard in-plane tensile tests following ASTM D3039M. The ultimate tensile strength is determined using

$$F^{tu} = \frac{P^{\max}}{A} \tag{4.1}$$

where:

F^{tu} = Ultimate tensile strength

P^{max} = Maximum load prior to failure

A = Initial cross sectional area

The tensile strength at each instant in time as the specimen was loaded is determined as:

$$\sigma_i = \frac{P_i}{A} \tag{4.2}$$

where:

σ_i = Tensile strength at the i^{th} instant

P_i = Load at the i^{th} instant

The tensile strain at each point of time the specimen was loaded is determined as:

$$\varepsilon_i = \frac{\delta_i}{L_g} \tag{4.3}$$

where:

ε_i = Tensile strain at the i^{th} instant

δ_i = Increase in gauge length at the i^{th} instant

L_g = Extensometer gage length

The elastic modulus can then be determined by utilizing Hook's law

$$E = \frac{\sigma_i}{\varepsilon_i} \tag{4.4}$$

The elastic modulus is calculated using data corresponding to the 0.1% to 0.3% strain range of the linear region.

4.1.3 Analyses and Results

4.1.3.1 Time Dependence

The data for tensile strength of carbon/epoxy composite materials exposed to various temperatures from ambient temperature to 260℃ are shown in Table 4.1. The strength data were obtained by data reduction as described in the previous chapter. The values of normalized strength were calculated by dividing the average thickness of the specimens by 1.930 mm, the nominal thickness of 2-layers wet-layup composite panels. The values of strength retention (%) were obtained by comparing with strength on as-received specimen which is exposed to ambient temperatures without thermal ageing. At the fixed exposure temperatures, test specimens were thermally aged from 1 hr to 72 hrs in the oven to investigate time-dependent tendency. Fig 4.1 shows the tensile strength, normalized strength, and strength retention of carbon/epoxy composite materials as a function of time at fixed temperatures.

Residual Post-curing effects resulted in an increase of the tensile strength as

shown in Table 4-1 and Figure 4-1. At lower exposure temperatures, more time is needed for attainment of full cure, while fully curing was attained within rapid time at higher exposure temperatures. Moreover, in the ranges of lower ageing temperatures (i.e. 66, 93, 121, 149 and 177℃), the values of tensile strengths initially increased and then leveled off or slightly decreased after reaching the maximum strength. At the ambient temperature, the maximum strength caused by post-curing effect did not occur. In the case of specimens exposed to 204 and 232℃, the time to reach the maximum strength was very short and the values of the maximum strength were lower compared to lower exposure temperatures. However, the values of tensile strength did not dramatically drop. On the other hand, thermal oxidation of specimens, thermal decomposition of the epoxy resin and debonding between carbon fiber and epoxy resin occurred on specimens exposed to 260℃ for more than 16 hrs and resulted in the rapid drop of tensile strengths. In particular, thermal oxidation resulting in surface deterioration causing additional decrease of the tensile strength in the case of the specimens exposed to 260℃ for more than 16 hrs.

Over the set of tensile tests, the maximum tensile strength was 775.59 MPa (154.42% in tensile strength retention) and occurred in environmental condition of 1 hr at 149℃, while the minimum tensile strength was 188 MPa (37.55% in tensile strength retention) and as expected, under conditions of 72 hrs at 260℃, which was the highest temperature of exposure.

In addition, standard deviations of the tensile strengths after exposure to higher temperatures were greater than those at lower exposure temperatures due to variation caused by thermal oxidation.

Table 4-1: Data for tensile strength (MPa) of carbon/epoxy composite materials after exposure to various temperatures

Exposure Temperature	Time (hr)	Thickness (mm)	Strength (MPa)	S.D (MPa)	Normalized Strength (MPa)	Strength Retention (%)
Ambient (23℃)	0	3.51	502.26	15.94	913.26	100
	1	3.31	501.34	16.66	859.81	99.81
	2	3.21	512.68	29.32	852.70	102.07
	4	3.48	505.18	23.45	910.89	100.58
	8	3.02	507.06	19.79	793.43	100.95
	16	3.33	522.71	27.66	901.88	104.07
	24	3.05	514.71	14.11	813.40	102.47
	48	3.11	523.45	22.61	843.49	104.21
	72	3.24	519.48	16.66	872.08	103.42
66℃	1	2.67	706.34	121.36	978.63	140.63
	2	2.43	751.05	35.12	944.65	149.53
	4	2.67	759.38	51.76	1050.53	151.19
	8	2.62	754.03	55.81	1022.62	150.13
	16	2.80	749.95	61.39	1087.03	149.31
	24	3.09	604.06	86.50	967.74	120.27
	48	2.65	584.97	43.80	804.41	116.47
	72	2.85	578.72	34.65	854.59	115.22
93℃	1	3.22	632.60	36.84	1055.43	125.95
	2	3.02	646.52	45.32	1011.65	128.72
	4	3.20	675.49	108.19	1120.69	134.49
	8	3.12	679.70	98.29	1100.20	135.33
	16	2.97	691.43	79.60	1065.45	137.66
	24	3.26	611.17	84.19	1032.98	121.68
	48	3.14	610.71	75.52	993.59	121.59
	72	3.26	602.29	28.56	1018.59	119.92
121℃	1	3.07	584.64	27.59	929.37	116.40
	2	3.16	583.46	77.91	954.09	116.17
	4	3.01	628.76	58.75	981.91	125.19
	8	2.73	662.12	77.57	935.20	131.83
	16	3.32	564.93	41.97	970.33	112.48
	24	3.19	524.36	48.69	866.14	104.40
	48	3.42	522.15	38.31	925.27	103.96
	72	3.21	526.22	35.73	875.90	104.77
149℃	1	2.62	775.59	43.74	1053.20	154.42
	2	2.71	768.83	92.07	1080.87	153.07
	4	2.73	757.77	42.45	1072.19	150.87
	8	2.73	752.08	68.54	1062.78	149.74
	16	2.79	720.81	93.11	1043.49	143.51
	24	2.84	691.34	90.38	1017.79	137.65
	48	2.91	638.38	63.88	961.97	127.10
	72	2.56	684.88	43.20	909.15	136.36

Table: 4-1 Continued

Exposure Temperature	Time (hr)	Thickness (mm)	Strength (MPa)	S.D (MPa)	Normalized Strength (MPa)	Strength Retention (%)
177℃	1	2.94	612.64	80.61	932.60	121.98
	2	3.21	623.52	61.66	1037.05	124.14
	4	2.77	684.95	56.01	982.35	136.37
	8	2.77	679.07	75.74	973.21	135.20
	16	2.53	671.43	53.52	879.47	133.68
	24	3.00	624.42	125.15	969.30	124.32
	48	3.00	570.72	92.71	886.53	113.63
	72	3.12	563.94	43.88	910.49	112.28
204℃	1	3.09	577.67	57.80	923.67	115.01
	2	2.89	652.35	70.31	977.51	129.88
	4	2.70	710.17	100.84	992.03	141.39
	8	3.02	673.62	59.69	1054.06	134.12
	16	2.98	669.59	72.74	1033.18	133.32
	24	2.94	625.50	103.24	952.83	124.54
	48	3.01	595.91	31.10	929.98	118.65
	72	3.07	582.49	68.98	925.95	115.97
232℃	1	3.11	559.53	113.78	901.04	111.40
	2	3.07	594.13	72.52	945.06	118.29
	4	2.71	635.30	109.41	890.73	126.49
	8	2.79	636.98	117.50	919.49	126.82
	16	2.66	623.21	66.32	860.22	124.08
	24	2.61	611.42	48.53	826.84	121.73
	48	2.71	603.00	52.38	847.95	120.06
	72	2.59	565.29	25.92	759.19	112.55
260℃	1	3.03	627.34	118.33	984.89	124.90
	2	3.10	638.44	77.55	1024.37	127.11
	4	3.08	667.76	124.99	1066.80	132.95
	8	2.99	537.66	145.04	833.33	107.05
	16	2.89	349.88	120.66	524.40	69.66
	24	3.31	303.20	61.99	520.52	60.37
	48	2.91	248.40	107.04	375.05	49.46
	72	3.02	188.60	79.34	295.44	37.55

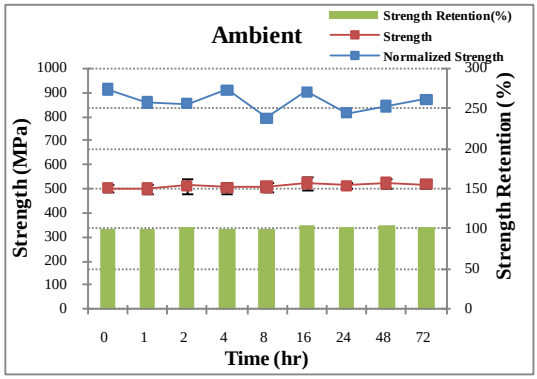

(a)

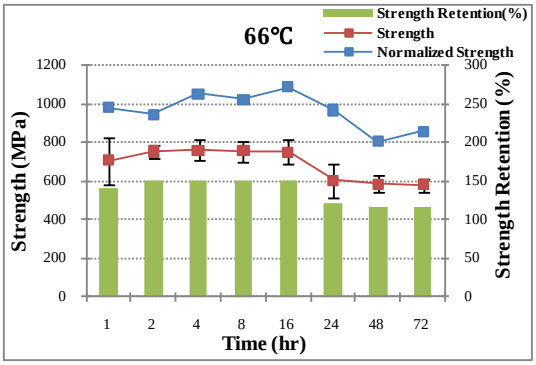

(b)

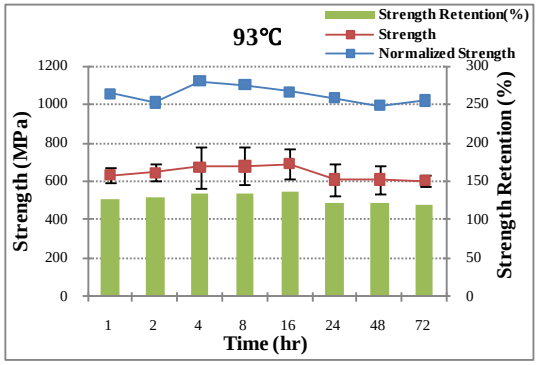

(c)

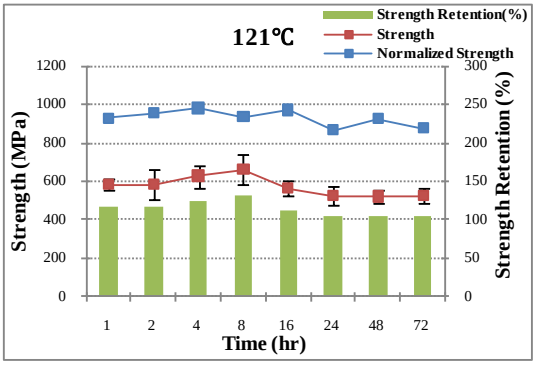

(d)

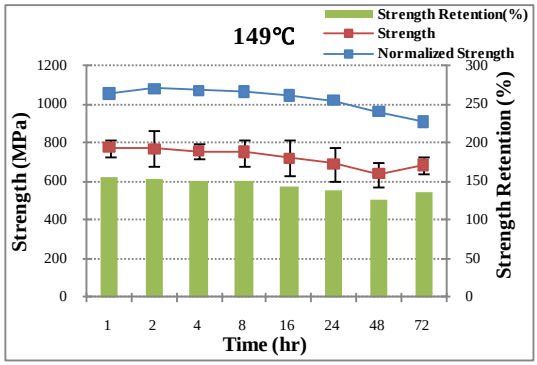

(e)

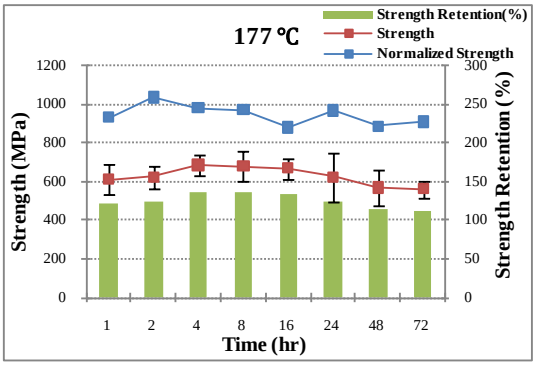

(f)

Figure 4-1: Tensile strengths and normalized tensile strengths of carbon/epoxy composite materials as a function of time at fixed temperatures, (a) ambient (b) 66 ℃ (c) 93℃ (d) 121℃ (e) 149℃ (f) 177℃ (g) 204℃ (h) 232℃ (i) 260℃

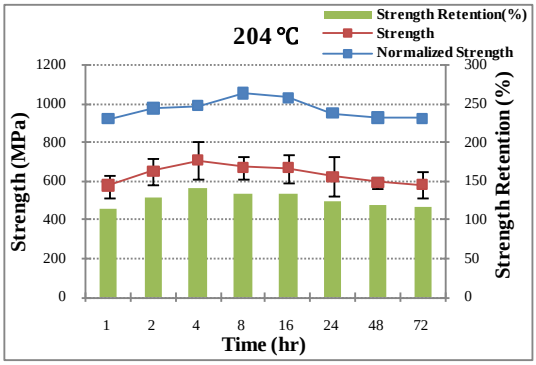

(g)

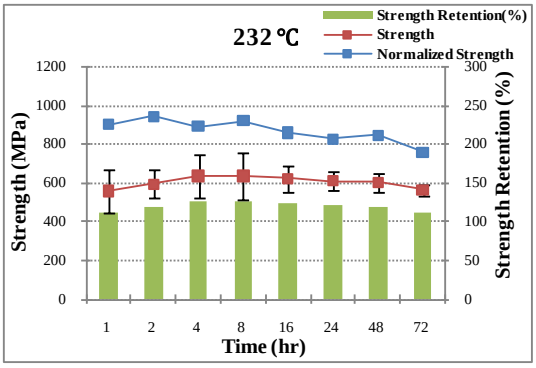

(h)

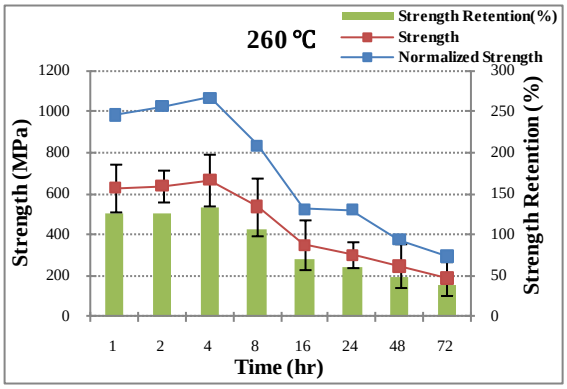

(i)

Figure 4-1: Continued

The data for tensile modulus of carbon/epoxy composite materials exposed to various temperatures from ambient temperature to 260℃ are shown in Table 4-2. The elastic modulus was calculated using data corresponding to 0.1% to 0.3% strain range within the linear region of test data.

Normalized strengths and modulus retentions (%) were obtained by same method mentioned for tensile strength. Figure 4-2 represents tensile modulus, normalized modulus, and modulus retention of the carbon/epoxy composite materials as a function of time at fixed temperatures. As shown in Figure 4-2, the data of tensile modulus show very similar tendency compared to the results of tensile strength. Initially, tensile modulus was enhanced due to post-curing effect. In all exposure temperatures, the maximum modulus values were initially attained and then showed consistency (ambient temperature) or slightly decrease (66, 93, 121, 149, 177, 204, 232℃) or a rapid drop (260℃). The distribution of the data within initial ageing time in terms of tensile modulus retention was mainly between 100 and 140%, while the distribution on tensile strength retention was mostly represented between 100% and 160%. This means the enhancement of the mechanical properties that would initially take place in tensile modulus was greater than that in tensile strength.

The maximum tensile modulus was 73.68 GPa (158.59% in tensile modulus retention) and occurred due to exposure of 16 hr at 66℃, while the minimum tensile modulus was 34.08 GPa (34.08% in tensile Modulus retention) at a condition of 72 hrs at 260℃. Tensile modulus retention of specimens exposed to 260℃ showed rapid loss in their mechanical properties compared to tensile strength retention.

Table 4-2: Data for tensile Modulus (GPa) of carbon/epoxy composite materials after exposure to various temperatures

Exposure Temperature	Time (hr)	Thickness (mm)	Modulus (GPa)	S.D (GPa)	Normalized Modulus	Modulus Retention (%)
Ambient (23℃)	0	3.51	46.46	3.60	84.48	100.00
	1	3.31	48.03	4.52	82.36	103.37
	2	3.21	50.26	3.69	83.59	108.18
	4	3.48	49.61	2.14	89.45	106.78
	8	3.02	48.24	3.56	75.48	103.83
	16	3.33	49.36	3.01	85.17	106.24
	24	3.05	53.21	4.28	84.09	114.53
	48	3.11	50.21	3.64	80.91	108.07
	72	3.24	49.52	5.22	83.13	106.59
66℃	1	2.67	56.88	4.62	78.81	122.43
	2	2.43	63.40	10.13	79.74	136.46
	4	2.67	66.18	4.48	91.55	142.43
	8	2.62	71.28	10.33	96.66	153.41
	16	2.80	73.68	9.15	106.80	158.59
	24	3.09	57.04	4.60	91.38	122.77
	48	2.65	57.08	10.82	78.49	122.86
	72	2.85	56.00	8.73	82.69	120.53
93℃	1	3.22	52.42	4.61	87.46	112.83
	2	3.02	57.86	3.39	90.54	124.54
	4	3.20	58.24	5.23	96.62	125.36
	8	3.12	60.21	8.63	97.45	129.59
	16	2.97	66.30	19.36	102.16	142.70
	24	3.26	61.20	4.09	103.44	131.73
	48	3.14	59.26	9.51	96.41	127.55
	72	3.26	51.00	8.22	86.25	109.77
121℃	1	3.07	52.54	8.67	83.52	113.09
	2	3.16	54.76	6.27	89.55	117.86
	4	3.01	56.00	2.36	87.45	120.53
	8	2.73	52.76	1.05	74.52	113.56
	16	3.32	51.49	4.37	88.44	110.82
	24	3.19	50.10	5.15	82.76	107.84
	48	3.42	45.86	7.17	81.27	98.72
	72	3.21	43.94	7.92	73.14	94.57
149℃	1	2.62	61.95	5.00	84.12	133.34
	2	2.71	60.11	5.25	84.51	129.38
	4	2.73	60.55	6.31	85.67	130.33
	8	2.73	60.58	6.63	85.61	130.40
	16	2.79	56.28	12.60	81.47	121.14
	24	2.84	56.65	5.06	83.40	121.93
	48	2.91	54.15	5.39	81.59	116.54
	72	2.56	52.78	5.40	70.06	113.59

Table 4-2: Continued

Exposure Temperature	Time (hr)	Thickness (mm)	Modulus (GPa)	S.D (GPa)	Normalized Modulus	Modulus Retention (%)
177℃	1	2.94	58.31	1.86	88.77	125.51
	2	3.21	59.44	4.67	98.86	127.94
	4	2.77	59.37	2.64	85.15	127.80
	8	2.77	56.06	4.38	80.34	120.66
	16	2.53	56.63	4.31	74.17	121.89
	24	3.00	51.76	13.28	80.35	111.41
	48	3.00	50.32	5.09	78.17	108.31
	72	3.12	49.18	5.76	79.40	105.86
204℃	1	3.09	53.46	3.57	85.48	115.07
	2	2.89	54.66	9.33	81.91	117.65
	4	2.70	60.34	2.16	84.29	129.88
	8	3.02	57.23	4.75	89.56	123.19
	16	2.98	55.18	6.39	85.14	118.77
	24	2.94	54.58	9.36	83.14	117.48
	48	3.01	53.83	5.47	84.00	115.86
	72	3.07	53.89	5.84	85.66	115.99
232℃	1	3.11	57.50	4.47	92.60	123.76
	2	3.07	59.88	3.34	95.24	128.88
	4	2.71	60.12	6.34	84.29	129.40
	8	2.79	60.82	6.11	87.80	130.91
	16	2.66	57.52	7.21	79.39	123.80
	24	2.61	55.15	3.04	74.57	118.69
	48	2.71	54.27	3.31	76.32	116.81
	72	2.59	48.15	3.68	64.66	103.63
260℃	1	3.03	49.14	6.78	77.15	105.77
	2	3.10	52.28	6.41	83.88	112.53
	4	3.08	52.61	6.37	84.05	113.24
	8	2.99	47.50	5.67	73.63	102.25
	16	2.89	35.41	4.44	53.07	76.21
	24	3.31	31.28	1.90	53.70	67.33
	48	2.91	19.68	3.86	29.71	42.35
	72	3.02	15.83	4.88	24.80	34.08

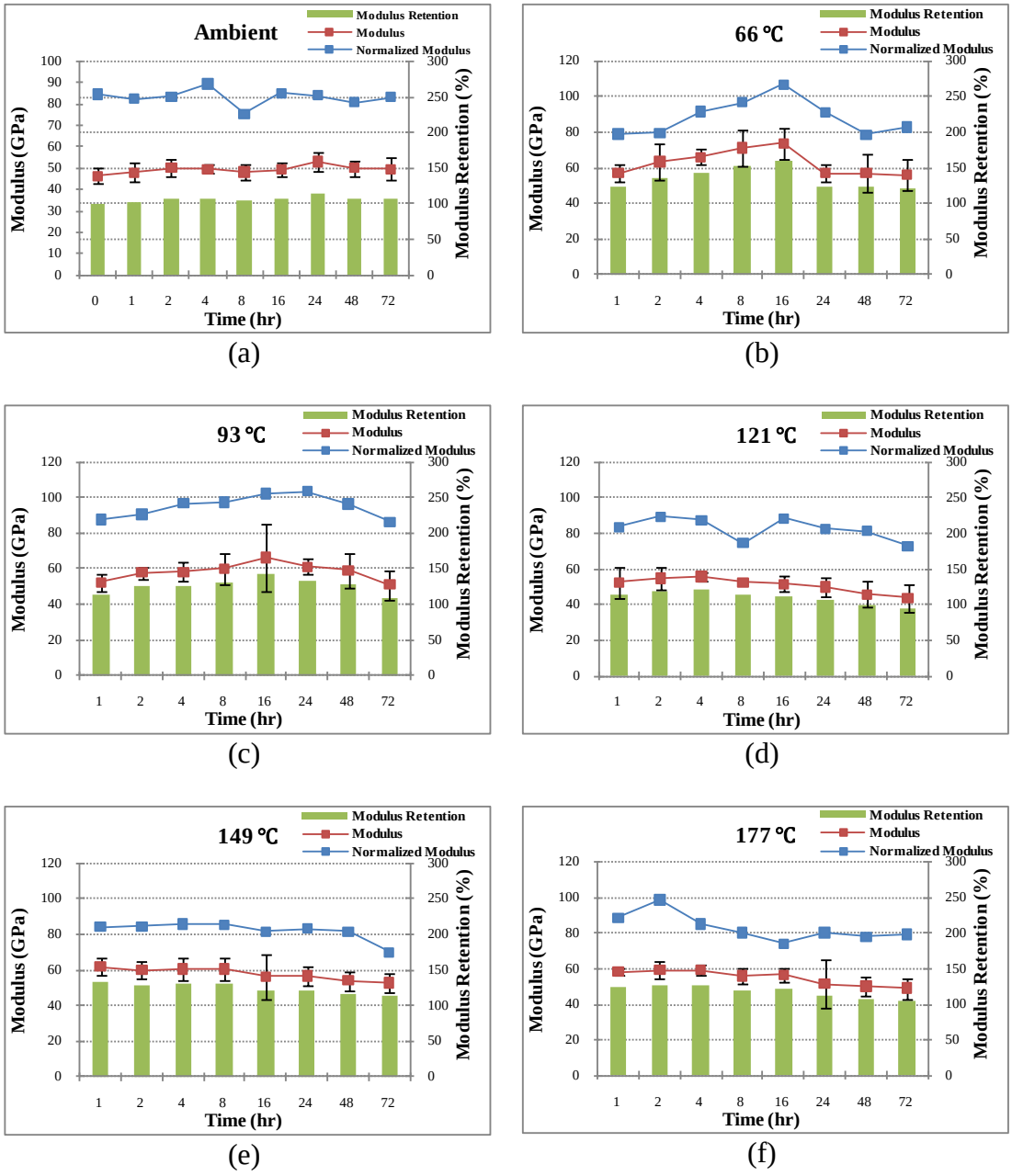

Figure 4-2: Tensile Modulus and normalized tensile modulus of carbon/epoxy composite materials as a function of time at fixed temperatures, (a) ambient (b) 66℃ (c) 93℃ (d) 121℃ (e) 149℃ (f) 177℃ (g) 204℃ (h) 232℃ (i) 260℃

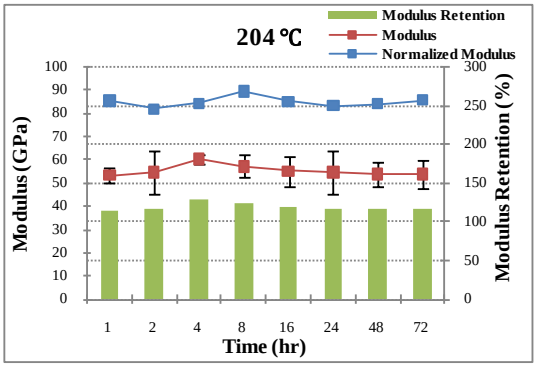

(g)

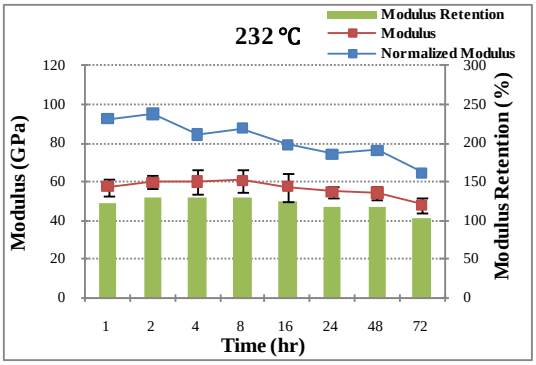

(h)

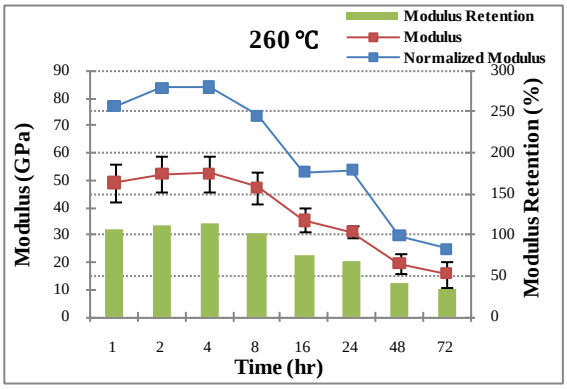

(i)

Figure 4-2: Continued

It is common engineering practice to "fit a line" to a set of data in order to determine some useful parameter in a mathematical model or perhaps to generate a calibration curve. A straight line is a simple polynomial and the goal of the fit is to determine the coefficients (the slope and intercept) of the polynomial that lead to the "best fit" of a line to the data. The fitting process can be generalized to determine the coefficients of the N^{th}-order polynomial that best fits N+1 (or more, usually) data points. The determination of the coefficients is usually termed "polynomial regression"

Table 4-3 and Table 4-4 show the time-dependent functions of tensile strength and modulus retention obtained by polynomial curve fittings. In looking at the data set of tensile strength and modulus retentions, it should be pointed out that time-dependent functions did not show linear tendency due to initial enhancement of the mechanical properties caused by post-curing effects. Therefore, the coefficients of regression (R^2) were relatively low compared to data sets without the initial increase and time-dependent functions were generally of the 2^{nd} order.

Table 4-3: Time-dependent functions of tensile strength retention (%) obtained by polynomial curve fitting

Temperature(℃)	a	b	c	d	R^2
Ambient (23)		-0.0017	0.1647	100.35	0.7359
66		0.0073	-1.0516	151.96	0.7732
93	3.E-04	-0.0316	0.6298	129.13	0.5794
121		0.0062	-0.7134	123.45	0.5709
149		0.0109	-1.071	156.08	0.9743
177	5.E-04	-0.0555	1.2256	125.25	0.7931
204	4.E-04	-0.0462	1.06	126.12	0.4772
232	2.E-04	-0.0286	0.9187	117	0.5115
260		0.0317	-3.5419	132.76	0.9362

Time-dependent function : $Y(t) = \frac{\sigma_t}{\sigma_i} \times 100 = at^3 + bt^2 + ct + d$

Table 4-4: Time-dependent functions of tensile modulus retention (%) obtained by polynomial curve fitting

Temperature(℃)	a	b	c	d	R^2
Ambient (23)		-0.005	0.3913	103.45	0.4527
66	8.E-04	-0.0923	2.2132	131.43	0.4938
93		-0.0172	1.0672	120.23	0.7162
121		0.0022	0.4867	117.99	0.9264
149		0.0042	-0.5545	132.32	0.9344
177		0.0054	-0.6963	128.22	0.9295
204	1.E-04	-0.0136	0.2273	120.08	0.2377
232		-0.002	-0.1895	128.23	0.8882
260		0.0181	-2.4333	115.95	0.977

Time-dependent function : $Y(t) = \frac{E_t}{E_i} \times 100 = at^3 + bt^2 + ct + d$

4.1.3.2 Temperature Dependence

The effect of elevated temperature on the mechanical properties of composites will be discussed in this section. Changes in temperature-dependent properties can be reversibly considered up to the point where decomposition of one of the phases, usually the polymer matrix, begins. Ideally, for a particular composite system, each modulus or strength value would be measured and expressed as a function of temperature. However, there are few composite systems where all the required data are available in this form. The accurate analysis regarding relations among mechanical properties, decomposition temperature, and glass transition temperature will be discussed in the thermal analysis chapter. In this section, temperature-dependent functions for longitudinal tensile strength and modulus at fixed time periods of exposure will be demonstrated by polynomial curve fittings.

Figure 4-3 shows tensile strength of carbon/epoxy composite materials as a

function of temperature at fixed times of exposure. As shown in Figure 4-3, in cases where tensile test specimens were exposed to short time such as 1, 2, 4 and 8 hrs, the values of the tensile strength properties had fluctuation which means post-curing effect act differently on aged specimens. As ageing times were prolonged to 16, 24, 48 and 72 hrs, the data of the tensile strength strongly depended on elevated temperatures. In particular, abrupt drop of the tensile strength occurred between 232℃ and 260℃. The amounts of tensile strength dropped by thermal decomposition at the each ageing times (16 24, 48, 72 hrs) between 232℃ and 260℃ were 43.9, 50.4, 58.8 and 66.6% respectively. In the overall tests, when test specimens were exposed to 149℃, tensile strengths were superior to the values on any other conditions.

Figure 4-4 represents tensile modulus of carbon/epoxy composite materials as a function of temperature at fixed periods of time. The data of the tensile modulus retention also had a similar tendency compared to those of the tensile strength retention but data fluctuation in short exposure times was not as high indicating that the values of the tensile modulus are more consistent. Similar to tensile strength retention, abrupt drop of the tensile modulus also took place between 232℃ and 260℃. The amounts of tensile modulus decreased by thermal decomposition at the each ageing times (16 24, 48, 72 hrs) between 232℃ and 260℃ were 38.4, 43.2, 63.7 and 67.1%, respectively.

From the data of the tensile strength and modulus retention, it can be seen that the rate of drop of the mechanical properties was higher in tensile modulus retention than in tensile strength retention in the case of high exposure temperature conditions where thermal decomposition can be expected to occur.

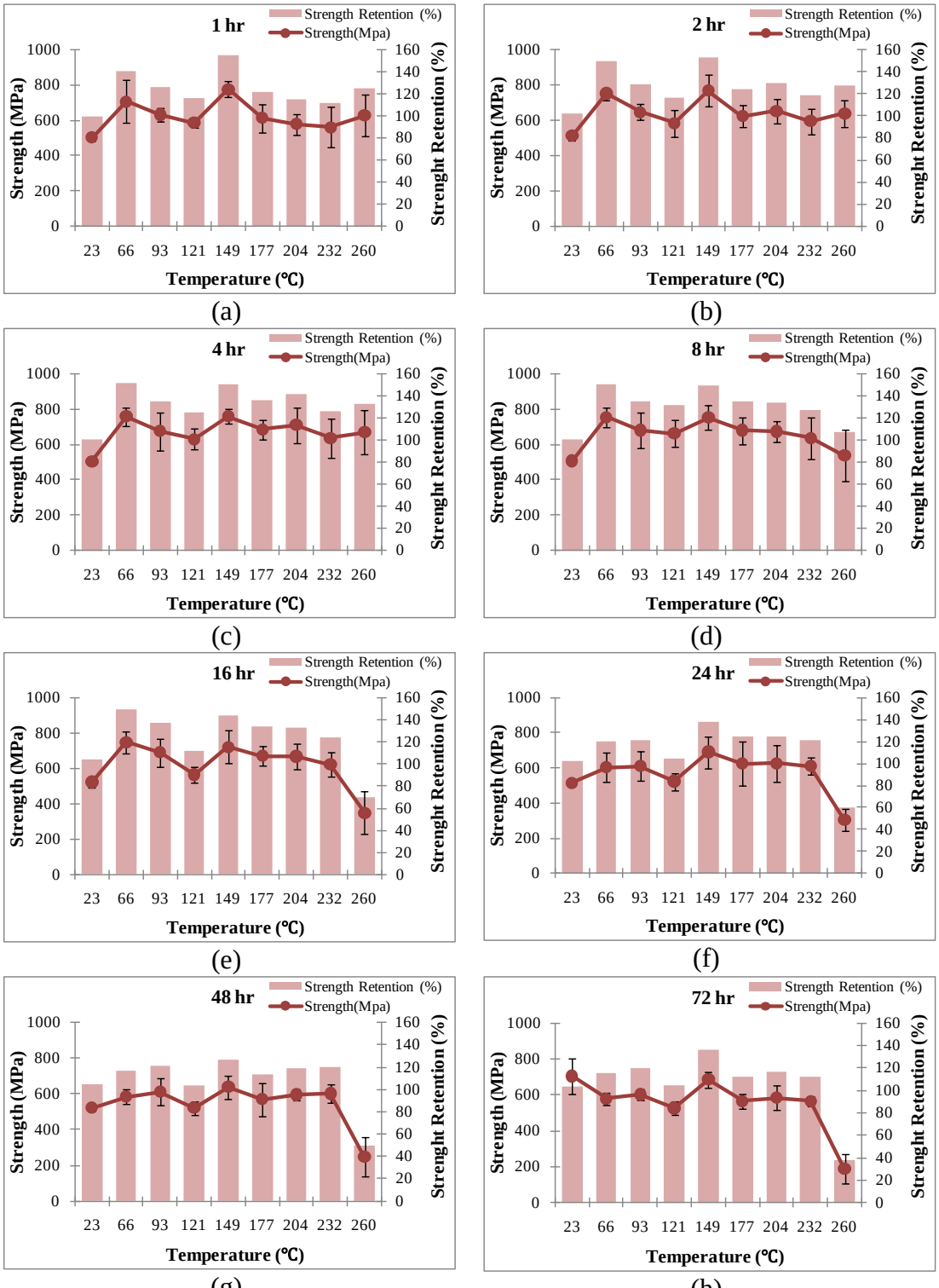

Figure 4-3: Tensile Strength of carbon/epoxy composite materials as a function of temperature at fixed periods of exposure, (a) 1 hr (b) 2 hrs (c) 4 hrs (d) 8 hrs (e) 16 hrs (f) 24 hrs (g) 48 hrs (h) 72 hrs

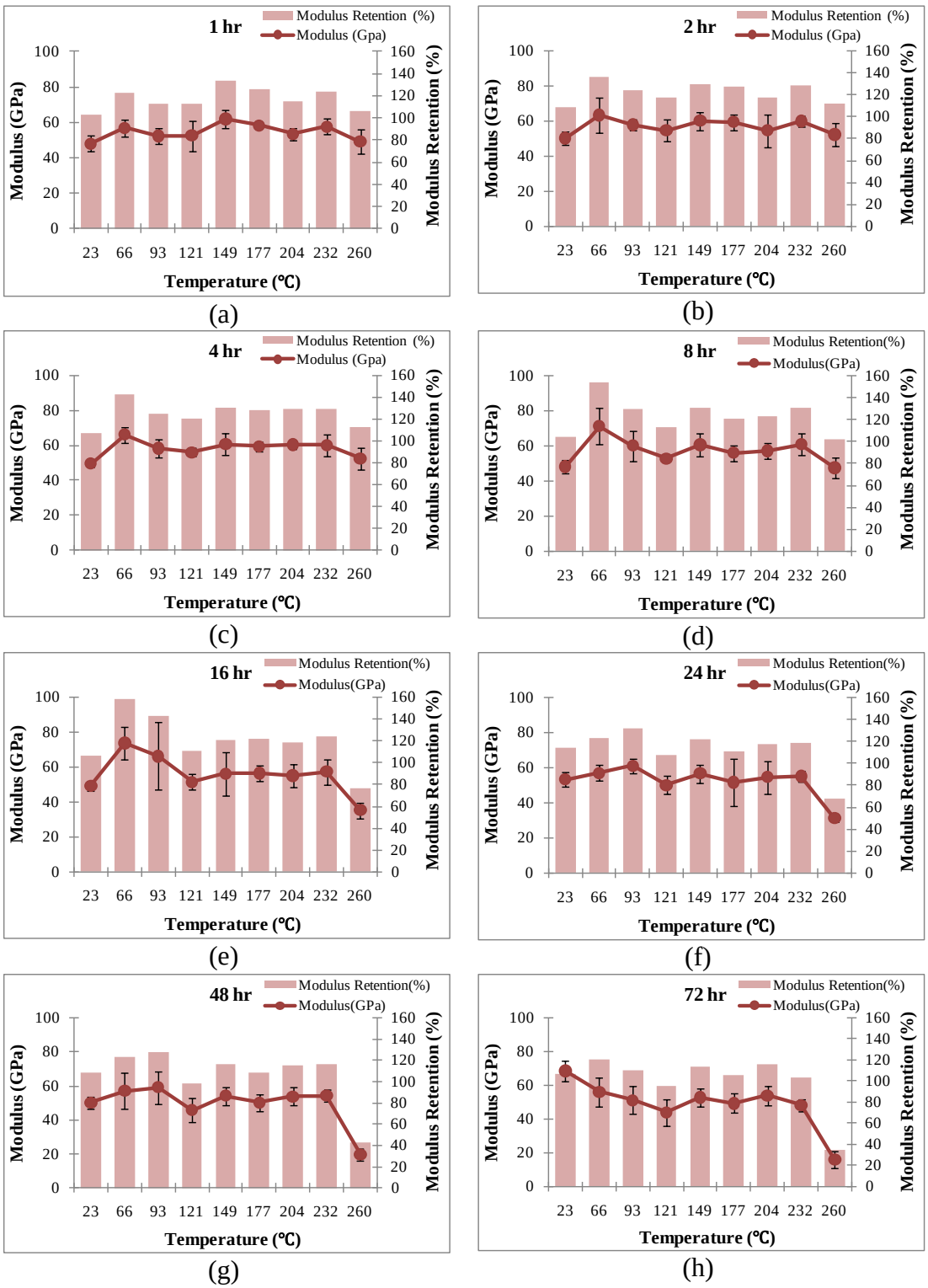

Figure 4-4: Tensile Modulus of carbon/epoxy composite materials as a function of temperature at fixed periods of exposure, (a) 1 hr (b) 2 hrs (c) 4 hrs (d) 8 hrs (e) 16 hrs (f) 24 hrs (g) 48 hrs (h) 72 hrs

Table 4-5 and Table 4-6 show the temperature-dependent functions of tensile strength and modulus retention obtained by polynomial curve fitting. Even though R-squared values are similar to the values of the time-dependent functions, temperature-dependent function had high order for good R-squared values.

Table 4-5: Temperature-dependent functions of tensile strength retention (%) obtained by polynomial curve fitting

Time (hr)	a	b	c	d	R^2
1			0.018	99.305	0.6899
2	9.E-06	-0.0044	0.5991	111.83	0.3216
4		-0.0007	0.1823	127.53	0.4414
8		-0.0016	0.3714	121.19	0.6859
16	-2.E-05	0.0073	-0.628	146.46	0.6967
24	-4.E-05	0.0141	-1.4661	159.13	0.7927
48	4.E-05	0.0151	-1.6784	168.37	0.7917
72	-5.E-05	0.0176	-1.9555	178.64	0.8552

Temperature-dependent function : $Y(T) = \frac{\sigma_t}{\sigma_i} \times 100 = a\mathrm{T}^3 + b\mathrm{T}^2 + c\mathrm{T} + d$

Table 4-6: Temperature-dependent functions of tensile modulus retention (%) obtained by polynomial curve fitting

Time (hr)	a	b	c	d	R^2
1		-0.0003	0.1046	97.959	0.4957
2	3.E-06	-0.0019	0.3418	109.86	0.2771
4		-0.0007	0.1633	120.23	0.2374
8		-0.0004	0.0309	133.06	0.3202
16		-0.0012	0.1604	132.38	0.5564
24	-2.E-05	0.0093	-1.1203	161.39	0.7578
48	-4.E-05	0.015	-1.8075	180.99	0.7736
72	-5.E-05	0.02	-2.4561	198.97	0.8913

Temperature-dependent function : $Y(T) = \frac{E_t}{E_i} \times 100 = a\mathrm{T}^3 + b\mathrm{T}^2 + c\mathrm{T} + d$

4.1.3.3 Morphological Analysis

First of all, if looking at the color of the test specimens exposed to elevated temperatures, the color of the specimens can be divided into five categories as represented in Figure 4-5.

Firstly, the surfaces of test specimens exposed to both ambient temperature and lower temperatures up to 121℃ kept the original morphology without the change of the color. In other words, the surfaces in ranges of these temperatures had the shining and black color. Secondly, as the aging time and exposed temperature were increased, the specimens showed a brown color and maintained a shiny surface between 149℃ and 177℃ in exposure temperature. Thirdly, in ranges of between 204 and 232℃, the specimens had red color and shiny surface. The color change is indicative of chemical changes occurring in the epoxy due to thermal oxidation. In addition, the color change is most likely due to an optical effect from the presence of carbon fibers in the composites. Fourthly, in specimens exposed to 232℃ for more than 8 hrs of ageing time and in 260℃ for less than 8 hrs in ageing time, the test specimens had darker color than black and more shining color due to resin melting caused by severe thermal oxidation. Finally, test specimens changed to char at 260℃ for more than 16 hrs of ageing time.

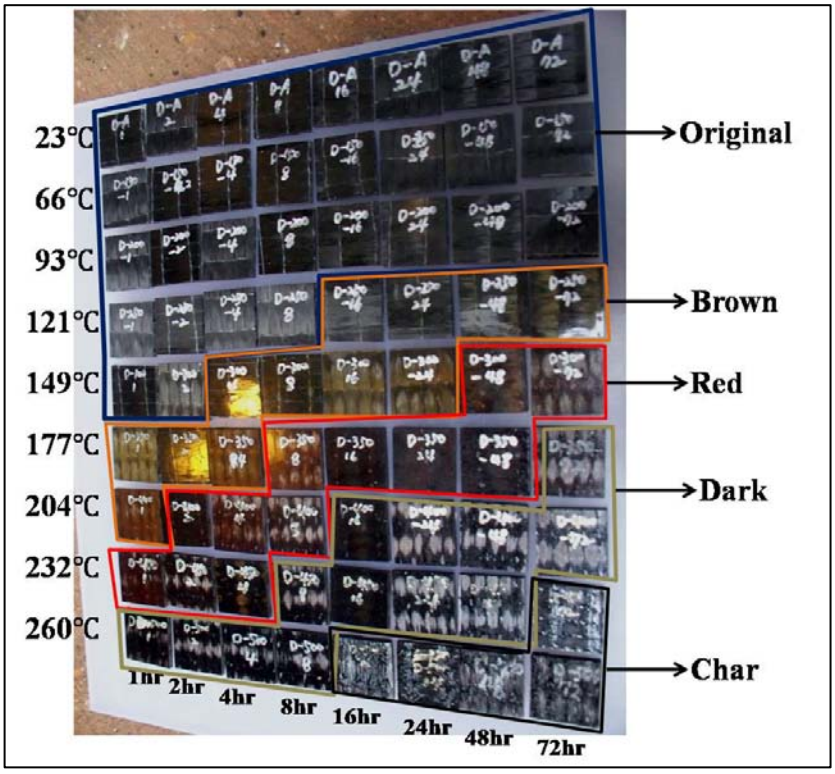

Figure 4-5: Color distribution of the test specimens after exposure to elevated temperatures for up to 72 hrs

Figure 4-6 shows test specimens fractured after tensile test after exposure to elevated temperatures at the ageing time of 72 hrs. Test coupons on Unaged and lower temperature exposures revealed visible protruding carbon fibers in the cross section fractured in brittle failure. In addition, test specimens were not fractured perpendicular to the fiber directions and the cross section fractured was not clean because fracture mechanisms were affected by cracks, voids, and poor interfaces between fiber and matrix or between layers of fabric in process of manufacturing the carbon/epoxy composite materials with the manual wet layup process. It should be noted that the fibers used in composite materials do not have perfect alignment along the longitudinal direction due to the use of manual wet layup process. On the other hand, the cross sections of the test specimen fractured under high temperature exposure conditions were approximately perpendicular to the length of the tensile bar due to bonding failure between the fiber and matrix and softening of the epoxy resin. The reason why the cross section is perpendicular and clean is that poor interface between fiber and matrix by thermal oxidation resulted in fiber pulling-out. Also, damage extended along the length of test specimen and damage area was not confined to the cross section.

Figure 4-7 shows the tensile testing results for the specimens exposed to 232℃ at 72 hrs and 260℃ at 72 hrs. Both tensile specimens demonstrated a brooming mode of failure due to thermal degradation of the matrix. The difference of the both pictures is whether carbon fibers are thermally degraded or not. At 232℃, carbon fibers of test specimens kept the stiffness up to certain points whereas even carbon fibers were perfectly degraded by thermal oxidation after exposure to 260℃ at 72 hrs.

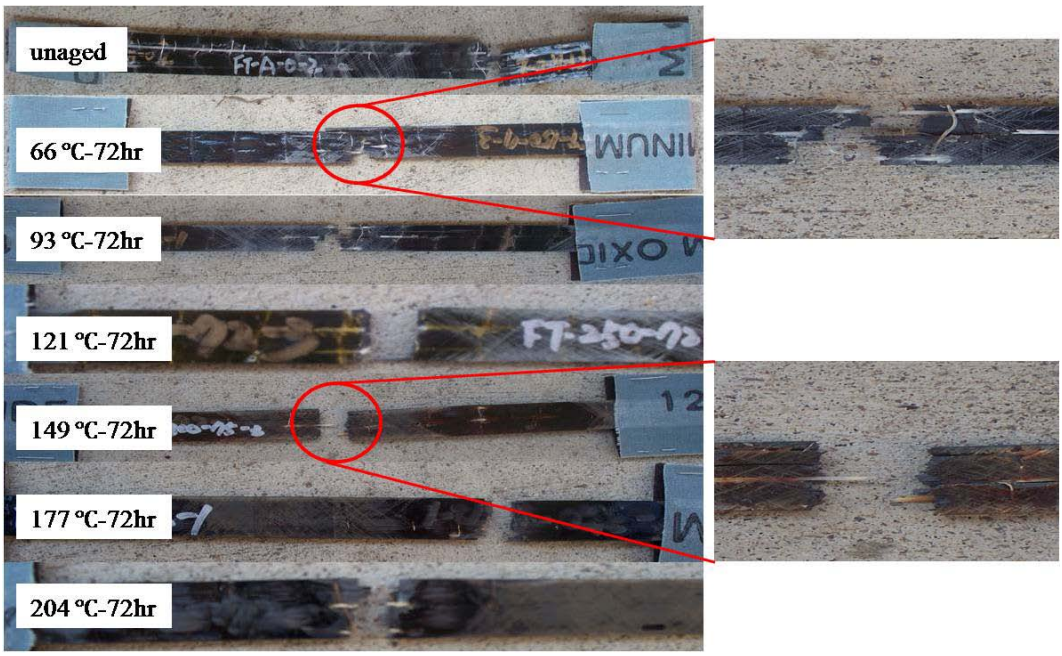

Figure 4-6: Test specimens fractured after tensile test after exposure to elevated temperatures at the ageing time of 72 hrs

(a) (b)

Figure 4-7: Tensile testing results for the specimens exposed to (a) 232 ℃ at 72 hrs and (b) 260℃ at 72 hrs

Figure 4-8 and Figure 4-9 exhibit the SEM images for comparison of as-received specimen and specimens exposed to 232℃ at the various ageing times. On fracture surfaces of as-received specimen fibers were well covered with the matrix representing a good adhesion and fractured surface included the evidence of fracture with a significant degree of ductility. The ultimate failure strain is generally greater in unaged specimen than in aged specimen. The strain effect will be explained in following chapter. On the other hand, in the cases of the specimens exposed to 232℃ for 1, 2, 4 hr, there were a little of resin debris and the interface between fiber and resin showed the good adhesion due to the additional post curing. As the ageing times were prolonged, the entire cross section of the aged specimens exhibits micro cracking, holes which fibers were pulled out, and some of the cracks have developed into delaminations. Especially, the severe delamination occurred in the specimen exposed to 232℃ at 72 hrs due to thermal decomposition of the epoxy resin and fibers were separated from the epoxy resin, indicating a low adhesion.

If seeing the surfaces of the fibers, the cross surfaces of the specimens unaged and aged within the short exposure time were not damaged and showed the good roughness. Contrary to the above cases, the roughness of the fiber surfaces was increased and the surface was damaged by thermal degradation in the higher exposure temperatures. As circled in Figure 4-9 (e), (f), (g) and (h), there were the pits on the fractured fibers because the fibers were also damaged by thermooxidation.

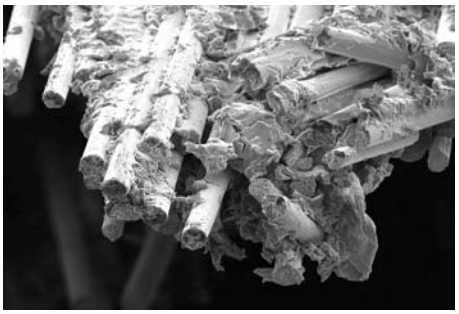

Figure 4-8: SEM image after tensile testing of as-received specimen: magnification 1000×

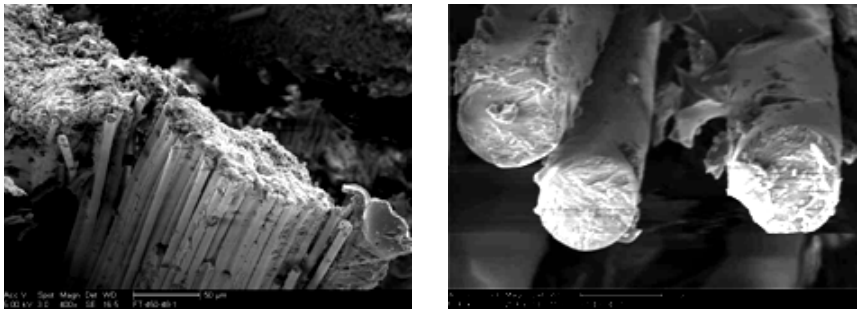

(a)

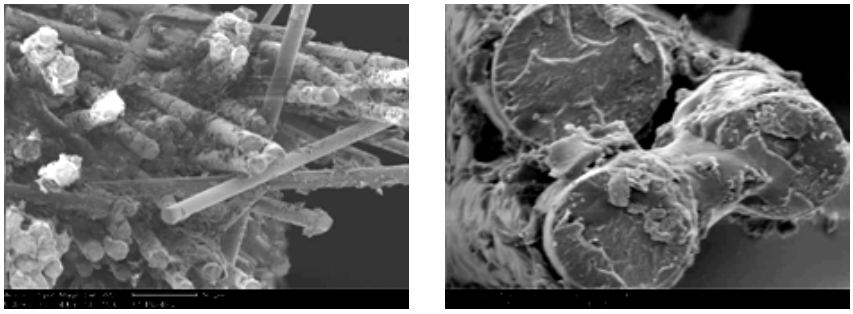

(b)

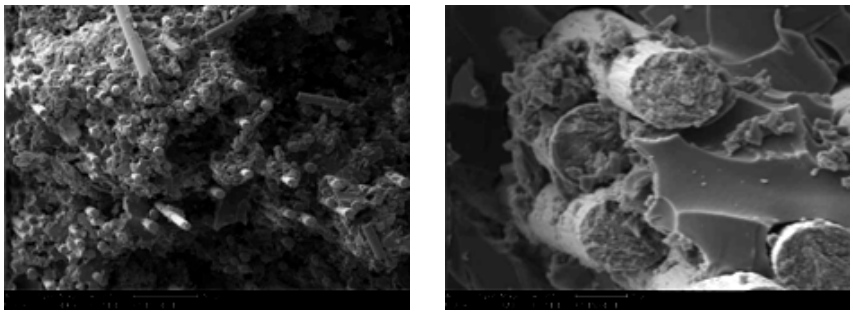

(c)

Figure 4-9: SEM images after tensile testing of specimens exposed to 232℃ for (a) 1 hr, (b) 2 hrs, (c) 4 hrs, (d) 8 hrs, (e) 16 hrs, (f) 24 hrs, (g)48 hrs, (h) 72 hrs - left images: magnification 400×, right images : magnification 500×

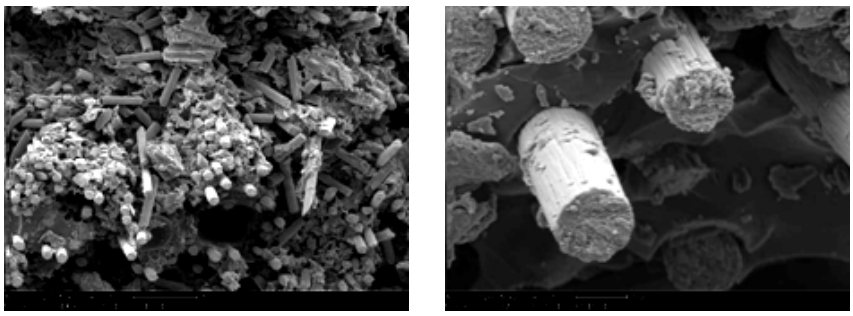

(d)

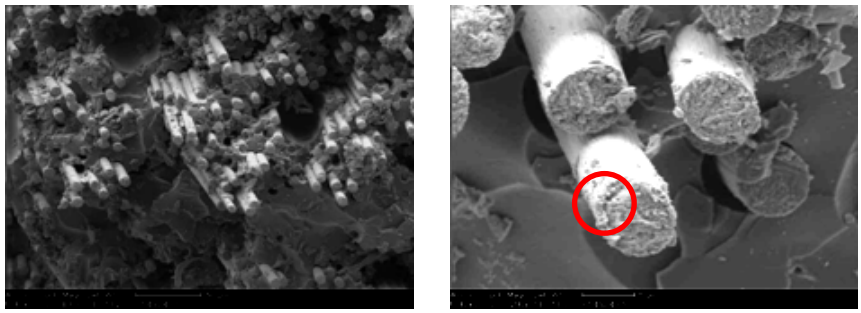

(e)

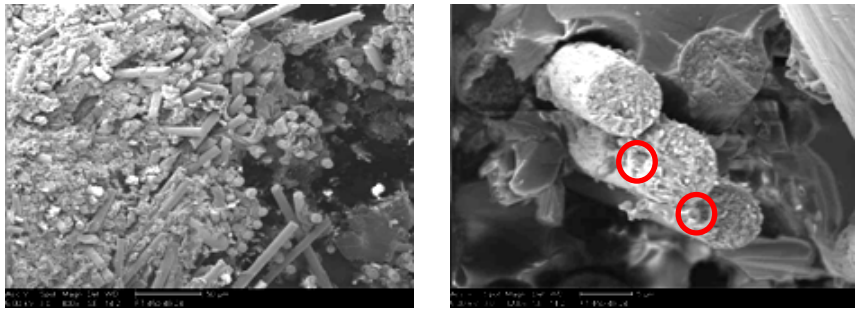

(f)

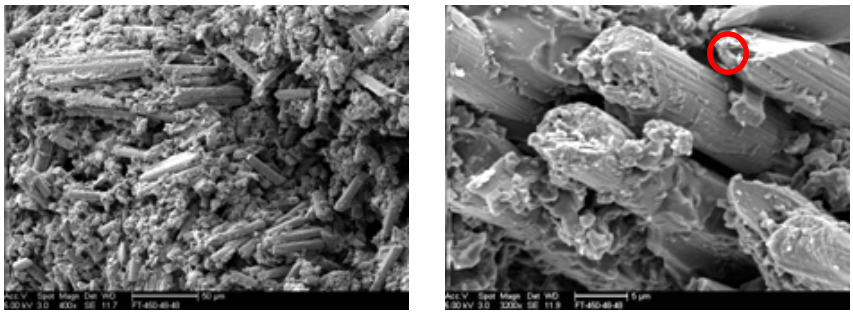

(g)

Figure 4-9: Continued

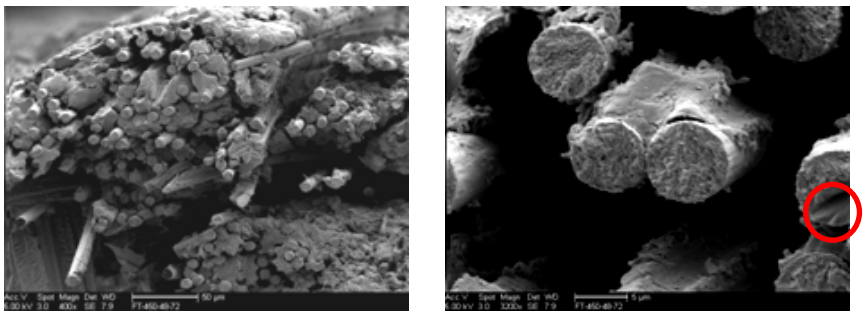

(h)

Figure 4-9: Continued

4.1.3.4 Strain Effect

Failure initiates when the fibers are elongated to their fracture strain in a unidirectional composite subjected to a longitudinal load. It is assumed that the failure strain of the fiber is less than that of the matrix and all the fibers fail at the same strain. Therefore, the ultimate longitudinal tensile strength of the composite can be assumed equal to the composite stress at the fiber fracture strain.

The ultimate failure strain of the fiber is

$$(\varepsilon_f)_{ult} = \frac{(\sigma_f)_{ult}}{E_f} \tag{4.3}$$

and the ultimate failure strain of the matrix is

$$(\varepsilon_m)_{ult} = \frac{(\sigma_m)_{ult}}{E_m} \tag{4.4}$$

Thus, the composite tensile strength is given by

$$(\sigma_1^T)_{ult} = (\sigma_f)_{ult} \mathrm{V}_f + (\varepsilon_f)_{ult} \mathrm{E}_m (1 - \mathrm{V}_f) \tag{4.5}$$

Figure 4-10 shows tensile stress-ultimate failure strain curve on specimens

exposed to various exposure temperatures at the fixed time, 72 hrs and tensile stress-ultimate failure strain curve until the strain reaches until 0.3%. Ultimate tensile strains were distributed between 2.8% and 3.2% except the result of the test specimens exposed to 260℃. The values of the ultimate failure strain were greater at the lower temperature than that at the higher temperatures. In the case of ageing time (72 hrs), perfect bonding between fibers and matrices due to fully cure occurred the strain elongation at the lower temperatures while thermal decompositions caused the ultimate failure strains to lower at the higher temperatures. The elastic modulus of the tensile test was calculated from slop between tensile stress and strain ranging from 0.1 to 0.3% before extensometer is taken off. Therefore, the slopes were changed from 0.3% strain as depicted in Figure 4-10 (a). As the slope is getting greater, test specimens are stiffer. As can be seen in Figure 4-10 (b), the slopes were increased from ambient temperature to 149℃ in exposure temperature, whereas the slopes were decreased after reaching the maximum slope between 177℃ and 232℃ due to thermal oxidation of the resin. In the case of 260℃, thermal decomposition of the resin as well as the carbon fibers caused the elasticity to lose before reaching the ultimate failure strain of 0.3%. As depicted in Figure 4-7, the epoxy resin was perfectly decomposed and carbon fibers had a brooming mode of failure.

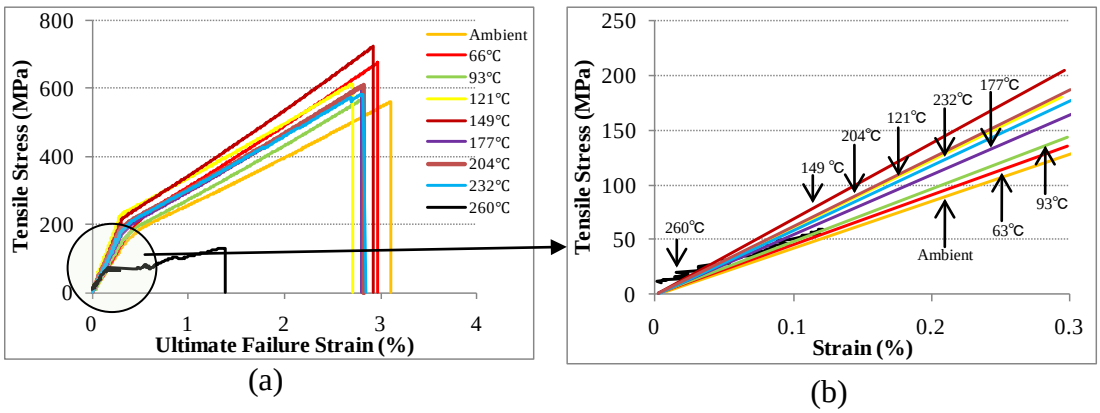

(a) (b)

Figure 4-10: (a) Tensile stress-ultimate failure strain curve exposed to various ageing temperatures at a fixed time of 72 hrs (b) Tensile stress-ultimate failure strain curve until the strain reaches until 0.3% (Note that the kink in figure 4-10 (a) is due to removal of the extensometer)

Figure 4-11 and Table 4-7 show the relations of the ultimate tensile strength, the tensile modulus and the longitudinal load as a function of the ultimate failure strain. Except the environmental conditions exposed to 260℃ for 16, 24, 48, and 72 hrs, the values of the tensile strength, the tensile modulus and load were distributed between 500 MPa and 750 MPa, 45 GPa and 73 GPa, 22 KN and 28 KN, respectively. The main range of the ultimate failure strain was between 2.4% and 3.4%. This range had the significant variation of the data because these specimens had the void due to hand wet layup process. As can be seen from R-squared values, the ultimate tensile strain showed the most linear relation with the longitudinal load. However, the linear relations between the ultimate tensile strain and the tensile modulus were poor than any other relations.

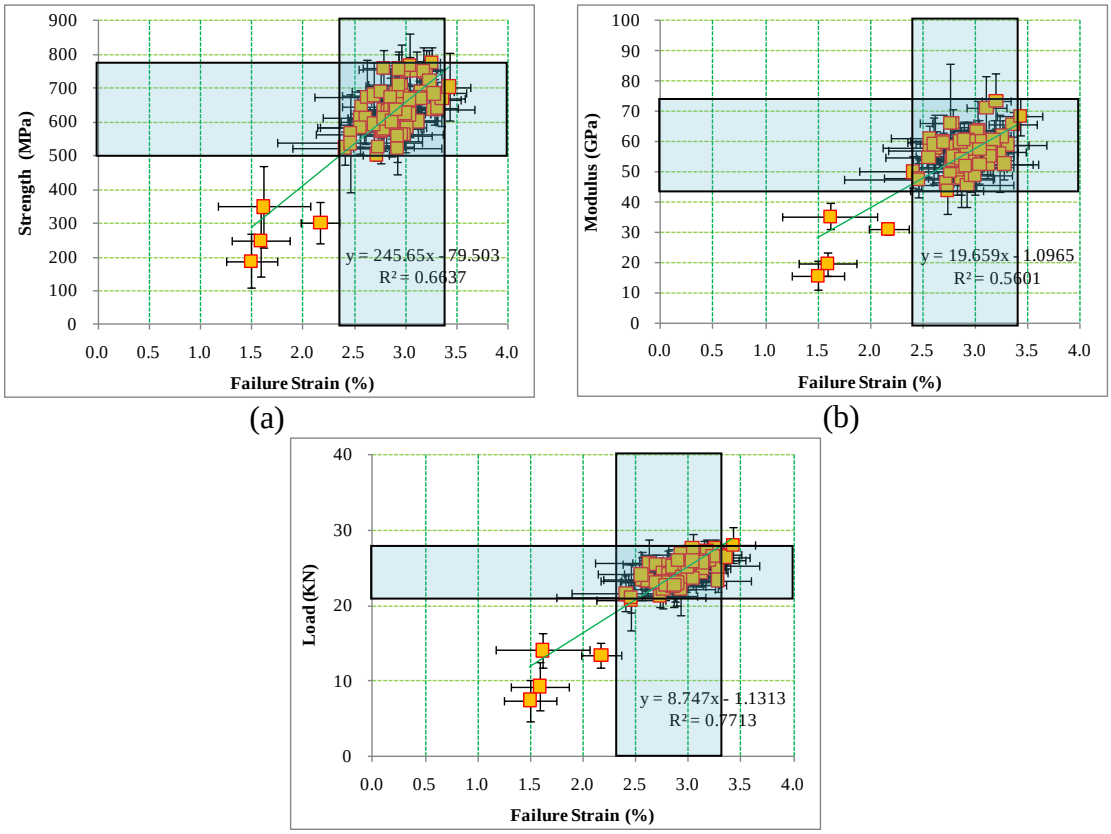

Figure 4-11: (a) Tensile Strength, (b) Tensile Modulus, (c) Load as a function of ultimate failure strains (%). Error bars indicate standard deviation

Table 4-7: Ultimate failure strain (%) after tensile testing

Exposure condition	Time (hr)	Load (KN)	S.D (KN)	Strength (MPa)	S.D (MPa)	Modulus (GPa)	S.D (GPa)	Failure strain (%)	S.D (%)
Ambient (23℃)	0	22.88	0.98	502.26	15.94	46.46	3.60	2.713	0.13
	1	23.68	1.89	501.34	16.66	48.03	4.52	2.862	0.31
	2	24.56	2.01	512.68	29.32	50.26	3.69	3.115	0.19
	4	22.74	0.98	505.18	23.45	49.61	2.14	2.784	0.26
	8	25.04	1.33	507.06	19.79	48.24	3.56	3.275	0.40
	16	23.05	0.89	522.71	27.66	49.36	3.01	3.306	0.20
	24	24.12	0.51	514.71	14.11	53.21	4.28	3.033	0.24
	48	23.91	1.22	523.45	22.61	50.21	3.64	3.353	0.23
	72	23.94	2.19	519.48	16.66	49.52	5.22	3.421	0.21
66℃	1	24.31	2.19	706.34	121.36	56.88	4.62	2.960	0.35
	2	24.86	1.15	751.05	35.12	63.40	10.13	3.012	0.24
	4	25.49	0.79	759.38	51.76	66.18	4.48	2.782	0.20
	8	25.54	1.24	754.03	55.81	71.28	10.33	3.102	0.19
	16	25.98	0.73	749.95	61.39	73.68	9.15	3.194	0.14
	24	24.20	1.92	604.06	86.50	57.04	4.60	2.866	0.31
	48	23.26	1.29	584.97	43.80	57.08	10.82	2.592	0.42
	72	23.61	1.25	578.72	34.65	56.00	8.73	2.933	0.22
93℃	1	23.97	1.34	632.60	36.84	52.42	4.61	2.830	0.18
	2	24.24	0.75	646.52	45.32	57.86	3.39	2.564	0.18
	4	25.71	3.13	675.49	108.19	58.24	5.23	2.620	0.51
	8	25.44	1.36	679.70	98.29	60.21	8.63	2.685	0.31
	16	24.45	1.67	691.43	79.60	66.30	19.36	2.754	0.28
	24	23.56	2.79	611.17	84.19	61.20	4.09	2.560	0.37
	48	23.40	1.97	610.71	75.52	59.26	9.51	2.605	0.18
	72	23.30	1.02	602.29	28.56	51.00	8.22	2.827	0.46
121℃	1	23.92	0.21	584.64	27.59	52.54	8.67	3.007	0.20
	2	24.13	2.92	583.46	77.91	54.76	6.27	2.552	0.41
	4	24.69	1.18	628.76	58.75	56.00	2.36	2.913	0.21
	8	24.01	1.55	662.12	77.57	52.76	1.05	2.916	0.25
	16	24.38	2.53	564.93	41.97	51.49	4.37	2.981	0.38
	24	21.59	2.38	524.36	48.69	50.10	5.15	2.405	0.52
	48	22.73	1.50	522.15	38.31	45.86	7.17	2.918	0.43
	72	21.31	1.51	526.22	35.73	43.94	7.92	2.726	0.35
149℃	1	27.66	1.02	775.59	43.74	61.95	5.00	3.251	0.08
	2	27.59	1.98	768.83	92.07	60.11	5.25	3.037	0.23
	4	26.86	0.52	757.77	42.45	60.55	6.31	2.928	0.38
	8	27.33	1.51	752.08	68.54	60.58	6.63	3.170	0.06
	16	26.64	1.11	720.81	93.11	56.28	12.60	3.232	0.12
	24	26.07	2.50	691.34	90.38	56.65	5.06	3.146	0.33
	48	24.71	3.42	638.38	63.88	54.15	5.39	2.968	0.39
	72	23.39	1.47	684.88	43.20	52.78	5.40	3.274	0.32

Table 4-7: Continued

Exposure condition	Time (hr)	Load (KN)	S.D (KN)	Strength (MPa)	S.D (MPa)	Modulus (GPa)	S.D (GPa)	Failure strain (%)	S.D (%)
177℃	1	24.21	3.13	612.64	80.61	58.31	1.86	2.809	0.13
	2	25.75	2.14	623.52	61.66	59.44	4.67	2.911	0.45
	4	25.91	0.48	684.95	56.01	59.37	2.64	2.910	0.18
	8	24.88	1.59	679.07	75.74	56.06	4.38	2.973	0.20
	16	25.03	0.93	671.43	53.52	56.63	4.31	3.138	0.26
	24	24.67	2.34	624.42	125.15	51.76	13.28	2.863	0.38
	48	22.21	2.47	570.72	92.71	50.32	5.09	2.759	0.30
	72	23.54	0.99	563.94	43.88	49.18	5.76	2.953	0.21
204℃	1	23.19	1.85	577.67	57.80	53.46	3.57	2.766	0.28
	2	24.38	1.30	652.35	70.31	54.66	9.33	2.948	0.11
	4	24.92	2.38	710.17	100.84	60.34	2.16	2.931	0.29
	8	25.20	0.80	673.62	59.69	57.23	4.75	2.849	0.19
	16	25.80	1.27	669.59	72.74	55.18	6.39	3.137	0.22
	24	23.81	2.38	625.50	103.24	54.58	9.36	2.935	0.30
	48	23.19	1.69	595.91	31.10	53.83	5.47	2.871	0.25
	72	23.09	1.97	582.49	68.98	53.89	5.84	2.784	0.33
232℃	1	22.16	3.42	559.53	113.78	57.50	4.47	2.921	0.33
	2	23.11	1.65	594.13	72.52	59.88	3.34	2.692	0.35
	4	22.59	2.73	635.30	109.41	60.12	6.34	2.853	0.31
	8	23.06	3.00	636.98	117.50	60.82	6.11	2.890	0.35
	16	23.71	1.44	623.21	66.32	57.52	7.21	3.039	0.15
	24	22.73	1.94	611.42	48.53	55.15	3.04	2.781	0.35
	48	22.73	2.24	603.00	52.38	54.27	3.31	2.867	0.42
	72	20.70	1.65	565.29	25.92	48.15	3.68	2.456	0.33
260℃	1	25.16	2.87	627.34	118.33	49.14	6.78	2.993	0.35
	2	26.06	1.65	638.44	77.55	52.28	6.41	2.902	0.15
	4	25.97	2.01	667.76	124.99	52.61	6.37	3.036	0.50
	8	21.06	4.35	537.66	145.04	47.50	5.67	2.455	0.71
	16	14.11	2.36	349.88	120.66	35.41	4.44	1.613	0.45
	24	13.43	1.62	303.20	61.99	31.28	1.90	2.170	0.19
	48	9.34	3.26	248.40	107.04	19.68	3.86	1.587	0.28
	72	7.51	2.74	188.60	79.34	15.83	4.88	1.495	0.25

4.1.3.5 Volume Fraction Effect

The mechanisms applying for composite materials during loading, and the progression of damage and fracture modes, are influenced by the properties, microgeometry and the interaction amongst the composite components since composite materials are composed of the various components such as fiber, matrix, void, and interfaces[49]. The strength and the stiffness properties of the composite materials are extremely dependent on the fiber volume fraction, and this parameter thus is an important quality measure of such materials. Especially, fiber volume fraction is more important factor since the fiber is the main load-bearing component in unidirectional composite materials. The fiber volume fraction of a composite may be determined by chemical matrix digestion, the burn-off technique, or by photomicrographic techniques. In this study, the volume fractions were determined by photomicrograph in some cases.

In addition, all volume fractions can be obtained by micromechanical analysis of composites as follows,

$$\mathrm{F}_c = \mathrm{F}_f + \mathrm{F}_m \tag{4.6}$$

$$\mathrm{F}_c = \sigma_c \mathrm{A}_c , \tag{4.7a}$$

$$\mathrm{F}_f = \sigma_f \mathrm{A}_f , \tag{4.7b}$$

$$\mathrm{F}_m = \sigma_m \mathrm{A}_m , \tag{4.7c}$$

Where:

$\mathrm{F}_{c,f,m}$ = The uniaxial load in composite, fiber, and matrix, respectively

$\sigma_{c,f,m}$ = stress of composite, fiber, and matrix, respectively

$A_{c,f,m}$ = area of composite, fiber, and matrix, respectively

Assuming that the fibers, matrix, and composite follow Hooke's law and that the fibers and the matrix are isotropic, the stress-strain relationship is

$$\sigma_c = E_1 \varepsilon_c \tag{4.8a}$$

$$\sigma_f = E_f \varepsilon_f \tag{4.8b}$$

$$\sigma_m = E_m \varepsilon_m \tag{4.8c}$$

Where

$\varepsilon_{c,f,m}$ = strains in composite, fiber, and matrix, respectively

$E_{1,f,m}$ = elastic modulus of composite, fiber, and matrix, respectively

Accordingly, Equation 4.6 by substituting Equation 4.7 and 4.8 can be changed as following equation.

$$E_1 \varepsilon_c A_c = E_f \varepsilon_f A_f + E_m \varepsilon_m A_m \tag{4.9}$$

In the uniaxial load, the strains in the composite, fiber and matrix are equal, then from Equation 4.9,

$$E_1 = E_f \frac{A_f}{A_c} + E_m \frac{A_m}{A_c} = E_f V_f + E_m V_m \tag{4.10}$$

In the case of carbon/epoxy composite materials, the elastic modulus (230 GPa) of the carbon fiber is much greater than the elastic modulus (3.4 GPa) of the epoxy. Therefore, following equation can be yielded.

$$E_1 \approx E_f V_f \tag{4.11}$$

Table 4-8 shows the volume fractions determined by using Equation 4.11.

Table 4-8: Volume fractions and normalized volume fractions determined by using Equation 4.11 (the elastic modulus of carbon fiber is assumed to be 230 GPa)

	Ambient (23℃)				66℃				93℃			
time	Modulus (GPa)	N Modulus (GPa)	V_f	N V_f	Modulus (GPa)	N Modulus (GPa)	V_f	N V_f	Modulus (GPa)	N Modulus (GPa)	V_f	N V_f
0	46.46	84.48	0.20	0.37								
1	48.03	81.66	0.21	0.36	56.88	78.81	0.25	0.34	52.42	87.46	0.23	0.38
2	52.48	86.69	0.23	0.38	63.40	79.74	0.28	0.35	57.86	90.54	0.25	0.39
4	55.48	87.81	0.24	0.38	66.18	91.55	0.29	0.40	58.24	96.62	0.25	0.42
8	58.84	91.28	0.26	0.40	71.28	96.66	0.31	0.42	60.21	97.45	0.26	0.42
16	59.14	101.22	0.26	0.44	73.68	106.80	0.32	0.46	66.30	102.16	0.29	0.44
24	63.84	99.21	0.28	0.43	57.04	91.38	0.25	0.40	61.20	103.44	0.27	0.45
48	65.85	104.80	0.29	0.46	57.08	78.49	0.25	0.34	59.26	96.41	0.26	0.42
72	68.44	108.75	0.30	0.47	56.00	82.69	0.24	0.36	51.00	86.25	0.22	0.38
	121℃				149℃				177℃			
time	Modulus (GPa)	N Modulus (GPa)	V_f	N V_f	Modulus (GPa)	N Modulus (GPa)	V_f	N V_f	Modulus (GPa)	N Modulus (GPa)	V_f	N V_f
1	52.54	83.52	0.23	0.36	61.95	84.12	0.27	0.37	58.31	88.77	0.25	0.39
2	54.76	89.55	0.24	0.39	60.11	84.51	0.26	0.37	59.44	98.86	0.26	0.43
4	56.00	87.45	0.24	0.38	60.55	85.67	0.26	0.37	59.37	85.15	0.26	0.37
8	52.76	74.52	0.23	0.32	60.58	85.61	0.26	0.37	56.06	80.34	0.24	0.35
16	51.49	88.44	0.22	0.38	56.28	81.47	0.24	0.35	56.63	74.17	0.25	0.32
24	50.10	82.76	0.22	0.36	56.65	83.40	0.25	0.36	51.76	80.35	0.23	0.35
48	45.86	81.27	0.20	0.35	54.15	81.59	0.24	0.35	50.32	78.17	0.22	0.34
72	43.94	73.14	0.19	0.32	52.78	70.06	0.23	0.30	49.18	79.40	0.21	0.35
	204℃				232℃				260℃			
time	Modulus (GPa)	N Modulus (GPa)	V_f	N V_f	Modulus (GPa)	N Modulus (GPa)	V_f	N V_f	Modulus (GPa)	N Modulus (GPa)	V_f	N V_f
1	53.46	85.48	0.23	0.37	57.50	92.60	0.25	0.40	49.14	77.15	0.21	0.34
2	54.66	81.91	0.24	0.36	59.88	95.24	0.26	0.41	52.28	83.88	0.23	0.36
4	60.34	84.29	0.26	0.37	60.12	84.29	0.26	0.37	52.61	84.05	0.23	0.37
8	57.23	89.56	0.25	0.39	60.82	87.80	0.26	0.38	47.50	73.63	0.21	0.32
16	55.18	85.14	0.24	0.37	57.52	79.39	0.25	0.35	35.41	53.07	0.15	0.23
24	54.58	83.14	0.24	0.36	55.15	74.57	0.24	0.32	31.28	53.70	0.14	0.23
48	53.83	84.00	0.23	0.37	54.27	76.32	0.24	0.33	19.68	29.71	0.09	0.13
72	53.89	85.66	0.23	0.37	48.15	64.66	0.21	0.28	15.83	24.80	0.07	0.11

Figure 4-12 shows volume fraction and the ultimate tensile strength as a function of temperature. The composites having higher volume fraction generally showed the good mechanical properties. It should be pointed out that the range between 0.3% and 0.4% in volume fraction did not show any correlation of the tensile strength and the volume fraction. In the case of composites cured up to certain point, voids created by hand wet layup process significantly resulted in the decrease of the ultimate tensile strength. As depicted in Figure 4-13, it can be seen that the data of the tensile strength were more scattered within range between 0.3% and 0.4% in volume fraction, whereas Figure 4-13 (b) demonstrated good correlation between the tensile strength and the volume fraction in range except 0.3% and 0.4% in volume fraction.

The relations of the volume fraction and the failure strain in composite materials are also meaningful in terms of the mechanical properties. Similar to the result of correlation of the tensile strength and the volume fraction, the higher volume fraction showed the higher failure strain as shown in Figure 4-14. The data of the ultimate failure strain were more scattered within range between 0.3% and 0.4% in volume fraction as demonstrated in the correlation of the tensile strength and the volume fraction.

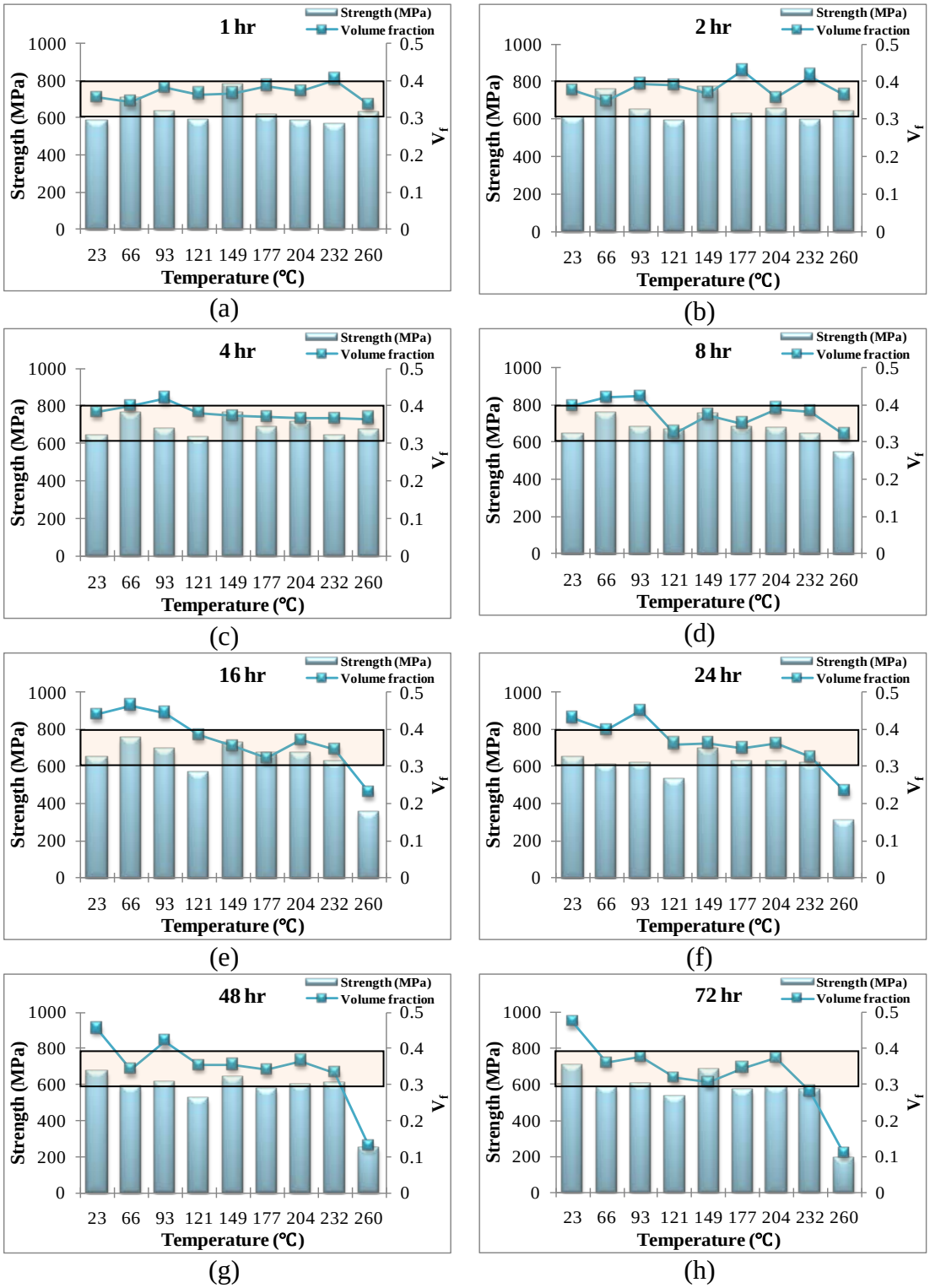

Figure 4-12: Volume fraction and the ultimate tensile strength as a function of temperature at fixed times of exposure (a) 1 hr, (b) 2 hrs, (c) 4 hrs, (d) 8 hrs, (e) 16 hrs, (f) 24 hrs, (g) 48 hrs, (h) 72 hrs

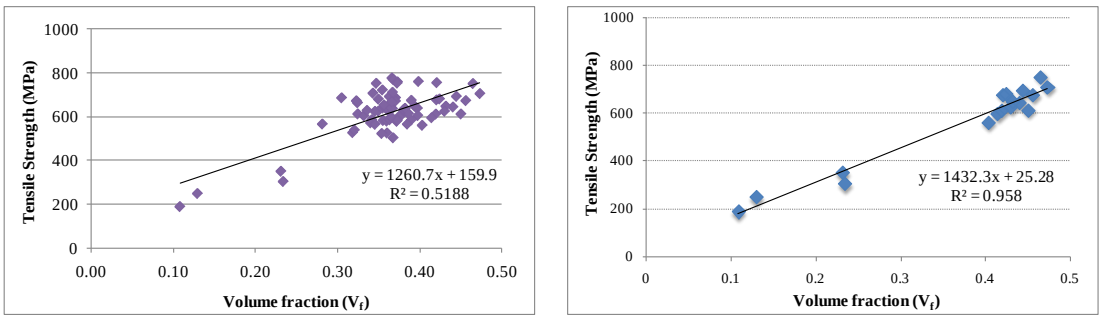

(a) (b)

Figure 4-13: (a) Volume fraction versus tensile strength (b) Volume fraction versus tensile strength without specimens having volume fractions ranging from 0.2% to 0.3%

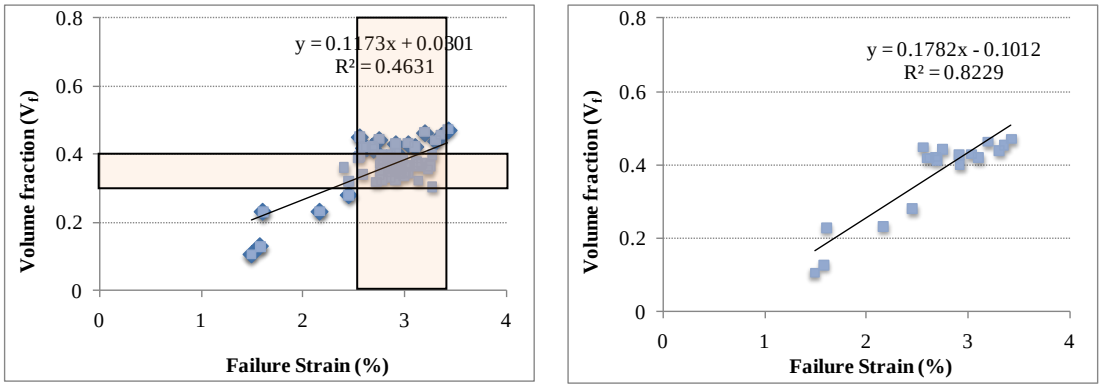

(a) (b)

Figure 4-14: (a) Volume fraction versus the ultimate failure strain (b) Volume fraction versus the ultimate failure strain without specimens having volume fractions ranging from 0.3% to 0.4%

4.2 Off-Axis Shear Testing

4.2.1 Introduction

While the unidirectional composite is very effective in providing strength and modulus in the direction of the fibers it should be pointed out that the application of small tangential stresses may lead to matrix cracking, layer delamination and fiber-matrix debonding, resulting in significant overall reductions in the load-bearing capacity of the composites[50]. It is obvious that off-axis shear resistance carefully assessed, especially as related to long-term response, since the efficiency of the strengthening technique can be consisted by the weakest materials characteristic. If the naval vessels made of composite materials are operating in the sea, off-axis shear force caused by rolling-pitching can be applied for ships. Therefore, it is very important to consider the off-axis shear as a design factor. The test specimen for the off-axis shear is relatively simple to prepare and requires no special test fixture other than standard tensile grips. The test method has been standardized as ASTM D 3518.

4.2.2 Data Reduction

When a $\pm 45^{o}$ laminate is loaded in uniaxial tension, a biaxial state of stress is induced within each of the +45 and -45 lamina. In this study, off-axis shear strength and modulus were determined through a standard $\pm 45^{o}$ laminate tensile test as outlined in ASTM D 3518. The off-axis shear strength as the specimen was loaded is determined as

$$\sigma_{11} = \frac{\sigma_{xx}}{2} + \tau_{xy} \tag{4.12}$$

$$\sigma_{22} = \frac{\sigma_{xx}}{2} - \tau_{xy} \tag{4.13}$$

$$\tau_{12} = \pm \frac{\sigma_{xx}}{2} \tag{4.14}$$

Where:

σ_{11}, σ_{22} = Normal stresses in the lamina coordinate system

σ_{xx} = The applied tensile stress

τ_{xy} = Induced shear strength

τ_{12} = Shear strength

The maximum off-axis shear strength is determined as

$$\tau_{12}^{\max} = \frac{P^{\max}}{2\mathrm{A}} \tag{4.15}$$

Where:

$\tau_{12}^{\max}$ = Maximum off-axis shear strength

$P^{\max}$ = Maximum load

The off-axis shear strain is determined as

$$\gamma_{12} = \varepsilon_{xx} - \varepsilon_{yy} \tag{4.16}$$

Where:

γ_{12} = Shear strain

ε_{xx} = Longitudinal normal strain

ε_{yy} = Lateral normal strain

The off-axis shear modulus can be determined by using the chord shear modulus.

$$G_{12}^{chord} = \frac{\Delta \tau_{12}}{\Delta \gamma_{12}} \tag{4.17}$$

Where:

G_{12}^{chord} = Shear chord modulus

$\Delta \tau_{12}$ = Difference in applied shear strength between two shear strain points

$\Delta \gamma_{12}$ = Difference of two strain points

4.2.3 Analyses and Results

4.2.3.1 Time Dependence

The data for off-axis shear strength of carbon/epoxy composite materials exposed to various temperatures from ambient temperature to 260°C are represented in Table 4-9. The off-axis shear strength was obtained by data reduction method. Also, the normalized off-axis shear strength and shear strength retention were calculated by same method described in tensile testing section. Figure 4-15 shows the off-axis shear strength, normalized strength, and strength retention of carbon/epoxy composite materials using uniaxial tensile test of a ± 45° laminate as a function of time at fixed temperatures.

Even though uniaxial tensile test of a ± 45° laminate is dominated by matrix properties, experimental results showed continuously decrease in shear strength except for test specimens exposed to ambient temperatures. Contrary to tensile testing, the

effect of residual post-cure did not initially occur in off-axis shear test. As the exposure temperature was increased, the rate of decrease of the off-axis shear strength was rapidly increased. The decreases of the off-axis shear strength exposed to 66, 93, 121, 149, 177, 204, and 232℃ from1 hr to 72 hrs in ageing time were 7.41, 17.88, 12.55, 20.36, 32.65, 34.68, and 79.30%, respectively. Especially, test specimens exposed to 232℃ abruptly underwent the decrease in off-axis shear strength. As can be seen in Table 4-9, there were no test results on test specimens exposed to 260℃ for more than 8 hrs because test specimens were already fractured when gripped for off-axis shear test.

The reason why test specimens experience continuous decrease of the off-axis shear strength is that test coupons were distorted by asymmetry when test specimens were taken out from the oven and kept in atmospheric condition before off-axis test. This phenomena means that heat transferred from the oven can be resulted in deformation of the test specimens in process of the thermal expansion and contraction. The more test specimens were exposed to high temperatures, the more distortion of the test specimens occurred.

Off-axis shear stresses applying in the plane of the laminate itself cause failure to be dominated by a single mechanism corresponding to delamination between layers and due to cracks formed across the coupon width[51].

Although the off-axis shear properties are intrinsically dependent on the resin characteristics, the increase of the shear strength which can be caused by residual post-cure effect was offset due to the distortion of the test coupons.

Table 4-9: Data for Off-axis shear strength (MPa) of carbon/epoxy composite materials after exposure to various temperatures

Exposure Temperature	Time (hr)	Thickness (mm)	Strength (MPa)	S.D (MPa)	Normalized Strength (MPa)	Strength Retention (%)
Ambient (23℃)	0	2.98	57.51	1.81	88.80	100.00
	1	2.89	58.73	2.19	87.95	102.12
	2	3.56	58.47	2.45	107.85	101.66
	4	3.16	58.40	3.58	95.63	101.55
	8	3.00	58.14	3.99	90.27	101.08
	16	3.58	58.15	1.82	107.86	101.10
	24	3.37	59.75	3.52	104.32	103.88
	48	3.53	62.30	4.91	113.83	108.31
	72	3.02	63.38	0.80	99.29	110.20
66℃	1	3.13	56.11	3.82	91.56	97.55
	2	3.13	55.32	5.75	90.09	96.19
	4	3.11	54.39	2.50	88.19	94.57
	8	3.27	53.79	1.47	91.61	93.52
	16	3.07	53.72	5.05	85.99	93.40
	24	3.49	52.68	6.06	95.76	91.60
	48	3.13	52.19	3.28	85.18	90.75
	72	3.25	51.95	4.61	88.03	90.33
93℃	1	3.20	53.94	3.31	89.80	93.78
	2	3.24	51.34	1.18	86.64	89.27
	4	3.48	51.19	4.74	92.79	89.01
	8	3.27	48.16	5.31	82.10	83.73
	16	3.01	47.59	5.05	74.61	82.75
	24	3.24	44.54	1.54	75.24	77.44
	48	3.68	42.41	2.50	81.29	73.74
	72	3.26	44.29	3.57	75.13	77.01
121℃	1	3.48	50.50	2.41	91.45	87.81
	2	3.26	50.38	3.00	85.63	87.60
	4	3.09	49.10	4.42	79.03	85.38
	8	3.29	45.19	4.57	77.44	78.57
	16	3.17	45.98	5.90	75.91	79.94
	24	3.27	44.56	4.03	75.96	77.47
	48	3.70	44.14	5.83	85.14	76.75
	72	3.32	44.16	4.78	76.37	76.79
149℃	1	3.40	49.18	5.39	87.09	85.51
	2	3.31	48.06	3.16	82.94	83.56
	4	3.09	47.95	1.16	77.17	83.37
	8	3.25	43.23	3.37	73.25	75.16
	16	3.42	42.06	2.57	74.99	73.13
	24	3.36	39.40	6.90	69.01	68.50
	48	3.20	39.69	4.38	66.15	69.01
	72	3.31	39.17	6.48	67.45	68.10

Table 4-9: Continued

Exposure Temperature	Time (hr)	Thickness (mm)	Strength (MPa)	S.D (MPa)	Normalized Strength (MPa)	Strength Retention (%)
177℃	1	3.20	47.90	4.91	79.75	83.28
	2	3.23	45.19	3.05	76.02	78.57
	4	3.11	41.85	5.62	67.71	72.76
	8	3.30	39.10	1.15	67.26	67.98
	16	3.32	37.82	4.06	65.33	65.75
	24	3.27	35.75	4.57	60.88	62.15
	48	3.53	33.28	8.07	61.14	57.87
	72	3.25	32.26	4.31	54.66	56.09
204℃	1	3.35	43.90	2.06	76.52	76.33
	2	3.31	41.72	0.69	71.99	72.54
	4	3.26	38.91	0.37	65.99	67.65
	8	3.31	36.34	4.21	62.64	63.18
	16	3.42	37.57	2.13	66.92	65.32
	24	3.23	31.38	2.75	52.84	54.55
	48	3.26	30.59	2.49	51.94	53.19
	72	3.48	28.67	1.82	51.92	49.85
232℃	1	3.28	37.22	4.30	63.52	64.71
	2	3.42	34.18	3.34	60.83	59.43
	4	3.19	33.20	3.25	55.10	57.72
	8	3.12	33.02	3.27	53.66	57.41
	16	3.40	29.09	2.11	51.56	50.57
	24	3.22	25.82	0.87	43.31	44.90
	48	3.22	16.92	5.74	28.34	29.41
	72	3.27	7.71	0.92	13.11	13.40
260℃	1	3.24	39.58	1.56	66.73	68.82
	2	3.25	35.36	3.43	59.91	61.48
	4	3.20	33.41	2.74	55.68	58.08

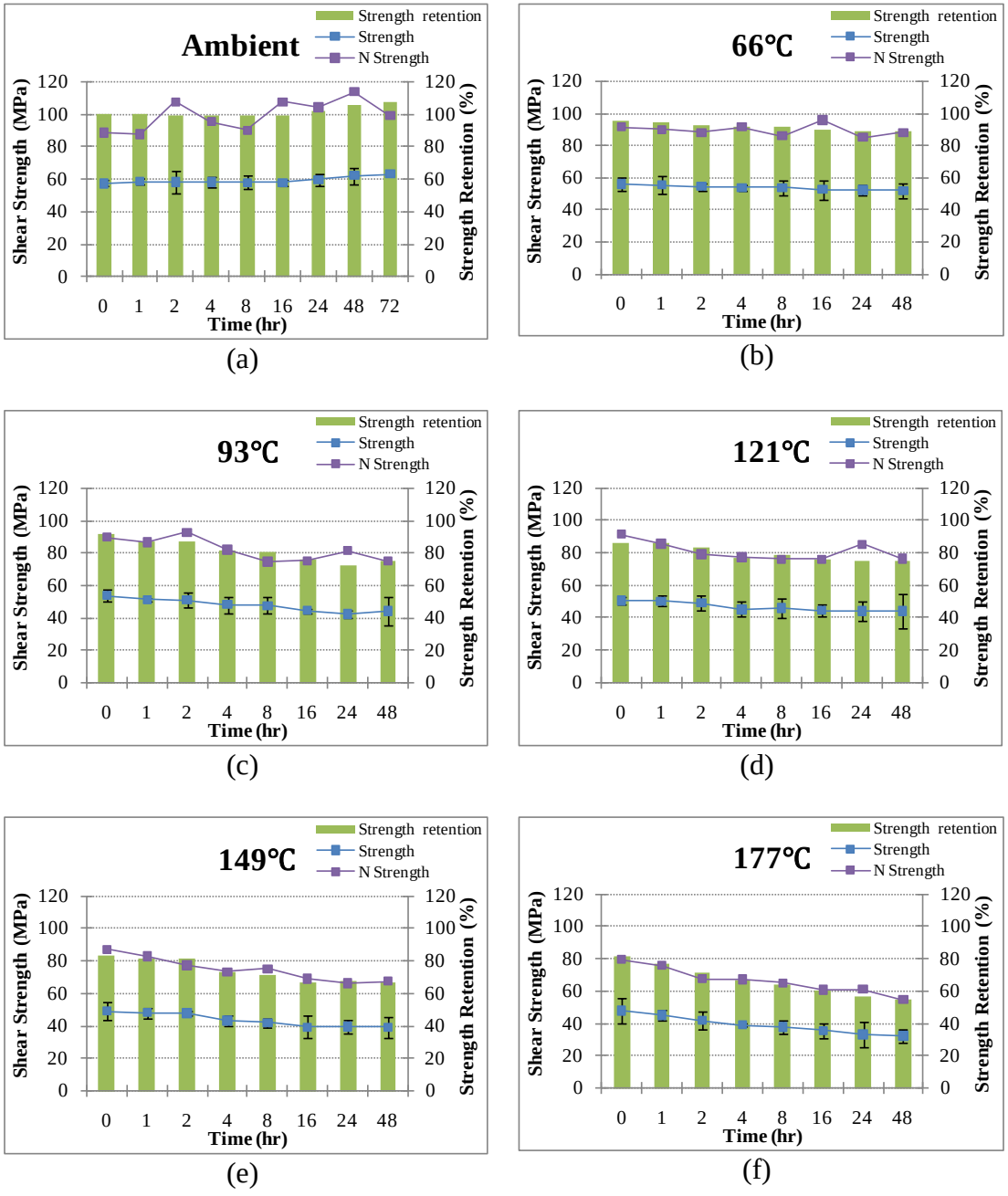

Figure 4-15: Off-axis shear strengths and normalized off-axis shear strengths of carbon/epoxy composite materials as a function of time at fixed temperatures, (a) ambient (b) 66℃ (c) 93℃ (d) 121℃ (e) 149℃ (f) 177℃ (g) 204℃ (h) 232℃ (i) 260℃

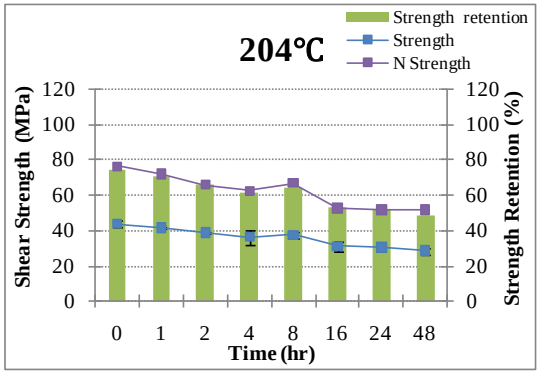

(g)

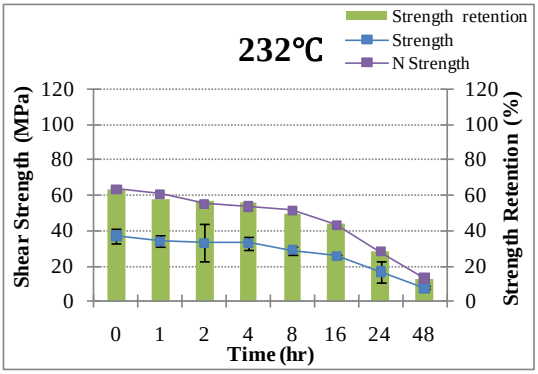

(h)

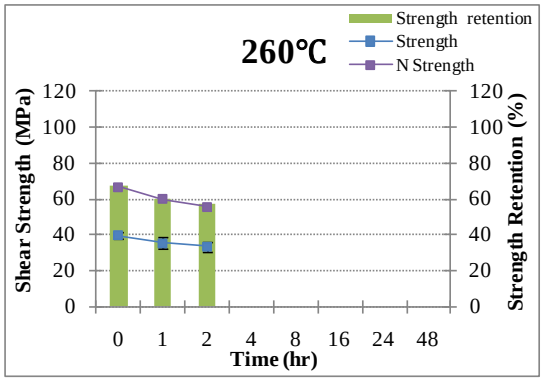

(i)

Figure 4-15: Continued

Table 4-10 lists the data for off-axis shear modulus of carbon/epoxy composite materials exposed to various temperatures from ambient temperature to 260°C . Unlike the values of the off-axis shear strength, the data of the modulus retention were relatively higher in all ageing conditions. The levels of the decreases of the off-axis shear modulus exposed to 66, 93, 121, 149, 177, 204, and 232°C from 1 hr to 72 hrs in ageing time were 5.63, 12.7, 9.14, 6.77, 5.04, 18.62, and 45.96%, respectively. These values are very low compared to the decrease of the off-axis shear strengths. This means that distortion caused by heat expansion and contraction of the test specimens did largely not affect the decrease of the shear modulus within ranges for measuring shear chord modulus. Figure 4-16 shows off-axis shear modulus of carbon/epoxy composite materials as a function of time at fixed temperatures.

Table 4-10: Data for off-axis shear Modulus (GPa) of carbon/epoxy composite materials after exposure to various temperatures

Exposure Temperature	Time (hr)	Thickness (mm)	Modulus (GPa)	S.D (GPa)	Normalized Modulus (GPa)	Modulus Retention (%)
Ambient (23℃)	0	2.98	6.78	0.10	10.47	100.00
	1	2.89	6.76	0.14	10.13	99.71
	2	3.56	6.88	0.38	12.70	101.47
	4	3.16	6.81	0.32	11.16	100.44
	8	3.00	6.80	0.27	10.56	100.25
	16	3.58	6.59	0.46	12.22	97.10
	24	3.37	6.71	0.18	11.72	98.92
	48	3.53	6.92	0.16	12.64	101.97
	72	3.02	7.25	0.47	11.35	106.83
66℃	1	3.13	6.45	0.20	10.48	95.14
	2	3.13	6.29	0.27	10.18	92.68
	4	3.11	6.25	0.44	10.09	92.19
	8	3.27	6.14	0.29	10.41	90.57
	16	3.07	6.14	0.57	9.77	90.47
	24	3.49	6.15	0.27	11.13	90.71
	48	3.13	6.11	0.23	9.92	90.07
	72	3.25	6.09	0.27	10.27	89.78
93℃	1	3.20	6.33	0.76	10.48	93.27
	2	3.24	5.75	0.29	9.66	84.82
	4	3.48	5.63	0.79	10.15	82.95
	8	3.27	5.62	0.48	9.53	82.85
	16	3.01	5.46	0.38	8.51	80.44
	24	3.24	5.32	0.28	8.93	78.38
	48	3.68	5.24	0.38	10.00	77.30
	72	3.26	5.21	0.31	8.79	76.76
121℃	1	3.48	5.54	0.58	9.99	81.72
	2	3.26	5.40	0.56	9.14	79.66
	4	3.09	5.54	0.34	8.86	81.62
	8	3.29	5.63	0.58	9.60	83.05
	16	3.17	5.64	0.41	9.27	83.19
	24	3.27	5.58	0.14	9.47	82.31
	48	3.70	5.31	0.53	10.18	78.23
	72	3.32	5.04	0.23	8.66	74.25
149℃	1	3.40	5.41	0.96	9.54	79.80
	2	3.31	5.40	0.95	9.27	79.61
	4	3.09	5.41	0.73	8.66	79.75
	8	3.25	5.12	0.46	8.62	75.43
	16	3.42	5.09	0.72	9.03	75.04
	24	3.36	5.01	0.57	8.74	73.91
	48	3.20	5.02	0.29	8.32	74.00
	72	3.31	5.05	0.07	8.65	74.40

Table 4-10: Continued

Exposure Temperature	Time (hr)	Thickness (mm)	Modulus (GPa)	S.D (GPa)	Normalized Modulus (Gpa)	Modulus Retention (%)
177℃	1	3.20	5.23	0.53	8.66	77.10
	2	3.23	5.19	0.25	8.68	76.46
	4	3.11	5.23	0.19	8.41	77.05
	8	3.30	5.21	0.08	8.91	76.76
	16	3.32	5.28	0.19	9.07	77.79
	24	3.27	5.19	0.62	8.80	76.56
	48	3.53	5.11	0.84	9.34	75.33
	72	3.25	4.97	0.23	8.37	73.22
204℃	1	3.35	6.14	0.12	10.65	90.52
	2	3.31	5.88	0.31	10.09	86.63
	4	3.26	5.24	0.62	8.85	77.30
	8	3.31	5.07	0.33	8.69	74.69
	16	3.42	5.06	0.51	8.96	74.55
	24	3.23	5.02	0.18	8.40	73.96
	48	3.26	5.02	0.19	8.49	74.05
	72	3.48	5.00	0.50	9.00	73.66
232℃	1	3.28	5.61	0.43	9.53	82.75
	2	3.42	5.43	0.26	9.62	80.10
	4	3.19	5.25	0.73	8.67	77.40
	8	3.12	5.21	0.18	8.42	76.81
	16	3.40	5.13	0.27	9.05	75.63
	24	3.22	5.12	0.49	8.55	75.53
	48	3.22	3.80	0.26	6.33	56.02
	72	3.27	3.03	0.28	5.13	44.72
260℃	1	3.24	5.63	0.11	9.44	82.95
	2	3.25	5.56	0.33	9.38	82.01
	4	3.20	5.55	0.50	9.21	81.87

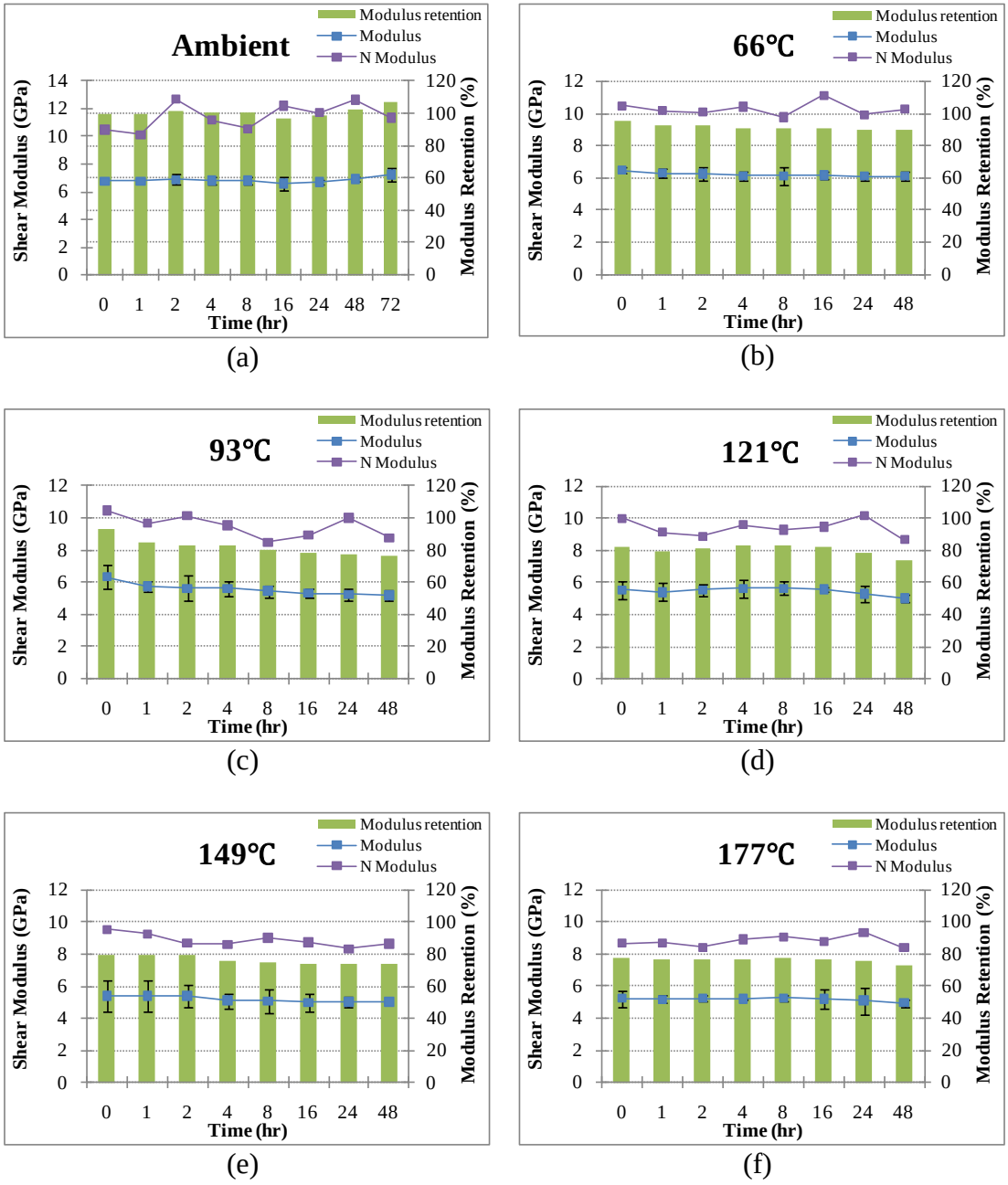

Figure 4-16: Off-axis shear modulus and normalized off-axis shear modulus of carbon/epoxy composite materials as a function of time at fixed temperatures, (a) ambient (b) 66°C (c) 93°C (d) 121°C (e) 149°C (f) 177°C (g) 204°C (h) 232°C (i) 260°C

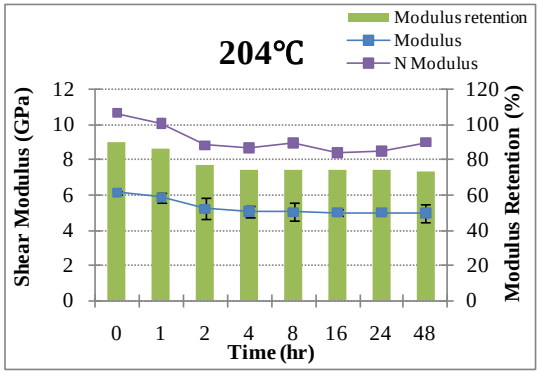

(g)

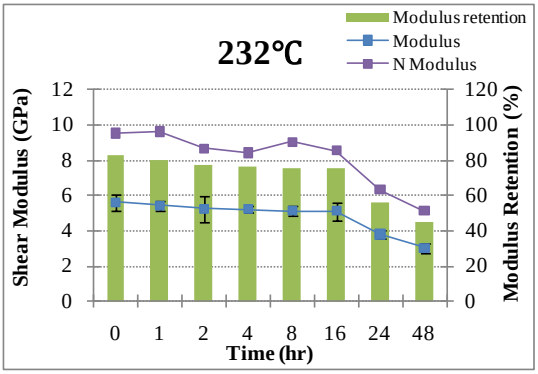

(h)

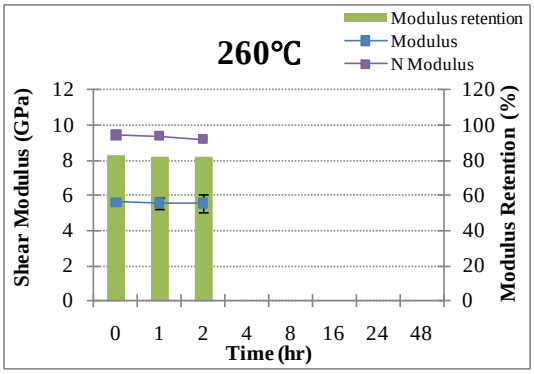

(i)

Figure 4-16: Continued

The time-dependent functions of off-axis shear strength and modulus retention obtained by polynomial curve fittings are represented in Table 4-11and Table 4-12. Compared to the data of the curve fitting regarding tensile strength and modulus, R-squared values were relatively higher because the residual post-cure effect did not enable the test specimens to enhance the initial shear properties. Especially, the functions showed nearly linear tendency in high temperatures such as 232 and 260℃ and R-squared values in off-axis shear strength were higher than values of modulus.

Table 4-11: Time-dependent functions of off-axis shear strength retention (%) obtained by polynomial curve fitting

Temperature(℃)	a	b	c	d	R^2
Ambient (23)			0.1257	98.966	0.9072
66	-6.E-05	0.008	-0.3787	94.915	0.9301
93		0.0078	-0.7584	90.045	0.9515
121	-2.E-04	0.0217	-0.9054	86.477	0.8911
149	-2.E-04	0.0321	-1.3697	84.936	0.9717
177	-2.E-04	0.0333	-1.5098	79.635	0.9456
204	-2.E-04	0.025	-1.2471	73.358	0.9178
232			-0.668	60.828	0.992
260			-3.2428	69.058	0.8489

Time-dependent function : $Y(t) = \frac{\sigma_t}{\sigma_i} \times 100 = at^3 + bt^2 + ct + d$

Table 4-12: Time-dependent functions of off-axis shear modulus retention (%) obtained by polynomial curve fitting

Temperature(℃)	a	b	c	d	R^2
Ambient (23)	-5.E-05	0.0081	-0.2603	100.82	0.8922
66	-7.E-05	0.0095	-0.3575	93.964	0.7743
93	-2.E-04	0.0216	-0.9109	89.259	0.7912
121	9.E-05	-0.0125	0.3405	80.445	0.9461
149	-9.E-05	0.0133	-0.5555	80.588	0.9234
177		-0.001	0.0226	76.882	0.9213
204	-3.E-04	0.0409	-1.4835	87.768	0.7666
232		-0.0026	-0.3337	81.123	0.9696
260			-0.3194	83.022	0.6926

Time-dependent function : $Y(t) = \frac{\sigma_t}{\sigma_i} \times 100 = at^3 + bt^2 + ct + d$

4.2.3.2 Temperature Dependence

Figure 4-17 represents the off-axis shear strength of the test specimens of the carbon/epoxy composite as a function of temperature at fixed time. As shown in Figure 4-17, the slopes which mean the drop of the off-axis shear strength were very steep as the ageing time is going up. The rate of decrease of the off-axis shear strength at each fixed times (1, 2, 4, 8, 16, 24, 48, 72 hrs), as the exposure time is increased, was 32.6, 39.53, 42.8, 43.2, 49.97, 56.78, 72.85 and 87.84%, respectively. It is apparent the distortion of the specimens for testing caused linear drop in off-axis shear strength and offset enhancement of the mechanical property due to residual post-cure effect. Accordingly, off-shear strength must be considered as an important design factor in many applications having high temperature variation.

Contrary to off-axis shear strength as shown in Figure 4-18 , off-axis shear modulus showed relatively a tendency to approach asymptotic levels except severe conditions (exposure temperature: more than 230℃, ageing time: more than 48 hrs). The level of reduction in off-axis shear modulus at fixed times (1, 2, 4, 8, 16, 24, 48, 72 hrs) from ambient temperature to 260℃ was 16.8, 19.17, 18.49, 23.38, 22.16, 23.65, 45.06, and 58.14%, respectively. Relatively, these values were very low than in the case of the off-axis shear strength.

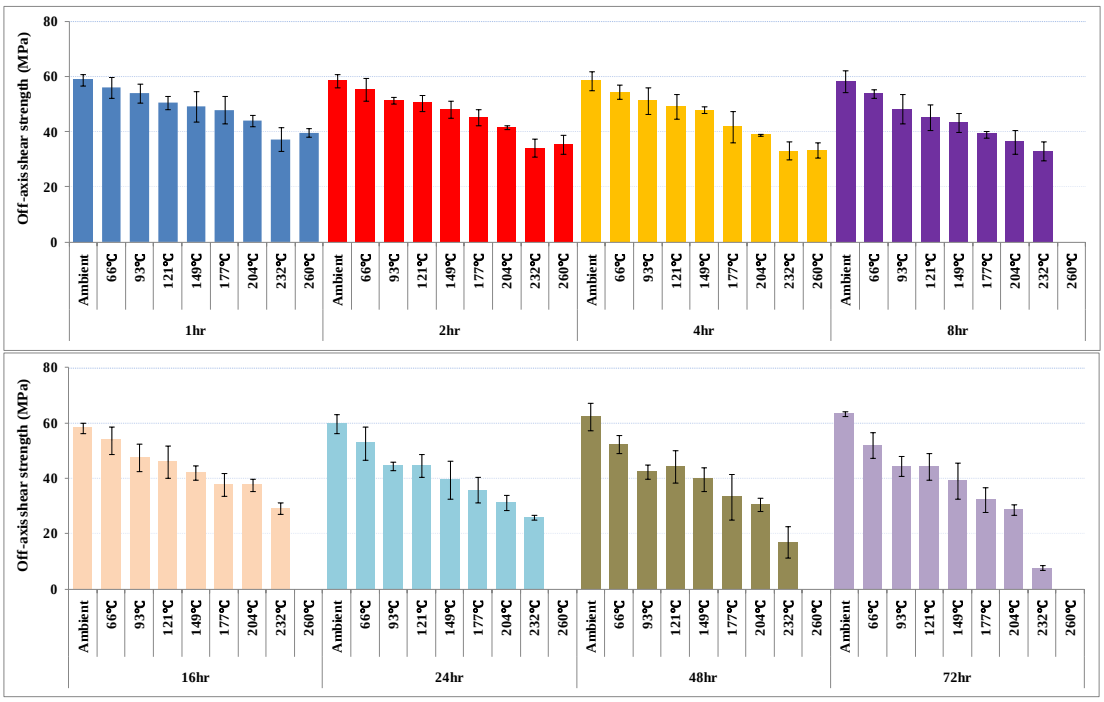

Figure 4-17: Off-axis shear strength of carbon/epoxy composite materials as a function of temperature at fixed periods of exposure

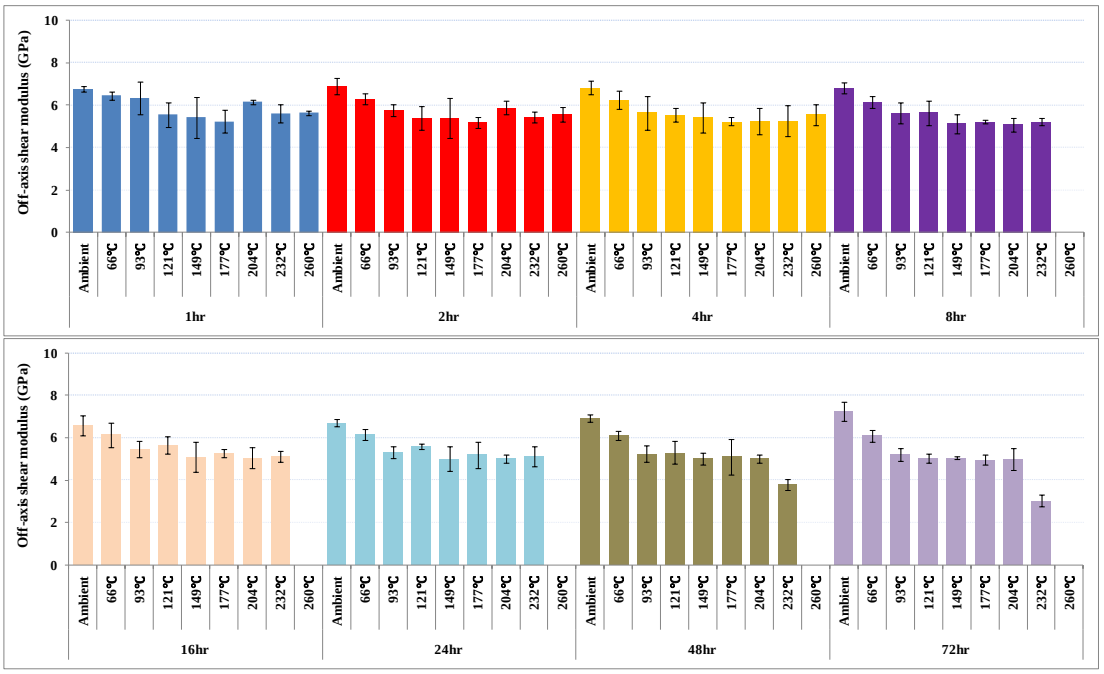

Figure 4-18: Off-axis shear modulus of carbon/epoxy composite materials as a function of temperature at fixed periods of exposure

Table 4-13 and Table 4-14 list the temperature-dependent functions of off-axis shear strength and modulus retention using polynomial curve fittings. Compared to the time-dependent functions, temperature-dependent functions showed more linear relations and R-squared values were superior to the results of the time-dependent functions. Especially, temperature-dependent functions on the off-axis strengths showed strongly linear correlation between shear strengths and exposure temperatures.

Table 4-13: Temperature-dependent functions of off-axis shear strength retention (%) obtained by polynomial curve fitting

Time (hr)	a	b	c	R^2
1	-0.0002	-0.1094	102.96	0.9539
2	-0.0002	-0.1063	101.82	0.9683
4		-0.1924	105.59	0.9742
8		-0.2047	103.21	0.9918
16		-0.222	104.46	0.974
24		-0.2634	106.13	0.9824
48		-0.3211	111.17	0.9421
72		-0.3211	117.26	0.9169

Temperature-dependent function : $Y(T) = \frac{\sigma_t}{\sigma_i} \times 100 = a\mathrm{T}^2 + b\mathrm{T} + c$

Table 4-14: Temperature-dependent functions of off-axis shear modulus retention (%) obtained by polynomial curve fitting

Time (hr)	a	b	c	R^2
1	0.0007	-0.26	107.05	0.6819
2	0.0009	-0.3192	108.13	0.8454
4	0.0008	-0.3214	107.85	0.9754
8	0.0008	-0.3212	107.44	0.9703
16	0.0006	-0.2684	103.29	0.9235
24	0.0009	-0.3294	106.29	0.9161
48	0.0003	-0.2467	104.74	0.8452
72	0.0002	-0.2656	108.03	0.7948

Temperature-dependent function : $Y(T) = \frac{E_t}{E_i} \times 100 = a\mathrm{T}^2 + b\mathrm{T} + c$

4.2.3.3 Morphological Analysis

The off-axis shear tests were accomplished in accordance with the procedure of uiaxial tensile test. Test specimens were comprised of 2 layers laminate with $+45^{o}$ and -45^{o} fiber directions. Figure 4-19 shows the test coupons distorted by asymmetry in process of thermal expansion and contraction by heat transfer and dissipation when test specimens were cooled in the atmospheric temperature after taken out from the oven. As can be seen in Figure 4-19, distortion of the test specimens by asymmetry and char formation by thermal oxidation resulted in the severe deterioration in terms of off-axial shear strength and modulus. The angles of the distortion which caused internal crack when test coupon was gripped were higher as the exposure temperatures were going up.

Figure 4-20 shows test specimens fractured after uniaxial tensile test of a $\pm 45^{o}$ laminate exposed to elevated temperatures at the ageing time, 72 hrs. All test specimens were fractured parallel to the fiber directions. In the lower exposure temperatures such as ambient temperature, 66, 93, and 121℃, crack was found around the fractured cross section and the surface between 2 layers was well kept the shape wrapping the fibers without thermal degradation of the resin. However, the delamination between 2 layers, thermal oxidations and char formation in the internal and outer surfaces, additional cracks except the cross section were discovered in the test specimens exposed to high temperatures (204, 232, and 260℃) as depicted in Figure 4-20.

Figure 4-19: Test specimens distorted by asymmetry in process of thermal expansion and contraction after exposure to 260℃ for 8 hrs

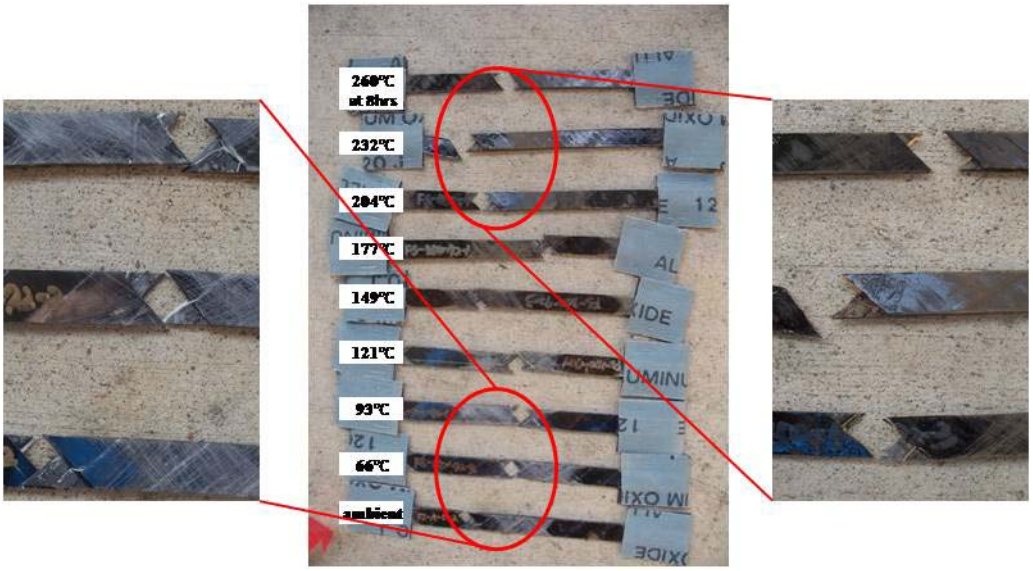

Figure 4-20: Test specimens fractured after uniaxial tensile test of a ± 45^{o} laminate exposed to elevated temperatures at an ageing time of 72 hrs

4.2.3.4 Strain Effect

Figure 4-21 shows tensile stress-ultimate failure strain curve by uniaxial tensile test of a ± 45^{o} laminate exposed to various exposure temperatures at the fixed time, 72 hrs. Like tensile test, off-axis shear modulus was calculated from slop between off-axis shear stress and strain ranging from 0.1% to 0.3% before extensometer is taken off. However, off-axis shear strain was rapidly reached to 0.3% compared to tensile strain because uniaxial tensile test of a ± 45^{o} laminate is matrix-dominant. Ultimate failure strains in off-axis shear test were lower than those of the tensile test and all test specimens were fractured before strains were reached 1.5% strain. As the exposure temperatures were going up, ultimate failure strain and off-axis shear strength were getting lower although the residual post-curing apparently happened in process of exposure to temperatures. In addition, the reason why the slopes of the off-axis shear stress versus the ultimate shear failure strains were not perfectly linear is that a ± 45^{o} laminates are ductile due to matrix-dominant characteristics. As can be seen in Figure 4-21, ductility is getting higher as the exposure temperatures are increased.

Figure 4-22 shows the off-axis shear strength and off-axis shear modulus as a function of ultimate failure strains (%). If looking at the comparison of two data related to shear strength and shear modulus, it should be pointed out that off-axis shear strengths were more strain-dependent with ultimate failure strains than in the case of off-axis shear modulus. All test coupons were fractured between 0.75% and 1.6 % in strain while off-axis shear strength and modulus were within 35 ~ 65 Mpa and 5 ~ 7 GPa, respectively. Off-axis shear strengths were widely distributed compared to off-axis shear modulus as shown in Figure 4-22 (a). As shown in Figure 4-23, in the case off-

axis shear strength and modulus were changed to logarithmic scale, the more linear data were obtained.

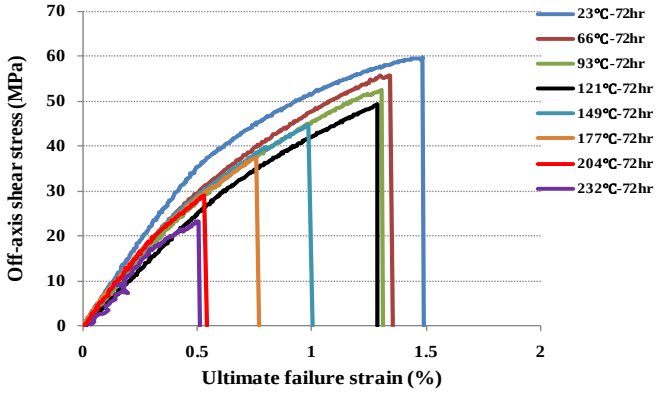

Figure 4-21: Off-axis shear stress-ultimate failure strain curves from specimens exposed to various ageing temperatures at the fixed period of 72 hrs

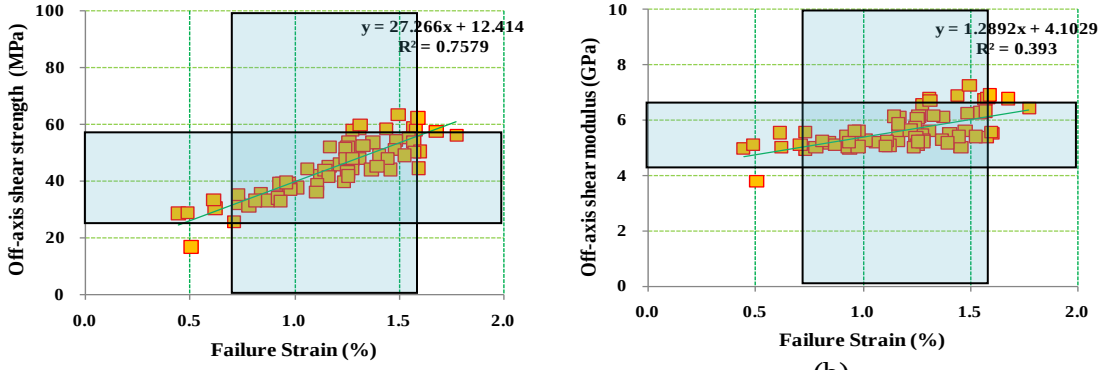

(a) (b)

Figure 4-22: (a) Off-axis shear strength and (b) Off-axis shear modulus as a function of ultimate failure strains (%). Error bars indicate standard deviation

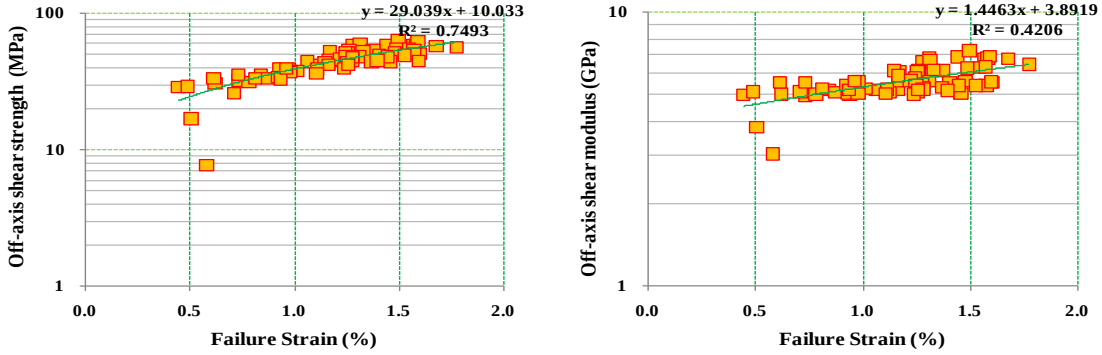

(a) (b)

Figure 4-23: (a) Off-axis shear strength and (b) Off-axis shear modulus as a function of ultimate failure strains (%) using a logarithmic scale

4.2.3.5 Correlation to Tensile Test Results

Correlations between tensile and shear results are very important to estimate the other properties from the values obtained by useful experimental test.

First, in case an off-axis shear stress applied to a representative volume element for finding off-shear modulus of a unidirectional composite, off-shear modulus can be calculated by following equation

$$G''_{12} = G_{\mathrm{m}}\left[\frac{G_{\mathrm{f}12}(1+V_{\mathrm{f}}) + G_{\mathrm{m}}V_{\mathrm{m}}}{G_{\mathrm{f}12}V_{\mathrm{m}} + G_{\mathrm{m}}(1+V_{\mathrm{f}})}\right] \tag{4.18}$$

$$G'''_{12} = \frac{G_m G_f}{G_m V_f + G_f V_m} \tag{4.19}$$

Where G''_{12} = shear modulus for cylinder shaped composites

G'''_{12} = shear modulus for rectangular shaped composites

G_m = nominal epoxy modulus (1.308 GPa)

G_f = nominal carbon fiber modulus (22 GPa)

In addition, the data of fiber volume fraction using Equation 4.11 were used to calculate the off-axis shear modulus. As shown in Table 4-15, calculated shear modulus had good correlation in the ranges which the tensile properties were enhanced by the residual post-cure effect.

Table 4-15: Comparison of experimental shear modulus and calculated shear modulus- G'_{12}: experimental off-axis shear modulus (G''_{12} = shear modulus for cylinder shaped composites, G'''_{12} = shear modulus for rectangular shaped composites)

	Ambient (23℃)						66℃					
Time (hr)	V_f	G'_{12} (GPa)	G''_{12} (GPa)	error (%)	G'''_{12} (GPa)	error (%)	V_f	G'_{12} (GPa)	G''_{12} (GPa)	error (%)	G'''_{12} (GPa)	error (%)
0	0.37	6.78	5.90	13.0	4.93	27.3						
1	0.36	6.76	5.79	14.4	4.86	28.2	0.34	6.45	5.68	12.0	4.79	25.8
2	0.38	6.88	5.99	12.9	4.99	27.5	0.35	6.29	5.71	9.1	4.81	23.5
4	0.38	6.81	6.04	11.4	5.02	26.3	0.40	6.25	6.20	0.9	5.12	18.1
8	0.40	6.80	6.19	9.0	5.12	24.8	0.42	6.14	6.42	-4.6	5.27	14.2
16	0.44	6.59	6.63	-0.7	5.41	17.8	0.46	6.14	6.90	-12.5	5.60	8.8
24	0.43	6.71	6.54	2.5	5.35	20.2	0.40	6.15	6.19	-0.6	5.12	16.8
48	0.46	6.92	6.81	1.6	5.53	20.0	0.34	6.11	5.67	7.3	4.78	21.8
72	0.47	7.25	7.00	3.4	5.66	21.8	0.36	6.09	5.83	4.3	4.88	19.8
	93℃						121℃					
Time (hr)	V_f	G'12 (GPa)	G"12 (GPa)	error (%)	G'"12 (GPa)	error (%)	V_f	G'12 (GPa)	G"12 (GPa)	error (%)	G'"12 (GPa)	error (%)
1	0.38	6.33	6.02	4.8	5.01	20.8	0.36	5.54	5.86	-5.8	4.91	11.5
2	0.39	5.75	6.15	-7.0	5.10	11.4	0.39	5.40	6.11	-13.1	5.07	6.2
4	0.42	5.63	6.42	-14.1	5.27	6.3	0.38	5.54	6.02	-8.8	5.01	9.5
8	0.42	5.62	6.46	-14.9	5.30	5.7	0.32	5.63	5.52	2.1	4.68	16.9
16	0.44	5.46	6.68	-22.4	5.44	0.2	0.38	5.64	6.07	-7.5	5.04	10.7
24	0.45	5.32	6.74	-26.8	5.49	-3.2	0.36	5.58	5.83	-4.5	4.89	12.5
48	0.42	5.24	6.41	-22.3	5.27	-0.4	0.35	5.31	5.77	-8.8	4.85	8.6
72	0.38	5.21	5.97	-14.7	4.98	4.4	0.32	5.04	5.46	-8.5	4.65	7.7
	149℃						177℃					
Time (hr)	V_f	G'12 (GPa)	G"12 (GPa)	error (%)	G'"12 (GPa)	error (%)	V_f	G'12 (GPa)	G"12 (GPa)	error (%)	G'"12 (GPa)	error (%)
1	0.37	5.41	5.89	-8.8	4.92	9.1	0.39	5.23	6.08	-16.2	5.05	3.5
2	0.37	5.40	5.90	-9.3	4.93	8.7	0.43	5.19	6.52	-25.8	5.34	-3.0
4	0.37	5.41	5.95	-10.0	4.96	8.3	0.37	5.23	5.93	-13.4	4.95	5.3
8	0.37	5.12	5.95	-16.2	4.96	3.0	0.35	5.21	5.74	-10.2	4.82	7.3
16	0.35	5.09	5.78	-13.6	4.85	4.6	0.32	5.28	5.50	-4.3	4.67	11.4
24	0.36	5.01	5.86	-16.9	4.90	2.2	0.35	5.19	5.74	-10.5	4.83	7.1
48	0.35	5.02	5.79	-15.3	4.86	3.3	0.34	5.11	5.65	-10.6	4.77	6.6
72	0.30	5.05	5.35	-6.1	4.58	9.3	0.35	4.97	5.70	-14.8	4.80	3.3

Table 4-15: Continued

	204℃						232℃					
Time (hr)	V_f	G'12 (GPa)	G"12 (GPa)	error (%)	G'"12 (GPa)	error (%)	V_f	G'12 (GPa)	G"12 (GPa)	error (%)	G'"12 (GPa)	error (%)
1	0.37	6.14	5.94	3.2	4.96	19.3	0.40	5.61	6.24	-11.2	5.15	8.2
2	0.36	5.88	5.80	1.3	4.86	17.2	0.41	5.43	6.36	-17.0	5.23	3.7
4	0.37	5.24	5.89	-12.4	4.93	6.0	0.37	5.25	5.89	-12.3	4.93	6.2
8	0.39	5.07	6.11	-20.6	5.07	0.0	0.38	5.21	6.04	-15.9	5.02	3.6
16	0.37	5.06	5.93	-17.2	4.95	2.1	0.35	5.13	5.70	-11.1	4.80	6.4
24	0.36	5.02	5.85	-16.6	4.90	2.4	0.32	5.12	5.52	-7.7	4.68	8.6
48	0.37	5.02	5.88	-17.1	4.92	2.1	0.33	3.80	5.58	-46.9	4.73	-24.4
72	0.37	5.00	5.95	-19.1	4.96	0.7	0.28	3.03	5.16	-70.2	4.46	-47.0

	260℃					
Time (hr)	V_f	G'12 (GPa)	G"12 (GPa)	error (%)	G'"12 (GPa)	error (%)
1	0.34	5.63	5.61	0.2	4.75	15.7
2	0.36	5.56	5.88	-5.7	4.92	11.6
4	0.37	5.55	5.88	-6.0	4.92	11.4
8	0.32		5.48		4.66	
16	0.23		4.78		4.22	
24	0.23		4.80		4.24	
48	0.13		4.11		3.82	
72	0.11		3.98		3.74	

Figure 4-24 shows the data distribution of the tensile properties and off-axis shear properties. The data of the tensile strength were distributed between 500 MPa and 790 MPa and off-axis shear strengths were widely distributed due to offset of residual post-cure effect. Meanwhile, the values of tensile and off-axis shear modulus were concentrated between 42 GPa and 75 GPa and between 5 GPa and 7 GPa, respectively. If changing the tensile properties into logarithmic scale because the values of the tensile property have more scale compared to off-axis shear property, more linear correlation can be obtained as shown in Figure 4-25.

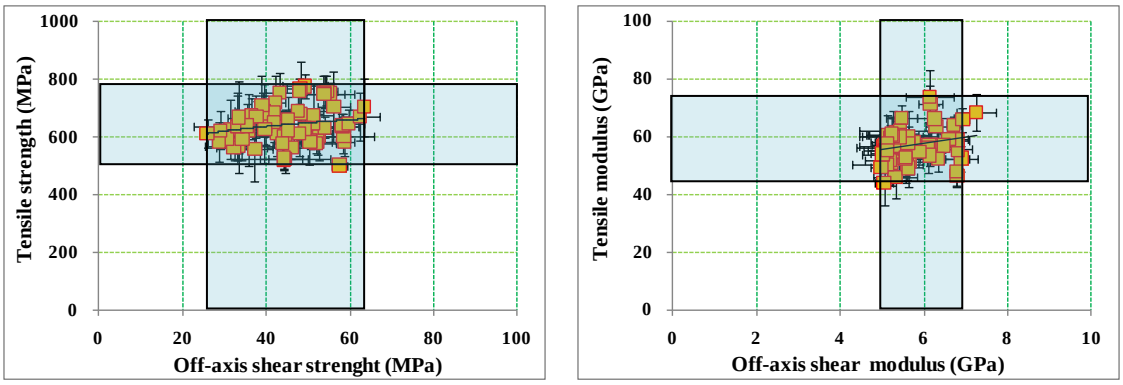

(a) (b)

Figure 4-24: Data distribution of (a) tensile strength versus off-axis shear strength and (b) tensile modulus versus off-axis shear modulus

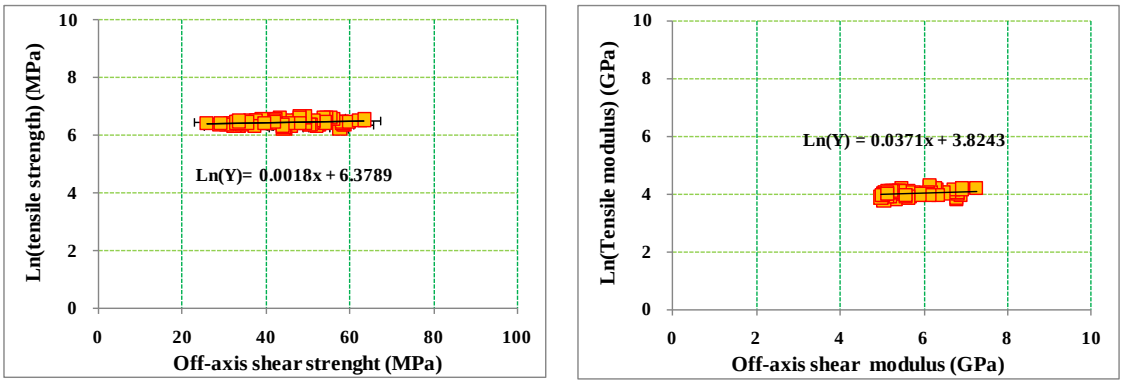

(a) (b)

Figure 4-25: Data distribution of (a) tensile strength versus off-axis shear strength and (b) tensile modulus versus off-axis shear modulus using a logarithmic scale

4.3 Flexural Testing

4.3.1 Introduction

Flexural properties provide important factor of composite materials as related to the response of naval vessels operating in the diverse environments. However, it is difficult to estimate values that can be directly utilized in design because flexural testing subjects the test specimens to a mixed state of stress and a stress gradient. The flexural characteristics and their change as a function of time and temperature are important and offer the crucial data to decide the deteriorative level after exposure to high temperatures and fire.

Flexure tests are very useful for characterizing mechanical properties of layered composite materials due to simplicity of the test method for determining characteristics where relative rather than absolute data are needed. Therefore, flexural data are used to derive the other mechanical properties because of simple test method. In case composite materials are bended since flexural loading in materials imposes both tensile and compressive stresses, these tests must be considered for determining the design data. As mentioned, flexural properties are a combination of the tensile and compressive properties of the composite materials[52] .

4.3.2 Data Reduction

For test specimens in 3 point bending comprised of simple beam supported at two points and loaded at midpoint, the flexural strength and modulus are determined through a three-point flexural test following method described in ASTM D790. A

support span-to-depth ratio of 16:1 was used for 2 layers laminate. The test specimens is deflected until rupture occurs in the outer surface of the test specimen or until a maximum strain of 5.0% is reached, whichever occurs first.

The flexural strength is obtained by following equation

$$\sigma_f = \frac{3PL}{2bh^2} \tag{4.20}$$

where:

σ_f = the stress in the outer fibers at midpoint, MPa

P = the load at a given point in the load-deflection curve, N

L = the support span, mm

b = the width of the specimen tested, mm

h = the thickness of the specimen tested, mm

Flexural strain is defined as nominal fractional change in the length of an element of the outer surface of the test specimen at midspan, where the maximum stress occurs. It may be calculated for any deflection using Equation 4.21.

$$\varepsilon_f = 6Dh / L^2 \tag{4.21}$$

where:

ε_f = strain in the outer surface, mm/mm

D = maximum deflection of the center of the beam, mm

Chord modulus may be calculated from two discrete points on the load deflection curve. The chord modulus is calculated using the following equation:

$$E_f = (\sigma_{f2} - \sigma_{f1}) / (\varepsilon_{f2} - \varepsilon_{f1}) \quad (4.22)$$

where:

E_f = chord modulus, GPa

4.3.3 Analyses and Results

4.3.3.1 Time Dependence

Flexural properties with regard to strength, modulus, strain and load were determined at room temperature after the test specimens had been exposed to a controlled temperature for times up to 72 hrs. A flat rectangular specimen was simply supported close to its ends and centrally loaded in three point bending. Each data were obtained by average value determined from five flexural tests. Flexural test is often utilized to characterize mechanical properties of layered laminate because they offer a simple means of determining bending response. However, Flexural test can be resulted in various failure modes as follows[50],

- Tensile fracture of fibers
- Tensile fracture of outer surface
- Compression fracture of outer surface
- Tensile fracture with interlaminar shear
- Compression fracture with interlaminar shear
- Interlaminar shear

Data for Flexural strength (MPa) of carbon/epoxy composite materials after exposure to various temperatures are tabulated in Table 4-16 and Flexural strengths as a function of time at fixed temperatures are depicted in Figure 4-26. The flexural strength retentions did not largely enhanced by residual post-cure effect compared to the result of tensile test. The maximum strength retention caused by post-curing was 117.43% in condition of 177℃ exposure temperature for 72hr. It should be noted that this value is much less than the maximum strength retention (154.42%) of tensile test. At lower exposure temperatures, the reason why the flexural strength data show fluctuation is that post-curing effects did not largely contribute to enhancement of the property. In other words, as mentioned previously, defects in process of hand wet layup fabrication had probably test specimens fractured in various failure modes. As ageing time was increased, the strength drops in ranges of ambient, 66, 93, 121, 149, 177, and 204℃ were only 5.23, 6.53, 3.19, 7.37, 11.54 and 13.26%, respectively. As strength enhancements were not highly affected by residual post-cure effect, strength reductions were largely not influenced by thermal degradation in low exposure temperatures. Big drop of the flexural strength took place in conditions of 232℃ exposure temperature for 72 hrs and 260℃ exposure temperature for more than 8 hrs. Since thermal oxidation caused catastrophic delamination between 2 layers in high exposure temperatures, the rate of drop of the flexural strength was higher than that of the tensile strength.

Table 4-16: Data for flexural strength (MPa) of carbon/epoxy composite materials after exposure to various temperatures (N denotes normalized)

Exposure Temperature	Time (hr)	Thickness (mm)	Width (mm)	load (KN)	Strength (MPa)	S.D (MPa)	N strength (MPa)	Strength retention(%)
Ambient (23℃)	0	2.83	12.88	0.74	513.13	36.64	753.48	100
	1	2.77	12.73	0.74	543.11	16.70	779.48	105.84
	2	2.73	12.84	0.78	565.72	15.28	799.48	110.25
	4	2.79	12.67	0.72	527.26	30.88	762.89	102.75
	8	2.84	12.73	0.75	532.05	76.51	782.91	103.69
	16	2.80	12.86	0.73	527.11	10.95	764.03	102.72
	24	2.78	12.71	0.70	515.97	75.90	742.14	100.55
	48	2.63	12.80	0.68	523.90	26.16	714.59	102.10
	72	2.88	12.49	0.73	514.70	59.23	768.72	100.31
66℃	1	3.00	12.80	0.81	525.82	34.01	816.79	102.47
	2	3.07	12.49	0.82	520.14	9.37	826.02	101.37
	4	2.78	12.70	0.77	558.61	73.47	804.64	108.86
	8	2.84	12.85	0.78	544.49	47.94	801.21	106.11
	16	2.56	12.71	0.64	523..72	55.05	693.32	102.06
	24	2.90	12.82	0.75	543.15	81.71	815.58	105.85
	48	2.82	12.75	0.70	495.65	63.63	724.73	96.59
	72	3.03	12.64	0.80	511.71	66.01	803.36	99.72
93℃	1	2.97	12.67	0.79	512.19	69.29	788.20	99.82
	2	2.67	12.74	0.68	540.10	24.67	747.88	105.26
	4	3.07	12.61	0.84	512.58	49.98	814.81	99.89
	8	3.08	12.73	0.79	483.48	55.38	772.19	94.22
	16	2.98	12.81	0.81	518.38	30.03	799.05	101.02
	24	3.13	12.71	0.85	495.93	109.24	804.80	96.65
	48	2.94	12.64	0.82	540.55	21.71	822.31	105.34
	72	2.91	12.84	0.84	545.66	41.23	822.03	106.34
121℃	1	2.69	12.56	0.70	535.95	30.11	747.69	104.45
	2	2.80	12.69	0.77	554.82	36.79	805.50	108.12
	4	2.87	12.86	0.78	529.80	44.94	787.29	103.25
	8	2.91	12.55	0.78	523.24	19.17	789.61	101.97
	16	2.66	12.87	0.68	543.61	69.20	748.52	105.94
	24	2.94	12.72	0.85	555.62	26.81	846.38	108.28
	48	3.13	12.74	0.82	523.16	70.08	848.43	101.95
	72	2.67	12.57	0.70	553.06	28.91	765.11	107.78
149℃	1	2.82	12.70	0.69	498.76	97.21	728.25	97.20
	2	2.73	12.74	0.72	574.78	46.37	814.22	112.01
	4	2.89	12.56	0.74	505.41	15.11	756.81	98.50
	8	2.78	12.73	0.81	594.22	53.17	855.16	115.80
	16	2.67	12.91	0.74	576.04	25.62	795.41	112.26
	24	2.72	12.63	0.71	553.59	48.29	779.47	107.88
	48	2.79	12.73	0.75	542.36	73.84	784.03	105.70
	72	2.99	12.78	0.73	461.98	25.12	714.51	90.03

Table 4-16: Continued

Exposure Temperature	Time (hr)	Thickness (mm)	Width (mm)	load (KN)	Strength (MPa)	S.D (MPa)	N strength (MPa)	Strength retention(%)
177℃	1	2.87	12.77	0.79	540.21	8.04	802.62	105.28
	2	2.64	12.69	0.73	586.62	37.05	803.18	114.32
	4	3.04	12.76	0.85	529.97	85.57	834.77	103.28
	8	2.91	12.77	0.81	548.39	83.06	826.85	106.87
	16	2.80	12.99	0.75	530.45	27.08	770.25	103.37
	24	2.77	12.93	0.73	527.56	8.66	756.48	102.81
	48	2.99	12.74	0.87	549.98	42.22	852.76	107.18
	72	2.73	12.73	0.80	602.56	47.72	853.58	117.43
204℃	1	3.08	12.72	0.89	530.27	43.87	847.33	103.34
	2	2.86	12.83	0.82	562.61	39.56	833.12	109.64
	4	3.14	12.71	0.85	492.13	48.51	800.67	95.91
	8	2.75	12.88	0.71	526.03	47.50	748.98	102.51
	16	2.80	12.62	0.76	545.35	44.81	790.47	106.28
	24	2.86	12.80	0.76	526.99	63.49	782.02	102.70
	48	3.00	12.75	0.87	548.88	68.89	853.19	106.97
	72	2.89	12.66	0.88	600.62	36.85	900.15	117.05
232℃	1	2.95	12.75	0.85	549.63	38.76	839.54	107.11
	2	2.82	12.57	0.72	516.77	60.33	754.40	100.71
	4	3.02	12.79	0.85	528.36	61.34	826.76	102.97
	8	2.83	12.88	0.77	540.63	45.01	791.33	105.36
	16	2.98	12.65	0.79	538.35	37.20	831.94	104.92
	24	2.80	12.73	0.78	557.54	54.28	808.86	108.65
	48	2.95	12.55	0.73	534.48	73.29	816.26	104.16
	72	2.86	12.70	0.50	356.95	138.39	528.21	69.56
260℃	1	2.99	12.95	0.80	494.27	18.27	764.46	96.32
	2	2.76	12.90	0.73	534.28	24.92	763.35	104.12
	4	2.84	12.71	0.82	575.69	12.04	847.13	112.19
	8	2.91	12.82	0.44	295.26	66.36	444.41	57.54
	16	2.68	12.78	0.15	122.17	14.30	169.33	23.81
	24	2.86	12.63	0.15	104.44	8.99	154.49	20.35
	48	3.06	12.88	0.13	76.88	13.18	122.00	14.98
	72	3.15	12.62	0.09	51.66	20.91	84.25	10.07

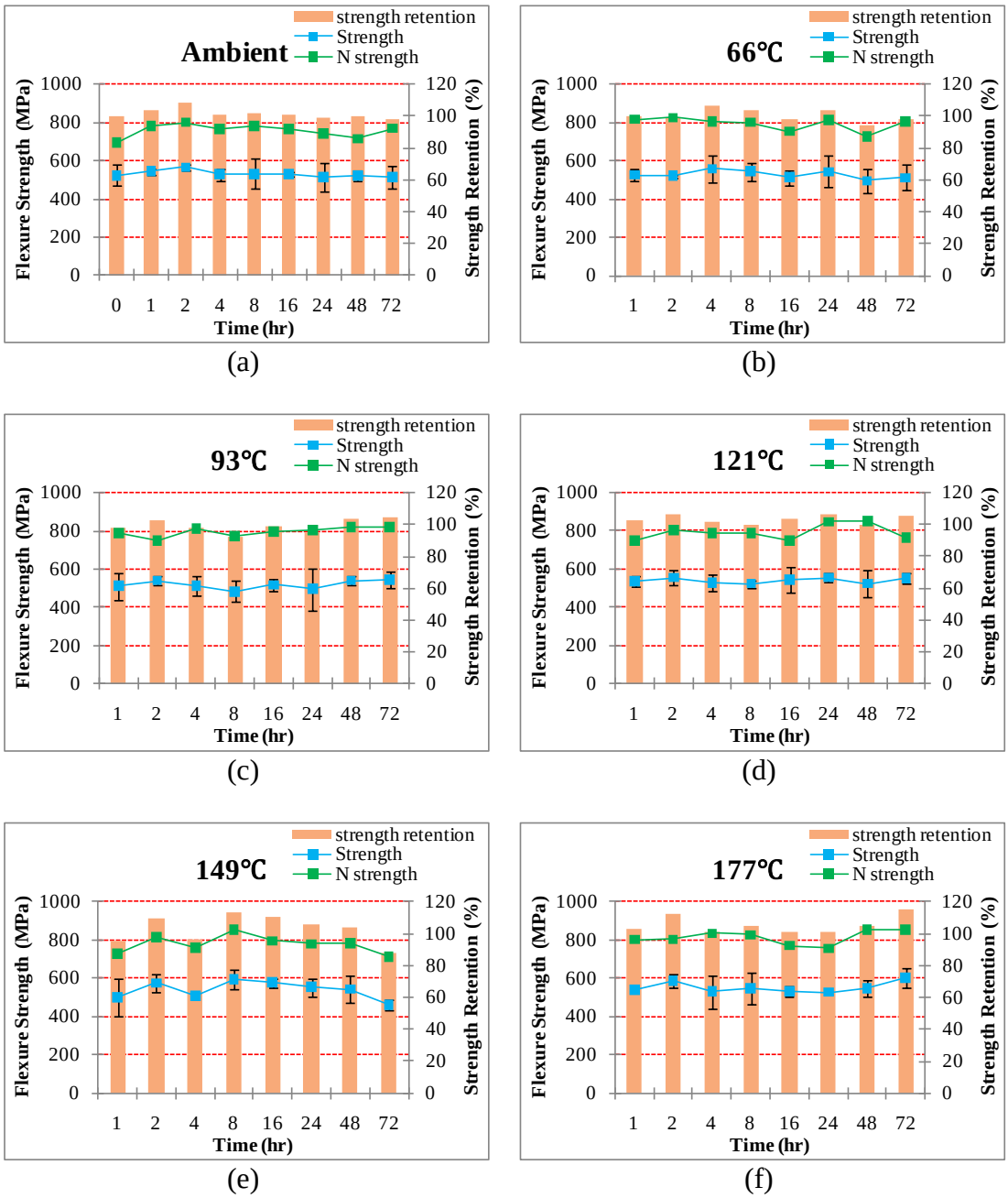

Figure 4-26: Flexural strengths and normalized flexural strengths of carbon/epoxy composite materials as a function of time at fixed temperatures of exposure, (a) ambient (b) 66℃ (c) 93℃ (d) 121℃ (e) 149℃ (f) 177℃ (g) 204℃ (h) 232℃ (i) 260℃

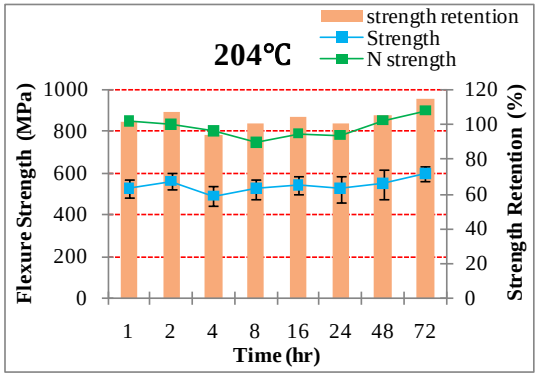

(g)

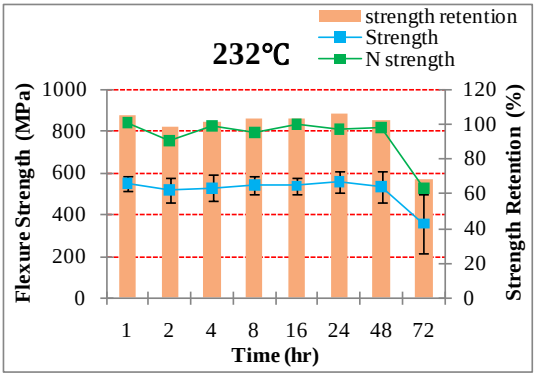

(h)

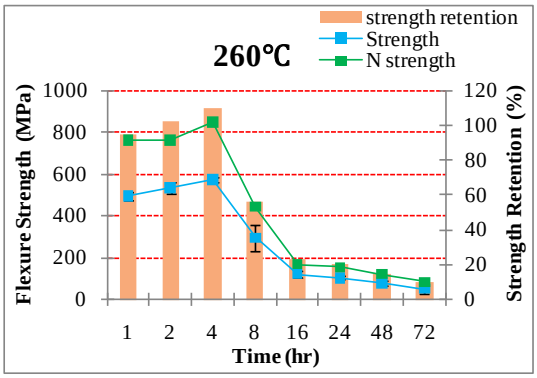

(i)

Figure 4-26: Continued

Table 4-17 shows data for flexural modulus (GPa) of carbon/epoxy composite materials after exposure to various temperatures and Figure 4-27 represents flexural modulus of carbon/epoxy composite materials as a function of time at fixed temperatures.

The chord modulus of flexural test initially showed a little increase by residual post-curing effect. The amount of increase in terms of property retention was lower than enhancement of the flexural strength. Similar to the result of flexural strength, data fluctuation existed in the low exposure temperatures and the values of the flexural modulus were rapidly reduced in high temperatures. The retention of flexural modulus in condition of the exposure temperature (260℃) for ageing time (72 hrs) was only 6.78%. It should be noted that the thickness of test specimens affected flexural modulus. As test specimens are thinner, the flexural modulus is getting higher. Since thicker test specimen means area containing more than the maximum allowable resin content which may arise from improper curing exist, the void and defect in resin-rich area resulted in the reduction of the flexural modulus due to big deflection in centrally loading.

In case the test specimens were subjected to experimental conditions of exposure temperature (260℃) for more than 8 hrs, flexural modulus can be catastrophically reduced because test specimens supported at two points and loaded at midpoint changed to char by thermal oxidation. When nose for loading passed the section of char, rapid deflection can be measured by flexural test equipment.

Table 4-17: Data for flexural modulus (GPa) of carbon/epoxy composite materials after exposure to various temperatures (N denotes normalized)

Exposure Temperature	Time (hr)	Thickness (mm)	Width (mm)	load (KN)	Modulus (GPa)	S.D (GPa)	N Modulus (GPa)	Modulus retention(%)
Ambient (23℃)	0	2.83	12.88	0.74	36.64	4.86	53.80	100.00
	1	2.77	12.73	0.74	41.70	1.08	59.84	113.79
	2	2.73	12.84	0.78	43.85	4.05	61.97	119.68
	4	2.79	12.67	0.72	39.52	5.26	57.18	107.85
	8	2.84	12.73	0.75	38.98	3.42	57.35	106.37
	16	2.80	12.86	0.73	40.52	3.36	58.73	110.57
	24	2.78	12.71	0.70	39.40	7.38	56.68	107.54
	48	2.63	12.80	0.68	40.78	1.62	55.62	111.28
	72	2.88	12.49	0.73	39.69	4.47	59.27	108.30
66℃	1	3.00	12.80	0.81	36.33	9.44	56.43	99.15
	2	3.07	12.49	0.82	36.65	0.83	58.21	100.03
	4	2.78	12.70	0.77	41.11	9.37	59.22	112.20
	8	2.84	12.85	0.78	39.88	6.30	58.69	108.84
	16	2.56	12.71	0.64	39.12	4.24	51.79	106.76
	24	2.90	12.82	0.75	36.01	5.96	54.07	98.28
	48	2.82	12.75	0.70	34.55	6.38	50.52	94.30
	72	3.03	12.64	0.80	33.29	4.91	52.26	90.85
93℃	1	2.97	12.67	0.79	35.69	7.44	54.92	97.41
	2	2.67	12.74	0.68	38.43	2.50	53.22	104.89
	4	3.07	12.61	0.84	34.13	5.58	54.26	93.16
	8	3.08	12.73	0.79	32.22	4.81	51.46	87.93
	16	2.98	12.81	0.81	31.64	4.24	48.76	86.34
	24	3.13	12.71	0.85	32.16	6.01	52.19	87.77
	48	2.94	12.64	0.82	34.50	4.54	52.49	94.16
	72	2.91	12.84	0.84	35.10	5.46	52.87	95.78
121℃	1	2.69	12.56	0.70	38.59	1.66	53.83	105.31
	2	2.80	12.69	0.77	37.99	3.57	55.16	103.69
	4	2.87	12.86	0.78	36.21	7.52	53.81	98.82
	8	2.91	12.55	0.78	37.11	4.10	56.00	101.27
	16	2.66	12.87	0.68	38.76	8.12	53.36	105.77
	24	2.94	12.72	0.85	35.70	4.07	54.39	97.44
	48	3.13	12.74	0.82	33.72	4.00	54.68	92.01
	72	2.67	12.57	0.70	34.82	2.39	48.17	95.02
149℃	1	2.82	12.70	0.69	34.65	10.32	50.60	94.57
	2	2.73	12.74	0.72	41.30	3.29	58.50	112.70
	4	2.89	12.56	0.74	34.99	4.78	52.39	95.48
	8	2.78	12.73	0.81	40.48	4.26	58.25	110.47
	16	2.67	12.91	0.74	36.52	3.86	50.43	99.67
	24	2.72	12.63	0.71	36.67	5.55	51.63	100.07
	48	2.79	12.73	0.75	35.46	3.93	51.25	96.76
	72	2.99	12.78	0.73	32.21	5.35	49.81	87.89

Table 4-17: Continued

Exposure Temperature	Time (hr)	Thickness (mm)	Width (mm)	load (KN)	Modulus (GPa)	S.D (GPa)	N Modulus (GPa)	Modulus retention(%)
177℃	1	2.87	12.77	0.79	32.72	2.13	48.61	89.28
	2	2.64	12.69	0.73	40.88	3.70	55.96	111.55
	4	3.04	12.76	0.85	32.66	6.00	51.45	89.14
	8	2.91	12.77	0.81	35.52	5.96	53.56	96.95
	16	2.80	12.99	0.75	33.41	2.77	48.51	91.17
	24	2.77	12.93	0.73	34.29	4.93	49.17	93.57
	48	2.99	12.74	0.87	34.58	3.27	53.61	94.37
	72	2.73	12.73	0.80	40.87	2.98	57.90	111.55
204℃	1	3.08	12.72	0.89	30.61	3.33	48.91	83.53
	2	2.86	12.83	0.82	36.86	4.18	54.59	100.60
	4	3.14	12.71	0.85	31.90	3.93	51.89	87.05
	8	2.75	12.88	0.71	36.98	2.35	52.66	100.93
	16	2.80	12.62	0.76	33.32	3.52	48.30	90.93
	24	2.86	12.80	0.76	33.93	6.18	50.35	92.60
	48	3.00	12.75	0.87	34.52	2.63	53.65	94.20
	72	2.89	12.66	0.88	35.56	2.50	53.29	97.04
232℃	1	2.95	12.75	0.85	36.15	4.64	55.22	98.66
	2	2.82	12.57	0.72	34.29	2.24	50.05	93.57
	4	3.02	12.79	0.85	35.57	6.86	55.67	97.09
	8	2.83	12.88	0.77	35.54	4.42	52.01	96.98
	16	2.98	12.65	0.79	37.72	4.47	58.29	102.95
	24	2.80	12.73	0.78	37.66	4.32	54.64	102.78
	48	2.95	12.55	0.73	35.08	6.48	53.57	95.73
	72	2.86	12.70	0.50	23.45	6.88	34.70	63.99
260℃	1	2.99	12.95	0.80	36.06	4.05	55.78	98.42
	2	2.76	12.90	0.73	35.72	2.00	51.03	97.47
	4	2.84	12.71	0.82	38.82	2.95	57.12	105.94
	8	2.91	12.82	0.44	19.24	1.80	28.96	52.51
	16	2.68	12.78	0.15	8.85	1.85	12.26	24.15
	24	2.86	12.63	0.15	8.22	1.51	12.16	22.43
	48	3.06	12.88	0.13	7.16	1.41	11.36	19.53
	72	3.15	12.62	0.09	2.48	0.86	4.05	6.78

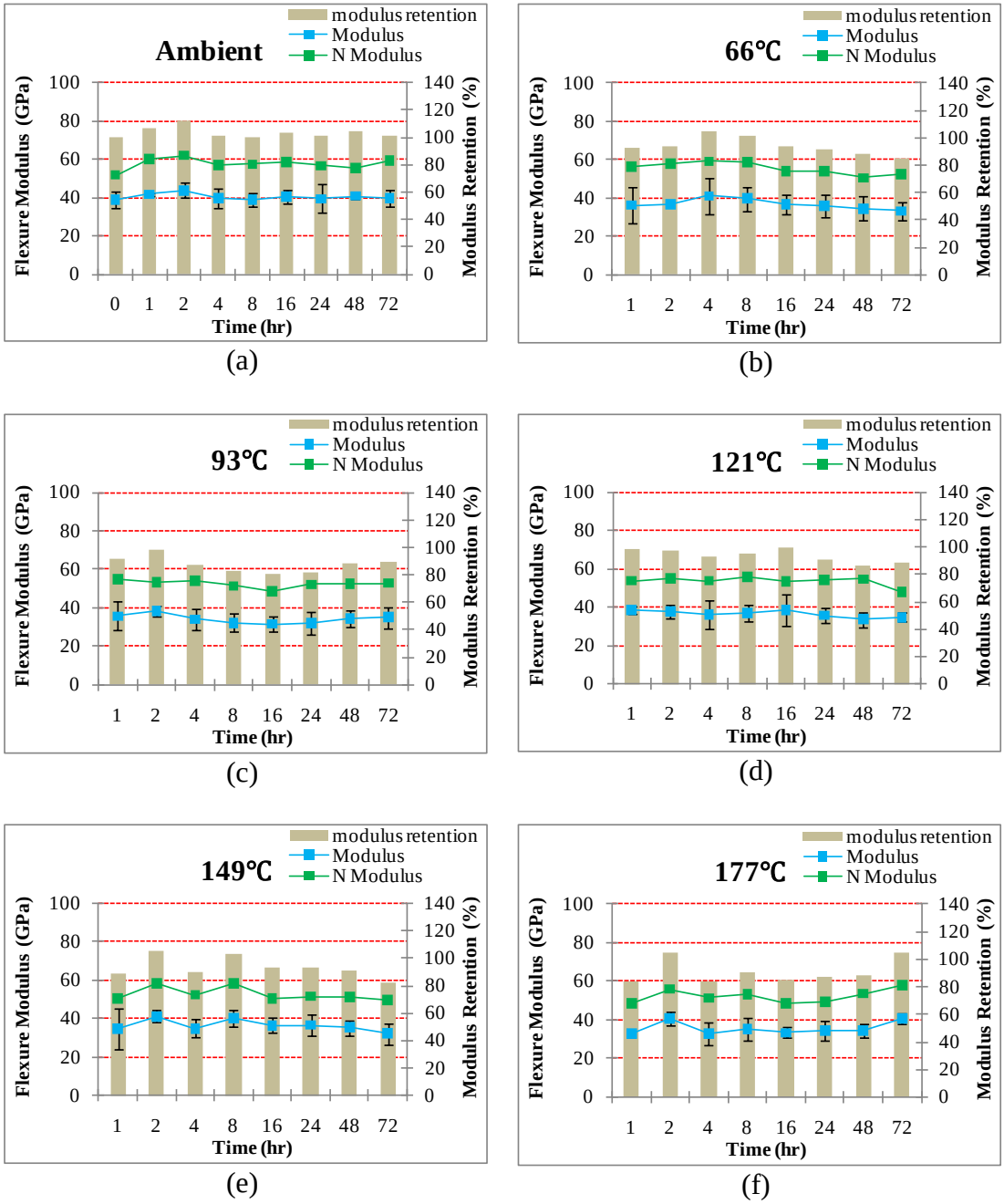

Figure 4-27: Flexural modulus and normalized flexural modulus of carbon/epoxy composite materials as a function of time at fixed temperatures, (a) ambient (b) 66℃ (c) 93℃ (d) 121℃ (e) 149℃ (f) 177℃ (g) 204℃ (h) 232℃ (i) 260℃

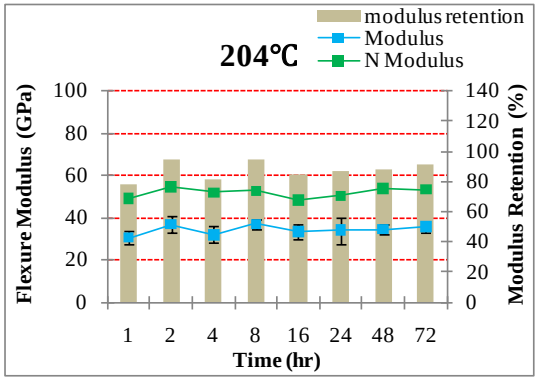

(g)

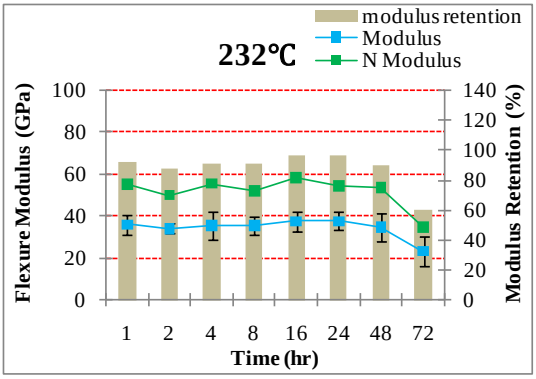

(h)

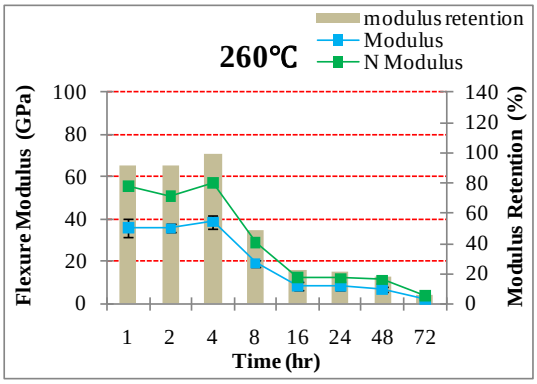

(i)

Figure 4-27: Continued

The time-dependent functions of flexural strength and modulus retention obtained by polynomial curve fittings are tabulated in Table 4-18 and Table 4-19. The coefficients of determination (R^2) of the time-dependent function in ranges of lower exposure temperatures were very low due to data fluctuation derived from thickness and defect. Especially, R-squared values in condition of ambient temperature showed the minimum values. Another reason why data variation was high than expected is that thermal oxidation did not largely affect the reduction of mechanical properties in the intermediate exposure temperatures. However, since degradations in flexural test rapidly occurred in exposure temperature of 260℃ compared to tensile test, the coefficient of determination (R^2) showed higher values.

Table 4-18: Time-dependent functions of off-axis shear strength retention (%) obtained by polynomial curve fitting

Temperature(℃)	a	b	c	d	R^2
Ambient (23)	-7.0E-05	0.0084	-0.3353	105.73	0.4012
66	2.0E-04	-0.0189	0.3454	103.22	0.4907
93	-2.0E-04	0.0261	-0.6874	102.46	0.5865
121	1.0E-04	-0.013	0.2979	104.05	0.2465
149	1.0E-04	-0.0265	0.9694	102.19	0.5885
177	-5.0E-05	0.013	-0.5409	109.14	0.679
204	3.0E-05	0.0009	-0.039	103.49	0.6074
232	-3.0E-04	0.0156	-0.0449	103.87	0.9782
260	-1.3E-03	0.1859	-7.9962	117.97	0.932

Time-dependent function : $Y(t) = \frac{\sigma_t}{\sigma_i} \times 100 = at^3 + bt^2 + ct + d$

Table 4-19: Time-dependent functions of off-axis shear modulus retention (%) obtained by polynomial curve fitting

Temperature(℃)	a	b	c	d	R^2
Ambient (23)	-1.0E-04	0.0165	-0.4739	112.33	0.1408
66		0.0003	-0.2224	105.05	0.5535
93	-4.0E-04	0.0518	-1.668	101.45	0.7312
121	2.0E-04	-0.016	0.1447	102.64	0.7227
149	3.0E-05	-0.0067	0.1114	102.18	0.3991
177	-7.0E-05	0.0027	-0.3472	97.793	0.4329
204	1.0E-04	-0.0115	0.3419	91.027	0.5847
232	-1.0E-04	-0.0035	0.4771	95.199	0.9809
260	-1.5E-03	0.1968	-7.9759	114.25	0.9428

Time-dependent function : $Y(t) = \frac{E_t}{E_i} \times 100 = at^3 + bt^2 + ct + d$

4.3.3.2 Temperature Dependence

As shown in Figure 4-28 of flexural strength of carbon/epoxy composite materials as a function of temperature at fixed time, the majority of the flexural strengths were distributed within a range from 500 MPa to 600 MPa except the conditions of exposure temperature, 232℃ for ageing timer, 72 hrs and exposure temperature, 260℃ for ageing times of 8, 16, 24, 48 and 72 hrs. If the ageing time is less than 8 hrs, flexural strengths were not largely affected by residual post-cure and thermal degradation in exposure temperature range up to 260℃.

Similar to the result of flexural strength, most of flexural chord modulus existed between 32 GPa and 45 GPa except the conditions mentioned in flexural strength as shown in Figure 4-29. At these conditions, data variation of the flexural modulus was much higher than in the case of flexural strength.

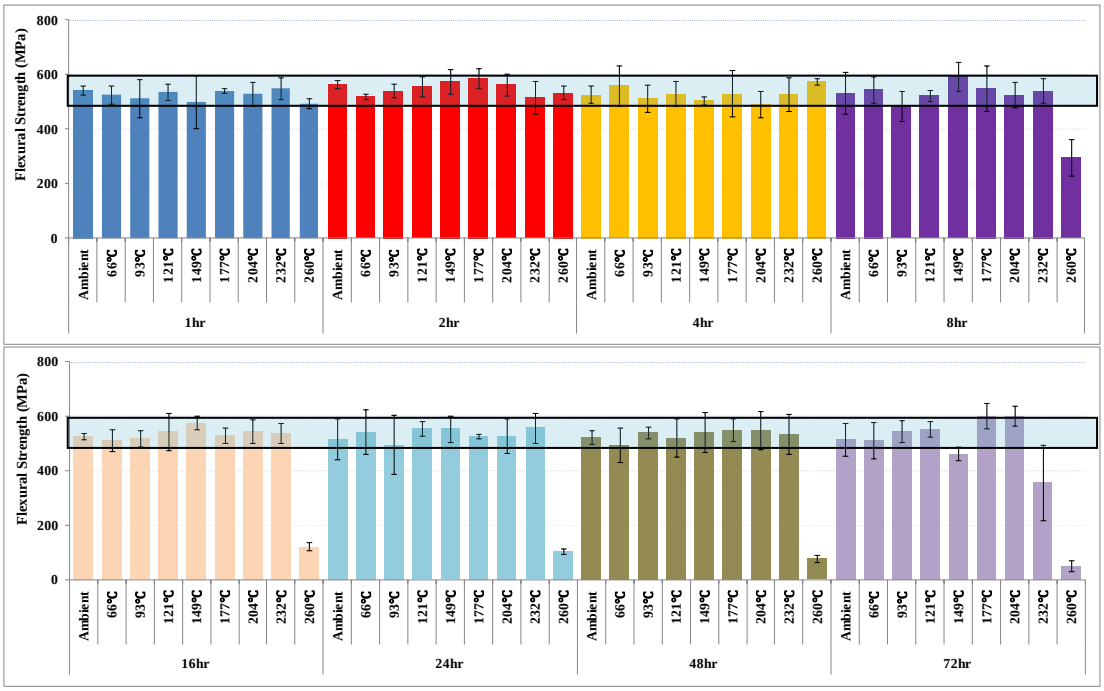

Figure 4-28: Flexural strength of carbon/epoxy composite materials as a function of temperature at fixed periods of exposure

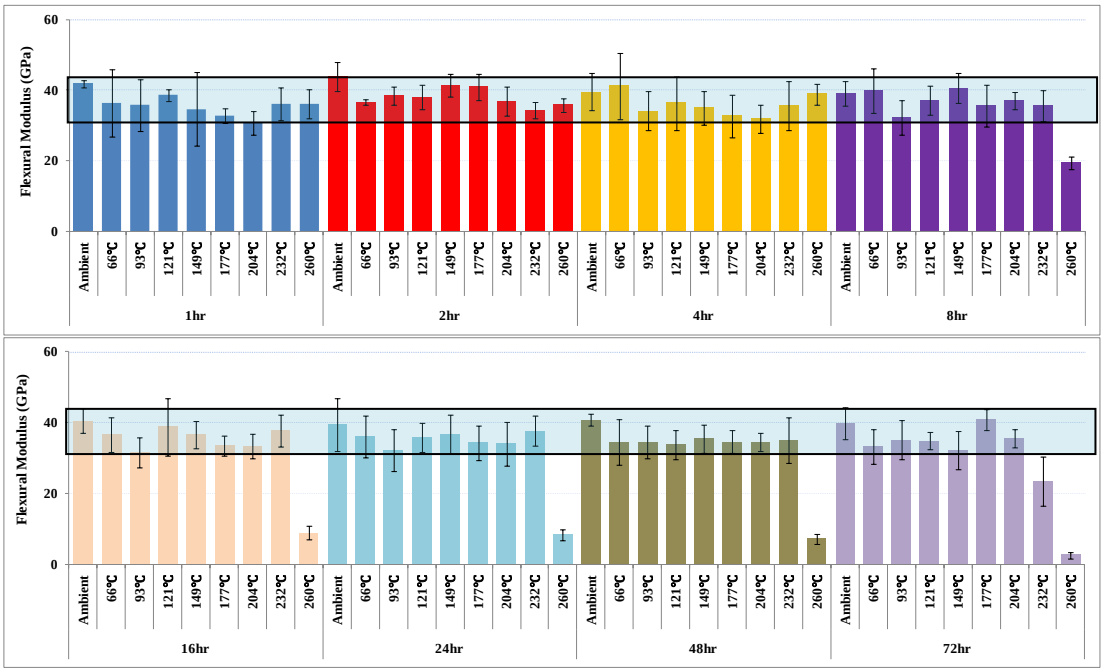

Figure 4-29: Flexural modulus of carbon/epoxy composite materials as a function of temperature at fixed periods of exposure

Based on the experimental data, temperature-dependent functions of flexural strength and modulus retention determined by polynomial curve fitting are drawn in Table 4-20 and Table 4-21. As mentioned in time and temperature dependent analysis, since the majority of the data did not show any tendency in the ranges of lower temperatures, temperature-dependent functions had high order and the coefficient of determination (R^2) were higher compared to the values of tensile and off-shear properties.

Table 4-20: Temperature-dependent functions of flexural strength retention (%) obtained by polynomial curve fitting

Time (hr)	a	b	c	d	R^2
1	-6.E-06	0.00028	-0.3364	112.94	0.571
2	-8.E-06	0.0029	-0.2958	113.93	0.8816
4	8.E-06	-0.003	0.27	98.481	0.6546
8	-3.E-05	0.0092	-0.8728	121.99	0.8121
16	-4.E-05	0.0137	-1.2568	128.4	0.8489
24	-4.E-05	0.013	-1.1904	126.62	0.7871
48	-4.E-05	0.0155	-1.4465	131.89	0.8458
72	-4.E-05	0.0142	-1.2546	126.26	0.8901

Temperature-dependent function : $Y(T) = \frac{\sigma_t}{\sigma_i} \times 100 = a\mathrm{T}^3 + b\mathrm{T}^2 + c\mathrm{T} + d$

Table 4-21: Temperature-dependent functions of flexural modulus retention (%) obtained by polynomial curve fitting

Time (hr)	a	b	c	d	R^2
1	4.E-06	-0.0008	-0.1093	114.44	0.7072
2	-1.E-05	0.0044	-0.5641	127.68	0.9183
4	1.E-05	-0.0033	0.1745	106.38	0.7596
8	-2.E-05	0.0091	-0.9504	127.01	0.7955
16	-4.E-05	0.0137	-1.487	141.05	0.7641
24	-4.E-05	0.048	-1.5817	140.52	0.7882
48	-4.E-05	0.0158	-1.7299	146.6	0.8586
72	-5.E-05	0.0166	-1.7061	141.49	0.9539

Temperature-dependent function : $Y(T) = \frac{E_t}{E_i} \times 100 = a\mathrm{T}^3 + b\mathrm{T}^2 + c\mathrm{T} + d$

4.3.3.3 Morphological Analysis

Figure 4-30 represents top view and side view of the test specimens fractured after flexural test after exposure to elevated temperatures at the ageing time, 72 hrs. As exposure temperatures were going up, the color of the test specimens was also changed as described in morphological analysis of the tensile test. Except for color change, test specimens fractured by flexural test did not have characterized morphology in ranges of the lower exposure temperatures. From the side view of test specimens, there were many stains in the side section of test coupons. There were no stains in the exposure conditions of ambient and 66℃ while stains were increased as exposure temperatures were going up. The reason why there are stains in the side of the test specimens is that the polymer matrix and organic fibers decomposed thermally yield volatile gases via a series of chemical reaction mechanisms and volatile gases were emitted from side section of the test specimen.

In ranges of lower exposure temperatures (ambient, 66, 93, 121, 149℃) for 72 hrs of ageing time, test specimens fractured by flexural test did not show the delamination between 2 layers whereas severe delamination caused by thermal oxidation occurred in ranges of the higher exposure temperatures (177, 204, 232, 260℃) for 72 hrs. As the exposure temperatures were going up, the delaminations between 2 layers were more severe. The reason why flexural properties were rapidly reduced in range of the exposure temperature of 260℃ compared to tensile properties is that additional delamination between 2 layers caused severe deterioration of the test specimens.

(a) (b)

Figure 4-30: Test specimens fractured after flexural testing after exposure to elevated temperatures at an ageing time of 72 hrs (a) top view (b) side view

4.3.3.4 Strain Effect

The strains of the flexure test were calculated by using Equation 4.2l. The ultimate failure strains and the maximum strains were obtained from the values which flexural stress reached the maximum and test specimens were perfectly fractured by test equipment, respectively.

Figure 4-31 shows flexural stress-ultimate failure strain curve exposed to various ageing temperatures at the fixed time, 72 hrs. The slopes of the linear range to measure the flexural chord modulus were gradually increased in exposure temperatures of from ambient to 149℃ while the values of flexural modulus were significantly reduced in ranges of high exposure temperatures more than 177℃. The maximum stresses were increased in lower exposure temperatures and were decreased by thermal oxidation in higher exposure temperatures. Because test specimens were perfectly not cured in ambient exposure temperature, they showed the ductile property until completely fractured after the maximum stress was reached. In case flexural modulus and strength were enhanced by residual post-cure effect, test specimen showed brittle property fractured promptly after reaching the maximum stress. In addition, the maximum strains of test specimens subjected to high temperatures of 232 and 260℃ were very high compared to any exposure temperatures. This phenomenon was attributed to softening of test specimens caused by char formation in process of thermal oxidation.

Figure 4-32 (a), Figure 4-33 (a) and Figure 4-34 (a) show flexural strength, modulus and load as a function of ultimate failure strains (%), respectively. Except for the data of the high exposure temperature (260℃), all data of the flexural strength,

modulus and load were distributed between 0.014 mm/mm and 0.021 mm/mm of ultimate failure strain. If the outlier data in high exposure temperatures are extracted and the data of the flexural strength, modulus and load are changed to log scale, more linear correlations between flexural properties and ultimate strain can be obtained as represented in Figure 4-32 (b), Figure 4-33 and Figure 4-34 (b).

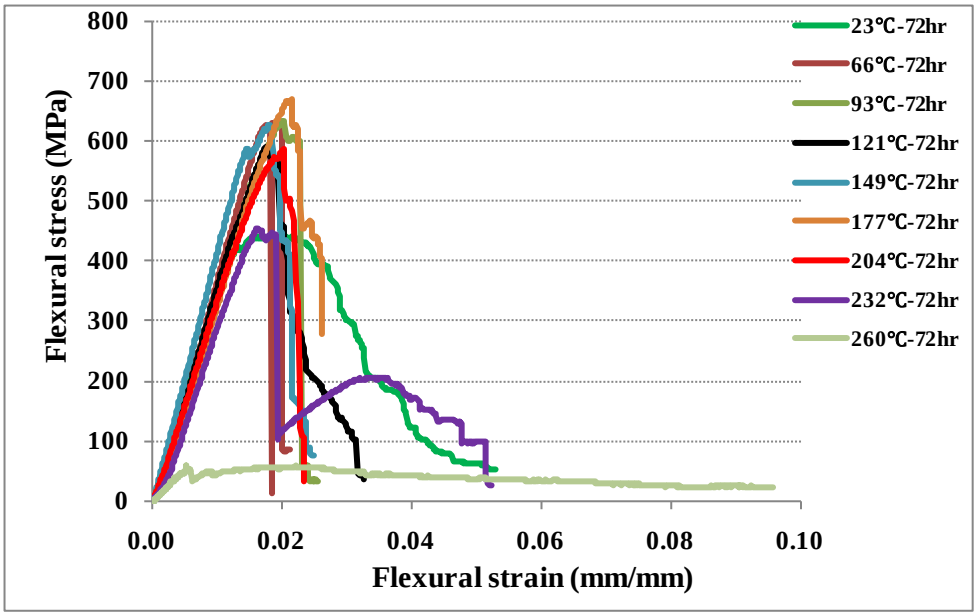

Figure 4-31: Flexural stress- strain curve resulting from specimens exposed to various ageing temperatures at a fixed time of 72 hrs

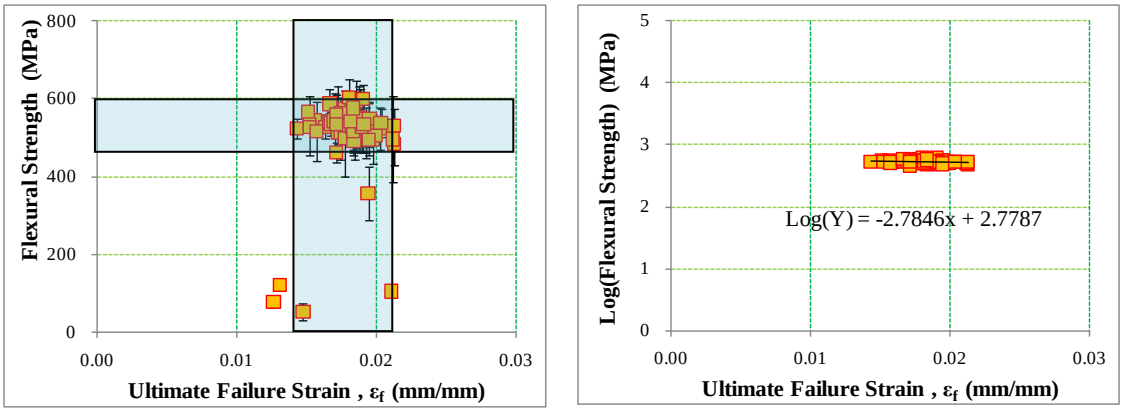

(a) (b)

Figure 4-32: (a) Flexural strength as a function of ultimate failure strains and (b) correlations of log (Flexural strength) versus ultimate failure strain

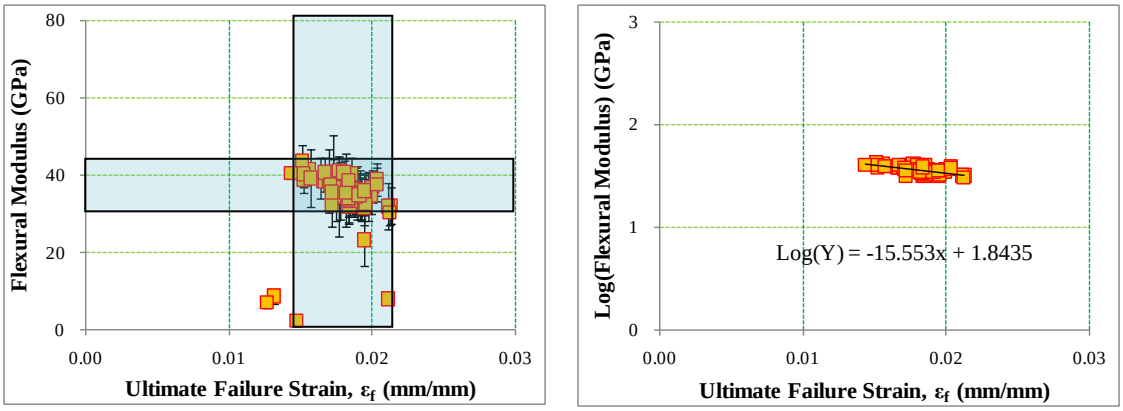

(a) (b)

Figure 4-33: (a) Flexural modulus as a function of ultimate failure strains and (b) correlations of log (Flexural modulus) versus ultimate failure strain

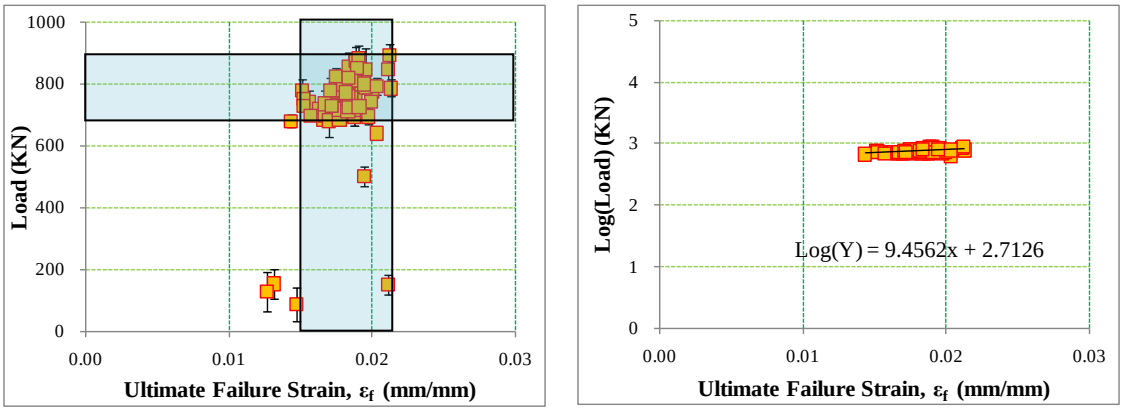

(a) (b)

Figure 4-34: (a) Flexural load as a function of ultimate failure strains and (b) correlations of log (Flexural load) versus ultimate failure strain

4.4 Short Beam Shear Testing

4.4.1 Introduction

It is well known that the original performance of fiber reinforced polymer (FRP) composites strongly depend on the properties of the fiber reinforcement and the resin, and the interface between the two components. Layered composite materials intrinsically have a weaken zone within interlaminar regions. If the composite materials are exposed to high temperature and fire, cracks and defects within weaken zone can result in catastrophic degradations such as macrocrack formation and delamination of reinforced layers along this regions.

In case the composite materials are applied for naval applications, the majority of the fiber reinforced polymer composites are wet laid-up in ambient temperature due to huge structures. FRP composites which incompletely cured over the expected service-life can influence the properties of resin and interfaces between layers or fiber and resin. Interlaminar shear strength (ILSS) depends primarily on the resin properties and fiber-matrix interfacial shear strengths rather than the fiber properties. Therefore, ILSS is an important characteristic to be assessed because this property can be criterion for potential failure modes. In general, ILSS refers to the shear strength parallel to the plane of lamination. In this study, short beam shear test having three-point bending fixture was executed in accordance with ASTM D2344. Because of its simplicity, the short beam shear test is widely accepted for materials screening and quality control purpose[53]. This method measures the apparent interlaminar shear strength of composite materials. Thus, short beam shear test method is not appropriate for

generating design information[54].

4.4.2 Data Reduction

Short beam shear (SBS) tests were executed to obtain the interlaminar shear strength of carbon/epoxy composite materials comprised of 2 layers laminate. In the case of SBS test in three-point bending, the test specimens are center-loaded with two ends on two supports enabling lateral motion, with the force applied by a loading nose placed in midpoint of the test specimens. Detail SBS test procedure is described in Chapter 3.5.4.

SBS strength can be calculated by Equation 4.23.

$$F^{sbs} = 0.75 \times \frac{P_m}{b \times h} \tag{4.23}$$

where:

F^{sbs} = the short beam shear strength, MPa

P_m = the maximum load, N

b = the width of the specimen tested, mm

h = the thickness of the specimen tested, mm

4.4.3 Analyses and Results

4.4.3.1 Time Dependence

Although layered unidirectional composite materials offer good mechanical properties in fiber direction they have very little resistance to crack propagation and delamination under transverse and shear loading. Therefore, short beam shear test can be resulted in various failure modes as follows[55],

- Discrete shear by irregular crack and side crack
- Homogenous shear by permanent deformation and compression jamming
- Tensile fracture of outer surface
- Compression fracture of outer surface

Short beam shear test can derive complicated fractures since failure mode can be combined with other failure mode or not. Thus, it is difficult to analyze the experimental test results in short beam shear test. In particular, when used in conjunction with thin unidirectional composites, which is common with the graphite/epoxy composites, the test does not usually yield interlaminar failure[54].

Data for short beam shear strength (MPa) of carbon/epoxy composite materials after exposure to various temperatures are tabulated in Table 4-22 and Short beam shear strength as a function of time at fixed temperatures are presented in Figure 4-35. Except for severe environments of exposure temperature (260℃) for more than 16 hrs in ageing time, all short beam shear strengths were distributed in ranging from 40 to 50 MPa. Compared to the strength retentions of tensile and flexural test, the strength retentions of short beam shear test were initially increased in the amount of more than

flexural strength retention and less than tensile strength retention by residual post-curing. Therefore, the fractures of short beams shear test can be resulted in mixed failure mode. Especially, it should be pointed out that strength retention of exposure temperature (232℃) for 72 hrs in ageing time, contrary to tensile and flexural test, was not decreased by thermal degradation. Interlaminar shear stress was not contributed to fracture of the test specimens since char was only formatted in the surface of composite materials and buckling failure near the load nose in the midpoint was not occurred. However, levels of deterioration measured in the environmental condition of exposure temperature (260℃) for more than 16 hrs in ageing time were higher than strength retention in tensile and flexural test as represented in Table 4-22 and Figure 4-35.

The time-dependent functions of short beam shear retention obtained by polynomial curve fittings are tabulated in Table 4-23. Even though 3 order polynomial curve fittings were executed, the coefficient of determination (R^2) of the time-dependent function except for condition of exposure temperature (260℃) was the lowest compared to tensile and flexural strengths. As mentioned about disadvantage of short beam shear test, since short beam shear test can derive complicated fractures, particularly, in carbon/epoxy composite materials, higher variation of experimental data resulted in lower coefficient of determination (R^2) in the ranges of intermediate exposure temperatures.

Table 4-22: Data for Short Beam Shear Strength (MPa) of carbon/epoxy composite materials after exposure to various temperatures (N denotes normalized)

Exposure temperature	Time (hr)	Thick (mm)	Width (mm)	Load (N)	Strength (MPa)	S.D (MPa)	N strength (MPa)	Strength Retention(%)
Ambient (23℃)	0	2.26	6.54	776.69	39.45	2.01	46.15	100.00
	1	2.33	6.50	829.30	41.85	1.67	50.48	106.08
	2	2.26	6.63	843.66	42.23	1.06	49.45	107.05
	4	2.28	6.58	830.12	41.44	1.48	49.05	105.06
	8	2.34	6.50	858.81	42.43	1.41	51.35	107.55
	16	2.27	6.60	824.88	41.19	1.18	48.54	104.42
	24	2.34	6.58	857.47	41.84	2.00	50.64	106.06
	48	2.29	6.56	843.39	42.07	3.10	49.92	106.64
	72	2.26	6.54	796.31	40.28	3.17	47.21	102.11
66℃	1	2.37	6.61	882.45	42.33	1.62	51.89	107.31
	2	2.28	6.67	930.24	45.76	3.12	54.15	115.99
	4	2.28	6.71	921.70	45.36	2.64	53.50	114.99
	8	2.34	6.46	912.26	45.45	2.25	55.02	115.22
	16	2.24	6.67	921.20	46.31	2.97	53.65	117.39
	24	2.30	6.35	909.20	46.44	3.53	55.25	117.73
	48	2.30	6.62	912.36	44.85	2.90	53.49	113.68
	72	2.30	6.56	923.86	46.02	3.23	54.75	116.66
93℃	1	2.25	6.67	857.23	42.89	1.98	49.96	108.73
	2	2.31	6.59	902.84	44.46	3.66	53.30	112.69
	4	2.28	6.74	917.38	44.91	2.18	52.96	113.84
	8	2.23	6.68	931.75	46.94	1.12	54.24	119.00
	16	2.10	6.70	981.39	47.75	3.87	52.05	121.03
	24	2.29	6.60	892.79	44.49	3.12	52.67	112.77
	48	2.25	6.81	947.45	46.29	1.44	54.02	117.35
	72	2.32	6.70	960.55	46.37	3.07	55.70	117.55
121℃	1	2.30	6.69	883.95	43.13	2.42	51.35	109.32
	2	2.27	6.77	926.38	45.29	2.01	53.22	114.80
	4	2.28	6.71	917.24	45.01	2.62	53.13	114.10
	8	2.29	6.65	973.76	47.93	1.50	56.87	121.51
	16	2.27	6.74	906.24	44.47	3.04	52.26	112.72
	24	2.27	6.71	914.62	44.96	1.95	52.97	113.97
	48	2.33	6.73	983.08	47.01	3.02	56.76	119.17
	72	2.29	6.40	918.65	47.01	2.86	55.83	119.16
149℃	1	2.29	6.72	955.55	46.35	2.95	55.10	117.50
	2	2.32	6.73	959.45	46.00	1.87	55.35	116.61
	4	2.27	6.66	923.42	45.69	2.77	53.74	115.83
	8	2.28	6.69	1033.25	50.69	1.51	59.99	128.49
	16	2.26	6.61	905.01	45.46	2.40	53.23	115.23
	24	2.26	6.72	951.32	46.93	2.00	54.96	118.97
	48	2.34	6.75	973.59	46.20	2.03	56.07	117.12
	72	2.28	6.66	980.43	48.43	4.51	57.21	122.77

Table 4-22: Continued

Exposure temperature	Time (hr)	Thick (mm)	Width (mm)	Load (N)	Strength (MPa)	S.D (MPa)	N strength (MPa)	Strength Retention(%)
177℃	1	2.26	6.71	934.46	46.17	2.50	54.11	117.03
	2	2.28	6.69	910.04	44.63	3.10	52.82	113.14
	4	2.33	6.73	905.27	43.27	2.29	52.28	109.69
	8	2.27	6.77	941.41	46.03	1.63	54.09	116.68
	16	2.35	6.63	945.68	45.41	1.02	55.39	115.12
	24	2.34	6.62	958.83	46.39	1.07	56.29	117.60
	48	2.27	6.73	950.46	46.86	3.02	55.01	118.78
	72	2.26	6.61	940.33	47.16	4.05	55.27	119.54
204℃	1	2.23	6.72	907.45	45.54	2.26	52.57	115.45
	2	2.31	6.72	933.51	45.08	1.63	54.00	114.27
	4	2.29	6.74	894.37	43.45	1.61	51.55	110.13
	8	2.25	6.65	957.13	48.08	0.60	55.95	121.87
	16	2.27	6.47	875.64	44.73	2.22	52.60	113.37
	24	2.29	6.76	938.53	45.49	2.88	53.98	115.32
	48	2.29	6.75	921.25	44.67	4.01	52.90	113.22
	72	2.20	6.36	918.40	48.91	3.83	55.81	123.99
232℃	1	2.30	6.71	909.84	44.28	1.14	52.72	112.24
	2	2.35	6.71	958.50	45.61	3.24	55.58	115.61
	4	2.17	6.73	936.50	48.06	2.91	54.04	121.84
	8	2.30	6.67	957.24	46.71	2.66	55.76	118.41
	16	2.24	6.19	859.29	46.48	1.74	53.85	117.83
	24	2.29	6.70	955.67	46.62	4.27	55.42	118.19
	48	2.25	6.73	1003.92	49.61	3.17	57.93	125.75
	72	2.27	6.48	955.59	48.97	5.11	57.70	124.14
260℃	1	2.23	6.71	872.91	43.64	2.94	50.51	110.61
	2	2.28	6.50	950.82	48.00	1.38	56.80	121.67
	4	2.22	6.71	999.02	50.13	2.99	57.77	127.09
	8	2.22	6.56	530.95	27.34	2.46	31.45	69.31
	16	2.26	6.74	373.01	18.37	1.27	21.51	46.57
	24	2.30	6.62	191.15	9.43	1.12	11.23	23.92
	48	2.29	6.74	130.06	6.26	1.85	7.43	15.87
	72	2.33	6.43	87.46	4.42	1.47	5.32	11.20

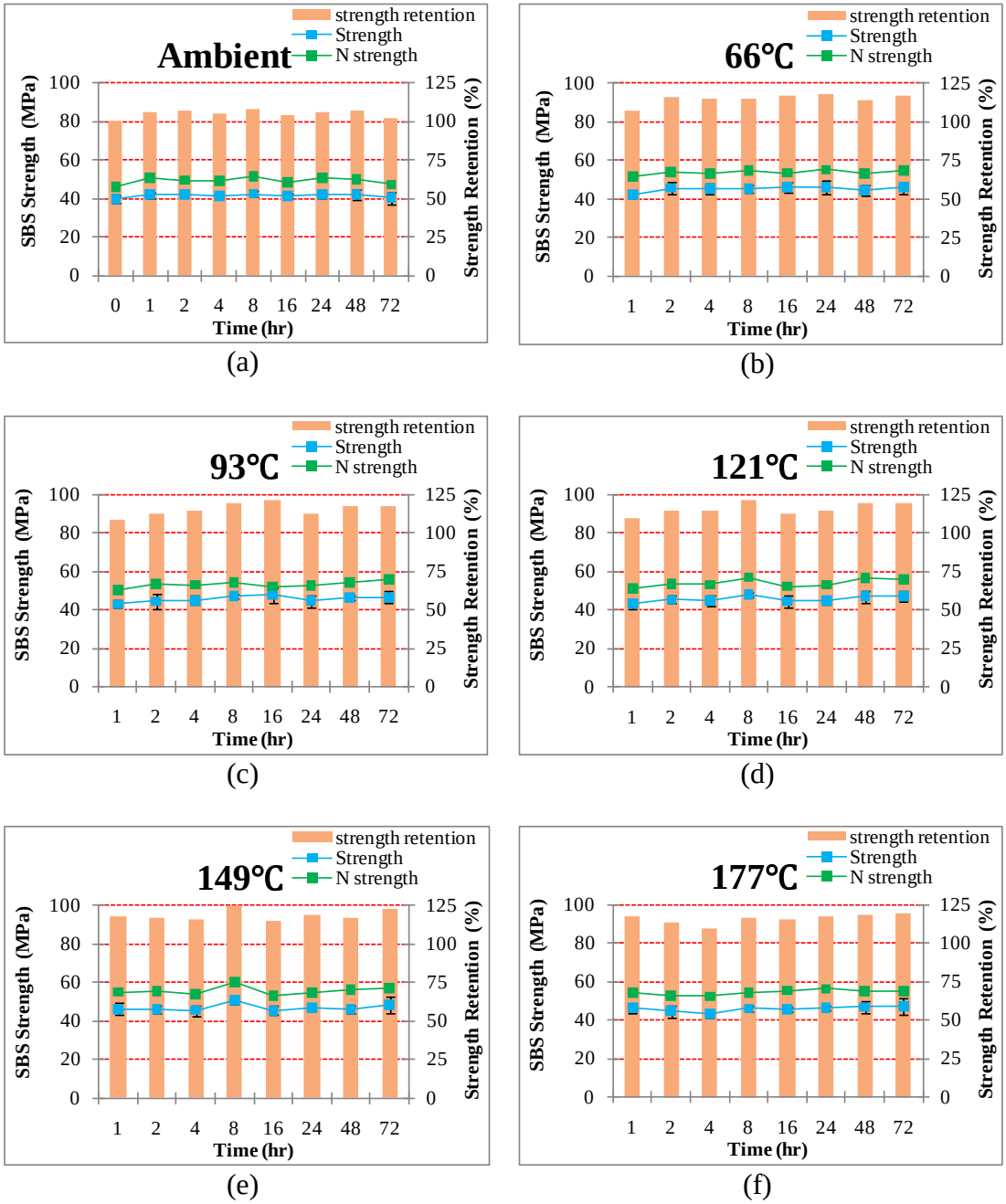

Figure 4-35: Short Beam Shear Strengths and normalized Short Beam Shear strengths of carbon/epoxy composite materials as a function of time at fixed temperatures, (a) ambient (b) 66°C (c) 93°C (d) 121°C (e) 149°C (f) 177°C (g) 204°C (h) 232°C (i) 260°C

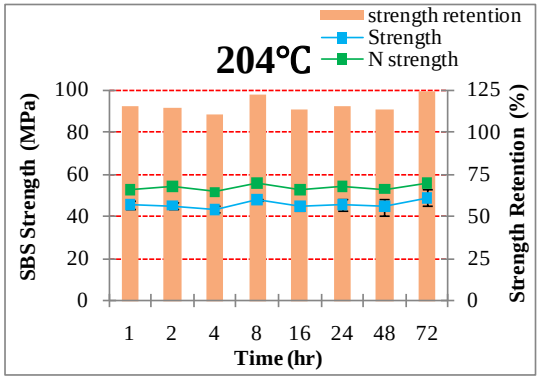

(g)

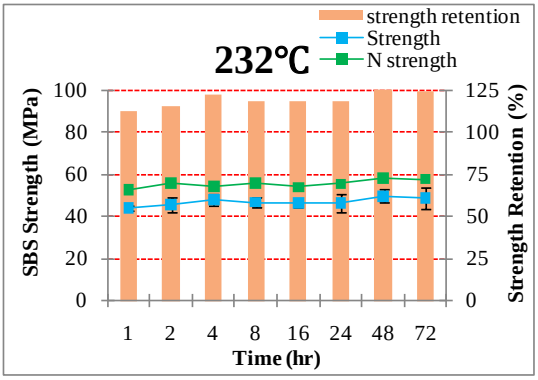

(h)

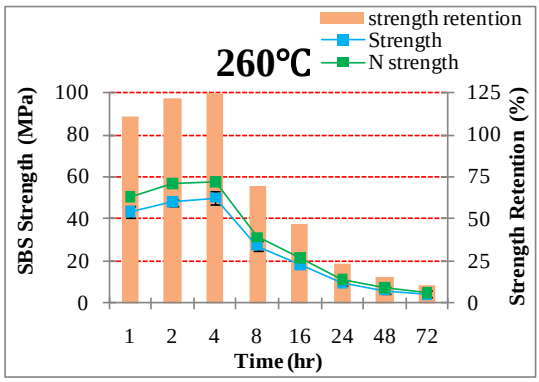

(i)

Figure 4-35: Continued

Table 4-23: Time-dependent functions of Short Beam Shear Strength retention (%) obtained by polynomial curve fitting

Temperature(℃)	a	b	c	d	R^2
Ambient(23)	-5.0E-06	-0.0021	0.1477	104.36	0.2788
66	2.0E-04	-0.027	0.8122	110.75	0.5601
93	2.0E-04	-0.024	0.7425	110.96	0.4209
121	8.0E-06	-0.0014	0.1411	113.47	0.2777
149	2.0E-04	-0.0162	0.3637	117.48	0.1819
177	-2.0E-05	0.0006	0.1239	113.66	0.5023
204	2.0E-04	-0.0176	0.3605	113.86	0.5356
232	-7.0E-05	0.0057	0.0694	116.19	0.6287
260	-1.1E-03	0.1645	-7.813	133.18	0.9469

Time-dependent function : $Y(t) = \frac{\sigma_t}{\sigma_i} \times 100 = at^3 + bt^2 + ct + d$

4.4.3.2 Temperature Dependence

Figure 4-36 and Figure 4-37 show the short beam shear strengths and loads of carbon/epoxy composite materials as a function of temperature at fixed time. The majority of the short beam shear strengths were distributed within ranging from 40 MPa and 50 MPa except for severe environments of exposure temperature (260℃) for more than 16 hrs in ageing time. In shorter ageing times (less than 8 hrs), short beam shear strengths were gradually increased although the exposure temperatures were going up. This phenomena means the residual post-curing effect and thermal oxidation by heat could not act on the change of short beam shear strengths. In other words, big data fluctuation appears to be stemmed from mixed failure modes of the defects and voids created in hand wet lay-up process. Data for short beam shear load were in good agreement with strength data and loads were existed between 800N and 1,000N as depicted in Figure 4-37.

Table 4-24 shows temperature-dependent functions of short beam shear strength retention (%) obtained by polynomial curve fitting. Compared to time-dependent functions, when each functions had 3 order equations, better coefficients of determination (R^2) were obtained by curve fitting.

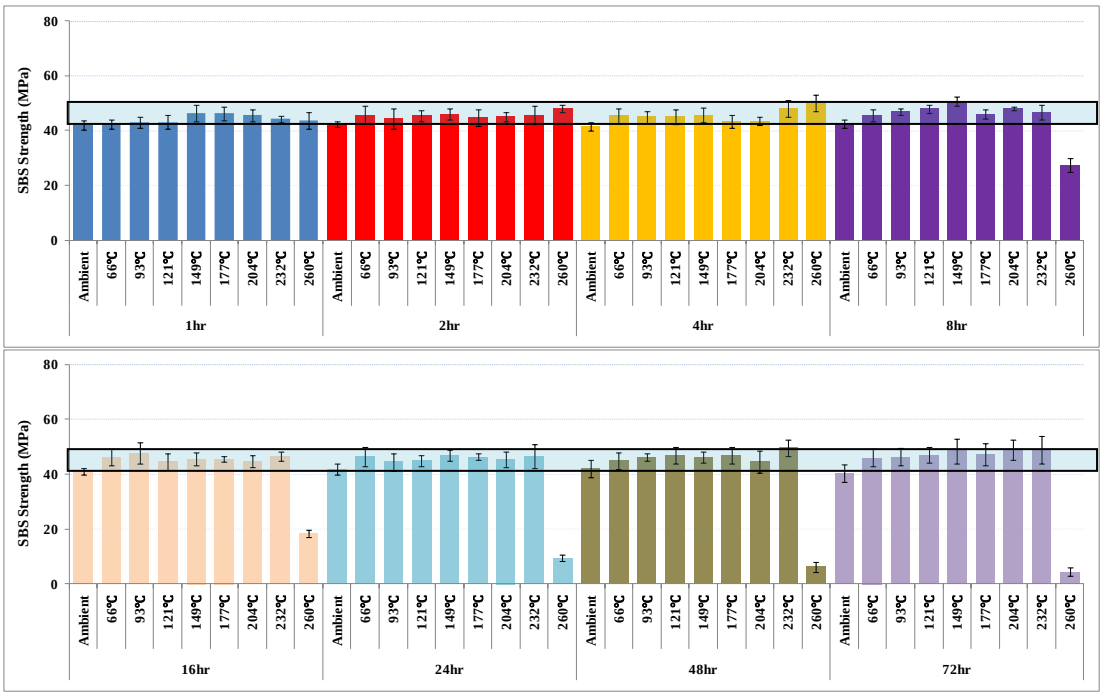

Figure 4-36: Short beam shear strength of carbon/epoxy composite materials as a function of temperature at fixed times of exposure

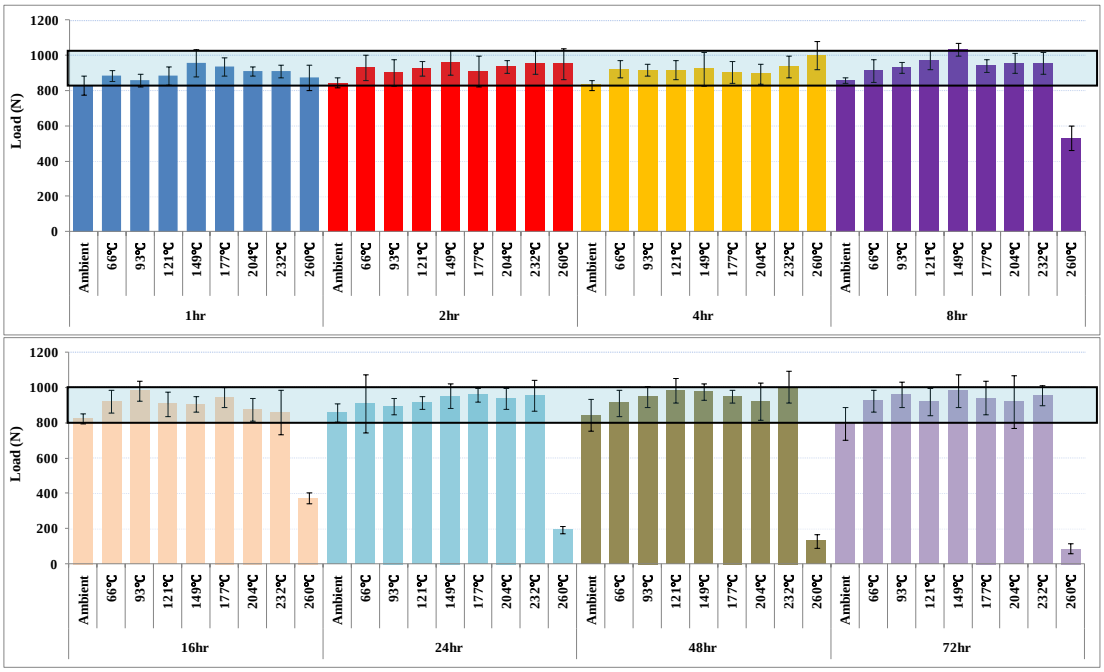

Figure 4-37: Short beam shear load of carbon/epoxy composite materials as a function of temperature at fixed times of exposure

Table 4-24: Temperature-dependent functions of Short Beam shear strength retention (%) obtained by polynomial curve fitting

Time (hr)	a	b	c	d	R^2
1	-5.E-06	0.0017	-0.0955	107.29	0.836
2	6.E-06	-0.0027	0.3598	100.4	0.8582
4	1.E-05	-0.0045	0.5412	94.954	0.8801
8	-2.E-05	0.0058	-0.3564	115.05	0.8404
16	-2.E-05	0.0073	-0.526	118.12	0.7482
24	-4.E-05	0.0131	-1.1202	131.82	0.7992
48	-4.E-05	0.0142	-1.2016	133.27	0.7595
72	-5.E-05	0.0152	-1.2157	129.9	0.7898

Temperature-dependent function : $Y(T) = \frac{\sigma_t}{\sigma_i} \times 100 = a\mathrm{T}^3 + b\mathrm{T}^2 + c\mathrm{T} + d$

4.4.3.3 Morphological Analysis

Figure 4-38 shows SEM images in region between the support and the load nose at midpoint of test specimen after short beams shear testing of specimens exposed to elevated temperatures for ageing time of 48 hrs. Left images show bottom section fractured by tension and right images show top section fractured by compression. In the ranges of lower exposure temperatures, both sections showed good bonding between fibers and matrix. Since debonding between fibers and matrix and pulling-out of fibers were observed in ranges of high exposure temperatures, experimental data showed the deterioration of the interlaminar shear strengths did not occur in short beam shear testing. Pure interlaminar shear stresses were not applied for test specimens due to thin thickness. Test specimen subjected to exposure temperature (260℃) for ageing time of 48 hrs caused the catastrophic degradation due to char formation and severe debonding between fibers and matrix as shown in Figure 4-38 (i). Also, it should be noted that resin was elongated away from the original surface and moved in a fiber direction as depicted in left images of Figure 4-38 (b), (c) and (f). Such failure shapes are often defined as 'hackles', which has been corresponded to mixed-mode (combined tension and shear) interlaminar fracture[56]. Accordingly, since these fracture modes means the horizontal split is not a pure shear failure and fracture modes is very complicated, it is very difficult to obtain the accurate short beam shear strengths using the thin test specimens of carbon/epoxy composite materials.

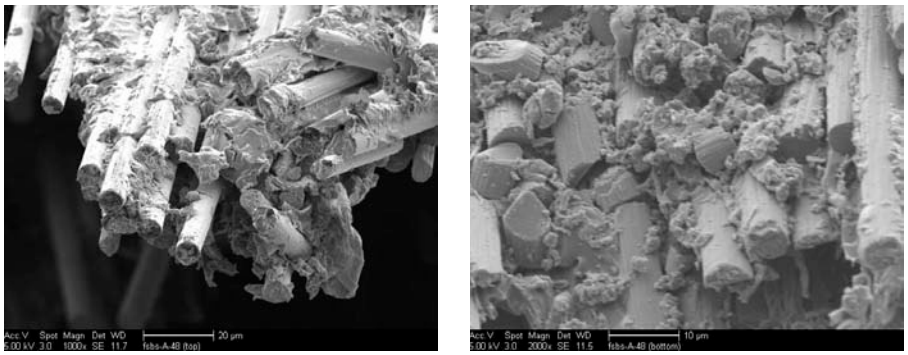

(a)

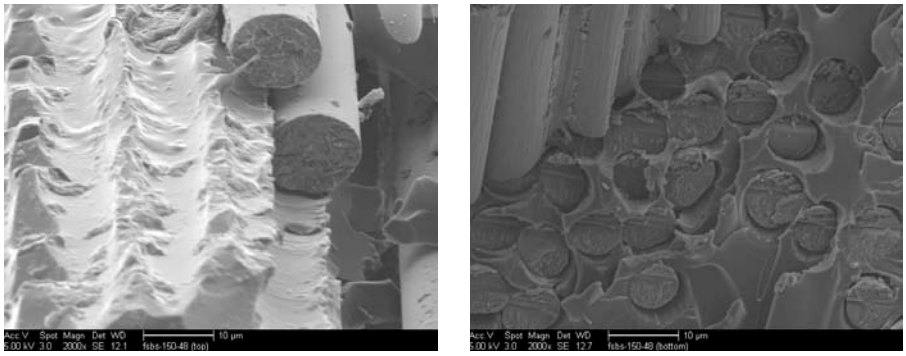

(b)

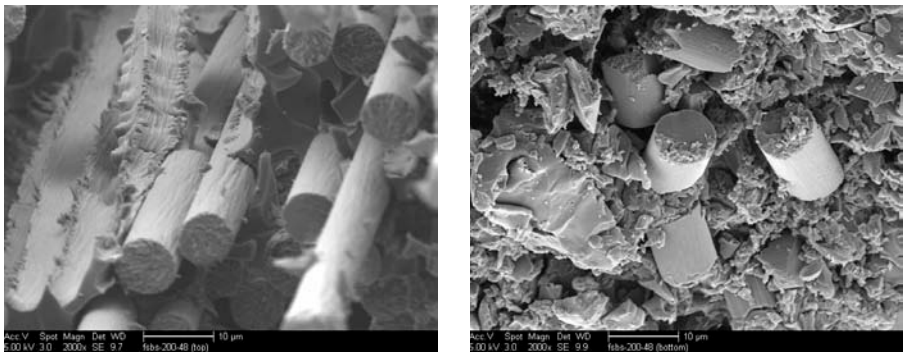

(c)

Figure 4-38: SEM images after short beam shear testing of specimens exposed to (a) ambient, (b) 66℃, (c) 93℃, (d) 121℃, (e) 149℃, (f) 177℃, (g)204℃, (h) 232℃, (i) 260℃ for 48 hrs in ageing time - left images : bottom section by tension, right images : top section by compression: Magnification 2000×

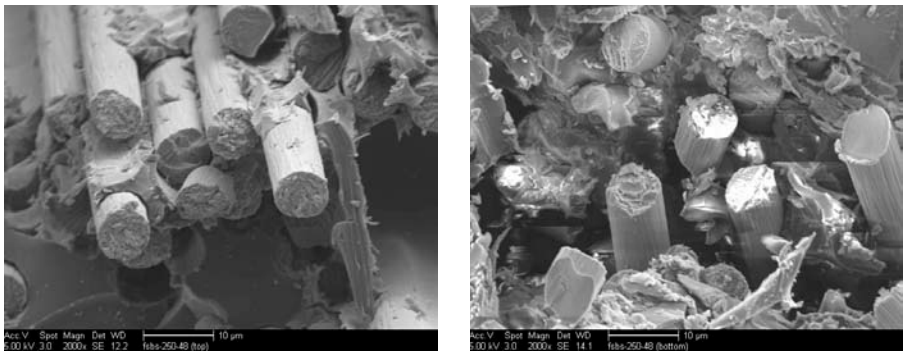

(d)

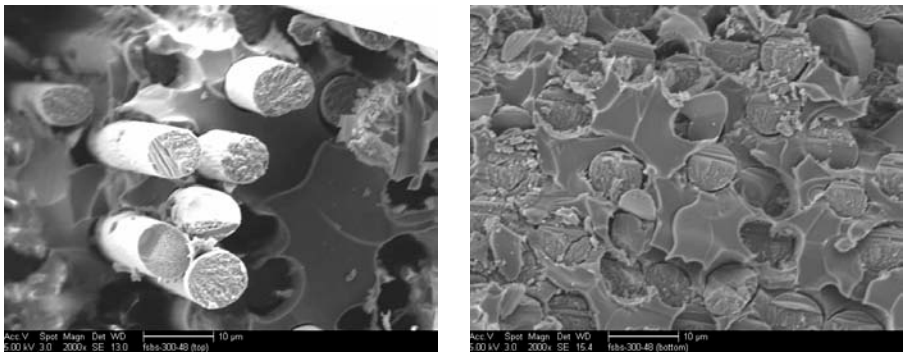

(e)

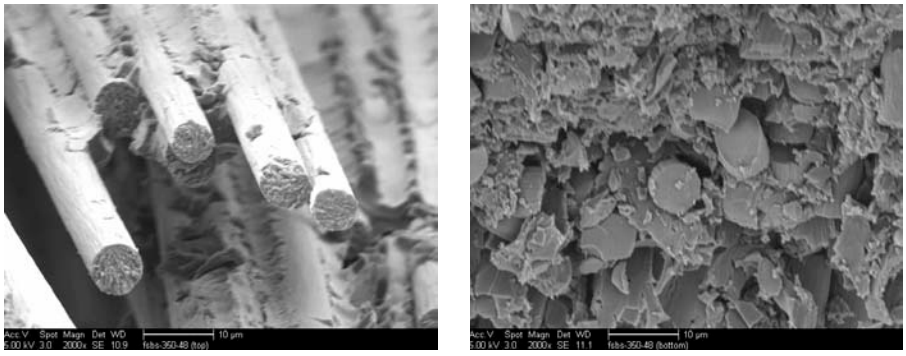

(f)

Figure 4-38: Continued

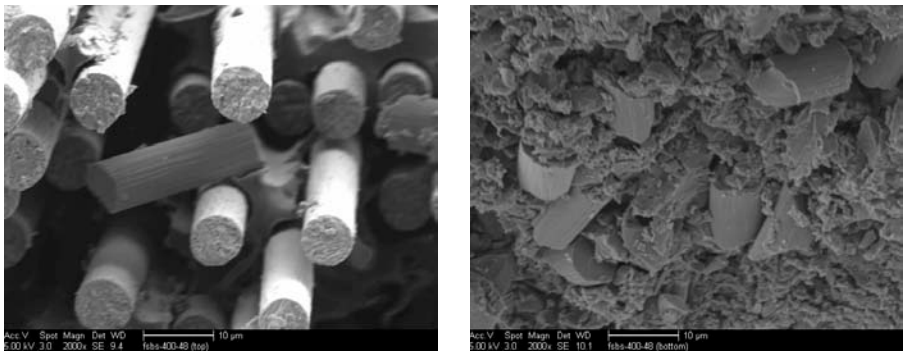

(g)

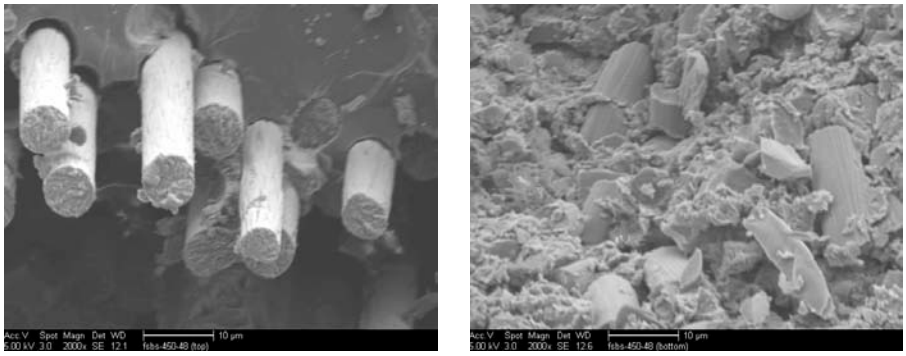

(h)

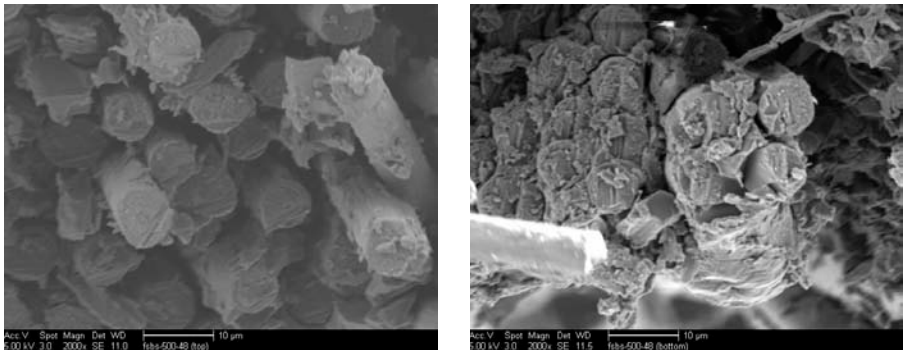

(i)

Figure 4-38: Continued

4.4.3.4 Correlation to Tensile Test Results

It is well known that the tensile properties are strongly dependent on interfacial adhesion between fibers and resin. Short beam shear testing are mainly used for the interlaminar shear strength of composite materials, though it has been recommended that short beam shear testing is proper for use as comparative measure of the fiber/matrix adhesion due to its sensitive to through thickness longitudinal shear strength. In addition, the short beam shear testing often shows a combination of failure mode such as delamination across the specimen depth, local crushing by the loading pin, bending failure, etc[57]. Therefore, through the comparison of tensile strength and short beam shear strength, it is necessary to analyze how failure mechanisms affect fracture of the test specimens in short beam shear test.

The stress applied at any point in the beam can be obtained by using strength of materials theory[58]. This theory is based on the necessary conditions for static equilibrium which pertains since the rate of deflection is small. The theory can be divided into two major components.

1. The normal stress has the maximum tensile value at midpoint between two supports. The maximum value of normal stress is

$$\sigma_x^* = \frac{3P_m L}{2bh^2} \tag{4.24}$$

2. Secondly, the longitudinal shear stress occurs at the mid-plane and is given by

$$\tau_{xy}^* \approx F^{sbs} = \frac{3P}{4bh} \tag{4.25}$$

According to Equation 4.24 and 4.25 of materials theory, test specimens of beam will be fractured by shear rather than tension or compression in outer surface at midpoint if

$$\sigma_x^* > \frac{2F^{sbs}L}{h} \tag{4.26}$$

Experimental data of tensile and flexural test are compared with materials theory as shown in Figure 4-39 and Figure 4-40. In short beam shear test, the span and average thickness of test specimens were 14 mm and 2.3 mm, respectively. Therefore, the slope of line drawn by red color in Figure 4-39 and Figure 4-40 was 12.17 according to Equation 4.26. The upper region from red line means the cases failed by short beam shear while the lower region represents the cases fractured by flexural tension at outer surface and pure tension. In particular, compared to experimental data of flexural test, the majority of failure modes of short beam shear test were occurred by not shear but flexural tension at outer surface. As a result, the reason why big variation of experimental data took place in lower exposure temperatures is that pure interlaminar shear stresses were not applied for test specimen of shear beam shear test.

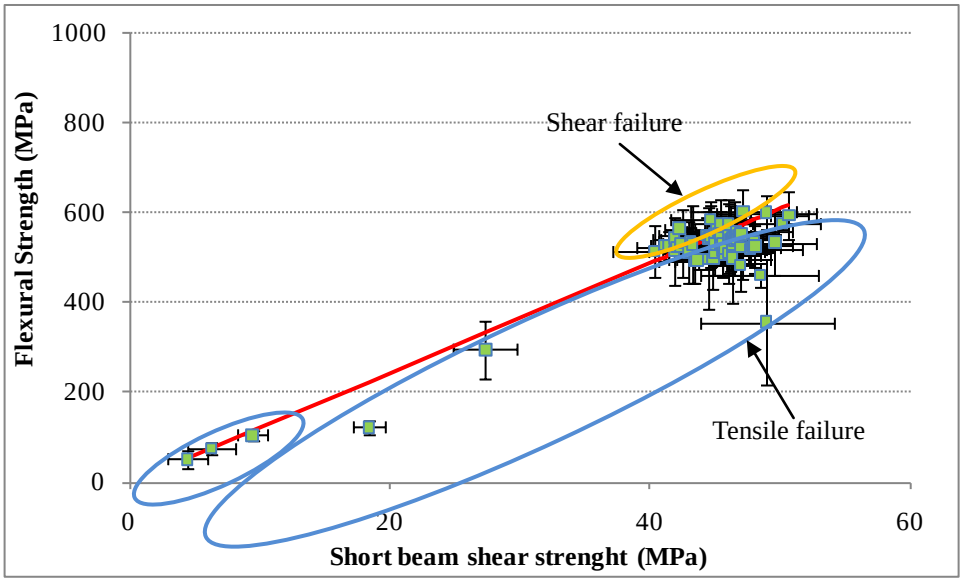

Figure 4-39: Boundary between interlaminar shear and flexural tension. L/h = $6.09(\sigma^{*}>12.17F^{sbs})$.

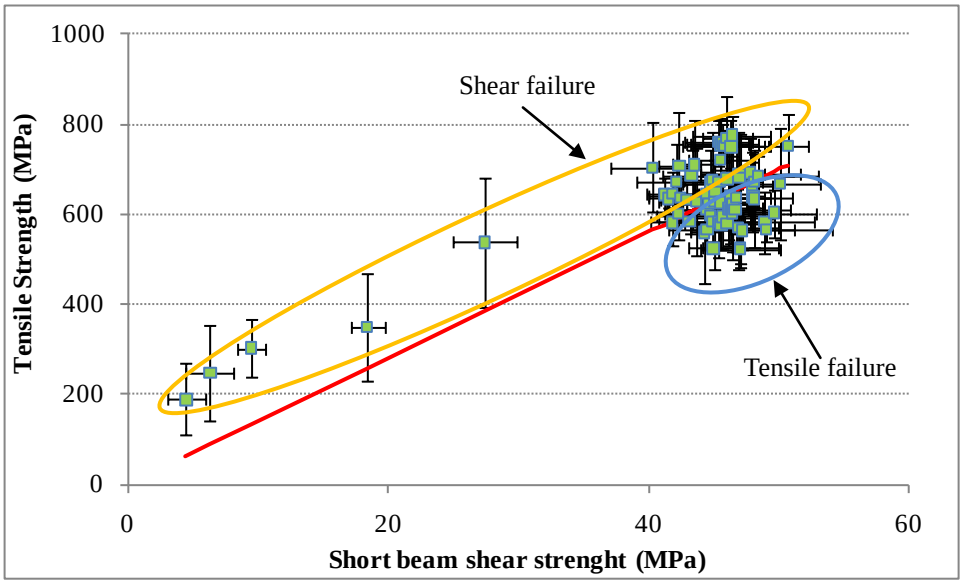

Figure 4-40: Boundary between interlaminar shear and pure tension. L/h = $6.09(\sigma^{*}>12.17F^{sbs})$.

5 Thermal Analysis

In general, thermal analysis refers to a variety of techniques in which properties of test specimens are continuously measured as the sample is programmed through a predetermined temperature profile. Therefore, thermal analysis can be used to characterize the physical and chemical properties of composite materials under conditions that simulate various environments. In particular, since polymers used in composite materials experience a diversity of properties according to temperatures, thermal analysis is necessary technique to assess the composite systems of this study focused on properties after exposure to elevated temperatures and fire.

5.1 Dynamic Mechanical Thermal Analysis

5.1.1 Introduction

Dynamic Mechanical Thermal Analysis (DMTA) is a powerful and sensitive analytical technique to determine the characteristic properties of polymer composites. DMTA measurements over a range of temperatures provide valuable insight into the structure, morphology and viscoelastic behavior of polymer materials[59]. DMTA comes from the field of rheology including the deformation and flow of materials[60]. As described in Chapter 3.5.5, an instrument is used to apply an oscillatory force on a sample in a temperature-controlled chamber. The sinusoidal stress and strain can be occurred by an oscillatory force. The instrument measures the amplitude of the peak deformation of the sine wave and the phase shift between them to determine data with regard to modulus, viscosity, and damping. Three important parameters that can be

determined from DMTA are 1) storage modulus, which is a measure of the maximum energy stored in the material during one cycle of oscillation and which gives an indication of the stiffness behavior of the sample; 2) loss modulus, which is directly proportional to the amount of energy that has been dissipated as heat by the sample; and 3) a mechanical damping term, tan delta, which is the ratio of the loss modulus to the storage modulus and is related to the degree of molecular mobility in the material[42]. Beside three important parameters, storage and loss compliance, dynamic and complex viscosity, creep compliance, and the stress-relaxation modulus can be determined by DMTA. In the case of thermoset polymers, DMTA can provide not only the glass transition temperature but also information regarding relative crosslink density and interfacial adhesion.

During measurement of the storage and loss modulus and damping property of a polymer composite over a wide range of temperatures, glass transition can be clearly detected. The glass transition is a reversible change of the polymer composite between rubbery and glassy states. The glass transition temperature can be detected as a sudden and considerable change in the elastic modulus and an attendant peak in the tangent delta curve. Since this temperature show the significant change in rigidity that polymer composites experience, glass transition temperature is a key factor in evaluating the polymer composites.

Most commonly, DMTA are accomplished in a fixed frequency in which the response of a material is studied as a function of temperature only. However, multi-frequency testing is often used for calculating activation energy, which can reveal transitions in response and structural change in the polymer composites. By using multi-

frequency test data, Time–Temperature Superposition (TTS) can be used to make long-term time-dependent predictions of some of the properties of the material. The shifting is usually done using the Arrhenius model[61] or the Williams–Landel–Ferry (WLF) model[62], depending on the reference temperature used during the master curve construction.

5.1.2 Data Reduction

DMTA test was performed in accordance with ASTM D5418[43] using the single cantilever frame fixture since the thickness of specimens was not uniform and specimen was made by wet layup process. First of all, the glass transition temperatures can be obtained by peak tan δ or modulus data recorded from Rheometric Scientific dynamic mechanical thermal analyzer.

The storage modulus (or elastic modulus) is calculated as

$$E' = \frac{\sigma_0}{\varepsilon_0}\cos\delta \tag{5.1}$$

where:

E' = Storage Modulus

σ_0= applied stress

ε_0= maximum amplitude of the strain

δ = Phase angle

The loss modulus (or viscous modulus) is calculated as

$$E'' = \frac{\sigma_0}{\varepsilon_0} \sin \delta \tag{5.2}$$

where:

E" = Loss Modulus

The tangent delta (or tan δ) is the ratio of the loss modulus to the storage modulus. The loss tangent, tan δ is called the internal friction or damping coefficient and is the ratio of energy dissipated per cycle to the maximum potential energy stored during the cycle.

$$\tan \delta = \frac{E''}{E'} \tag{5.3}$$

5.1.3 Analyses and Results

5.1.3.1 Glass transition temperature

Identifying the glass transition and how various system modifications affect glass transition temperature is a major application for DMTA. The glass transition is easily identified from dynamic mechanical data because of the sharp decrease in storage modulus, and the corresponding loss dispersion in E" or tan δ that occur at glass transition temperature[63]. In general glass transition temperature, also changes based on the frequency used in testing and the rate of heating used. An increase in the heating rate is known to shift T_g to a higher temperature and an increase in test frequency for a constant heating rate also results in the increase of T_g[41].

Glass transition temperatures based on peak tan δ determined at different frequencies (0.3, 1, 3, 10, and 30Hz) on longitudinal and transverse test specimens after exposure to elevated temperatures are represented in Table 5-1. In addition, changes in glass transition temperature based on peak tangent delta as a function of time at fixed temperatures are shown in Figure 5-1 and Figure 5-2 shows the Schematic diagram for detecting the glass transition temperature at peak tangent delta. As shown in Table 5-1, glass transition temperatures determined from both fiber oriented test specimens showed very similar data for all environmental conditions. However, because specimens were tested in bending with single cantilever fixture in longitudinal direction, glass transition temperatures were slightly delayed compared to transverse test specimens. Thermal ageing initially caused a significant T_g increase, which is attributed to the post-cure effect on ambient cured system. As known in previous study, glass transition temperature of an epoxy resin is directly relevant to the reached crosslinkage[64]. T_gs showed no change by post-curing effect in ambient condition. In the ranges of lower exposure temperatures (66, 93 and 121℃), glass transition temperatures continuously increased as ageing time went up and the amounts of increase of the glass transition temperature by post-cure effect were 42.6, 67.2 and 69.1%, respectively. In the ranges of intermediate exposure temperatures (149, and 177℃), glass transition temperatures slightly started to decrease after reaching the maximum value. On the contrary, under 204 and 232℃ condition, glass transition temperatures rapidly decrease due to serious polymer structural breakage. Under 260℃ condition, glass transition temperatures dramatically decreased by thermal degradation. In the conditions of more than 24 hrs of ageing time at 260℃, DMTA was not performed since test specimens were broken in

the process of tests. The measured glass transition temperatures did not reflect the effect of the oxidation of the specimen surfaces. Therefore, specimens aged at low temperatures showed stable values in glass transition temperature after initial increase.

Glass transition is strongly influenced by the rate or frequency of mechanical energy input due to kinetic. It is well known that substantial molecular relaxation involving cooperative segmental motions of the polymer chains occurs in the region of glass transition temperature. The rate of this segmental motion depends on temperature, so that if the test frequency is increased, the relaxations corresponding to the glass transition is hard to reflect the mechanical strain input, and the polymer composites may have rigid property[63]. Therefore, glass transition temperatures increase as the rate of frequency is increased as shown in Figure 5-1. Figure 5-3 showed the height of tan δ at different frequencies of test specimen exposed to 121℃ for 4 hrs. It should be pointed out that glass transition at peak tan δ was shifted to high temperature range and was broaden in the peak as the rate of frequencies were increased. This is related to a broadening of the relaxation spectrum in the glass transition temperature.

Table 5-1: T_g based on the peak of tangent delta determined from longitudinal and transverse test specimens after exposure to elevated temperatures

Exposure Temperature	Time	T_g(℃)-Longitudinal					T_g(℃)-Transverse				
		0.3Hz	1Hz	3Hz	10Hz	30Hz	0.3Hz	1Hz	3Hz	10Hz	30Hz
Ambient (23℃)	0	68.30	68.55	71.65	74.05	78.39	68.47	68.66	70.61	74.63	80.22
	1	63.89	68.75	72.68	76.64	79.33	63.79	69.53	72.38	74.89	79.30
	2	66.75	68.64	71.94	77.03	79.39	66.39	66.90	71.60	75.97	80.18
	4	64.88	69.29	73.29	74.58	77.46	63.02	67.95	73.75	73.86	81.99
	8	64.12	66.67	71.70	75.59	77.29	62.54	68.44	70.93	74.82	81.71
	16	64.29	68.95	70.25	72.63	76.50	65.46	68.95	72.54	75.44	81.55
	24	62.22	66.45	71.39	72.97	75.34	64.18	69.64	75.45	76.15	81.31
	48	64.04	67.84	70.31	73.01	75.35	71.56	71.95	73.74	78.72	84.39
	72	64.15	68.82	71.81	74.88	78.58	66.17	68.08	75.25	78.52	81.83
66℃	1	79.52	85.73	87.13	89.98	94.72	79.72	82.68	86.78	89.25	93.75
	2	84.05	84.27	87.38	91.22	95.11	80.67	82.90	88.74	93.68	97.27
	4	87.19	90.85	95.07	95.16	99.07	86.85	90.38	91.97	97.09	102.89
	8	94.86	95.94	97.10	98.79	104.09	88.15	92.02	95.56	99.33	103.00
	16	96.55	96.80	100.40	102.13	105.98	95.12	97.71	100.02	104.46	107.86
	24	98.80	100.13	100.24	102.22	106.80	93.07	96.08	98.37	101.17	103.38
	48	94.94	97.77	99.25	100.89	104.71	97.54	99.57	99.71	104.11	107.10
	72	97.44	100.12	102.62	104.43	107.45	103.80	104.01	104.15	108.76	112.96
93℃	1	89.61	93.09	98.01	101.33	104.33	92.17	93.86	97.59	102.75	105.46
	2	92.99	99.00	100.30	101.57	105.58	96.98	106.02	106.14	109.38	109.51
	4	99.55	104.49	107.31	110.25	112.62	107.20	106.59	109.97	112.78	118.42
	8	102.51	106.81	107.77	111.96	115.32	107.16	108.91	110.04	113.47	117.09
	16	102.73	107.50	112.08	114.38	115.90	108.24	111.53	113.31	117.56	121.86
	24	107.94	111.46	112.97	115.84	119.18	109.76	111.50	112.79	116.64	119.81
	48	113.53	113.89	116.05	118.52	120.90	113.51	115.19	116.75	119.26	124.64
	72	114.25	114.41	116.25	118.76	121.10	112.45	115.40	118.20	118.91	122.47
121℃	1	97.45	103.08	106.18	111.29	114.25	103.59	106.88	110.15	114.82	117.57
	2	98.50	104.05	109.96	113.99	116.00	104.12	106.81	110.87	114.29	117.62
	4	109.10	113.84	116.28	119.04	121.19	109.79	113.14	117.93	122.54	126.22
	8	111.53	117.32	117.45	122.21	124.58	111.12	115.47	119.52	122.09	124.51
	16	109.15	113.83	113.96	118.25	120.74	11.08	113.10	115.33	119.72	122.58
	24	109.23	115.30	116.63	118.71	121.82	108.18	113.97	116.22	119.32	124.64
	48	115.50	120.24	120.44	124.14	127.38	115.25	118.25	121.84	125.08	127.29
	72	114.58	120.85	119.80	124.97	127.33	115.42	119.59	119.73	123.48	128.46
149℃	1	110.43	115.56	116.52	119.06	121.24	110.71	112.40	115.70	120.94	123.95
	2	114.14	117.60	117.73	122.22	125.98	115.72	118.40	119.43	123.27	125.53
	4	113.49	117.18	117.31	121.79	124.21	114.45	119.74	118.37	124.93	127.23
	8	110.83	115.48	118.77	120.38	122.59	114.20	115.81	117.09	119.69	123.38
	16	115.91	121.17	121.27	124.39	127.53	118.98	120.80	120.93	125.23	129.92
	24	107.46	110.23	114.38	116.65	118.36	108.89	115.55	114.58	116.87	121.28
	48	108.12	113.21	113.19	118.29	119.64	112.96	115.49	116.77	120.94	125.27
	72	108.66	113.41	113.62	115.89	119.28	109.44	112.93	114.57	119.18	123.03

Table 5-1: Continued

Exposure Temperature	Time	T_g(℃)-Longitudinal					T_g(℃)-Transverse				
		0.3Hz	1Hz	3Hz	10Hz	30Hz	0.3Hz	1Hz	3Hz	10Hz	30Hz
177℃	1	107.52	113.47	113.69	117.42	120.53	109.92	110.14	113.70	117.81	122.10
	2	108.37	113.53	114.88	116.63	119.79	112.30	113.91	117.75	120.91	123.23
	4	109.45	113.90	114.02	118.53	121.77	109.09	112.08	114.78	118.77	121.65
	8	107.83	112.74	113.90	117.05	120.28	110.29	112.77	114.83	118.10	123.30
	16	111.00	114.60	115.97	118.88	121.93	111.23	114.02	115.42	120.08	122.32
	24	106.08	112.26	115.03	118.12	119.33	111.97	114.42	114.56	117.34	121.24
	48	111.56	112.97	114.94	117.48	119.08	103.00	109.12	114.23	116.09	121.99
	72	108.94	110.45	113.64	117.44	118.66	109.07	112.70	115.44	118.05	122.48
204℃	1	107.97	113.08	115.17	116.09	119.15	107.31	109.34	113.21	115.93	119.74
	2	112.34	112.70	114.14	117.68	120.09	110.84	112.43	111.14	115.92	119.02
	4	105.74	109.19	111.87	113.63	117.51	103.57	109.67	111.28	115.87	118.10
	8	109.98	111.92	114.79	117.22	120.16	108.62	110.36	112.00	115.32	119.69
	16	110.53	110.00	111.06	111.96	116.25	102.44	108.63	110.21	114.26	117.78
	24	106.63	107.75	111.28	113.68	116.91	101.54	106.63	109.79	112.31	115.66
	48	99.54	102.04	102.98	108.51	110.79	100.62	104.37	108.80	110.45	113.29
	72	103.39	105.64	109.07	112.37	114.56	96.54	100.69	103.71	108.13	110.29
232℃	1	107.48	112.91	112.27	115.39	119.29	109.71	111.39	114.93	119.31	122.27
	2	106.51	107.78	109.69	111.59	114.96	102.24	107.42	106.52	110.77	114.01
	4	103.45	108.56	109.61	113.90	115.39	103.96	109.88	116.00	116.12	120.57
	8	105.25	103.43	105.57	109.14	111.55	96.94	101.63	105.87	109.90	112.11
	16	91.14	98.73	101.69	103.26	106.36	90.66	96.70	99.47	103.34	105.57
	24	92.32	96.37	98.22	100.48	103.68	88.23	90.35	94.28	98.96	101.96
	48	86.24	90.57	89.94	95.44	98.63	82.43	84.74	92.89	96.05	101.74
	72	87.33	87.61	92.37	94.14	98.05	78.48	80.16	90.10	94.26	97.14
260℃	1	101.15	103.40	104.45	109.00	112.31	101.22	107.42	103.86	108.84	113.96
	2	99.00	99.30	102.77	104.57	107.68	95.12	98.70	98.83	102.58	106.29
	4	86.49	88.96	90.24	93.27	97.14	85.50	88.85	90.55	96.95	99.84
	8	68.80	71.23	81.70	81.80	86.03	75.53	80.74	85.72	89.18	93.08
	16	72.98	72.24	78.11	80.99	85.26	70.42	74.88	78.11	84.35	87.83
	24	71.71	71.53	78.06	84.28	90.29					

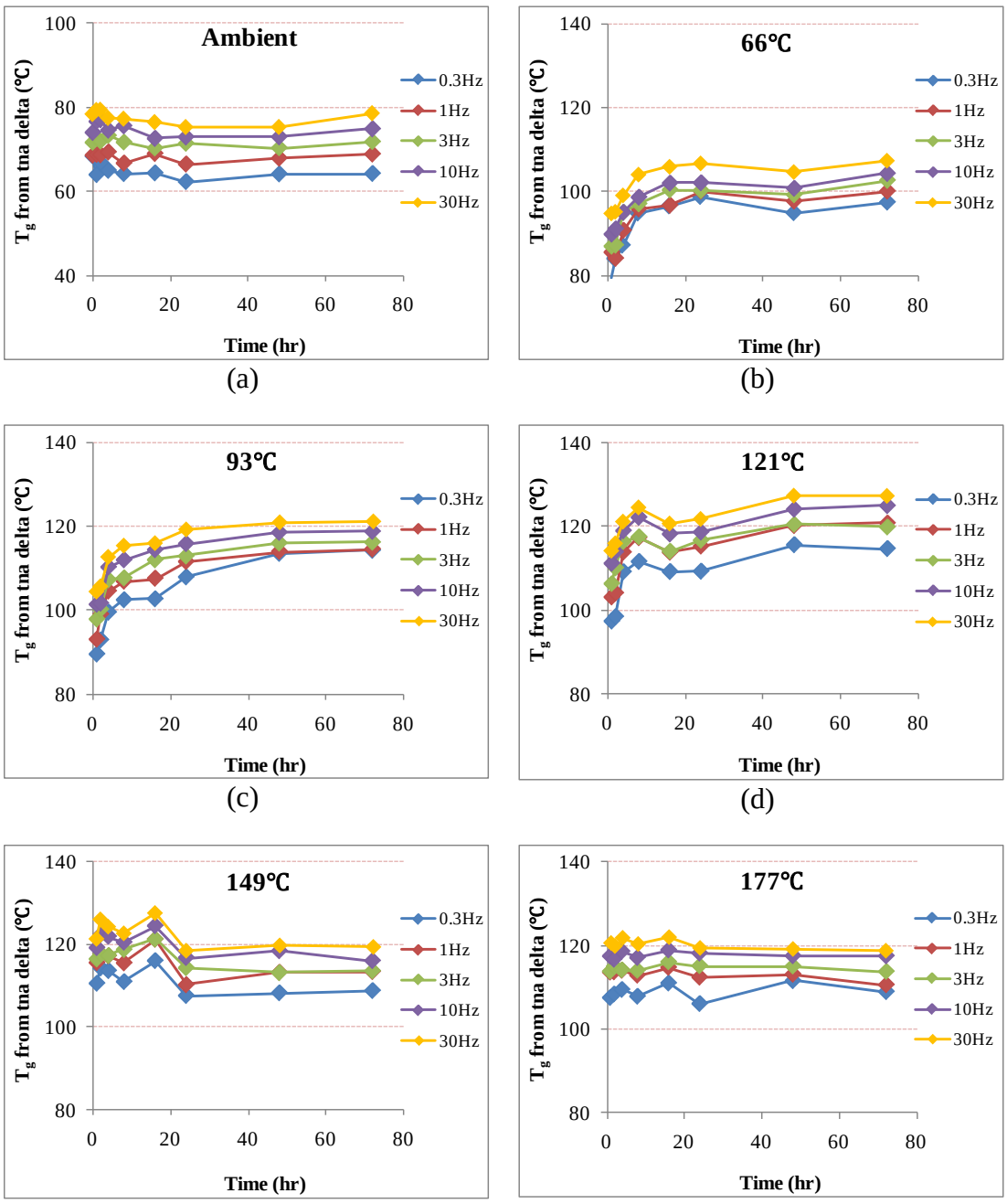

Figure 5-1: Change in T_g based on peak tangent delta as a function of time at fixed temperatures, (a) ambient (b) 66℃ (c) 93℃ (d) 121℃ (e) 149℃ (f) 177℃ (g) 204℃ (h) 232℃ (i) 260℃

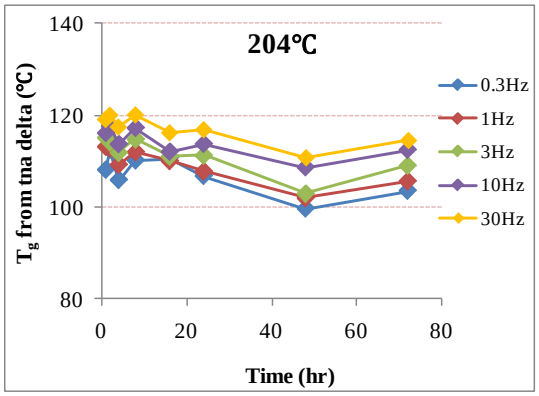

(g)

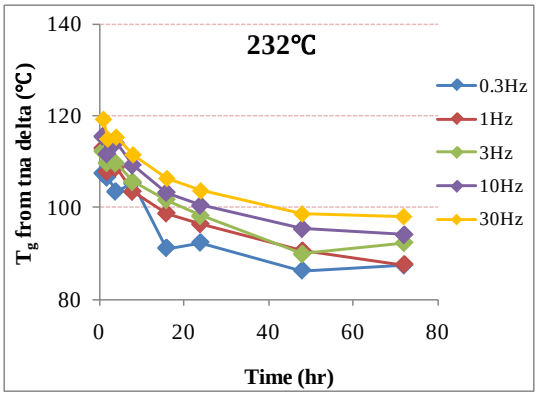

(h)

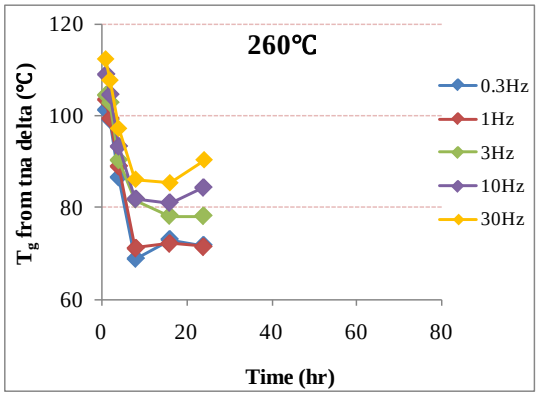

(i)

Figure 5-1: Continued

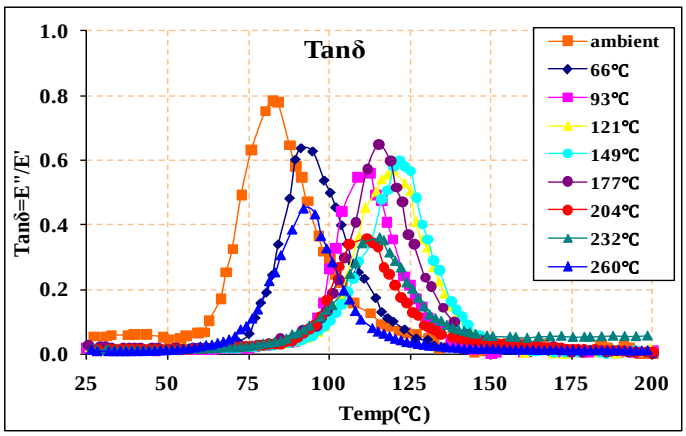

Figure 5-2: Schematic diagram for detecting the glass transition temperature at peak tangent delta in conditions of elevated temperatures for 4 hrs

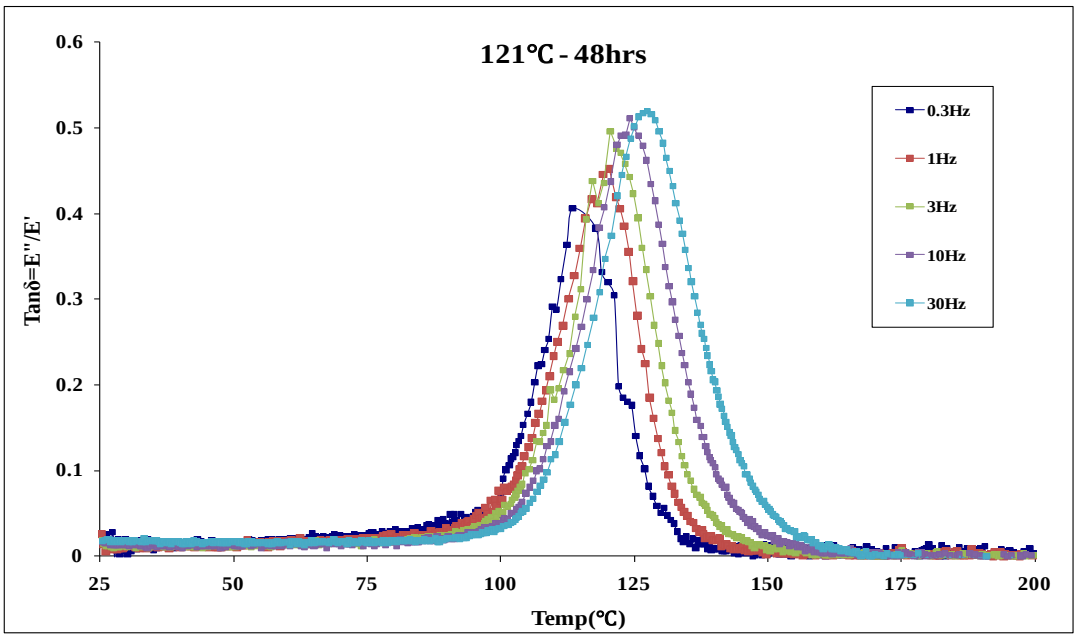

Figure 5-3: Height of tangent delta at different frequencies of test specimen exposed to 121℃ for 4 hrs

Beside the method using the peak tan δ, glass transition temperature can be detected by the inflection point in the middle portion of the storage modulus profile. An analysis program of Rheometric Scientific Instruments Orchestrator can be used to detect the first derivative of the storage modulus curve, which is typically a parabolic curve. Analysis of the midpoint of the parabolic curve yields the glass transition temperature based on the storage modulus as shown in Figure 5-4. Glass transition temperatures obtained by storage modulus were lower than those of peak tan δ in all conditions. Table 5-2 and Figure 5-5 show the comparison of glass transition temperatures determined by peak tangent delta at 1Hz and storage modulus on longitudinal and transverse test specimens. As the glass transition temperatures were increased due to post-cure effect, the differences between both values occurred. In this study, the values determined by peak tan δ at 1Hz will be used as a representative glass transition temperature. The reason why 1Hz values were used is that these values are close to the glass transition temperatures determined by other widely used methods such as Differential Scanning Calorimetry (DSC), dilatometry, and Thermomechanical Analysis (TMA).

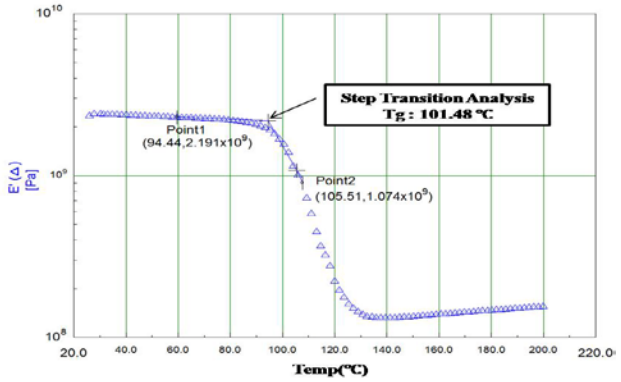

Figure 5-4: Schematic diagram for detecting the glass transition temperature from storage modulus (Exposure temperature: 93℃, Ageing time: 72hr)

Table 5-2: Comparison of glass transition temperatures determined by peak of tangent delta at 1Hz and storage modulus from longitudinal and transverse test specimens

Exposure Temperature	Time	T_g(℃)-Longitudinal		T_g(℃)-Transverse		Exposure Temperature	T_g(℃)-Longitudinal		T_g(℃)-Transverse	
		1Hz	E'	1Hz	E'		1Hz	E'	1Hz	E'
Ambient (23℃)	0	68.55	60.35	68.66	61.11	66℃				
	1	68.75	57.46	69.53	60.50		85.73	80.12	82.68	72.53
	2	68.64	68.15	66.90	58.54		84.27	80.04	82.90	77.15
	4	69.29	62.19	67.95	60.00		90.85	83.43	90.38	78.12
	8	66.67	65.64	68.44	58.07		95.94	84.95	92.02	83.84
	16	68.95	62.15	68.95	59.54		96.80	88.64	97.71	89.66
	24	66.45	61.25	69.64	60.23		100.13	90.54	96.08	88.31
	48	67.84	60.54	71.95	59.54		97.77	91.12	99.57	90.74
	72	68.82	61.16	68.08	60.12		100.12	92.34	104.01	93.06
93℃	1	93.09	91.07	93.86	87.50	121℃	103.08	97.07	106.88	100.15
	2	99.00	89.31	106.02	95.12		104.05	101.74	106.81	101.25
	4	104.49	98.87	106.59	101.46		113.84	105.12	113.14	105.34
	8	106.81	100.12	108.91	99.98		117.32	108.81	115.47	105.44
	16	107.50	103.58	111.53	102.70		113.83	105.40	113.10	104.86
	24	111.46	104.58	111.50	104.57		115.30	107.07	113.97	102.54
	48	113.89	106.31	115.19	104.64		120.24	111.84	118.25	107.62
	72	114.41	105.41	115.40	103.16		120.85	110.84	119.59	107.19
149℃	1	115.56	106.54	112.40	104.56	177℃	113.47	100.03	110.14	102.95
	2	117.60	109.64	118.40	106.30		113.53	102.45	113.91	104.43
	4	117.18	108.64	119.74	106.62		113.90	99.62	112.08	101.24
	8	115.48	103.05	115.81	106.24		112.74	103.33	112.77	101.99
	16	121.17	112.25	120.80	109.07		114.60	101.36	114.02	103.27
	24	110.23	101.58	115.55	103.20		112.26	101.41	114.42	101.19
	48	113.21	103.85	115.49	104.14		112.97	103.44	109.12	100.00
	72	113.41	103.89	112.93	102.34		110.45	98.97	112.70	99.87
204℃	1	113.08	102.22	109.34	101.21	232℃	112.91	100.00	111.39	105.90
	2	112.70	101.97	112.43	101.70		107.78	97.72	107.42	97.87
	4	109.19	100.01	109.67	102.06		108.56	97.98	109.88	98.90
	8	111.92	100.00	110.36	100.00		103.43	97.07	101.63	90.66
	16	110.00	96.36	108.63	98.52		98.73	83.24	96.70	82.95
	24	107.75	96.71	106.63	97.17		96.37	71.55	90.35	78.85
	48	102.04	86.61	104.37	95.51		90.57	68.20	84.74	80.27
	72	105.64	90.04	100.69	88.58		87.61	65.43	80.16	73.74
260℃	1	103.40	99.48	107.42	97.40					
	2	99.30	89.72	98.70	87.91					
	4	88.96	76.81	88.85	79.84					
	8	71.23	59.27	80.74	65.17					
	16	72.24	52.02	74.88	52.63					
	24	71.53	49.06							

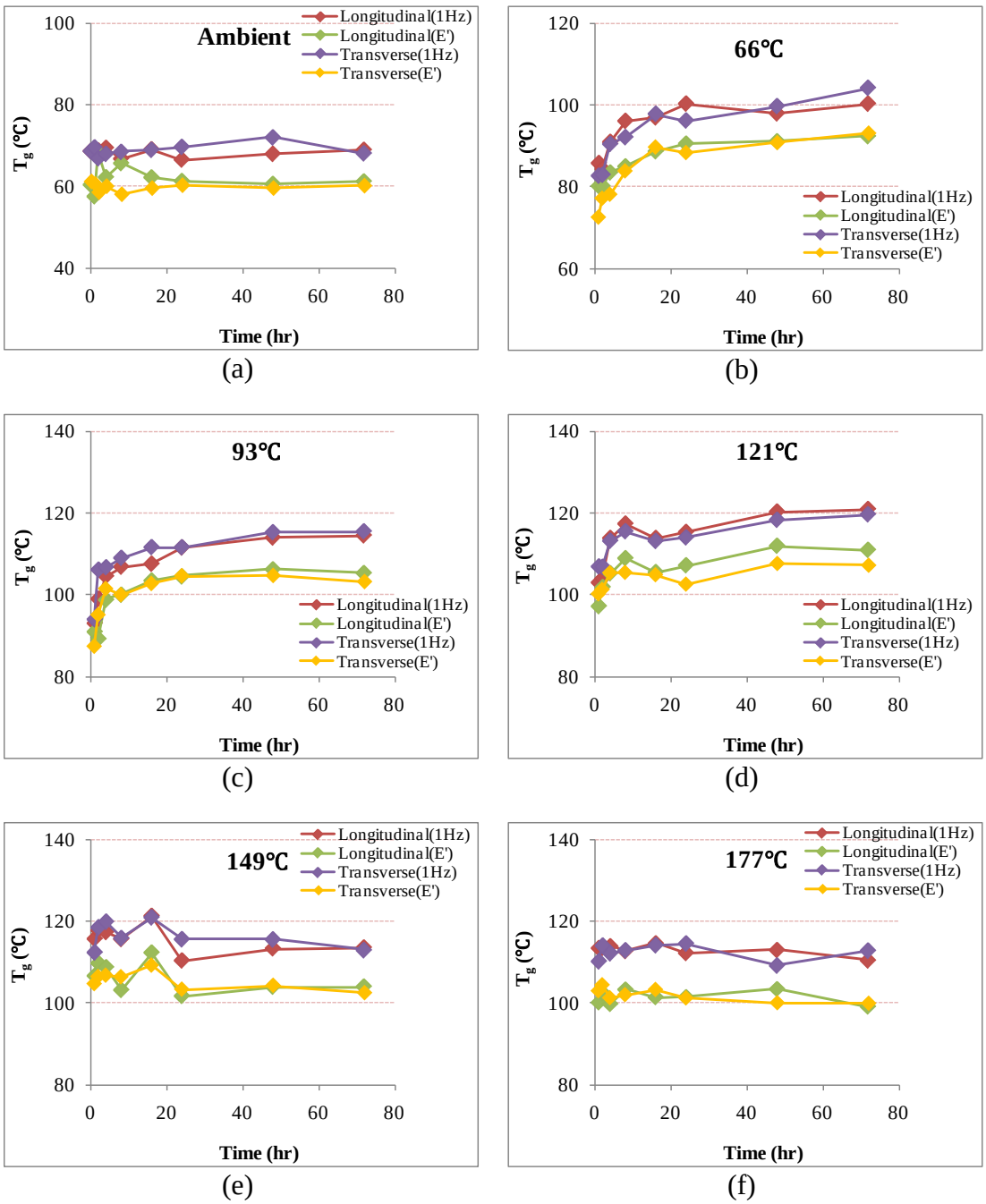

Figure 5-5: Difference in T_g based on peak tangent delta at 1Hz and storage modulus as a function of time at fixed temperatures, (a) ambient (b) 66°C (c) 93°C (d) 121°C (e) 149°C (f) 177°C (g) 204°C (h) 232°C (i) 260°C

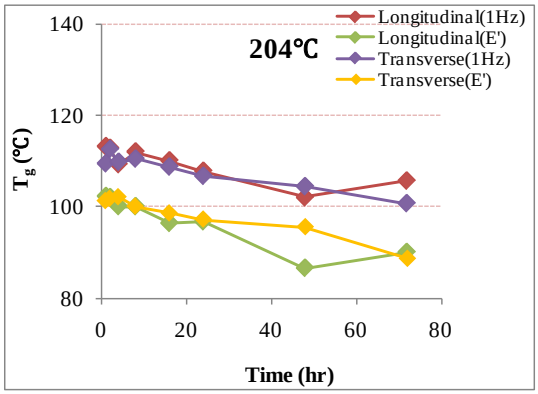

(g)

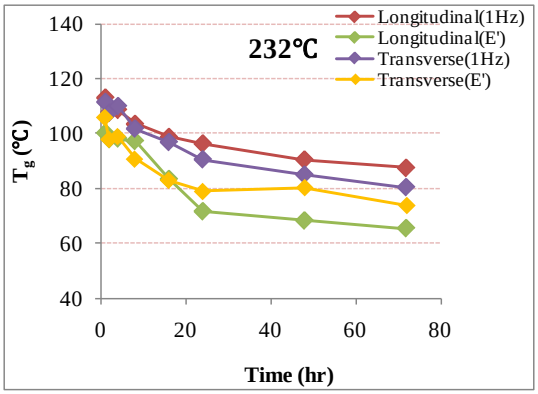

(h)

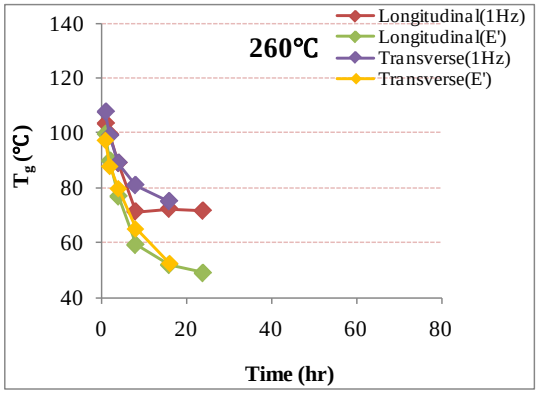

(i)

Figure 5-5: Continued

5.1.3.2 Height of Tangent Delta

The tan δ curve provides information about the ability of a material to lose energy due to molecular rearrangements and internal friction. Moreover, this value reflects the energy dissipation ratio during dynamic strain cycles, and is relevant to the amount of epoxy chain segments undergoing the glass transition.

The storage modulus moved to higher temperature range without changing the shape or slope of change between elastic and viscoelastic region as shown in Figure 5-6. In addition, the loss modulus shifted to higher temperatures and the level of the peak loss modulus also was increased with increase in test frequency as depicted in Figure 5-7. As described in data reduction section of chapter 5, since the tan δ is the ratio of the loss modulus to the storage modulus, the values of tan δ and glass transition temperatures shifted to higher levels with increase in test frequency as shown in Table 5-1.

The height of the tan δ curve is related to interfacial adhesion performance[65]. An increase in damping loss is correlated to a loss in interfacial adhesion since perfect bonding between fibers and matrix restrict the mobility of the polymer structure, leading to a rapid response when a load is applied. Therefore, as the fiber/matrix bond performance increase, the height of peak tan δ decreases. In other words, in case post-cure effect contributes to increase of interfacial bonding, broadened transition region and decreased tan δ value are observed due to the stiffness or rigid of test specimen. Table 5-3 and Figure 5-8 show the variation of the height of peak tan δ at different frequencies as a function of ageing time for both longitudinal and transverse specimens. All specimens exposed to ambient temperature showed higher height of peak tan δ

compared to other conditions. This phenomenon was attributed to increase of mobility since fully-cure was not applied for specimens. In ranges of lower exposure temperatures, the heights of peak tan δ continued to decrease up to 72 hrs of ageing time due to residual post-cure effect. During the thermooxidative process occur, initially, the small molecules will diffuse out and evaporate into air, and the residual post-cure effect will be occurred leading to high crosslinkage. All those reactions definitely reduce epoxy segments undergoing the glass transitions, responsible for the abrupt depression of the height of tan δ peak.

Figure 5-9 shows comparison of the height of tangent delta at 1Hz on longitudinal and transverse test specimens as a function of time at fixed temperatures. From this figure, the heights of peak tan δ on specimens in transverse direction were extremely higher than in longitudinal direction. The reason why the transverse specimens showed tan δ peaks of higher value compared to the longitudinal specimens is that fibers in longitudinal specimen result in the interruption of mobility on specimens when a load is applied.

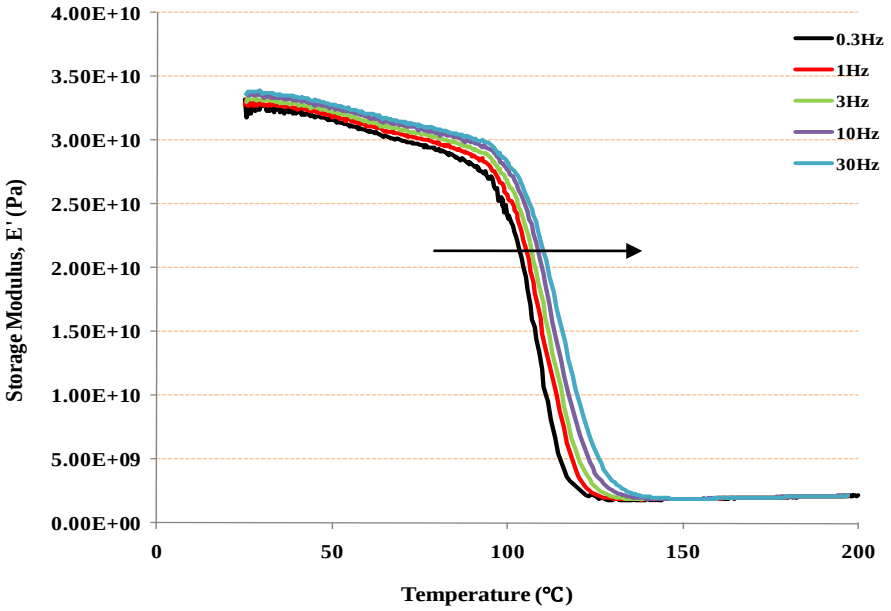

Figure 5-6: Effect of test frequency on storage modulus (specimen exposed to 121℃ for 4 hrs)

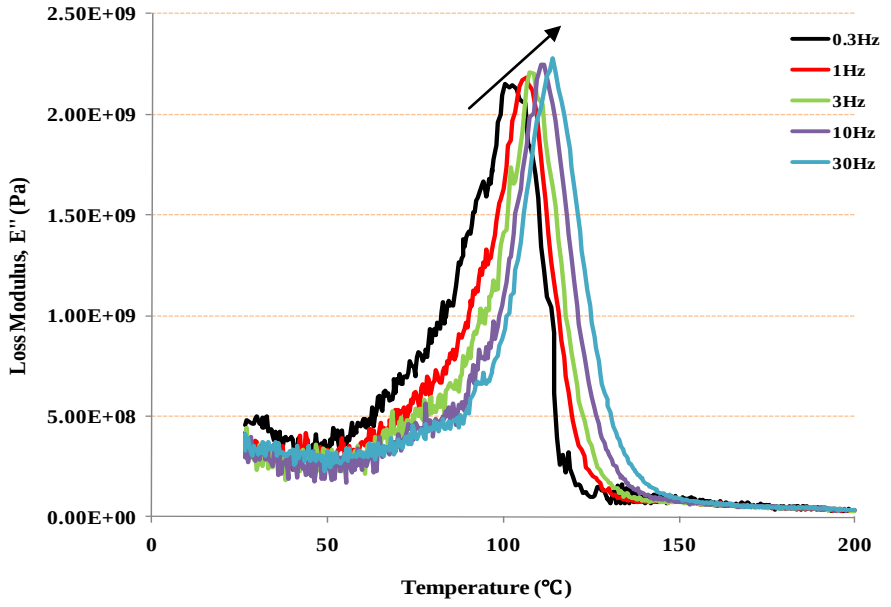

Figure 5-7: Effect of test frequency on loss modulus (specimen exposed to 121℃ for 4 hrs)

Table 5-3: Height of tangent delta at the different frequencies on longitudinal and transverse test specimens after exposure to elevated temperatures

Exposure Temperature	Time	Height of tangent delta -Longitudinal					Height of tangent delta -Transverse				
		0.3Hz	1Hz	3Hz	10Hz	30Hz	0.3Hz	1Hz	3Hz	10Hz	30Hz
Ambient (23℃)	0	0.633	0.825	0.760	0.729	0.714	0.821	0.847	0.913	0.878	0.928
	1	0.598	0.645	0.601	0.578	0.588	0.945	1.060	0.945	0.986	1.004
	2	0.624	0.631	0.609	0.603	0.600	1.064	0.944	1.043	1.023	1.057
	4	0.648	0.664	0.724	0.760	0.761	0.880	0.901	0.948	0.972	0.984
	8	0.585	0.634	0.699	0.703	0.718	0.871	0.894	0.934	1.071	1.111
	16	0.615	0.649	0.683	0.685	0.698	0.887	0.900	0.925	0.965	1.025
	24	0.641	0.693	0.713	0.731	0.728	0.900	0.902	0.915	0.925	0.953
	48	0.598	0.603	0.661	0.665	0.665	0.791	0.800	0.805	0.830	0.864
	72	0.625	0.645	0.687	0.704	0.699	0.785	0.792	0.817	0.858	0.909
66℃	1	0.634	0.737	0.680	0.701	0.776	0.854	0.955	0.993	0.954	0.950
	2	0.665	0.687	0.708	0.697	0.688	0.796	0.871	0.876	0.883	0.892
	4	0.612	0.608	0.622	0.646	0.639	0.712	0.784	0.780	0.774	0.815
	8	0.568	0.581	0.592	0.596	0.682	0.832	0.865	0.850	0.861	0.866
	16	0.565	0.590	0.571	0.583	0.586	0.710	0.728	0.795	0.793	0.804
	24	0.585	0.575	0.583	0.579	0.582	0.761	0.835	0.878	0.886	0.895
	48	0.591	0.609	0.615	0.614	0.603	0.685	0.719	0.765	0.814	0.835
	72	0.595	0.570	0.619	0.634	0.632	0.583	0.657	0.672	0.684	0.757
93℃	1	0.449	0.454	0.481	0.458	0.461	0.701	0.730	0.693	0.698	0.754
	2	0.490	0.526	0.551	0.547	0.548	0.654	0.664	0.611	0.644	0.666
	4	0.436	0.448	0.457	0.459	0.477	0.624	0.647	0.633	0.658	0.686
	8	0.521	0.546	0.545	0.545	0.546	0.642	0.684	0.680	0.665	0.687
	16	0.455	0.467	0.479	0.500	0.512	0.586	0.611	0.625	0.633	0.653
	24	0.471	0.489	0.537	0.546	0.552	0.602	0.655	0.655	0.641	0.659
	48	0.487	0.443	0.466	0.489	0.494	0.596	0.616	0.623	0.633	0.660
	72	0.442	0.460	0.460	0.491	0.507	0.661	0.538	0.560	0.577	0.633
121℃	1	0.512	0.537	0.542	0.556	0.566	0.571	0.590	0.623	0.647	0.694
	2	0.501	0.549	0.523	0.514	0.520	0.602	0.638	0.691	0.688	0.708
	4	0.492	0.501	0.540	0.561	0.575	0.569	0.631	0.667	0.677	0.713
	8	0.441	0.446	0.483	0.501	0.508	0.552	0.610	0.644	0.664	0.698
	16	0.461	0.486	0.538	0.551	0.560	0.581	0.605	0.620	0.631	0.662
	24	0.469	0.504	0.513	0.553	0.568	0.508	0.551	0.587	0.595	0.660
	48	0.450	0.452	0.496	0.512	0.520	0.602	0.636	0.627	0.659	0.689
	72	0.505	0.529	0.519	0.544	0.562	0.636	0.667	0.679	0.673	0.714
149℃	1	0.475	0.496	0.530	0.557	0.570	0.631	0.654	0.646	0.652	0.691
	2	0.433	0.455	0.471	0.493	0.537	0.625	0.642	0.679	0.695	0.730
	4	0.481	0.506	0.552	0.566	0.579	0.625	0.633	0.646	0.657	0.692
	8	0.459	0.461	0.480	0.514	0.527	0.635	0.648	0.691	0.682	0.716
	16	0.501	0.518	0.518	0.562	0.570	0.591	0.617	0.630	0.656	0.709
	24	0.446	0.460	0.444	0.458	0.414	0.646	0.679	0.715	0.737	0.775
	48	0.501	0.514	0.525	0.524	0.538	0.640	0.672	0.683	0.656	0.693
	72	0.538	0.438	0.475	0.474	0.476	0.528	0.571	0.559	0.568	0.593

Table 5-3: Continued

Exposure Temperature	Time	Height of tangent delta -Longitudinal					Height of tangent delta -Transverse				
		0.3Hz	1Hz	3Hz	10Hz	30Hz	0.3Hz	1Hz	3Hz	10Hz	30Hz
177℃	1	0.495	0.514	0.526	0.531	0.544	0.621	0.638	0.618	0.640	0.665
	2	0.452	0.470	0.483	0.508	0.515	0.627	0.674	0.690	0.695	0.722
	4	0.462	0.476	0.471	0.481	0.502	0.650	0.653	0.671	0.726	0.756
	8	0.394	0.403	0.422	0.443	0.437	0.641	0.680	0.672	0.674	0.700
	16	0.390	0.416	0.421	0.425	0.434	0.433	0.453	0.465	0.453	0.473
	24	0.446	0.464	0.455	0.462	0.448	0.417	0.420	0.435	0.445	0.459
	48	0.358	0.367	0.392	0.406	0.422	0.359	0.344	0.346	0.355	0.366
	72	0.341	0.375	0.400	0.412	0.404	0.292	0.303	0.302	0.308	0.319
204℃	1	0.508	0.515	0.515	0.551	0.556	0.645	0.657	0.716	0.752	0.786
	2	0.418	0.439	0.451	0.446	0.454	0.581	0.597	0.601	0.603	0.626
	4	0.370	0.389	0.412	0.431	0.439	0.381	0.398	0.412	0.418	0.427
	8	0.345	0.354	0.376	0.380	0.387	0.327	0.359	0.353	0.352	0.365
	16	0.338	0.345	0.353	0.395	0.388	0.336	0.342	0.351	0.348	0.350
	24	0.319	0.306	0.317	0.326	0.333	0.324	0.334	0.332	0.330	0.361
	48	0.280	0.300	0.289	0.296	0.299	0.302	0.313	0.302	0.303	0.301
	72	0.294	0.314	0.326	0.340	0.341	0.301	0.312	0.300	0.301	0.300
232℃	1	0.385	0.394	0.408	0.425	0.428	0.519	0.534	0.542	0.534	0.592
	2	0.364	0.375	0.389	0.403	0.413	0.402	0.414	0.451	0.433	0.442
	4	0.345	0.358	0.362	0.377	0.386	0.332	0.363	0.367	0.372	0.378
	8	0.365	0.382	0.398	0.410	0.421	0.352	0.372	0.374	0.367	0.372
	16	0.385	0.407	0.412	0.395	0.409	0.378	0.389	0.375	0.362	0.342
	24	0.320	0.331	0.314	0.315	0.315	0.417	0.444	0.422	0.413	0.407
	48	0.305	0.323	0.332	0.325	0.329	0.313	0.334	0.332	0.329	0.329
	72	0.344	0.364	0.376	0.378	0.376	0.353	0.347	0.359	0.358	0.354
260℃	1	0.369	0.379	0.397	0.401	0.403	0.481	0.476	0.477	0.521	0.524
	2	0.475	0.477	0.520	0.517	0.518	0.470	0.474	0.470	0.463	0.466
	4	0.462	0.464	0.484	0.502	0.500	0.466	0.471	0.503	0.523	0.548
	8	0.525	0.545	0.568	0.568	0.557	0.409	0.403	0.386	0.390	0.397
	16	0.516	0.530	0.492	0.488	0.484	0.432	0.460	0.454	0.447	0.457
	24	0.534	0.536	0.503	0.488	0.483					

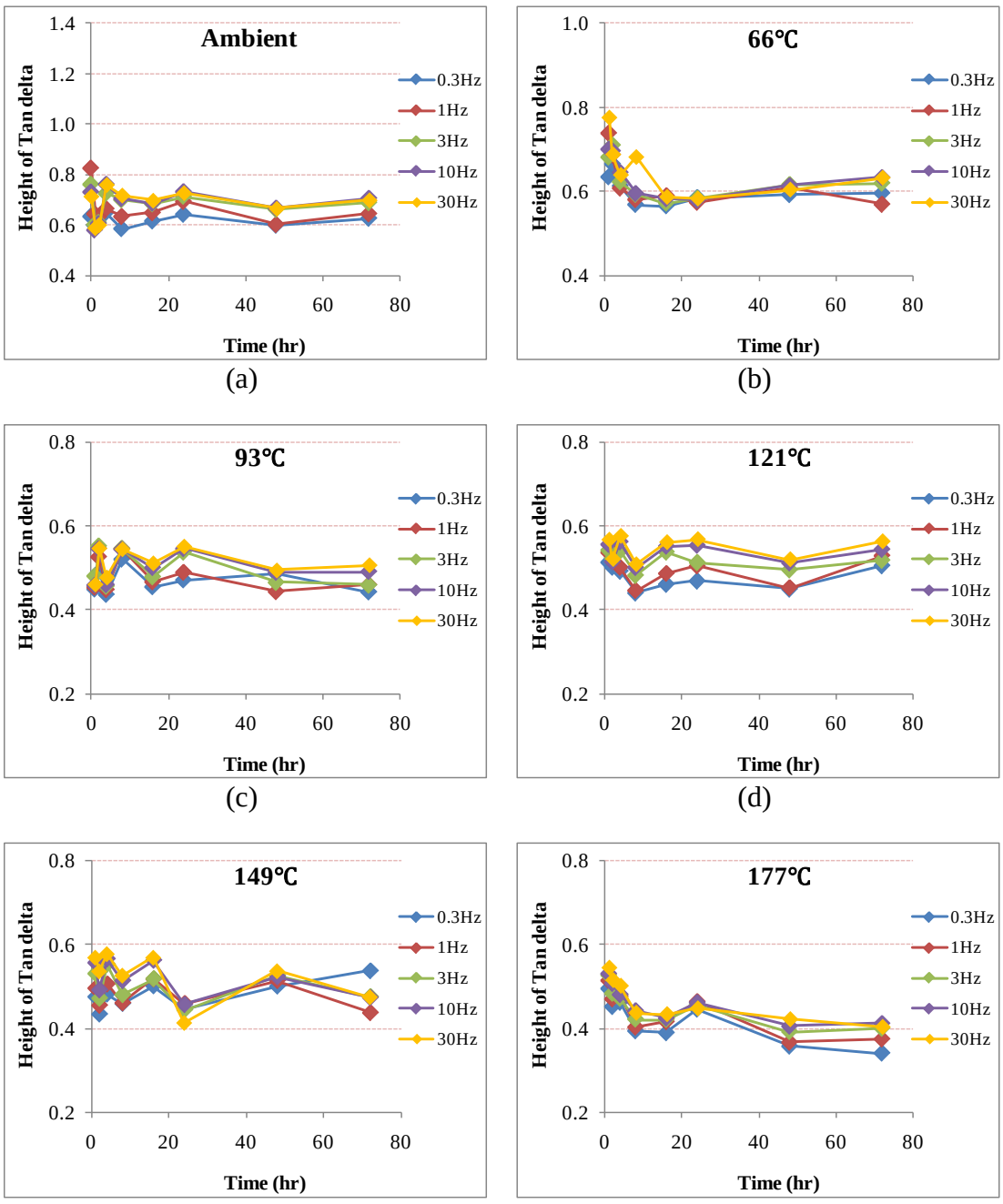

Figure 5-8: Difference of the peak of tangent delta at different frequencies on longitudinal test specimens as a function of time at fixed temperatures, (a) ambient (b) 66℃ (c) 93℃ (d) 121℃ (e) 149℃ (f) 177℃ (g) 204℃ (h) 232℃ (i) 260℃

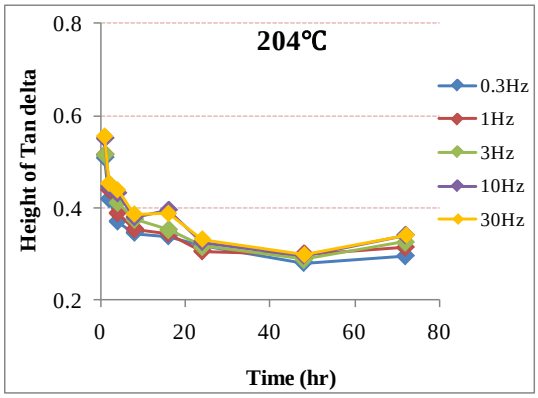

(g)

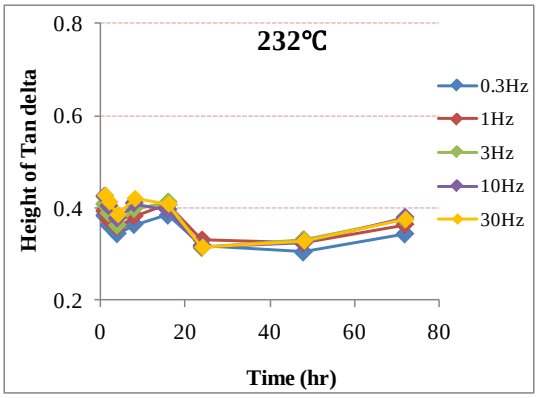

(h)

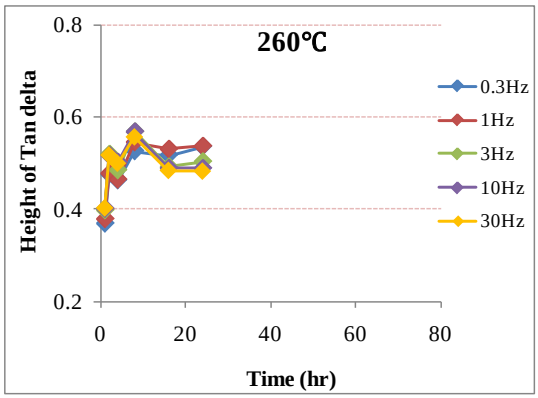

(i)

Figure 5-8: Continued

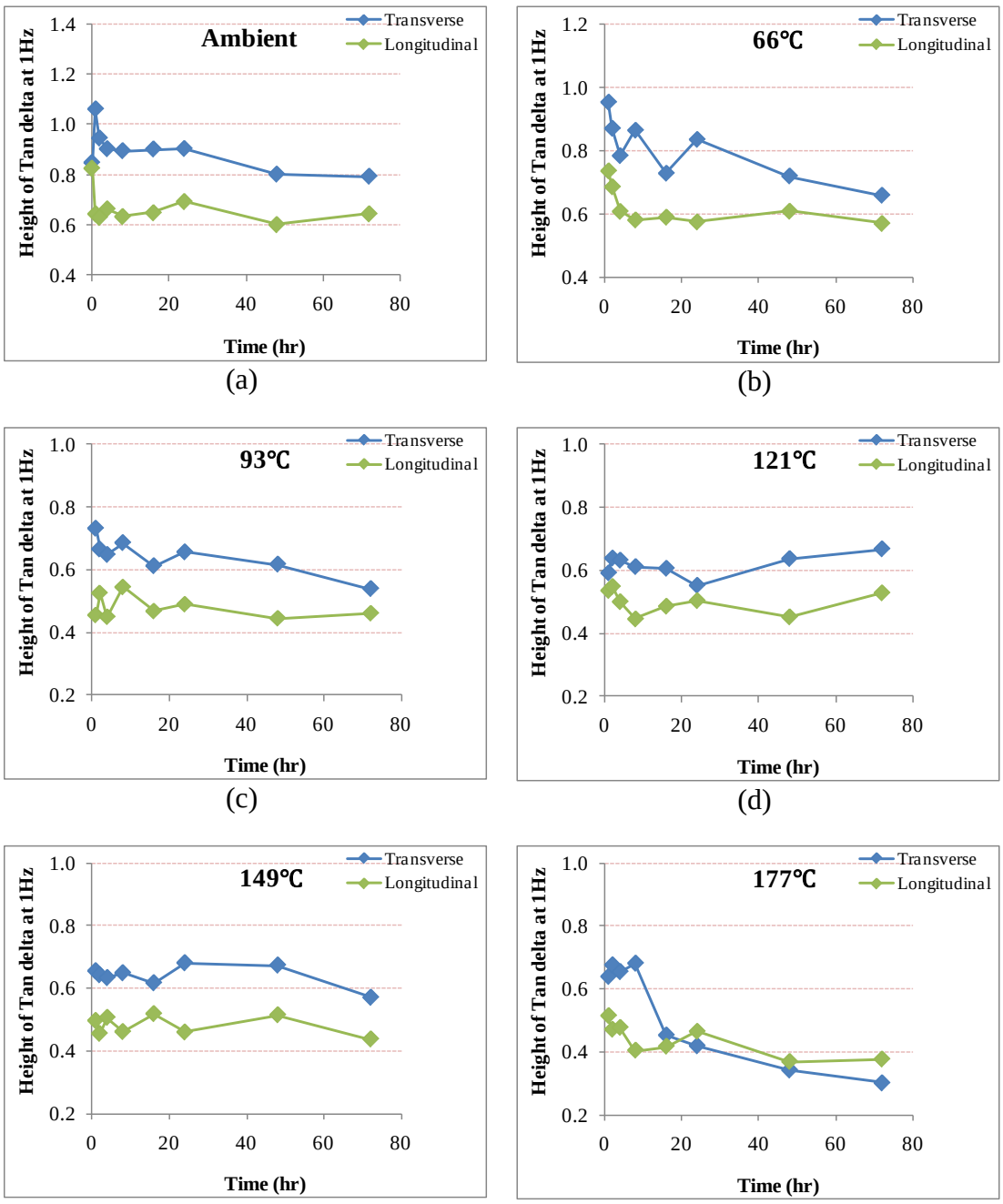

Figure 5-9: Comparison of the height of tangent delta at 1Hz from longitudinal and transverse test specimens as a function of time at fixed temperatures, (a) ambient (b) 66℃ (c) 93℃ (d) 121℃ (e) 149℃ (f) 177℃ (g) 204℃ (h) 232℃ (i) 260℃

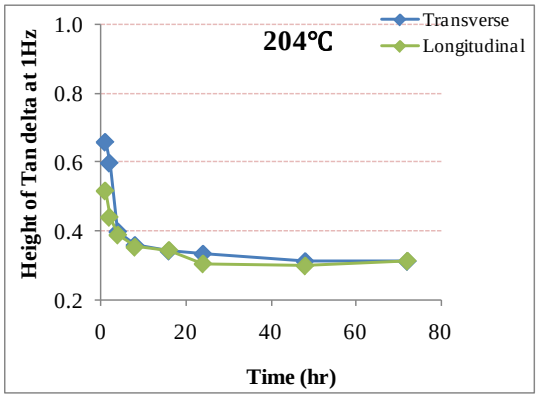

(g)

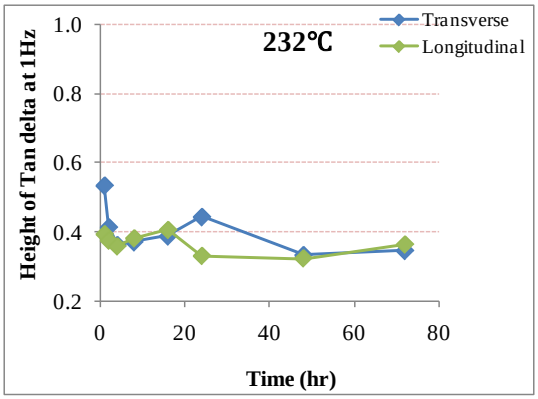

(h)

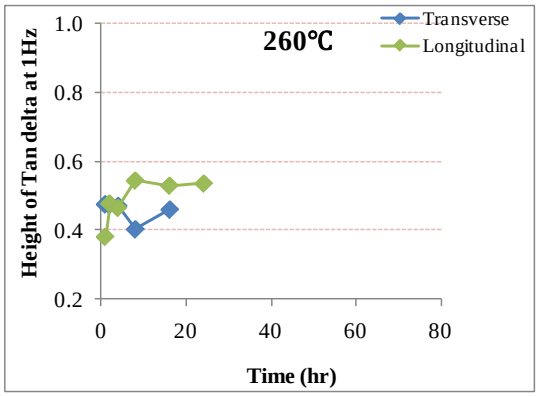

(i)

Figure 5-9: Continued

5.1.3.3 Activation Energy

The activation energy (ΔE_a) for glass transition can be obtained from the relationship between the shift of glass transition temperature and test frequency. The glass transition temperature reflects the relationship between the mobility of polymer chains and temperature while ΔE_a represents a relationship between mobility and time scale[39]. In addition, ΔE_a could be characterized as representing the energy barrier of glass transition relaxation.

Activation energy of the glass transition is calculated by Arrhenius relationship (time-temperature superposition principles) using superimposing either peak tan δ or E" determined over a range of frequencies.

$$f = Ae^{-(\Delta E_a / RT)} \tag{5.4}$$

where:

f = the frequency applied for DMTA test

A = a constant as the pre-exponet

R = universal gas constant

T = temperature at peak tan δ

The shift of glass transition temperatures can be related to the different frequencies from following equation.

$$\frac{f_1}{f_2} = \frac{e^{-(\Delta E_a / RT_{g1})}}{e^{-(\Delta E_a / RT_{g2})}} \tag{5.5}$$

Where:

f_1 and f_2 are corresponding values of the glass transition temperature T_{g1} and T_{g2},

respectively. Equation 5.5 can simply be changed as

$$\Delta E_a = -R\left[\frac{d(\ln f)}{d(\frac{1}{T_g})}\right] \tag{5.6}$$

The value of ΔE_a can be found by plotting the natural logarithm of the frequency against the reciprocal of the glass transition temperature. Consequently, ΔE_a is yielded by multiple of the slope of curve and the universal gas constant. Activation energies are summarized on longitudinal and transverse specimens in Table 5-4 and Figure 5-10 shows comparison of the activation energy on longitudinal and transverse test specimens as a function of time at fixed temperatures.

Activation energies were continuously increased up to 72 hrs of ageing time in the ranges of lower exposure temperatures (66, 93, 121 and 149℃). Continuous increases were attributed to residual post-cure effect, which leaded to an intense crosslinkage and the mobility of the polymer segment was constrained significantly. In ranges of intermediate temperatures (177, 204 and 232℃), activation energies were leveled off after initially reaching to the maximum value. In light of level off, since the breakage of polymer crosslinkage was responsible for shifting easily to glass transition as the exposure temperature and ageing time were increased, activation energies were decreased. As expected, activation energies in higher exposure temperature (260℃) were catastrophically decreased in ageing time of more than 8 hrs.

Moreover, the longitudinal specimens showed higher activation energy than the transverse specimens. It should be noted that the mobility of the epoxy matrix in the unidirectional specimens is interrupted by the fibers and require more energy for the

glass transition. As the fully cure was progressed, the differences on activation energy between the longitudinal and transverse specimens were more severe compared to unaged or insufficient- cured specimens.

Table 5-4: Activation energies using DMTA on longitudinal and transverse test specimens after exposure to elevated temperatures

Exposure Temperature	Time	Activation energy (KJ/mol)		Exposure Temperature	Time	Activation energy (KJ/mol)	
		Longitudinal	Transverse			Longitudinal	Transverse
Ambient (23℃)	0	379.36	321.45	66℃			
	1	372.74	338.67		1	343.69	354.96
	2	333.36	374.25		2	335.35	325.13
	4	349.16	302.45		4	333.65	337.99
	8	383.37	347.71		8	410.29	348.47
	16	386.10	298.45		16	374.91	397.43
	24	447.51	339.54		24	448.21	394.92
	48	408.25	340.03		48	445.14	386.96
	72	368.25	291.78		72	483.75	397.38
93℃	1	381.48	364.51	121℃	1	435.58	461.90
	2	485.46	442.33		2	457.79	458.08
	4	422.35	401.29		4	479.13	543.72
	8	421.33	554.35		8	422.03	539.04
	16	384.01	425.57		16	533.90	588.25
	24	527.36	548.54		24	547.79	516.74
	48	520.79	515.99		48	520.83	541.06
	72	546.69	578.34		72	465.99	542.34
149℃	1	476.69	420.28	177℃	1	451.60	455.81
	2	518.18	437.92		2	390.80	472.61
	4	486.95	500.76		4	549.22	498.93
	8	484.50	539.56		8	477.83	386.07
	16	481.37	511.31		16	548.73	504.24
	24	493.71	516.27		24	475.25	565.73
	48	491.84	521.90		48	455.92	423.07
	72	511.35	432.74		72	488.44	446.08
204℃	1	524.85	479.24	232℃	1	508.09	487.98
	2	584.87	486.09		2	511.23	409.92
	4	499.78	435.69		4	442.32	354.50
	8	559.46	481.02		8	475.45	287.67
	16	561.32	373.18		16	488.17	275.66
	24	493.64	298.05		24	483.42	289.38
	48	421.74	313.00		48	424.63	259.42
	72	416.47	300.67		72	486.28	231.67
260℃	1	460.74	393.17				
	2	463.07	405.91				
	4	531.03	275.55				
	8	244.83	270.15				
	16	254.18	265.68				
	24	229.14					

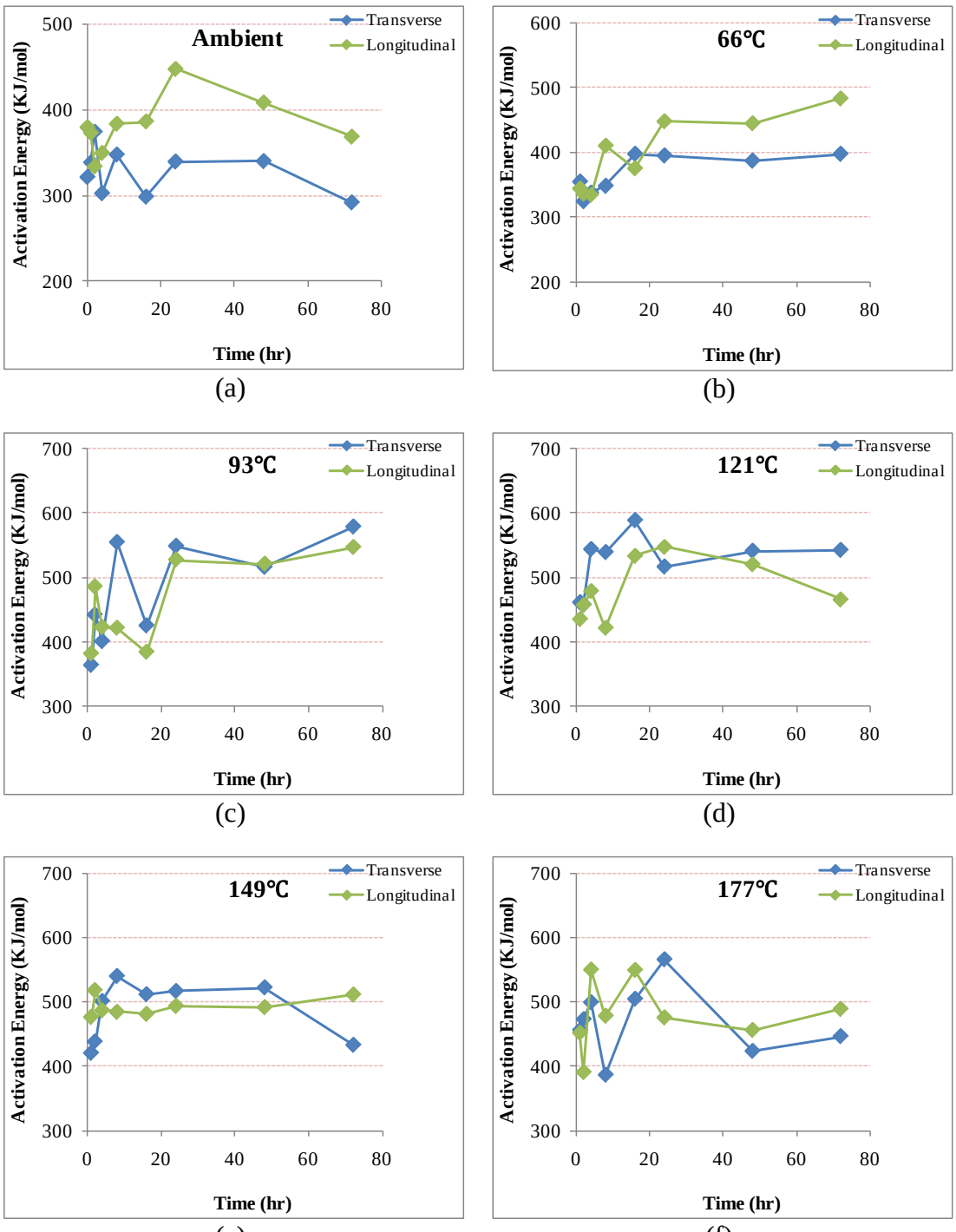

Figure 5-10: Comparison of the activation energies on longitudinal and transverse test specimens as a function of time at fixed temperatures, (a) ambient (b) 66℃ (c) 93℃ (d) 121℃ (e) 149℃ (f) 177℃ (g) 204℃ (h) 232℃ (i) 260℃

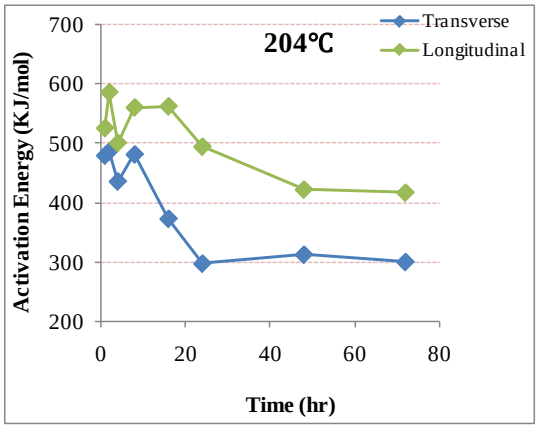

(g)

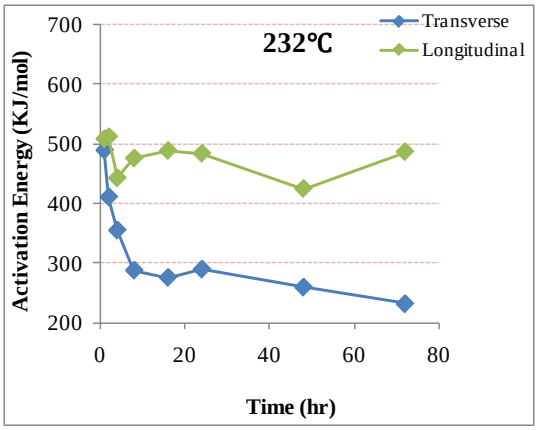

(h)

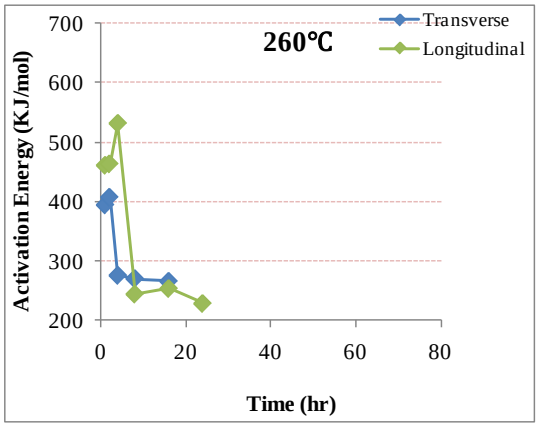

(i)

Figure 5-10: Continued

5.1.3.4 Modulus

Storage modulus or elastic modulus (E') means, as mentioned previously, the ability of a material to store energy or the elasticity of a composite materials. It is well known that the value of the initial storage modulus is determined as T_g-50℃ following bounds from T_g suggested by Fraga et al[66]. In this investigation, the initial storage modulus is considered as the storage modulus of T_g-40℃. Initial storage modulus increases with degree of cross-linking and molecular weight, with post-cure not only causing a higher modulus and increased brittleness, but also stronger interfacial bonds, which result in an increase in the storage modulus as well[67]. Due to post cure effect, the values of initial storage modulus were increased in the ranges of the exposure temperature and ageing time showing higher glass transition temperatures as shown in Table 5-5. The rubber plateau region of the storage modulus is taken into account to determine the extent of chemical change occurring within the composite materials. The rubbery modulus (E'_r) was determined as values of the storage modulus at a position of T_g+40℃ These values are taken as rubbery modulus to ensure that the asymptotic value is measured well away from the transition region. The rubbery modulus (E'r) at a position of T_g+40℃ are also tabulated in Table 5-5. It is known that the rubber plateau is related by the degree of crystallinity in a composite material.

A number of relationships have been developed between molecular weight and mechanical properties, as well as for unfilled polymers relating T_g to molecular weight and degree of cross-linking[68]. Therefore, it is necessary to consider changes at the level of average inter-crosslink molecular weight which is directly proportional to the ratio of materials density and cross-link density. The intercrosslink molecular weight

(M_c) can be calculated according to a method proposed by De'Neve and Shanahan[69]. The average inter-crosslink molecular weight can be expressed as:

$$M_c = \frac{3RT\rho}{E_M} \tag{5.7}$$

where:

E_M= the modulus of the polymer in the rubbery state

R = universal gas constant (8.3143J/mol^{o}K)

T = the temperature in the absolute scale at which the modulus was measured

ρ= the density of polymer

The rubbery modulus (E'_r) can be simplified by a rule of mixture,

$$E'_r = \frac{E_m E_f}{V_f E_m + (1-V_f)E_f} \tag{5.8}$$

where E_f and E_m are the modulus of the fiber and matrix, respectively. If assuming that $E_f >> E_m$, from Equation 5.7 and 5.8, a relationship between average inter-crosslink molecular weight and the rubbery modulus can be obtained by following equation,

$$M_c = \frac{3\rho RT}{(1-V_f)E'_r} \tag{5.9}$$

In order to calculate inter-crosslink molecular weight, following values were used.

T = the temperature in Kelvin (T_g based on tan delta at 1Hz+40℃)

V_f = volume fraction determined by tension test

E'_r = the rubber modulus corresponding to the temperature at T_g based on tan delta at 1Hz+40℃

Table 5-5 also shows normalized inter-crosslink molecular weight obtained from

dividing inter-crosslink molecular weight on unaged specimen by cases on aged specimens as a function of temperature and time. Normalized inter-crosslink molecular weights on longitudinal test specimens as a function of time at fixed temperatures are represented in Figure 5-11. Except for the conditions of ambient temperature and high temperatures (232 and 260℃), the majority of normalized inter-crosslink molecular weights showed $M_c/(M_c)_{time}$ <1 due to residual post-cure effect. Since fully curing did not occur in ambient temperature and thermal oxidation and degradation in the ranges of severe exposure temperatures leaded to chain scission and breakage, normalized inter-crosslink weights showed $M_c/(M_c)_{time}$ >1.

Table 5-5: Storage modulus at $T_g \pm 40$℃ and normalized inter-crosslink molecular weight from longitudinal and transverse specimens

Exposure Temperature	Time	Longitudinal (Pa)		Transverse (Pa)		Normalized inter-crosslink molecular weight	
		T_g-40℃	T_g+40℃	T_g-40℃	T_g+40℃		
		E'	E'	E'	E'	longitudinal	Transverse
Ambient (23℃)	1	4.4E+10	4.4E+09	3.96E+10	3.96E+09	1.105	0.906
	2	4.66E+10	4.66E+09	4.2E+10	4.2E+09	0.993	0.894
	4	4.14E+10	4.14E+09	3.73E+10	3.73E+09	1.032	1.020
	8	4.08E+10	4.08E+09	3.67E+10	3.67E+09	1.083	1.075
	16	4.26E+10	4.26E+09	3.84E+10	3.84E+09	1.007	1.140
	24	4.13E+10	4.13E+09	3.72E+10	3.72E+09	0.998	1.155
	48	4.29E+10	4.29E+09	3.86E+10	3.86E+09	0.984	1.185
	72	4.16E+10	4.16E+09	3.75E+10	3.75E+09	1.128	1.262
66℃	1	5.23E+10	6.02E+09	4.6E+10	5.29E+09	0.743	0.682
	2	5.28E+10	6.07E+09	4.64E+10	5.34E+09	0.741	0.683
	4	5.92E+10	6.81E+09	5.21E+10	5.99E+09	0.755	0.698
	8	5.74E+10	6.6E+09	5.05E+10	5.81E+09	0.831	0.761
	16	5.28E+10	6.07E+09	4.64E+10	5.34E+09	1.008	0.934
	24	5.19E+10	5.96E+09	4.56E+10	5.25E+09	0.881	0.807
	48	4.98E+10	5.72E+09	4.38E+10	5.04E+09	0.803	0.746
	72	4.79E+10	5.51E+09	4.22E+10	4.85E+09	0.873	0.815
93℃	1	4.28E+10	5.35E+09	3.68E+10	4.6E+09	0.927	0.879
	2	4.61E+10	5.76E+09	3.97E+10	4.96E+09	0.901	0.867
	4	4.1E+10	5.12E+09	3.52E+10	4.4E+09	0.891	1.040
	8	3.87E+10	4.83E+09	3.32E+10	4.16E+09	0.875	1.118
	16	3.8E+10	4.75E+09	3.26E+10	4.08E+09	0.865	1.203
	24	3.86E+10	4.82E+09	3.32E+10	4.15E+09	0.832	1.199
	48	4.14E+10	5.18E+09	3.56E+10	4.45E+09	0.801	1.048
	72	4.21E+10	5.26E+09	3.62E+10	4.53E+09	0.813	0.930
121℃	1	4.63E+10	6.48E+09	3.94E+10	5.51E+09	0.754	0.729
	2	4.56E+10	6.38E+09	3.88E+10	5.43E+09	0.815	0.786
	4	4.34E+10	6.08E+09	3.69E+10	5.17E+09	0.857	0.820
	8	4.45E+10	6.23E+09	3.78E+10	5.3E+09	0.742	0.708
	16	4.65E+10	6.51E+09	3.95E+10	5.53E+09	0.809	0.773
	24	4.28E+10	6E+09	3.64E+10	5.1E+09	0.833	0.795
	48	4.05E+10	5.66E+09	3.44E+10	4.81E+09	0.879	0.838
	72	4.18E+10	5.85E+09	3.55E+10	4.97E+09	0.787	0.751
149℃	1	4.16E+10	6.45E+09	3.45E+10	5.35E+09	0.786	0.765
	2	4.96E+10	7.68E+09	4.11E+10	6.38E+09	0.665	0.654
	4	4.2E+10	6.51E+09	3.48E+10	5.4E+09	0.794	0.783
	8	4.86E+10	7.53E+09	4.03E+10	6.25E+09	0.683	0.670
	16	4.38E+10	6.79E+09	3.64E+10	5.64E+09	0.736	0.721
	24	4.4E+10	6.82E+09	3.65E+10	5.66E+09	0.728	0.723
	48	4.25E+10	6.59E+09	3.53E+10	5.47E+09	0.745	0.734
	72	3.86E+10	5.99E+09	3.21E+10	4.97E+09	0.733	0.718

Table 5-5: Continued

Exposure Temperature	Time	Longitudinal (Pa)		Transverse (Pa)		Normalized inter-crosslink molecular weight	
		T_g-40℃	T_g+40℃	T_g-40℃	T_g+40℃		
		E'	E'	E'	E'	longitudinal	Transverse
177℃	1	3.93E+10	5.89E+09	3.34E+10	5.01E+09	0.897	0.852
	2	4.91E+10	7.36E+09	4.17E+10	6.25E+09	0.796	0.763
	4	3.92E+10	5.88E+09	3.33E+10	5E+09	0.867	0.827
	8	4.26E+10	6.39E+09	3.62E+10	5.44E+09	0.758	0.726
	16	4.01E+10	6.01E+09	3.41E+10	5.11E+09	0.762	0.729
	24	4.11E+10	6.17E+09	3.5E+10	5.25E+09	0.785	0.755
	48	4.15E+10	6.22E+09	3.53E+10	5.29E+09	0.763	0.724
	72	4.9E+10	7.36E+09	4.17E+10	6.25E+09	0.649	0.625
204℃	1	3.67E+10	4.96E+09	3.31E+10	4.46E+09	1.030	0.923
	2	4.42E+10	5.97E+09	3.98E+10	5.37E+09	0.824	0.745
	4	3.83E+10	5.17E+09	3.44E+10	4.65E+09	0.967	0.876
	8	4.44E+10	5.99E+09	3.99E+10	5.39E+09	0.885	0.798
	16	4E+10	5.4E+09	3.6E+10	4.86E+09	0.936	0.844
	24	4.07E+10	5.5E+09	3.66E+10	4.95E+09	0.896	0.808
	48	4.14E+10	5.59E+09	3.73E+10	5.03E+09	0.876	0.797
	72	4.27E+10	5.76E+09	3.84E+10	5.18E+09	0.872	0.780
232℃	1	4.34E+10	4.55E+09	3.99E+10	4.19E+09	1.203	1.061
	2	4.11E+10	4.32E+09	3.79E+10	3.97E+09	1.288	1.138
	4	4.27E+10	4.48E+09	3.93E+10	4.12E+09	1.114	0.988
	8	4.26E+10	4.48E+09	3.92E+10	4.12E+09	1.140	1.005
	16	4.53E+10	4.75E+09	4.16E+10	4.37E+09	0.977	0.860
	24	4.52E+10	4.75E+09	4.16E+10	4.37E+09	0.928	0.809
	48	4.21E+10	4.42E+09	3.87E+10	4.07E+09	0.999	0.871
	72	2.81E+10	2.95E+09	2.59E+10	2.72E+09	1.324	1.149
260℃	1	4.33E+10	3.89E+09	4.02E+10	3.62E+09	1.179	1.042
	2	4.29E+10	3.86E+09	3.99E+10	3.59E+09	1.260	1.102
	4	4.66E+10	4.19E+09	4.33E+10	3.9E+09	1.422	1.314
	8	2.31E+10	2.08E+09	2.15E+10	1.93E+09	1.971	1.767

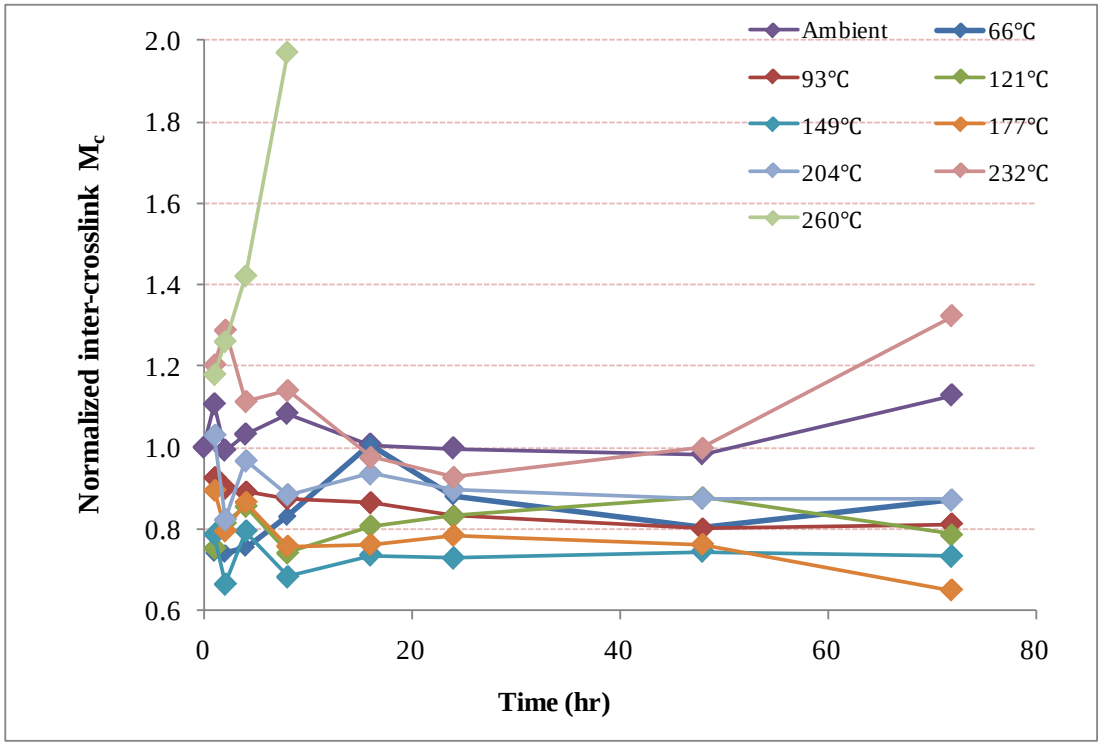

Figure 5-11: Normalized inter-crosslink molecular weights on longitudinal test specimens as a function of time at fixed temperatures

5.1.3.5 Mechanical Retention based on T_g

Mechanical properties are strongly dependent on glass transition temperature as shown in Figure 5-12. The retention of mechanical properties was enhanced with increasing glass temperatures. Tensile properties related to interfacial bond between fibers and matrix showed great enhancement due to post-cure effect compared to the properties of flexure, short beam shear and off-axis shear. As mentioned in off-axis shear test section, although glass transition temperatures increased, the distortion of test specimens caused by asymmetry leaded to deterioration of mechanical property. Mechanical properties on short beam shear test were slightly higher than those on flexural test in all test environments. It should be pointed out that tensile properties were rapidly and greatly increased in the ranges of lower exposure temperatures. On the other hand, if the glass transition reached the maximum due to fully curing, there was a little difference in mechanical properties such as tension, flexure and short beam shear. Therefore, glass transition temperatures can be crucial criterion to evaluate the mechanical properties on polymer-based composites.

Figure 5-13 shows the characterization of four mechanical properties in terms of strength retentions (%) as a function of glass transition temperatures determined by the peak of tan δ at 1Hz. The majority of test data were distributed between 100℃ and 120℃ in glass transition temperature. Except for the exposure conditions of severe and ambient temperature and off-axis shear test, the enhancement of mechanical properties were attributed to increase of glass transition temperature. The reason why the retention of tensile properties has big variation is that tensile characteristic is greatly affected by defects created in process of hand wet layup.

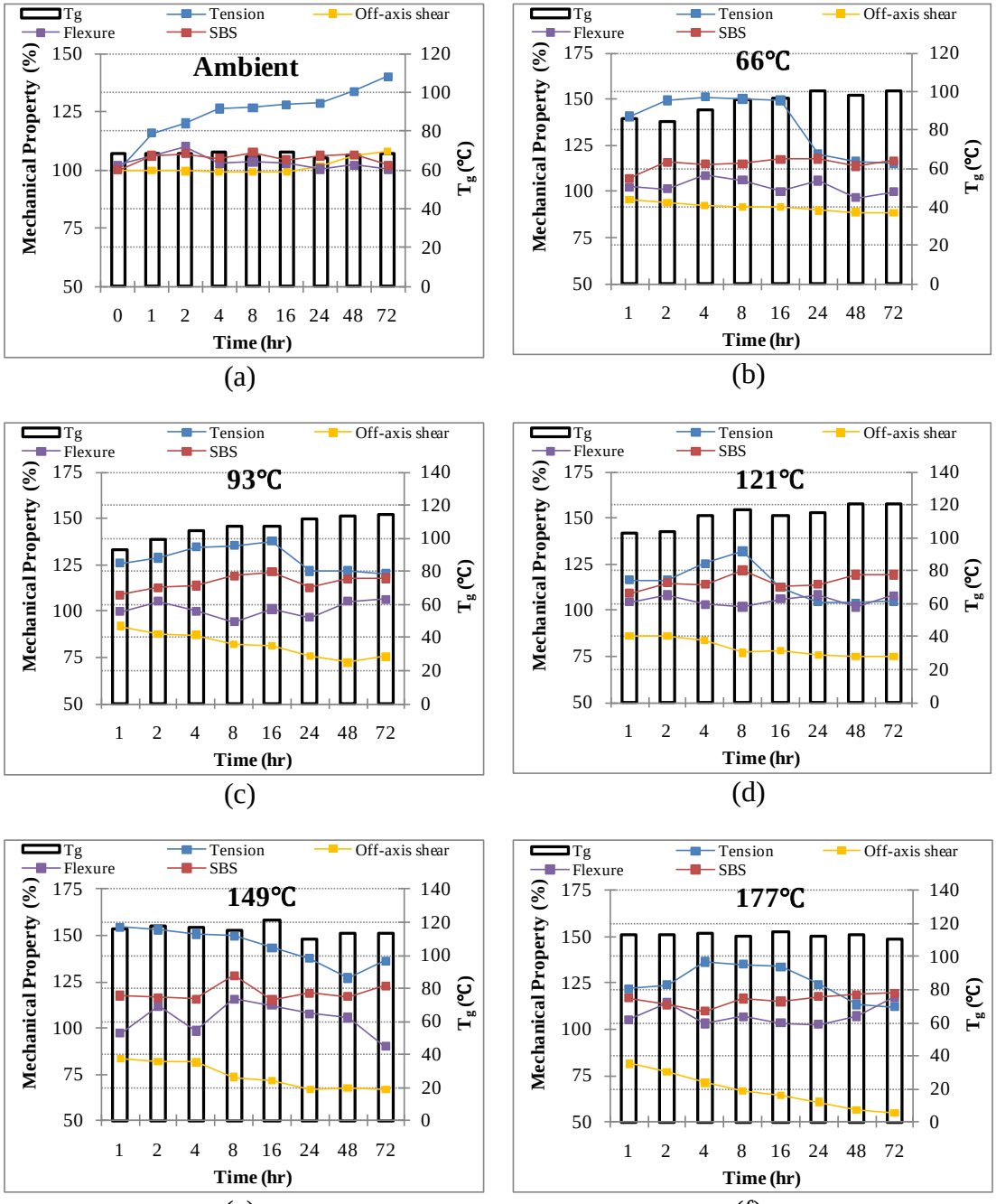

Figure 5-12: Mechanical properties versus glass transition temperatures on longitudinal and transverse test specimens as a function of time at fixed temperatures, (a) ambient (b) 66℃ (c) 93℃ (d) 121℃ (e) 149℃ (f) 177℃ (g) 204℃ (h) 232℃ (i) 260℃

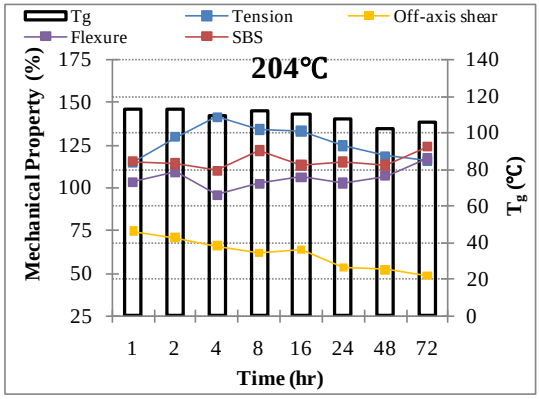

(g)

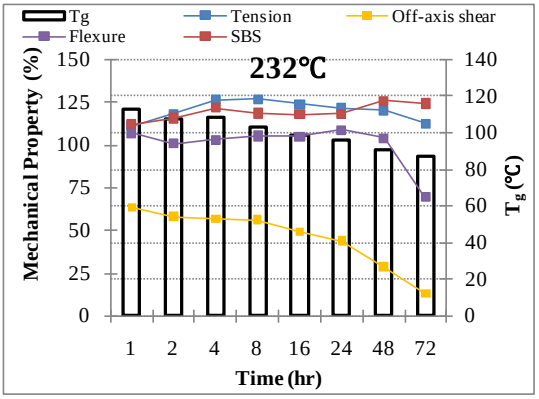

(h)

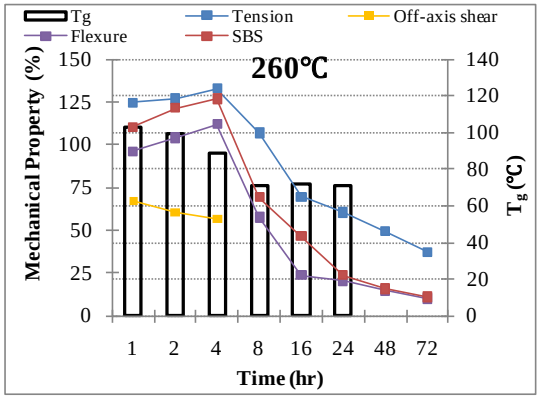

(i)

Figure 5-12: Continued

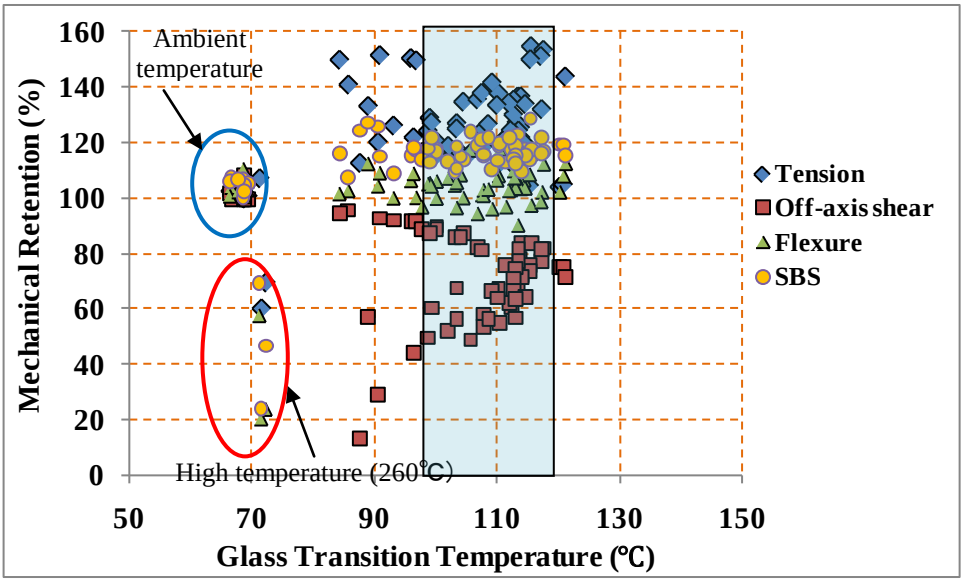

Figure 5-13: Characterization of four mechanical properties in terms of strength retention (%) as a function of glass transition temperatures determined by the peak of tan δ at 1Hz

5.2 Differential Scanning Calorimetry

5.2.1 Introduction

As mentioned in chapter 3.5.6, Differential scanning calorimetry (DSC) is a technique to study what happens to polymers when they're heated. DSC is mainly used to investigate the thermal transitions of a polymer.

The operation of a Differential Scanning Calorimeter (DSC) is based on measurement of the thermal response of a sample pan containing polymer composites as compared with a reference pan when the two are heated uniformly at a constant rate. A flow of nitrogen gas is maintained over the samples to create a reproducible and dry atmosphere. The nitrogen atmosphere also eliminates air oxidation of the samples at high temperatures. The sample is sealed into a small aluminum pan. The reference is usually an empty pan and cover. The sample sits upon a constantan disc on a platform in the DSC cell. A thermocouple under the constantan disc measures the sample temperature. An empty reference pan sits on a symmetric platform with its own underlying wafer and thermocouple. Heat flow is measured by comparing the difference in temperature across the sample and the reference pan. The applications of DSC are as follows:

1) Exothermal energy of polymer cure (as in epoxy adhesives), allows determination of the degree and rate of cure.

2) Measurement of plastic or glassy material glass transition temperatures or softening temperatures.

3) Determines crystalline to amorphous transition temperatures in polymers and

plastics and the energy associated with the transition.

4) Determine the thermal stability of a material.

5) Determine the reaction kinetics of a material.

5.2.2 Data Reduction

5.2.2.1 Glass Transition Temperature

As described in dynamic mechanical thermal analysis, glass transition is a method to characterize a property of a polymeric material. The glass transition is the temperature where the polymer goes from like a hard, glass to a state of rubber. DSC defines the glass transition as a change in the heat capacity as the polymer matrix goes from the glass state to the rubber state. This is a second order endothermic transition (requires heat to go through the transition) so in the DSC the transition appears as a step transition and not a peak such as might be seen with a melting transition. In other words, polymers have a higher heat capacity above the glass transition temperature than they do below it. Because of this change in heat capacity that occurs at the glass transition, DSC is used to measure a polymer's glass transition temperature. It should be pointed out that the change doesn't occur suddenly, but takes place over a temperature range. This makes picking one discreet T_g kind of tricky. T_g is taken the middle of the incline to be the T_g as shown in Figure 5-14.

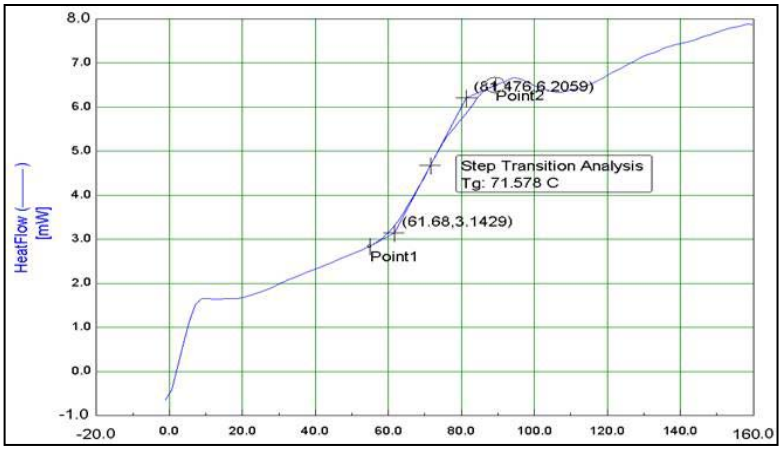

Figure 5-14: Schematic diagram for detecting the glass transition temperature from heat flow versus temperature (Exposure temperature: 23℃ Ageing time: 4 hrs)

5.2.2.2 Heat Capacity

When heating reference and sample pan, the software of DSC sp equipment by Rheometric Scientific corporation will plot the difference in heat output of the two heaters against temperature. That is to say, the heat absorbed by the polymer against temperature is plotted. The heat flow is going to be shown in units of heat, q supplied per unit time, t. The heating rate is temperature increase T per unit time, t.

$$\frac{\text{Heat}}{\text{Time}} = \frac{q}{t} = \dot{q} = \text{heat flow} \tag{5.10}$$

$$\frac{\text{Temperature increase}}{\text{Time}} = \frac{\Delta T}{t} = \text{heating rate} \tag{5.11}$$

If dividing the heat flow by heating rate, heat capacity can be calculated as follow:

$$\frac{\frac{q}{t}}{\frac{\Delta T}{t}} = \frac{q}{\Delta T} = C_p = \text{heat capacity} \tag{5.12}$$

Heat capacity can be changed by variations in the material, either from its formulation or its heat history. While most investigations regarding DSC are only interested in the changes of heat capacity at the glass transition temperature to determine the glass transition temperature, information on the amount of oriented amorphous material.

5.2.3 Analyses and Results

First of all, in the analysis of differential scanning calorimetry (DSC), it should be noted that the changes affecting the mechanical properties and service life of polymer composites are often subtle and may not be seen on heating. In particular, to obtain accurate experimental results you should calibrate the DSC cell periodically. Two pans and DSC cell keep from contamination to obtain the accurate data. Since sample size is usually limited to 10-20mg and sample is extracted from big specimens, it is difficult to get consistent data. In addition, the amount of the thermal oxidation between surface and core of bulk materials can be resulted in bad data. Therefore, DSC is often used in conjunction with DMTA if reaction is endothermic or exothermic.

In this study, the analysis of DSC is only focused on detecting of the glass transition temperatures in order to compare to results determined by DMTA due to noise of DSC data.

Table 5-6 and Figure 5-15 show the comparison among glass transition temperatures determined by peak height of tan δ at 1Hz, storage modulus and DSC on specimens exposed to elevated temperatures as a function of time. Glass transition temperatures determined by the analysis of DSC were overall higher than the results detected by the height of peak tan δ and storage modulus using DMTA in all environmental conditions. As post-curing effect was applied to specimens, glass transition temperatures were getting higher compared to other values while glass transition temperatures show the similarity in the ranges of higher temperatures (232 and 260℃).

Table 5-6: Comparison among glass transition temperatures determined by tan δ, storage modulus and DSC (percent error means the difference between tan δ and DSC)

Exposure Temperature	Time	T_g			Percent error(%)	Exposure Temperature	T_g			Percent error(%)
		1Hz	E'	DSC			1Hz	E'	DSC	
Ambient (23℃)	0	68.55	60.35	73.35	6.54					
	1	68.75	57.46	72.82	5.59	66℃	85.73	80.12	87.33	1.83
	2	68.64	68.15	71.79	4.39		84.27	80.04	89.45	5.79
	4	69.29	62.19	73.89	6.22		90.85	83.43	98.45	7.72
	8	66.67	65.64	72.18	7.64		95.94	84.95	102.12	6.05
	16	68.95	62.15	74.44	7.38		96.80	88.64	102.56	5.62
	24	66.45	61.25	69.45	4.33		100.13	90.54	105.37	4.97
	48	67.84	60.54	74.31	8.71		97.77	91.12	104.12	6.10
	72	68.82	61.16	69.51	1.00		100.12	92.34	103.88	3.62
93℃	1	93.09	91.07	90.57	-2.78	121℃	103.08	97.07	114.59	10.04
	2	99.00	89.31	100.58	1.57		104.05	101.74	119.78	13.13
	4	104.49	98.87	112.52	7.14		113.84	105.12	118.58	4.00
	8	106.81	100.12	115.40	7.44		117.32	108.81	115.47	-1.60
	16	107.50	103.58	117.90	8.82		113.83	105.40	118.72	4.12
	24	111.46	104.58	122.02	8.65		115.30	107.07	120.70	4.47
	48	113.89	106.31	121.81	6.50		120.24	111.84	122.92	2.18
	72	114.41	105.41	123.68	7.50		120.85	110.84	121.93	0.89
149℃	1	115.56	106.54	124.89	7.47	177℃	113.47	100.03	126.13	10.04
	2	117.60	109.64	125.34	6.18		113.53	102.45	126.69	10.39
	4	117.18	108.64	122.99	4.72		113.90	99.62	127.99	11.01
	8	115.48	103.05	125.00	7.62		112.74	103.33	126.17	10.64
	16	121.17	112.25	125.47	3.43		114.60	101.36	126.78	9.61
	24	110.23	101.58	125.28	12.01		112.26	101.41	124.61	9.91
	48	113.21	103.85	124.67	9.19		112.97	103.44	123.74	8.70
	72	113.41	103.89	124.34	8.79		110.45	98.97	121.16	8.84
204℃	1	113.08	102.22	126.58	10.67	232℃	112.91	100.00	121.63	7.17
	2	112.70	101.97	125.78	10.40		107.78	97.72	118.66	9.17
	4	109.19	100.01	125.05	12.68		108.56	97.98	121.90	10.94
	8	111.92	100.00	124.88	10.38		103.43	97.07	116.61	11.30
	16	110.00	96.36	125.47	12.33		98.73	83.24	106.27	7.10
	24	107.75	96.71	118.30	8.92		96.37	71.55	101.01	4.59
	48	102.04	86.61	112.74	9.49		90.57	68.20	91.01	0.48
	72	105.64	90.04	105.41	-0.22		87.61	65.43	86.95	-0.76
260℃	1	103.40	99.48	117.62	12.09					
	2	99.30	89.72	108.03	8.08					
	4	88.96	76.81	94.73	6.10					
	8	71.23	59.27	72.82	2.18					
	16	72.24	52.02	69.62	-3.76					
	24	71.53	49.06	70.06	-2.09					
	48			71.83						
	72			70.77						

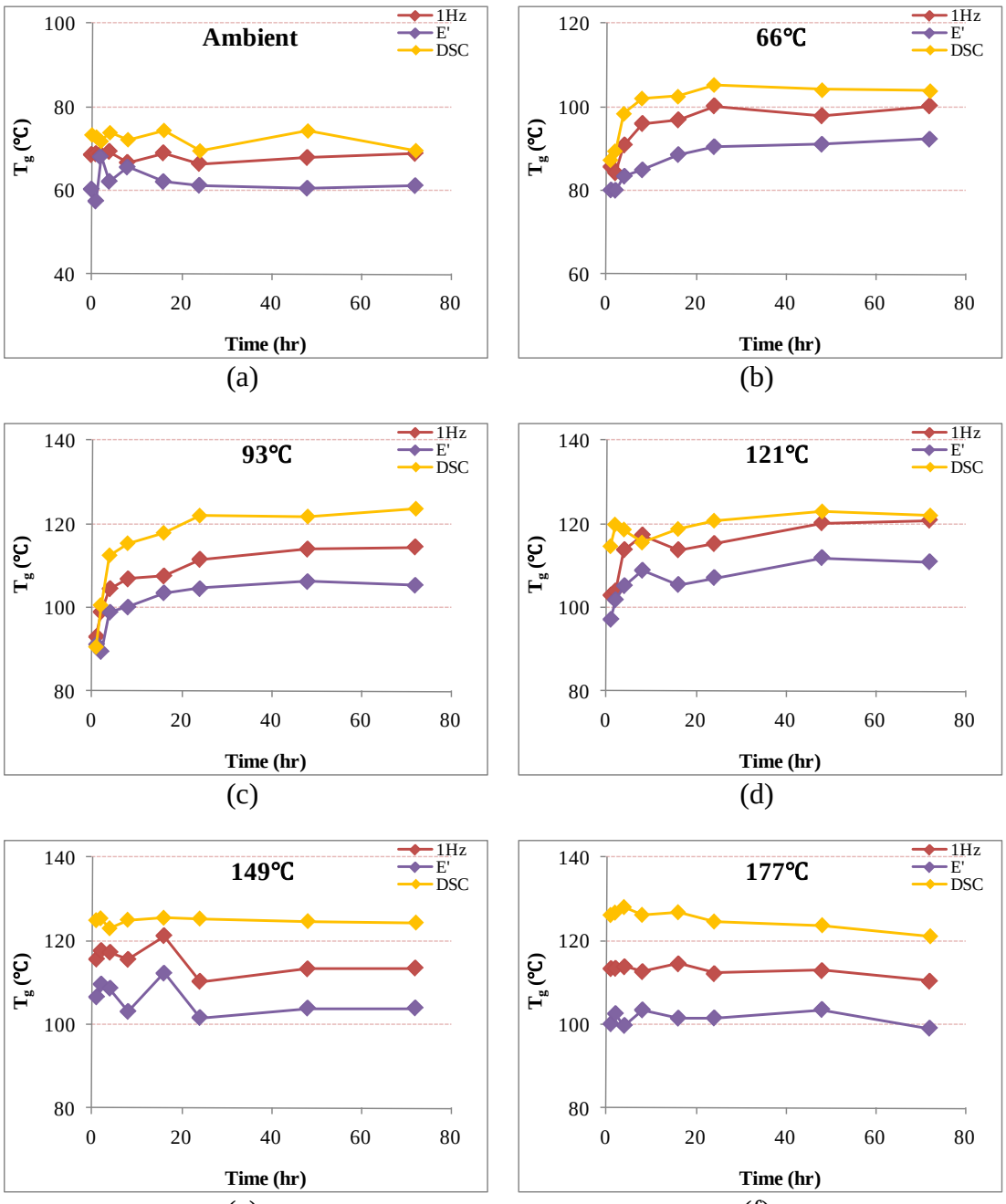

Figure 5-15: Comparison among glass transition temperatures determined by peak height of tan δ at 1Hz, storage modulus and DSC as a function of time at fixed temperatures, (a) ambient (b) 66℃ (c) 93℃ (d) 121℃ (e) 149℃ (f) 177℃ (g) 204℃ (h) 232℃ (i) 260℃

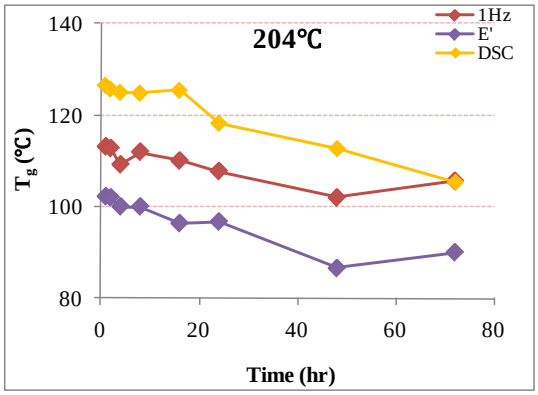

(g)

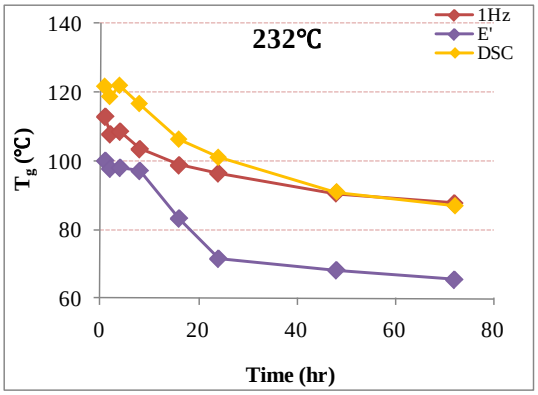

(h)

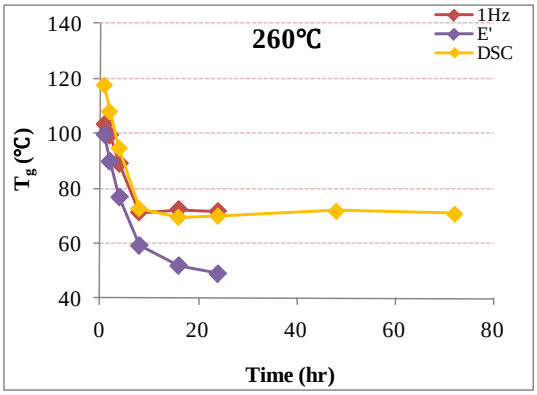

(i)

Figure 5-15: Continued

5.3 Thermogravimetric Analysis

5.3.1 Introduction

When fiber reinforced polymer composites are subjected to elevated and high temperatures, physical and chemical processes including glass transition and decomposition can greatly affect their physical and mechanical properties in various manners. To evaluate the thermal and mechanical responses of polymer composites in the ranges of the diverse exposure temperatures, thermophysical and thermomechanical properties should be considered. Thermogravimetric Analysis (TGA) is powerful and simple tool to estimate the thermophysical and thermomechanical properties exposed to a controlled temperature. In general, TGA is an analytical technique used to determine the thermal stability of composite materials and their fraction of volatile components by monitoring the mass loss that occurs when a specimen is heated. The measurement is normally performed in air or in an inert atmosphere. In this study, nitrogen gas is used to set inert condition as described in chapter 3.5.7. Mass loss can be categorized as volatile components such as absorbed moisture, residual solvents, or low-molecular-mass additive between ambient and 300℃; reaction products, such as water and amino resins, which generally form between 100℃ and 250℃, and generation of volatile degradation products from polymer chain scission that generally require temperatures above 200℃ but not more than 800℃[63]. All of these mass loss processes may be characterized by TGA to get information such as composition and thermal stability. In addition, kinetic information is important for estimating the times and temperatures corresponding to the processing, service lifetimes, and storage of materials. In an inert

atmosphere, the rate of many thermally activated processes can be described as a function of two variables: the temperature and the extent of conversion. The extent of conversion is conveniently determined from mass loss measurements.

The temperature-dependent effective thermophysical and thermomechnical properties of composite materials from thermal analysis using TGA combined with DMTA, DSC can be summarized in Figure 5-16. When decomposition of the composite materials due to elevated temperatures occurs, the effective specific heat capacity increases by decomposition heat emitted during endothermic process while the effective thermal conductivity definitely decreases at this region because significant thermal resistance results from the decomposed gas. As mentioned in DMTA section, the storage modulus apparently decreases in glass transition region, ant drops further at decomposition.

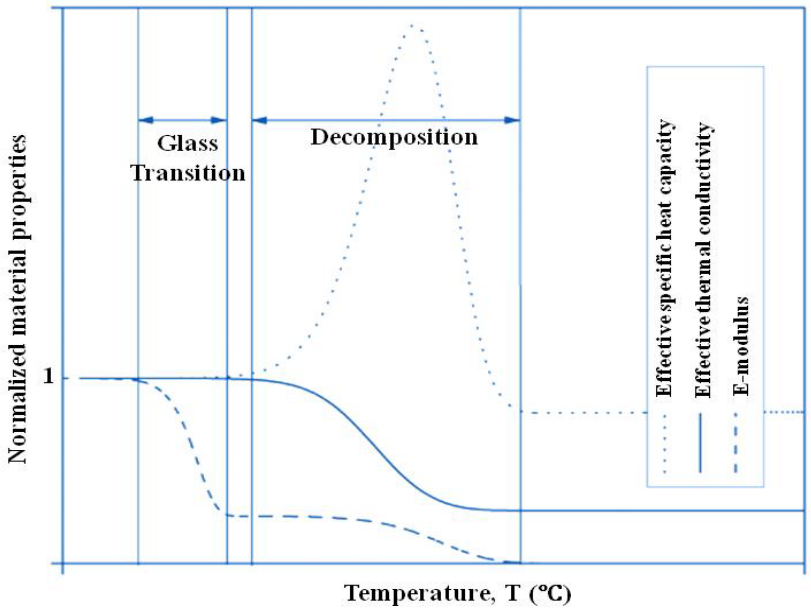

Figure 5-16: Temperature-dependent effective specific heat capacity, thermal conductivity and E-modulus for composite materials[70]

5.3.2 Analyses and Results

5.3.2.1 Weight loss

In order to compare to the results of weight loss using TGA, the characteristics of weight loss during thermooxidation process was evaluated with the weight change at various temperatures for different ageing time using DMTA specimens. When reached at required time and temperature, test specimens were removed to the atmospheric condition. After cooling in this condition, weight of DMTA specimens was recorded using analytical balance with a 10^{-5} grams resolution.

Table 5-7 and Figure 5-17 show the results of weight loss (%) on DMTA specimens exposed to elevated temperatures for up to 72 hrs using balance. In ranges of lower exposure temperatures (66, 93, 121, and 149℃), the data of weight loss only existed within 1%. As exposure temperatures were going up to 177, 204, and 232℃, weight loss rapidly increased. In addition, at these temperatures, the slopes of weight loss versus time, which means the weight loss per hour, were steeper compared to lower ageing temperatures. Weight loss in 260℃ was increased up to 18.2%. The slope of weight loss was 0.004, 0.005, 0.006, 0.009, 0.034, 0.039, 0.053, and 0.23 at 66, 93, 121, 149, 177, 204, 232 and 260℃, respectively. In other words, characterization of weight loss can be categorized into 4 regions in this study as follows:

1) no-changed region: ambient temperature (~0%)

2) slight-changed region: 66, 93, 121,149℃ (~1.5%)

3) intermediate-changed region: 177, 204, 232℃ (~5.6%)

4) catastrophic-changed region: 260℃ (~18.2%)

Since the epoxy resin used in this study is cured at room temperature and is not fully cured, it is expected that the weight loss is coming from following reasons:

1) Evaporating of uncured small molecules

2) The small molecular part spilt from long polymer chain

Evaporating resulted in initial weight loss whereas separation of the small molecular part from long polymer chain due to intensive themooxidaiton contributed to the abrupt weight loss. Therefore, weigh loss in ranges of lower exposure temperatures was smaller than that in higher exposure temperatures since serious chain splitting was not occurred due to severe thermooxidation.

Table 5-7: Data of weight loss (%) on DMTA specimens exposed to elevated temperatures using balance

Time	Weight Loss (%)							
	66℃	93℃	121℃	149℃	177℃	204℃	232℃	260℃
1	0.1405	0.3015	0.4803	0.6380	0.8389	1.1203	1.5616	2.2166
2	0.1677	0.3431	0.5695	0.7408	0.9919	1.4126	1.9864	2.7661
4	0.2031	0.4064	0.6520	0.8425	1.1400	1.7654	2.3837	3.6499
8	0.2412	0.4801	0.7613	0.9064	1.3921	2.0724	2.8212	5.1066
16	0.2953	0.6060	0.7807	0.9668	1.8138	2.5399	3.3807	8.8491
24	0.3672	0.6474	0.8284	1.0569	2.2278	2.8100	3.9378	10.9842
48	0.4443	0.7192	0.8696	1.2555	2.9053	3.3003	4.8256	15.6297
72	0.4887	0.7334	0.8859	1.4111	3.2853	3.6310	5.6593	18.2231

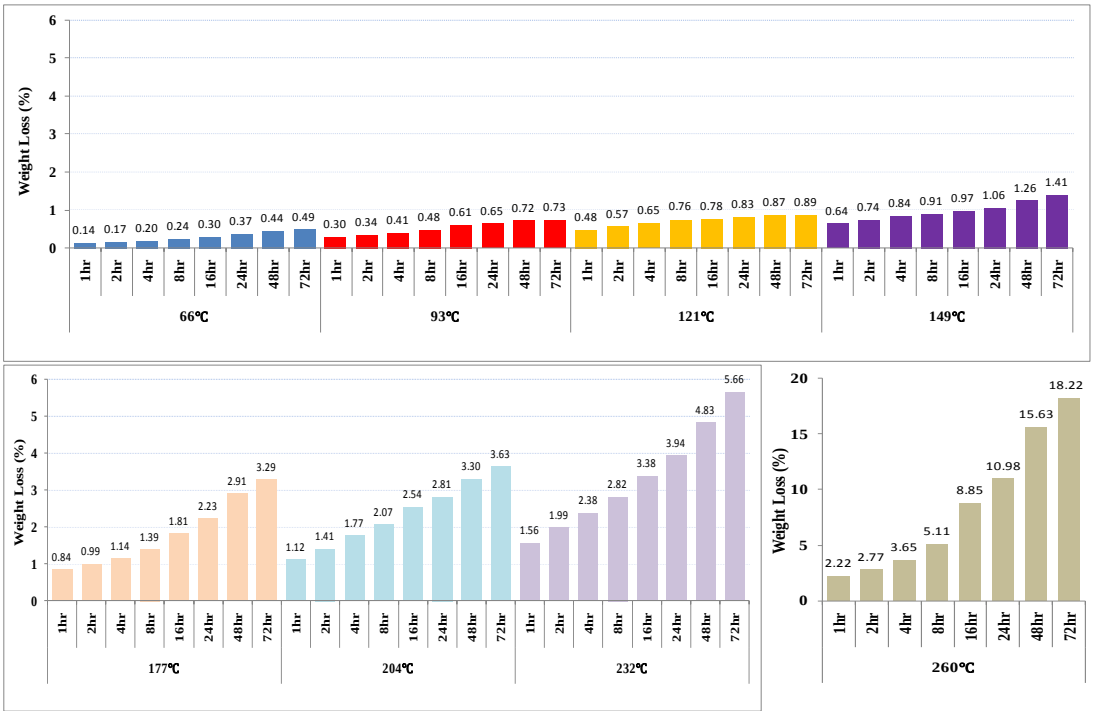

Figure 5-17: Weight loss (%) on DMTA specimens exposed to elevated temperatures using balance

Weight percent (%) of specimens at initial and final point of decomposition using TGA is presented in Table 5-8. As described in chapter 3.5.7, Samples were heated from 25℃ to 750℃ with the heating rate of 10℃/min in nitrogen environment (25 ml/min). m_i and m_e indicate the mass (%) that decomposition of specimens is initiated and finished and two masses can be detected using software of TGA instrument. The majority of m_i shows the value more than 99% except for some conditions (232℃ more than 24 hrs of ageing time and 260℃ more than 4 hrs of ageing time). This phenomenon means evaporating of uncured small molecules was only applied for weight loss before decomposition is initiated. Weakened or damaged polymer structures due to severe thermooxidation contributed to additional weight loss in higher exposure temperatures. On the contrary to the results of m_i, m_e did not show the tendency. It appears that this reason resulted from complicated mechanism of decomposition and variations having hand wet layup process.

Weight loss using TGA on specimens exposed to elevated temperatures for 72 hrs of ageing time is presented as a function of temperatures ranging from 25℃ to 750℃ in Figure 5-18. Based on graphs, no significant changes occurred before decomposition is initiated in all exposure temperatures except for 232℃ and 260℃. However, abrupt weight loss occurred after decomposition. Finally, in ranges of 232℃ and 260℃, a little of weight loss happened before decomposition while weight loss after decomposition were smaller compared to lower exposure temperatures. It should be pointed out that the un-uniformly distribution of carbon/epoxy composite materials contributed to the variation of the residual char weight.

Table 5-8: Weight percent (%) of specimens at initial and final point of decomposition using TGA

Time	Ambient (23℃)		66℃		93℃		121℃		149℃	
	m_i(%)	m_e(%)	m_i(%)	m_e(%)	m_i(%)	m_e(%)	m_i(%)	m_e(%)	m_i(%)	m_e(%)
0	99.57	55.57								
1	99.36	43.63	99.22	48.25	99.40	52.59	99.25	52.27	99.28	52.82
2	99.34	43.70	99.37	49.27	99.18	46.25	99.64	55.97	99.52	38.14
4	99.46	52.19	99.54	49.23	99.08	39.90	99.88	45.11	99.85	45.73
8	99.32	46.43	99.36	47.29	99.39	44.58	99.81	53.34	99.76	50.01
16	99.20	49.25	99.61	56.10	99.83	55.72	99.30	57.40	99.33	52.21
24	99.43	61.09	99.21	54.11	99.76	50.27	99.08	46.63	99.57	56.15
48	99.52	59.80	99.21	42.29	99.43	55.77	99.50	46.73	99.96	45.87
72	99.27	46.30	99.59	47.17	99.27	57.93	99.51	41.52	99.90	54.38

Time	177℃		204℃		232℃		260℃	
	m_i(%)	m_e(%)	m_i(%)	m_e(%)	m_i(%)	m_e(%)	m_i(%)	m_e(%)
1	99.73	51.67	99.62	43.84	99.58	53.25	99.36	46.55
2	99.77	51.20	99.36	50.44	99.24	54.40	99.06	61.98
4	99.50	49.30	99.15	54.28	99.41	48.04	98.24	40.97
8	99.68	45.67	99.24	52.09	99.13	48.37	94.84	59.08
16	99.48	44.03	99.63	59.58	99.59	58.01	93.19	64.77
24	99.37	51.55	98.70	50.91	98.64	60.74	92.64	69.72
48	99.21	54.71	97.02	57.03	97.00	56.39	93.47	71.21
72	99.49	57.37	96.84	45.88	94.26	59.77	93.15	75.57

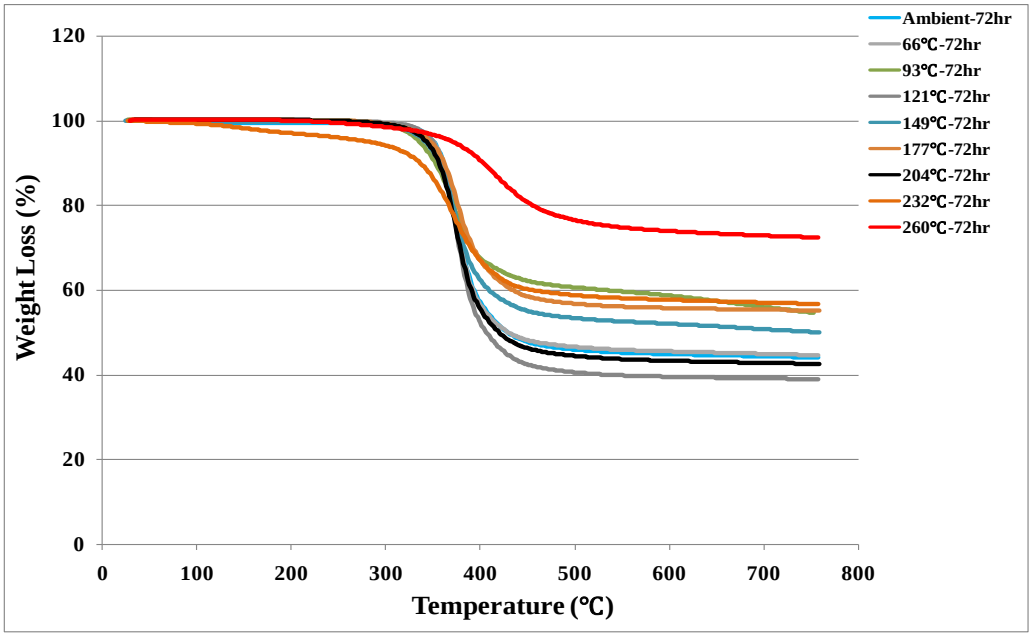

Figure 5-18: Weight loss (%) on specimens heated from 25℃ to 750℃ with the heating rate of 10℃/min in nitrogen environment (ageing time: 72 hrs)

5.3.2.2 Determination of Thermal Stability Parameters

Thermal stability parameters determined by the TGA curve are summarized in Table 5-9. First, the onset temperature of decomposition (T_{onset}) means what the maximum processing and manufacturing temperatures can be used without initiating decomposition. Therefore, T_{onset} is the main criteria for heat stability of polymers and polymer composites[71]. The endset temperature of decomposition (T_{endset}) indicate threshold temperature which decomposition show the asymptotic value due to char formation. T_{onset} and T_{endset} can be easily detected by software attached to TGA instrument. As shown in Figure 5-19, the values of T_{ondset} initially increased due to the dominant increase of the crosslinkage with thermal treatment. For lower exposure temperatures (~149℃), the values of T_{ondset} continuously increased even though ageing time went up. In the exposure temperatures ranging from 177 to 260℃, the values of T_{ondset} continuously decreased with the extended ageing time. The higher exposure temperature led to the more serious drop in the values of T_{ondset}. In the highest temperature (260℃), the absence of the initial increase of T_{ondset} means the degradation of the polymer structures occurred even in a short time. After 8 hr of ageing time in 260℃, the reason why T_{ondset} showed the asymptotic values is that serious thermooxidative degradation already occurred in the process of environmental conditions and this resulted in char formation. In the case of T_{endset}, the values of T_{endset} were very consistent except for exposure temperatures of more than 177℃ as shown in Figure 5-20. The values of T_{endset} were slightly increased in temperature raging from 177 to 232℃ while these values were abruptly increased in 260℃. The increase of T_{endset} indicates decomposition occur for long time period.

Table 5-9: Thermal stability parameters determined by TGA curves- T_m and α_m mean the maximum temperature and degree of decomposition at the maximum reaction

Temperature	Time	T_{onset} (℃)	T_{endset} (℃)	T_m (℃)	α_m	E_d (KJ/mol)	n
Ambient (23℃)	0	352.25	397.56	441.00	0.881	170.10	0.89
	1	354.72	397.78	448.82	0.933	188.56	0.93
	2	353.62	399.83	444.31	0.932	185.99	0.93
	4	354.34	400.15	444.09	0.929	179.71	0.92
	8	354.85	400	444.15	0.932	179.62	0.92
	16	354.79	397.11	444.87	0.897	155.95	0.9
	24	353.25	398.67	442.67	0.921	173.83	0.91
	48	353.61	398.59	444.25	0.929	181.13	0.93
	72	355.64	400.28	445.45	0.928	176.48	0.92
66℃	1	353.81	399.49	441.20	0.923	182.52	0.93
	2	353.79	399.42	442.78	0.928	181.29	0.93
	4	354.08	399.82	439.86	0.929	196.59	0.93
	8	354.2	399.15	443.29	0.907	184.47	0.92
	16	354.13	399.53	444.50	0.928	187.47	0.93
	24	354.04	398.54	440.17	0.903	192.34	0.98
	48	354.01	399.51	443.27	0.906	235.36	0.94
	72	354.54	399.09	441.38	0.913	235.68	0.94
93℃	1	352.14	397.72	444.68	0.889	167.60	0.89
	2	351.94	397.67	441.28	0.928	190.10	0.93
	4	355.18	400.48	445.56	0.933	216.86	0.94
	8	355.35	400.71	441.76	0.931	201.87	0.93
	16	356.29	400.04	442.59	0.929	230.81	0.93
	24	356.84	398.26	444.79	0.899	183.87	0.9
	48	354.07	396.26	442.31	0.873	186.98	0.91
	72	352.74	399.06	441.43	0.914	180.71	0.92
121℃	1	348.7	396.88	440.54	0.878	144.91	0.86
	2	354.48	400.7	445.83	0.922	215.57	0.9
	4	355.9	400.66	445.62	0.937	259.41	0.95
	8	353.92	399.63	441.01	0.922	293.76	0.95
	16	354.71	400.97	445.76	0.926	200.08	0.93
	24	353.74	399.37	441.59	0.925	209.04	0.93
	48	354.17	399.92	447.59	0.939	226.32	0.94
	72	354.25	399.24	444.45	0.935	218.02	0.94
149℃	1	348.63	397.75	440.49	0.897	158.22	0.9
	2	354.75	400.24	444.53	0.930	213.24	0.94
	4	355.4	399.3	446.20	0.936	232.36	0.94
	8	353.36	399.58	441.62	0.930	204.41	0.93
	16	352.39	398.46	442.48	0.873	147.25	0.86
	24	354.07	399.39	434.34	0.887	186.80	0.9
	48	352.88	400.73	443.24	0.930	207.79	0.93
	72	347.73	400.3	446.47	0.894	154.56	0.89

Table 5-9: Continued

Temperature	Time	T_{onset} (℃)	T_{endset} (℃)	T_m (℃)	α_m	E_d (KJ/mol)	n
177℃	1	353.07	399.7	443.47	0.924	192.42	0.93
	2	353.48	399.72	440.11	0.928	205.31	0.93
	4	353.48	401.08	446.17	0.939	231.23	0.95
	8	354.48	401.01	443.04	0.929	178.93	0.93
	16	351.91	401.79	448.92	0.936	171.72	0.93
	24	350.86	400.75	442.17	0.894	145.51	0.88
	48	351.87	402.94	449.14	0.928	159.79	0.91
	72	350.63	405.18	449.03	0.925	151.22	0.91
204℃	1	354.82	400.26	447.91	0.941	236.69	0.94
	2	354.21	399.43	443.43	0.935	210.09	0.94
	4	353.08	398.52	444.20	0.882	226.16	0.94
	8	347.47	396.98	445.90	0.875	154.03	0.87
	16	347.16	397.75	448.76	0.883	175.12	0.88
	24	347.73	399.93	441.87	0.922	163.40	0.91
	48	347.02	400.47	442.47	0.894	132.06	0.89
	72	346.53	402.42	443.37	0.927	169.25	0.91
232℃	1	355.05	401.5	449.15	0.936	204.89	0.92
	2	355.26	400.61	449.32	0.936	206.11	0.92
	4	354.8	399.6	447.69	0.933	215.18	0.92
	8	348.91	402.46	447.90	0.923	167.20	0.92
	16	345.2	403.89	448.00	0.933	169.10	0.92
	24	343.28	402.56	448.93	0.876	121.83	0.84
	48	342.91	407.55	446.70	0.908	104.18	0.85
	72	335.78	409.85	441.85	0.909	66.94	0.78
260℃	1	350.96	398.86	437.40	0.929	211.91	0.94
	2	346.4	399.25	447.30	0.881	149.67	0.87
	4	346.4	404.4	446.69	0.929	148.12	0.91
	8	318.6	403.84	440.60	0.895	63.25	0.74
	16	314.23	420.3	463.72	0.848	41.64	0.75
	24	318.54	436.12	473.92	0.871	32.73	0.78
	48	323.68	456.18	498.00	0.879	29.65	0.74
	72	320.65	467.73	543.01	0.845	28.42	0.72

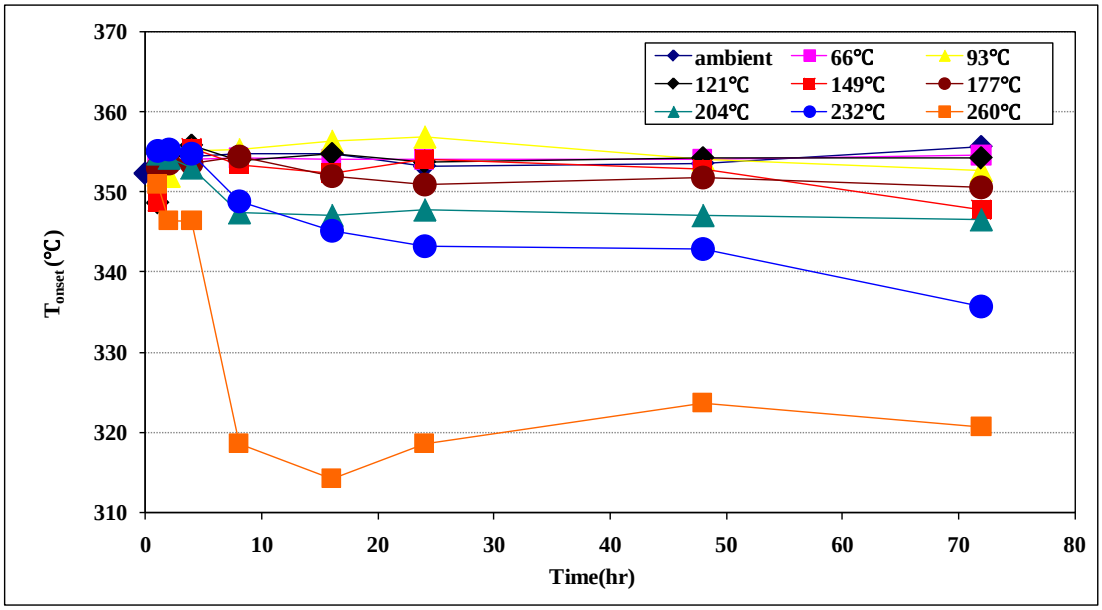

Figure 5-19: Onset temperatures of decomposition on specimens exposed to elevated temperature as a time function

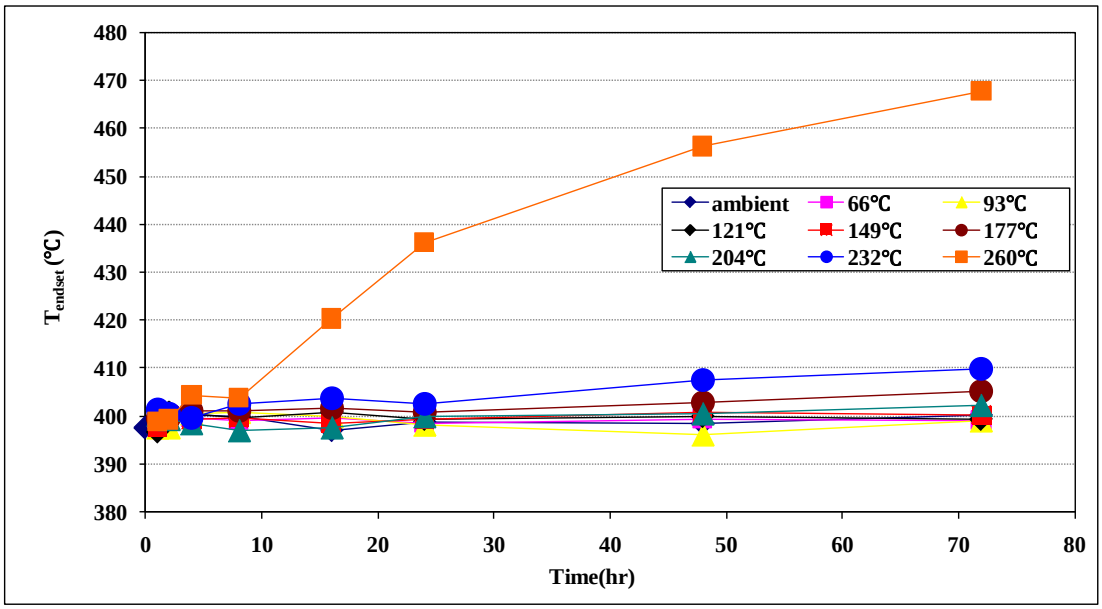

Figure 5-20: Endset temperatures of decomposition on specimens exposed to elevated temperature as a time function

In general, the mass of composite materials indicates little change until decomposition is initiated as mentioned previously. The degree of decomposition (α) can be expressed as

$$\alpha = \frac{(M_i - M)}{(M_i - M_e)} \tag{5.13}$$

where:

M = instantaneous mass

M_i = initial mass

M_e = final mass after decomposition

As can be seen in Figure 5-21, the values of decomposition degree at single heat rate (10℃/min) on specimens exposed to elevated temperature for 72 hrs show a little change before and after decomposition in the majority of exposure temperatures. Meanwhile, from Figure 5-21 decomposition was started at lower temperatures and was finished at higher temperatures in exposure temperatures, i.e., 232 and 260℃ compared to other environmental conditions. The reaction rate ($d\alpha/dT$) can be expressed by dividing the decomposition degree into temperatures and reaction rate of decomposition at single heat rate (10℃/min) on specimens exposed to elevated temperature for 72 hrs are depicted in Figure 5-22. The maximum reaction rate occurs $d^2\alpha/dT^2 = 0$. T_m and α_m can be defined as the maximum temperature and degree of decomposition at the maximum reaction, respectively. The values of T_m and α_m are tabulated in Table 5-9. In the case of exposure temperature (260℃) for 72 hrs, T_m shows the highest value and α_m indicates the lowest value compared to other environmental conditions.

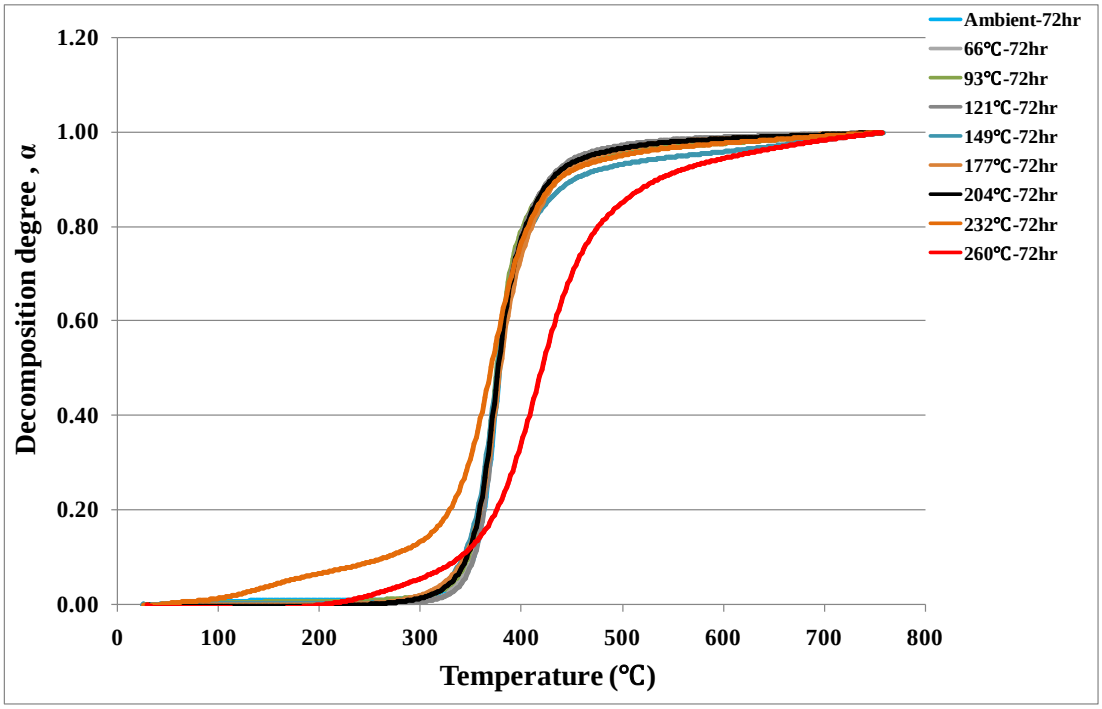

Figure 5-21: Decomposition degree at single heat rate (10℃/min) on specimens exposed to elevated temperature for 72 hrs

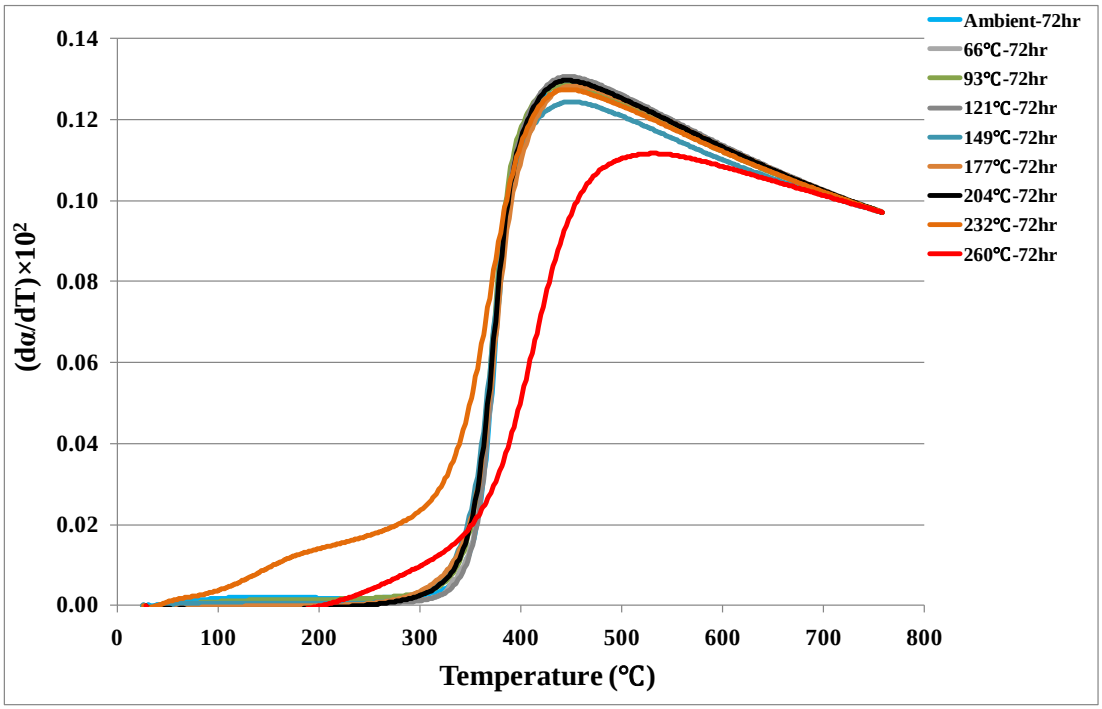

Figure 5-22: Reaction rate of decomposition at single heat rate (10℃/min) on specimens exposed to elevated temperature for 72 hrs

To determine the decomposition activation energy (E_d), the modified Coats and Redfern methods[72, 73] were applied. This method is suitable for experiment with single heating rate TGA curve. The decomposition process can be expressed by the theory of chemical reaction rate and the Arrhenius law[74]. The rate of decomposition is determined by the temperature and the quantity of reactants as follows:

$$\frac{d\alpha}{dt} = k(T)\, f(\alpha) \tag{5.14}$$

where k(T) and f(α) mean the effect of temperature and the effect of the reactant quantity to the reaction rate, respectively. Also, k(T) and f(α) can be expressed as follows:

$$f(\alpha) = (1-\alpha)^n \tag{5.15}$$

$$k(T) = A\exp\left(\frac{-E_d}{RT}\right) \tag{5.16}$$

where A is the pre-exponential factor, E_d is the activation energy, R is the universal gas constant, n is the reaction order. Moreover, a constant heating rate is express by

$$\frac{dT}{dt} = \beta \tag{5.17}$$

Consequently, from Equation 5.14~5.17, the rate of decomposition can be described below:

$$\frac{d\alpha}{dT} = \frac{A}{\beta}\exp(-\frac{E_d}{RT})(1-\alpha)^n \tag{5.18}$$

By integrating and logarithm, Equation 5.18 can be transformed as

$$\ln(\frac{\alpha}{T^2}) = \ln(\frac{AR}{\beta E_d}) \cdot (1 - \frac{2RT}{E_d}) - \frac{E_d}{RT} \quad (5.19)$$

From Equation 5.19, a slope of E_d/R can be obtained by a straight line of a plot of $\ln(\alpha/T^2)$ versus 1/T. In this TGA, a good linearity of $\ln(\alpha/T^2)$ versus 1/T was found in the α range between 1% and 30%. The coefficient of determination (R^2) was more than 0.99 in linear region.

Meanwhile, Reaction order, n, of the decomposition reaction is determined according to Kissinger model[75] according to the following equations.

$$\text{For } n \neq 1, \quad n(1-\alpha_m)^{n-1} = 1 + (n-1)\frac{2RT_m}{E_d} \quad (5.20)$$

The values of activation energy and reaction order using Equation 5.19 and 5.20 are tabulated in Table 5-9. Figure 5-23 shows activation energy of decomposition on specimens exposed to elevated temperatures as a function of time. Activation energies for un-aged specimens were less than 190 KJ/mol. With increased exposure temperatures, the value of activation energy was increased up to 293.76 KJ/mol (exposure temperature: 121℃, ageing time: 8 hrs) due to post-cure effect. Higher activation energy is required to decompose polymer composites since the higher degree of crosslinking due to post-cure effect brings more bonds in polymer chain. As expected, activation energies catastrophically dropped less than 100 KJ/mol in severe conditions exposed to 232℃ for 72 hrs and 260℃ for more than 8 hrs. The breakage of polymer chains in severe conditions due to thermooxidation resulted in decrease in activation energy.

In the case of reaction order, the majority of reaction order existed between 0.85

and 0.95. The reason why reaction order showed the similar values is that the same degradation mechanisms are applied for specimens, which severe breakage of polymer chain did not occurred in the process of ageing. Similar to the results of activation energy, reaction order decreased less than 0.8 in severe conditions exposed to 232℃ for 72 hrs and 260℃ for more than 8 hrs. The decrease of reaction order means extreme change of degradation mechanisms. In other words, it is indicative that a serious degradation occurred in chemical structures of the molecular chains.

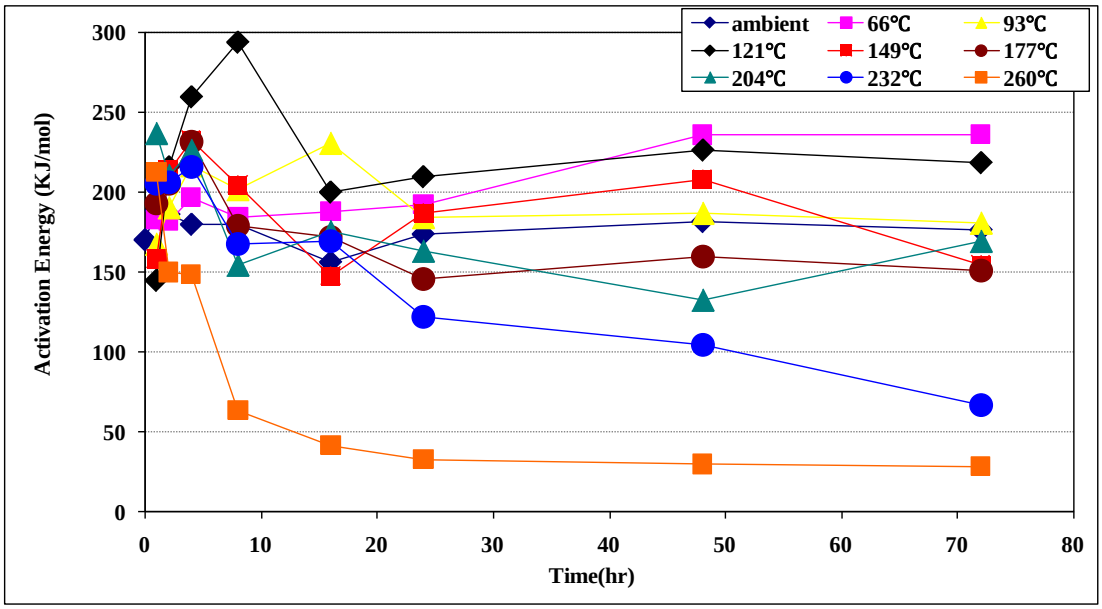

Figure 5-23: Activation Energy of decomposition (E_d) on specimens exposed to elevated temperatures as a function of time

5.3.2.3 Mechanical Retention based on Weight loss

As mechanical properties are strongly dependent on glass transition temperature, weight loss (%) of composite materials also is also associated with mechanical characterization. In Figure 5-24, mechanical retentions for four tests (Tension, off-axis shear, flexure and SBS) are represented as a function of weight loss. Most data of mechanical retention existed between 0 and 4% except for severe environmental conditions. Within 4% of weight loss, the majority of mechanical retentions showed higher values than un-aged specimens except for the properties of off-axis shear test. This phenomenon means the increase of mechanical property due to post-cure effect is more dominant than decrease of mechanical property by weight loss. The continuous decrease of off-axis shear property regardless of post-cure effect resulted from the distortion of specimens by asymmetry. In the case of tension, tensile properties showed retention more than 100% until weigh loss was reached 6% and after 6%, linearly were decreased.

In the ranges within 4% of weight loss, the mechanical retentions of flexure and short beam shear test were slightly increased due to residual post-cure effect. As shown in Figure 5-24, if the weigh losses of polymer composites were more than 6%, since the retentions of all mechanical properties were decreased up to 50%, polymer composites could not play a role as structures. Consequently, thermal stability parameters including weight loss and glass transition are important criteria to evaluate the performance and functionality of fiber reinforced polymer composites.

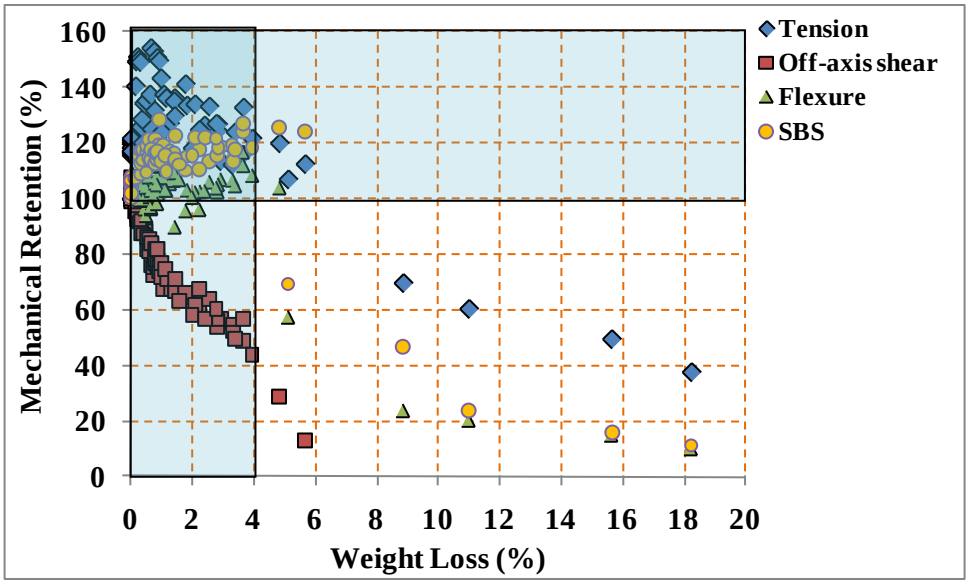

Figure 5-24: Characterization of four mechanical properties as a function of weigh loss (%)

6 Immersion Analysis

6.1 Introduction

From past researches, it is known that polymer composites are very sensitive and are friendly to water and moisture in any forms. Moisture in polymer composites often causes swelling and degradation. Especially, since polymer composite used in marine environments can easily be exposed to moisture regarding relative humidity and immersion, degradation mechanisms related to moisture must be investigated to evaluate the service life and long term effects. Matrix and/or interface degradation resulting from moisture absorption is a concern in most composite applications subject to normal atmospheric moisture, which can range from precipitation to mild humidity. Complete immersion in water constitutes the most severe environment, while humid air generally results in lower maximum moisture content[76]. Since this study is focused on assessment of composite materials for naval vessel applications, immersion analysis will be mainly performed in accordance with related theories.

While general investigations regarding moisture uptake are focused on the specimens cured in ambient temperature, this study is concentrated on the immersion effects of specimens exposed to elevated temperatures because naval vessels of composite materials exposed to the various heat sources such as electrical faults, ignition of flammable gases or liquids and weapon strikes must be estimated in terms of operating life. Consequently, mechanisms of complicated degradation including temperature and immersion effect can be applied for naval vessels. In following section, the theories regarding moisture effects on polymer composites will be introduced.

6.1.1 Moisture Effect on Polymer Composites

The effect of moisture sorption on the degradation of polymer composite materials was well established from a lot of investigations and studies. The degradation of polymers due to moisture can be divided into chemical and physical degradation. Chemical changes include hydrolysis of the polymer chain and interfacial bond while physical degradation means swelling, plasticization, and relaxation of the polymer[77, 78]. As swelling by moisture ingress promotes microcracking in the hydrolyzed damaged resin and interfacial debonding at the hydrolyzed interface, physio-mechanical degradation may also take place.

By moisture ingress on polymer composites, degradation mechanisms can be summarized as followings; 1) Hydrolysis: Hydrolysis is related to plasticization and this process occurs from separation of side groups from the polymer chains[17]. From the separation of polymer chains, weight loss generally occurs at the fiber-matrix interface region. This process cause permanent and irreversible degradation. 2) Plasticization: Polymer composite first experiences the plasticization due to moisture. Plasticization occurs in the matrix when bonds between ethers, secondary amines, and hydroxyl groups are broken[79]. This process involves swelling of the matrix. Unlike hydrolysis, this mechanism for degradation is reversible process on drying. 3) Microcracking: Composite materials can undergo matrix microcracking occurring when the composite reaches a stress level where the matrix begins to crack away from the fibers. Wicking created by matrix microcracking results in the ingress of large amounts of moisture into composite materials. Therefore, crack also results in high amounts of strength loss. 4) Debonding: composite materials made by hand wet layup process can have flaws in

terms of bond between the fiber and matrix. This process can be occurred by a pressure difference resulting from the moisture that is absorbed by the composite materials. This process is also irreversible degradation. 5) Delamination: Poor interface between layers can occur an acceleration of the delamination due to moisture. This is also irreversible process. Beside degradation mechanisms described above, moisture can cause fiber pitting, chain scission, leaching and microvoids in the form of reversible or irreversible degradation.

Accordingly, moisture uptake is important parameter to assess susceptibility of composite materials to deterioration and is used in the prediction of long-term durability. Under steady state conditions, moisture uptake in a composite can be expressed as a percent of the original dry mass,

$$M = \frac{(W_t - W_i)}{W_i} \times 100 \tag{6.1}$$

Where:

M = percent moisture uptake (change in weight)

W_i = initial weight of the specimen (prior to immersion)

W_t = Weight of the specimen after time t

6.1.2 Diffusion in Polymer Composites

In general definition, diffusion is the movement of molecules from a region of high concentration to a region of low concentration by means of random molecular motion. Fick's laws provide a theoretical basis for the diffusion of a fluid into a distinct

sorbing medium from a higher concentration to a lower concentration. Also, Fick's second law provides a theory for non-steady-state diffusion. Fick's law refer to that the mass of absorbed water increases linearly with the square root of time and then gradually slows until an equilibrium plateau or saturation is reached. The rate of diffusion and the attainment of an equilibrium content can be affected by materials characteristics, processing factor, environmental condition, and geometry. Since Fickian diffusion assumes no chemical reaction between the diffusion solution and composite materials, composites technically do not follow Fick's law. However, in a number of researches, the diffusion of moisture in fiber reinforced composites and crosslinking resin has been shown Fickian behavior[80, 81]. Fickian diffusion has following features.

1) Linear in the initial stage and the linear region until at least $M_t/M_m=0.6$

where:

M_t = the moisture absorbed by the composites at time t

M_m= the maximum moisture content absorbed by the composite

2) The decrease of the rate of diffusion until an equilibrium of moisture content

3) Diffusion coefficient as a function of temperature

$$D = D_0 \exp\left(\frac{-E_a}{RT}\right) \tag{6.2}$$

where:

D = diffusion coefficient

D_0= a constant

E_a= activation energy

R = the universal gas constant

The theory of Fickian diffusion also assumes that only reversible physical reactions take place in the polymer matrix during the process of moisture sorption.

Figure 6-1 shows schematic curves representing four categories of recorded non-Fickian weight-gain sorption compared to linear Fickian diffusion. This Figure was postulated by Weitsman[82]. Curve A means pseudo-Fickian diffusion characterized by a initial uptake in the beginning stages of immersion similar to Fickian behavior. However, saturation or equilibrium is not attained in this case. In the case of curve B describing two-stage diffusion behavior, the weight of composite materials initially increases due to moisture while this process experiences a quasi-equilibrium by the competition between moisture uptake and mass loss. Curve C caused by deformations, wicking, or mechanical failure is a type of diffusion where moisture is rapidly increasing. Curve D in Figure 6-1 shows weight loss that is attributed to hydrolysis or other types of irreversible degradations. Curve LF, which has the solid line, stand for linear Fickian diffusion that follows the Fick's law.

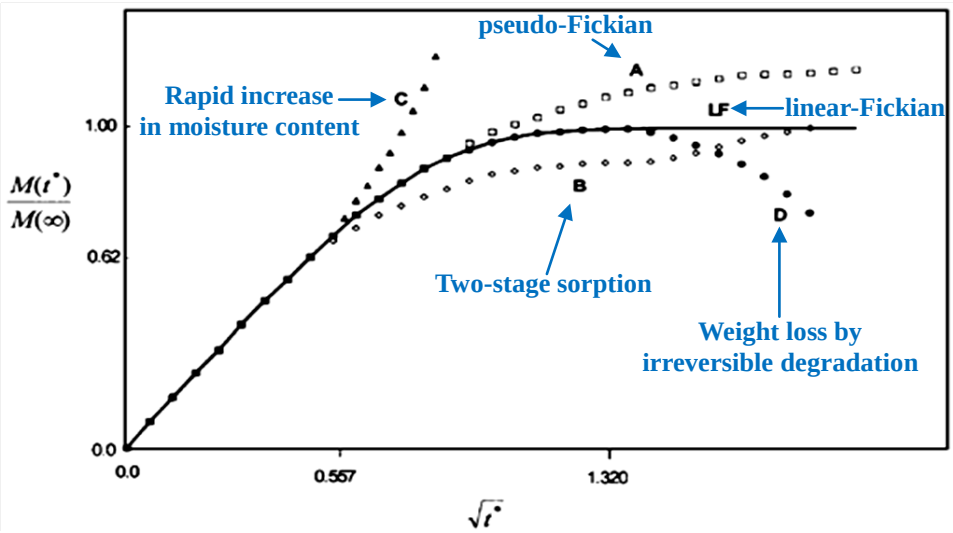

Figure 6-1: Schematic curves representing four categories of recorded non-Fickian weight-gain sorption [82]

The diffusion coefficient can be calculated either by monitoring the concentration characteristic from the volume of composite materials or via gravimetric measurements[83]. Ultimately, the diffusion coefficient can be determined according to a theoretical model used to fit experimental data trends. In case moisture uptake shows the Fickian diffusion, diffusion coefficient can be determined using the short-term approximation as expressed by Equation 6.3[84].

$$D = \frac{\pi h^2}{16 M_\infty^2}\left(\frac{M_2 - M_1}{\sqrt{t_2} - \sqrt{t_1}}\right)^2 \tag{6.3}$$

where:

D = the Fickian coefficient of diffusion, mm^2/s

h = the thickness of the specimen, mm

M_∞ = the weight gain after equilibrium, g

M_1, M_2 = the percent changes in weight at time t_1 and t_2, %

The test specimens used for moisture absorption tests are made in the form a thin plate so that the moisture enters predominantly through the surface marked by the length (l) and the width (b). However, as shown in Figure 6-2, contact angles of specimens in top and edge surface are 69^o and 43^o, respectively. Considering the edge effects on Equation 6.3, the diffusion coefficient multiplied by a correction factor is obtained in the form of the one-dimensional diffusion coefficient[84] as

$$D_{corr} = \frac{\pi h^2}{16 M_\infty^2}\left(\frac{M_2 - M_1}{\sqrt{t_2} - \sqrt{t_1}}\right)^2 \left(l + \frac{h}{l} + \frac{h}{b}\right)^{-2} \tag{6.4}$$

where:

h = the thickness of the specimen, mm

l = the length of the specimen, mm

b = the width of the specimen, mm

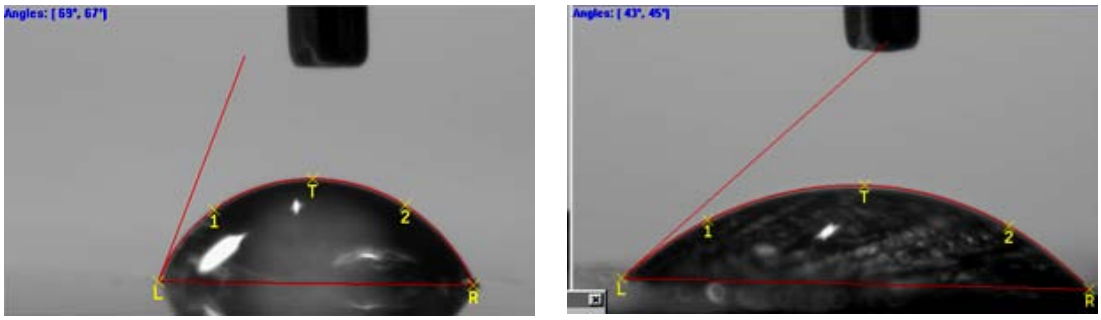

(a) (b)

Figure 6-2: Contact angle of specimens in (a) top surface and (b) edge surface

6.2 Analyses and Results

6.2.1 Water Uptake

Glass fiber laminates have low Young's modulus, which makes it difficult to build ultralight marine structures including naval vessels with adequate stiffness. Therefore, marine composite structures requiring high stiffness are often made of carbon fiber composite. However, a little of published papers are available on the effect of long-term seawater immersion on carbon fiber composite[85]. In addition, atmospheric ageing at high humidity has been reported to cause water uptake similar to that from immersion for epoxy laminates[86], while Gutierrez reported that ageing in sea air was as severe as in seawater for a range of marine composite. Especially, this study is focused on the effect of long-term seawater immersion on carbon fiber composites exposed to elevated temperatures for up to 72 hrs of ageing time using comparison with the effect of immersion in deionized water.

Before analysis of the effect of immersion on composites, the use of terms "absorption" and "adsorption" has to be clarified. Absorption is a capillary uptake by existing pores in materials and this process does not plasticize the matrix and generate little heat or swelling. Meanwhile, adsorption is the process by which a solution is formed and this process generates heat and swelling. If a polymer composite involves pores, air bubbles, or other such defects, both absorption and adsorption take place. In such a case, the term uptake is usually used[87].

The moisture uptake profiles for the carbon/epoxy composite specimens immersed in deionized water for 72 weeks are shown in Figure 6-3. Moisture uptake seems to follow two-stage diffusion response, with an initial period of linearity suggesting a diffusion-controlled process followed by a decrease in rate of moisture uptake. In other words, the results of the gravimetric measurements showed that the specimens immersed in deionized water displayed a Fickian response in all conditions. In the case of as-received specimens as shown in Figure 6-3 (a), saturation of weight gain did not occur until 1 year of immersion time and the levels of the maximum weight gain existed between 1.3% and 1.7%. These values were the lowest compared to the specimens in aged conditions. Specimens post-cured from the increase of ageing time and exposure temperature showed the rapid saturation and the higher maximum weight gain than in the case of un-cured specimens. The partially cured composite could be expected to have a greater concentration of unreacted chemical species with the epoxy resin and it appears that these were released more rapidly into water resulting in a slower net mass gain. Therefore, from experimental data, it should be pointed out that the degree of cure is proportional to the maximum mass uptake. The levels of the

maximum weight gain showed between 2.3% and 2.8% in exposure temperature, 177℃ and these levels were the highest compared to any other exposure temperatures. The deterioration of composite due to thermooxidaiton lowered the level of the maximum weight gain from the exposure temperatures of more than 232℃. Therefore, the level of maximums weight gain can be crucial criteria to evaluate the degree of cure on specimen under-cured in ambient condition. In severe environmental conditions (ageing time: more than 16 hrs, exposure temperature: 260℃), the moisture uptake profiles did not show the Fickian behavior. The reason why Fickian behavior did not occur is that the char formed by extreme heat played a role of sponge to absorb the water and thus the amount of moisture involving in specimens was different whenever the specimens were weighed in balance.

The chemical structure and morphology of a polymer are known to influence moisture uptake. Especially, a high concentration of polar functional groups can cause increased sorption of polar penetrants. The significant concentration of hydrophilic hydroxyl groups located along the backbone exists in epoxy resin. Therefore, many investigations reported that the maximum mass gain in epoxy is higher compared to the vinylester, polyester and phenolic resins. In addition, it is known that glass fibers chemically react with water, usually alkali elements to leach out while carbon fibers do not absorb moisture and are resistant to any corrosive effects of water[88].

The coefficient of diffusion provides a valuable characteristic in describing the rate at which water uptake is occurring. The Fickian diffusion uses an initial linear uptake period that is characterized by saturation at the maximum moisture content. General diffusion coefficients and corrective diffusion coefficients including edge effect

on specimens immersed in deionized water for 72 weeks are obtained from experimental data and are tabulated in Table 6-1. Similar to the maximum mass uptake, diffusion coefficient was also increased with the degree of cure. The diffusion coefficients of the specimens aged in ambient condition existed between 5.5×10^{-8} mm^2/s and 8.6×10^{-8} mm^2/s. As the specimens reached fully cure, diffusion coefficients increased up to 29.152×10^{-8} mm^2/s on specimen exposed to 121℃ for 1 hr of ageing time. It is well known that although the epoxy resin exhibited the highest equilibrium uptake or solubility (i.e., the mass of sorbed penetrant per unit volume of specimen) compared to vinylester, polyester and phenolic resins, it has the lowest diffusion coefficients. Since diffusion coefficient is a function of permeability and solubility, this means the permeability of the epoxy is lower than that of other resins.

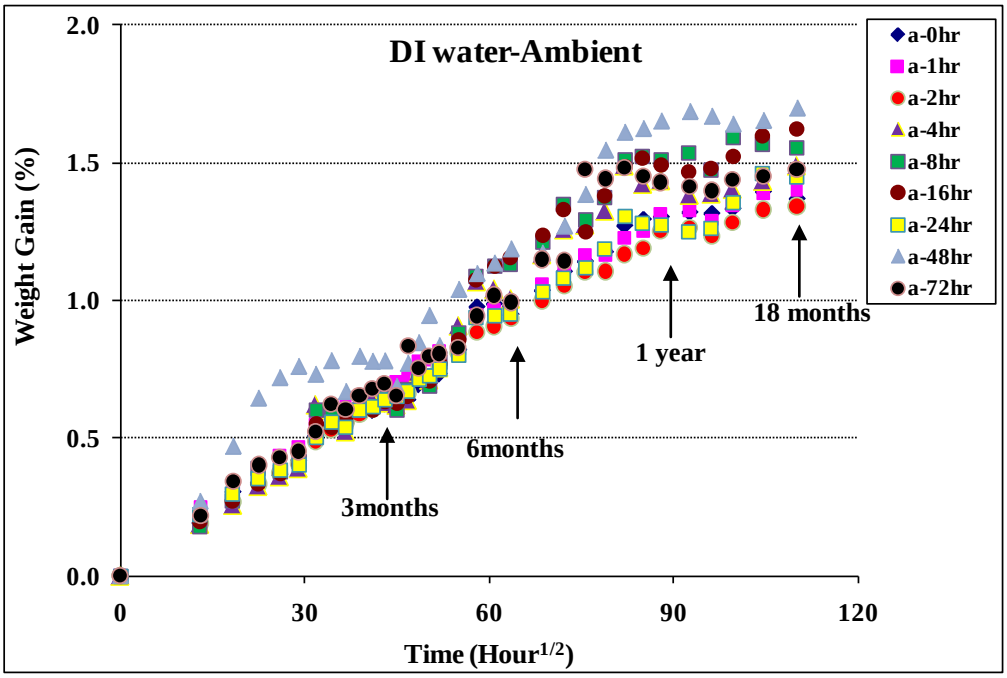

(a)

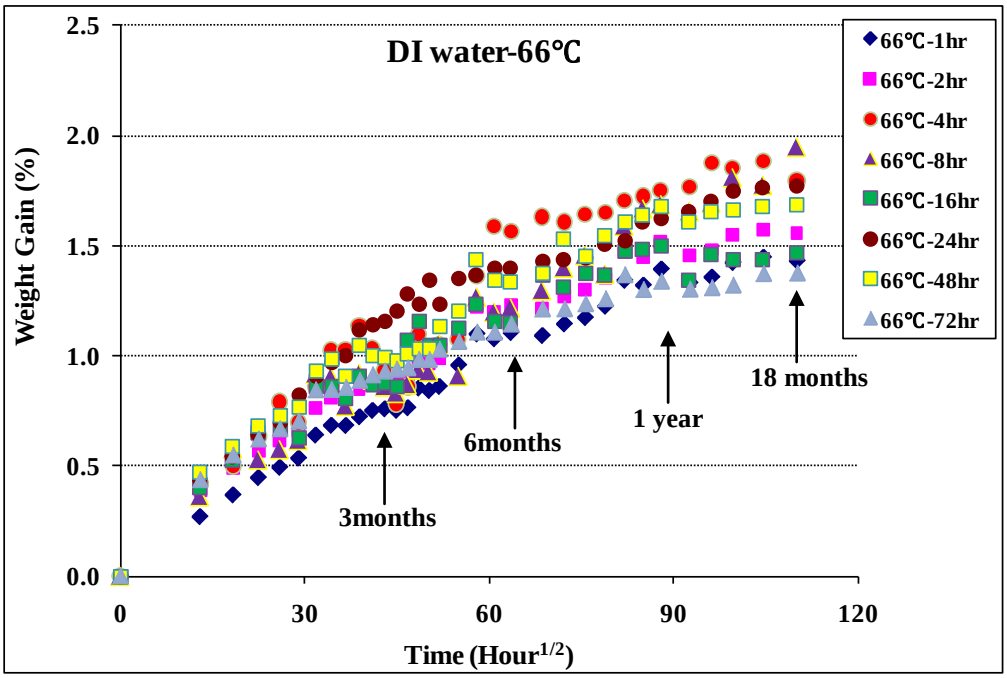

(b)

Figure 6-3: Weight Gain (%) on specimens immersed in deionized water for 72 weeks after exposure to elevated temperatures, (a) ambient (b) 66℃ (c) 93℃ (d) 121℃ (e) 149℃ (f) 177℃ (g) 204℃ (h) 232℃ (i) 260℃

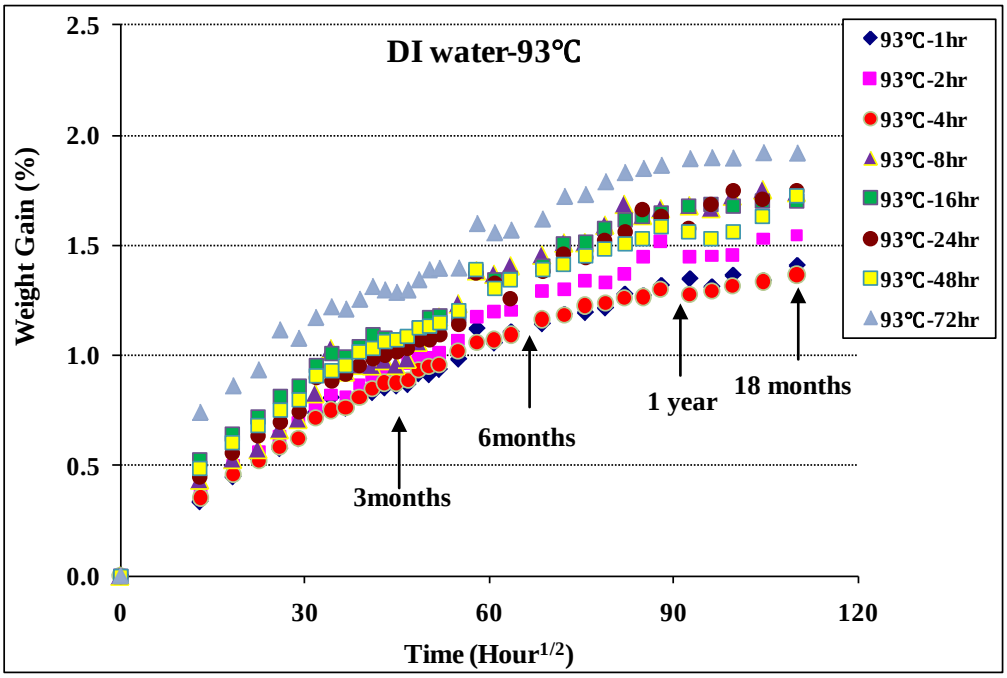

(c)

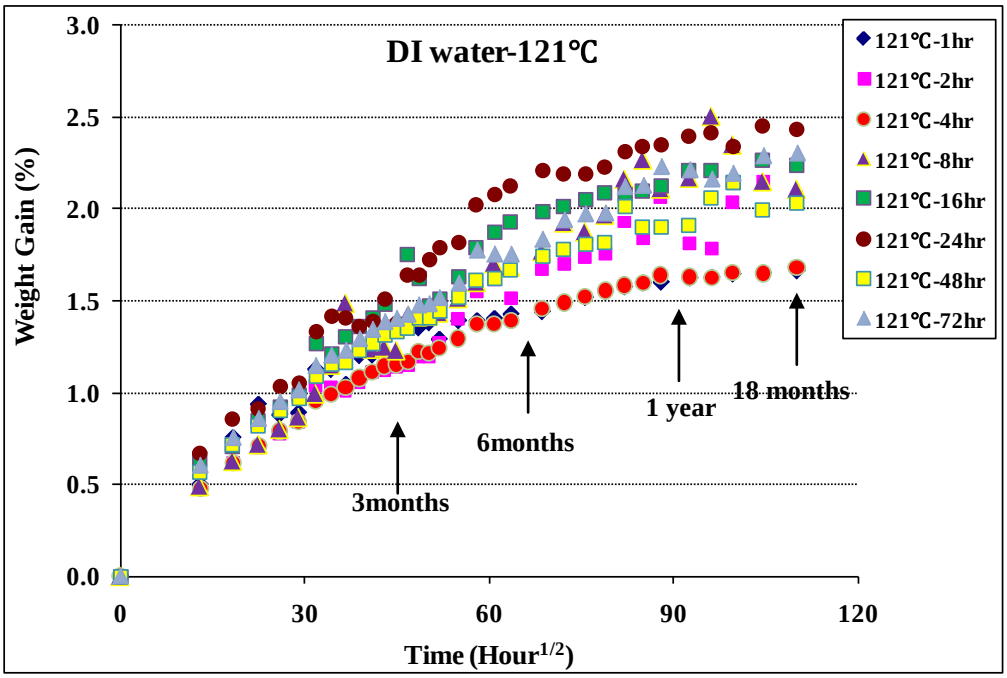

(d)

Figure 6-3: Continued

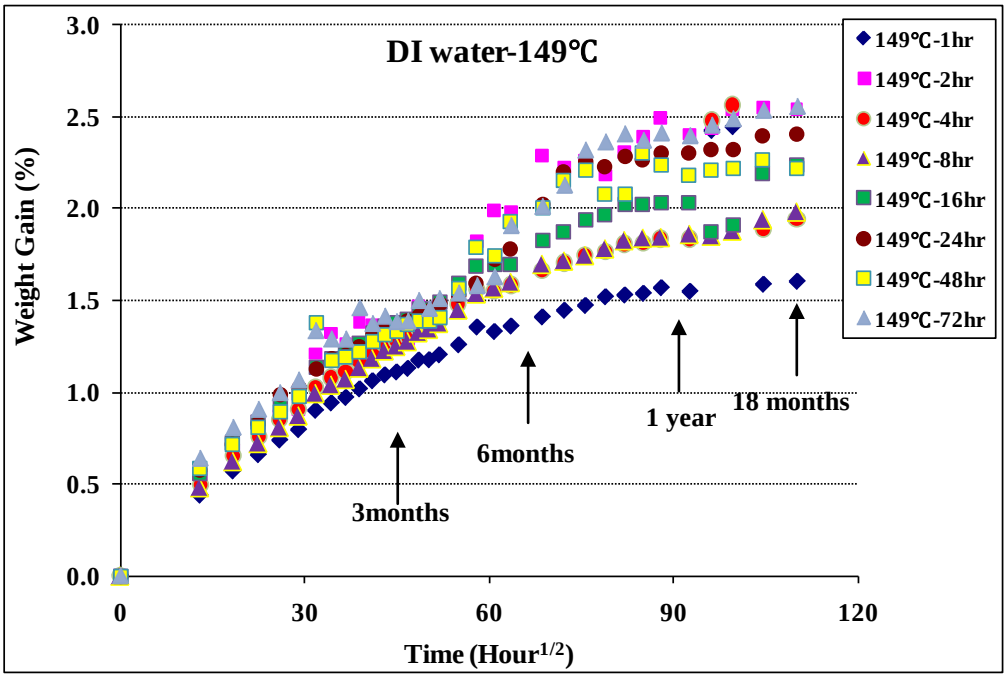

(e)

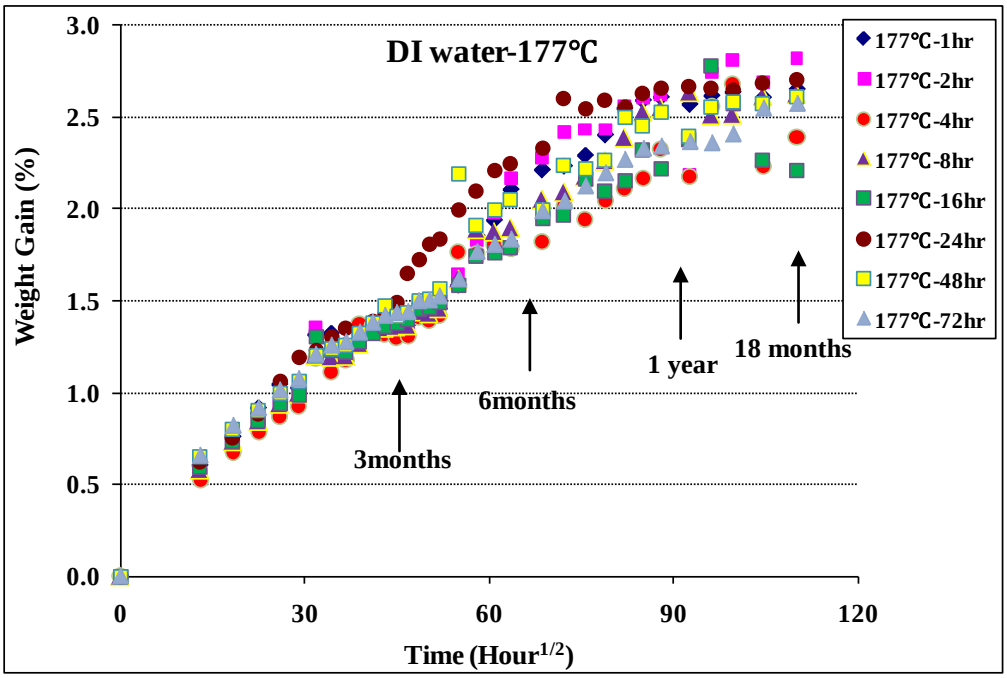

(f)

Figure 6-3: Continued

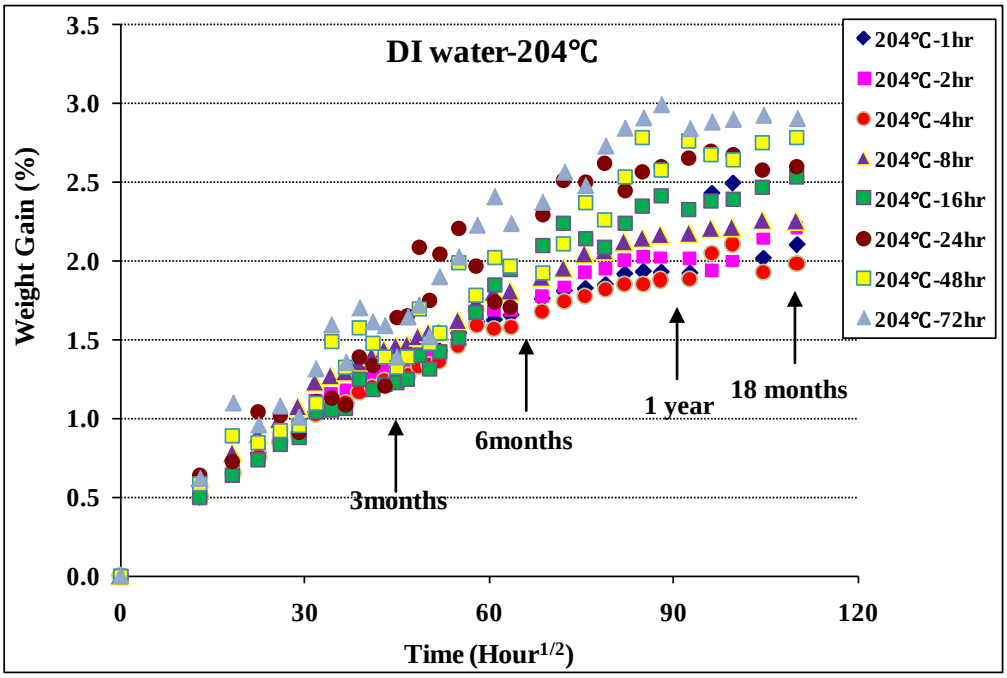

(g)

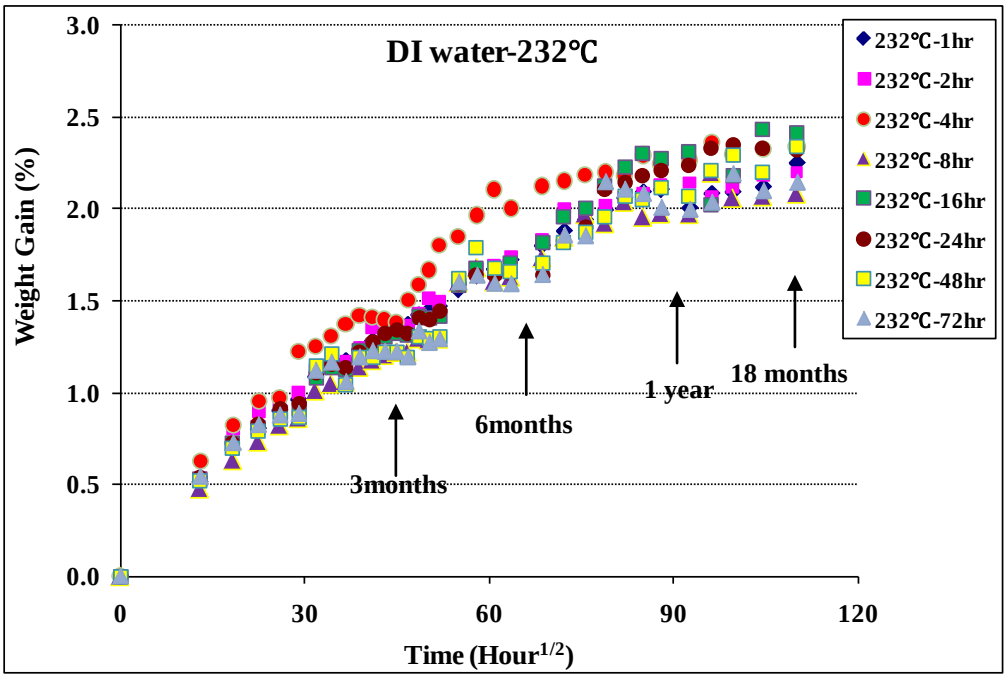

(h)

Figure 6-3: Continued

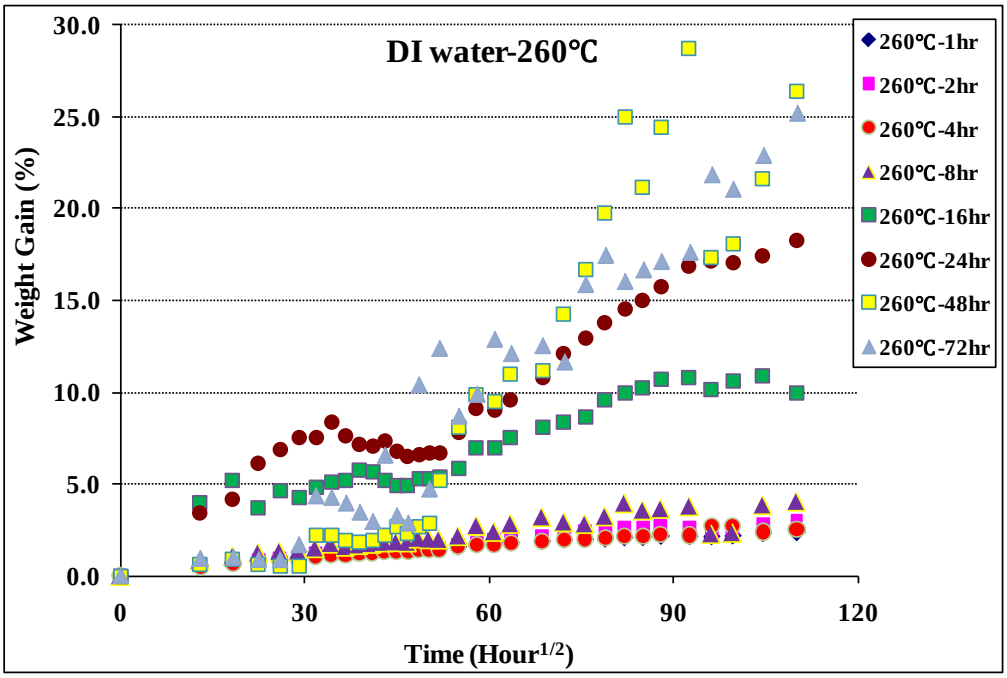

(i)

Figure 6-3: Continued

Table 6-1: Characteristics on specimens immersed in deionized water for 72 weeks after exposure to elevated temperatures

Exposure Temperature	Time	DI water							
		width (mm)	length (mm)	thickness (mm)	Mass (g)	M_∞ (%)	$D\times10^8$ (mm^2/s)	$D_{corr}\times10^8$ (mm^2/s)	slope
Ambient (23℃)	0	25.9	25.74	3.01	2.235	1.392	6.762	0.0100	0.0138
	1	24.41	25.7	2.73	2.012	1.390	6.756	0.0101	0.0152
	2	25.71	25.4	3.15	2.443	1.330	8.672	0.0132	0.0146
	4	25.74	25.91	2.89	2.290	1.431	7.065	0.0103	0.0149
	8	25.63	25.88	3.01	2.325	1.566	6.363	0.0093	0.0142
	16	25.36	25.53	2.82	2.256	1.599	5.625	0.0085	0.0144
	24	25.94	25.99	3.03	2.430	1.459	6.920	0.0101	0.0142
	48	26.12	25.58	2.86	2.277	1.656	5.588	0.0084	0.0144
	72	25.83	25.72	2.9	2.427	1.450	7.599	0.0113	0.0155
66℃	1	25.86	25.74	3.15	2.423	1.448	10.050	0.0149	0.0164
	2	25.06	25.83	2.95	2.223	1.573	9.558	0.0141	0.0178
	4	25.78	24.78	3.17	2.262	1.886	10.382	0.0166	0.0189
	8	24.9	25.84	3.25	2.317	1.774	9.608	0.0141	0.0172
	16	25.87	25.61	3.15	2.390	1.439	14.300	0.0214	0.0195
	24	25.57	25.87	2.9	2.131	1.763	17.316	0.0254	0.0258
	48	25.83	26.02	3.1	2.426	1.675	11.181	0.0162	0.0189
	72	26.06	25.69	3.15	2.462	1.376	12.604	0.0187	0.0179
93℃	1	25.67	26.01	3.05	2.425	1.339	11.604	0.0168	0.0175
	2	25.94	26.02	3.17	2.530	1.530	12.799	0.0186	0.0189
	4	26	25.69	3.03	2.378	1.334	12.025	0.0179	0.0179
	8	26.04	25.68	2.87	2.307	1.752	10.673	0.0159	0.0204
	16	25.4	25.87	3	2.159	1.705	12.221	0.0179	0.0206
	24	25.96	25.83	3.08	2.365	1.709	11.992	0.0176	0.0199
	48	26.21	25.73	3.05	2.465	1.629	13.348	0.0198	0.0207
	72	25.75	25.88	3.15	2.285	1.919	14.535	0.0213	0.0227
121℃	1	25.94	25.52	2.92	2.152	1.654	29.152	0.0440	0.0322
	2	25.97	25.47	3.15	2.242	2.154	22.016	0.0333	0.0296
	4	25.94	25.2	2.95	2.184	1.648	22.905	0.0354	0.0282
	8	25.97	25.62	3.28	2.385	2.146	26.107	0.0390	0.0309
	16	25.46	26.1	2.98	2.219	2.262	23.597	0.0340	0.0332
	24	25.75	25.72	2.84	2.186	2.451	20.505	0.0305	0.0338
	48	25.47	25.81	3.12	2.512	1.991	23.516	0.0346	0.0297
	72	25.91	25.97	3.1	2.506	2.291	22.417	0.0326	0.0313
149℃	1	25.63	25.96	3.05	2.322	1.586	16.926	0.0247	0.023
	2	25.92	25.82	3.07	2.363	2.550	14.261	0.0210	0.0266
	4	25.66	25.93	3.19	2.580	1.886	25.442	0.0371	0.0294
	8	25.89	25.82	3.36	2.614	1.941	25.591	0.0376	0.0284
	16	25.94	25.61	3.17	2.550	2.193	20.730	0.0310	0.0288
	24	25.85	25.56	3.02	2.289	2.399	16.488	0.0248	0.0282
	48	25.92	25.52	3.2	2.422	2.267	19.730	0.0297	0.0283
	72	25.4	25.8	2.94	2.149	2.535	15.106	0.0223	0.0285

Table 6-1: Continued

Exposure Temperature	Time	DI water							
		width (mm)	length (mm)	thickness (mm)	Mass (g)	M_∞ (%)	$D\times10^8$ (mm^2/s)	$D_{corr}\times10^8$ (mm^2/s)	slope
177℃	1	25.86	25.78	2.91	2.216	2.606	11.343	0.0168	0.0253
	2	25.98	25.9	3.08	2.383	2.692	14.219	0.0208	0.272
	4	25.87	25.73	3.2	2.510	2.229	17.592	0.0261	0.0265
	8	25.68	25.89	2.99	2.312	2.615	12.797	0.0188	0.0262
	16	25.64	25.77	3.18	2.363	2.264	17.235	0.0255	0.0266
	24	24.69	25.79	3.23	2.359	2.682	22.132	0.0326	0.0323
	48	25.67	25.99	3.1	2.340	2.574	15.063	0.0219	0.0272
	72	25.4	26	3	2.306	2.553	13.810	0.0201	0.0268
204℃	1	25.94	25.74	3.16	2.570	2.015	16.620	0.0246	0.0248
	2	25.83	25.89	2.96	2.290	2.142	13.941	0.0204	0.025
	4	25.95	25.88	3.04	2.417	1.929	14.427	0.0212	0.0235
	8	25.52	25.82	3.04	2.238	2.257	14.867	0.0219	0.0258
	16	26.01	25.51	3.19	2.470	2.463	16.424	0.0248	0.027
	24	26.06	25.06	3.08	2.173	2.582	19.011	0.0297	0.0308
	48	25.86	25.97	3.25	2.553	2.747	17.638	0.0257	0.029
	72	26.08	25.9	3.3	2.538	2.930	21.946	0.0321	0.0329
232℃	1	25.8	25.82	3.14	2.529	2.118	14.872	0.0219	0.0242
	2	25.88	25.91	3	2.447	2.183	13.063	0.0191	0.0241
	4	25.07	25.81	3.08	2.358	2.326	17.938	0.0264	0.0284
	8	25.97	25.82	2.89	2.263	2.068	12.585	0.0186	0.0239
	16	24.93	25.92	2.87	2.293	2.435	10.893	0.0159	0.0243
	24	25.69	25.95	2.89	2.346	2.329	10.081	0.0147	0.0227
	48	25.48	25.89	2.98	2.212	2.203	11.936	0.0175	0.0233
	72	25.89	25.58	3.04	2.311	2.097	11.740	0.0176	0.0221
260℃	1	26.01	25.88	3.11	2.631	2.308	8.512	0.0125	0.0193
	2	25.74	25.87	3.07	2.449	2.816	13.110	0.0192	0.0268
	4	25.82	25.88	2.85	2.363	2.390	8.808	0.0129	0.0218
	8	25.77	25.98	3.06	2.274	2.846	9.512	0.0197	0.0319

Meanwhile, Figure 6-4 shows weight Gain (%) on specimens immersed in seawater for 72 weeks after exposure to elevated temperatures. Similar to the result of the immersion effect in deionized water, moisture uptake profile in seawater showed the Fickian behavior. The degree of cure is also proportional to the maximum weight gain and diffusion coefficient. If looking at Figure 6-4 (a), saturation of weight gain did not occur until 1 year of immersion time and the levels of the maximum weight gain existed between 1.3% and 1.8% similar to result of immersion in deionized water. The maximum weight gain did not largely increase until exposure temperature of 149℃. Also, in severe environmental conditions, weight gain was not accurately measured due to char created by thermooxidation and damage in the form of debonding, microcraking, and other types of morphological changes, thus allowing additional sorption to occur[89]. In this condition, although the variation of weight gain existed, continuous increase of weight gain was shown.

Table 6-2 shows diffusion coefficient and slope in linear region ($M_t/M_m<0.6$) on specimens immersed in seawater for 72 weeks after exposure to elevated temperatures. Diffusion coefficient and corrective diffusion coefficient considering edge effect on specimens exposed to ambient temperature up to 72 hrs existed from 7.5×10^{-8} mm^2/s to 13.3×10^{-8} mm^2/s and from 0.01×10^{-8} mm^2/s to 0.02×10^{-8} mm^2/s, respectively. Even though ageing time and exposure temperatures were increased, diffusion coefficient did not excess 20×10^{-8} mm^2/s except for some environmental conditions.

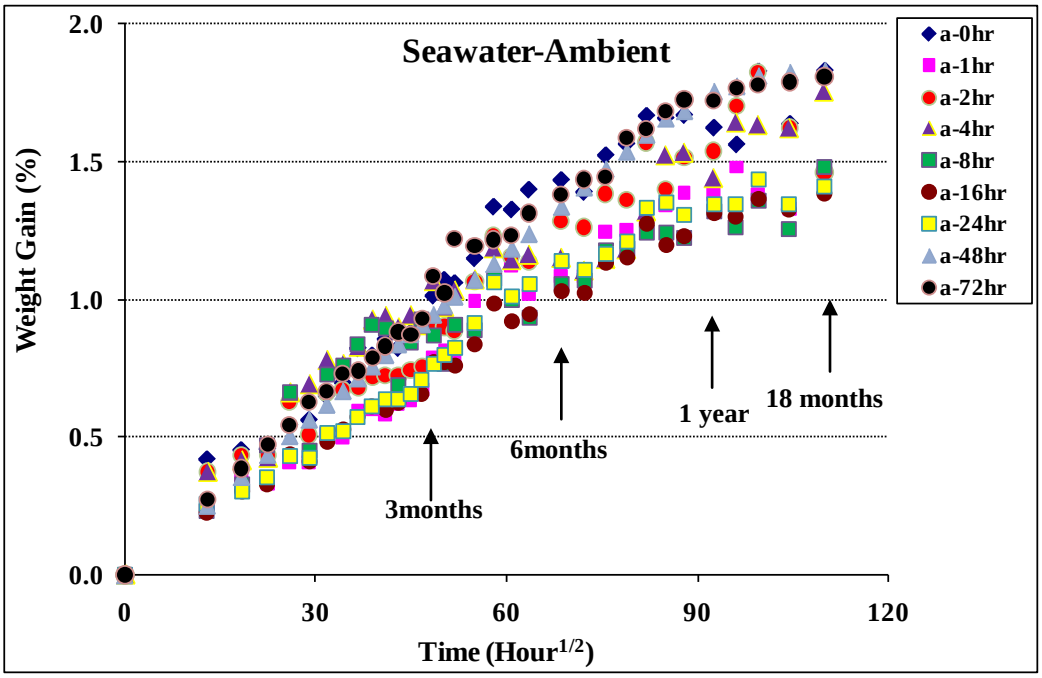

(a)

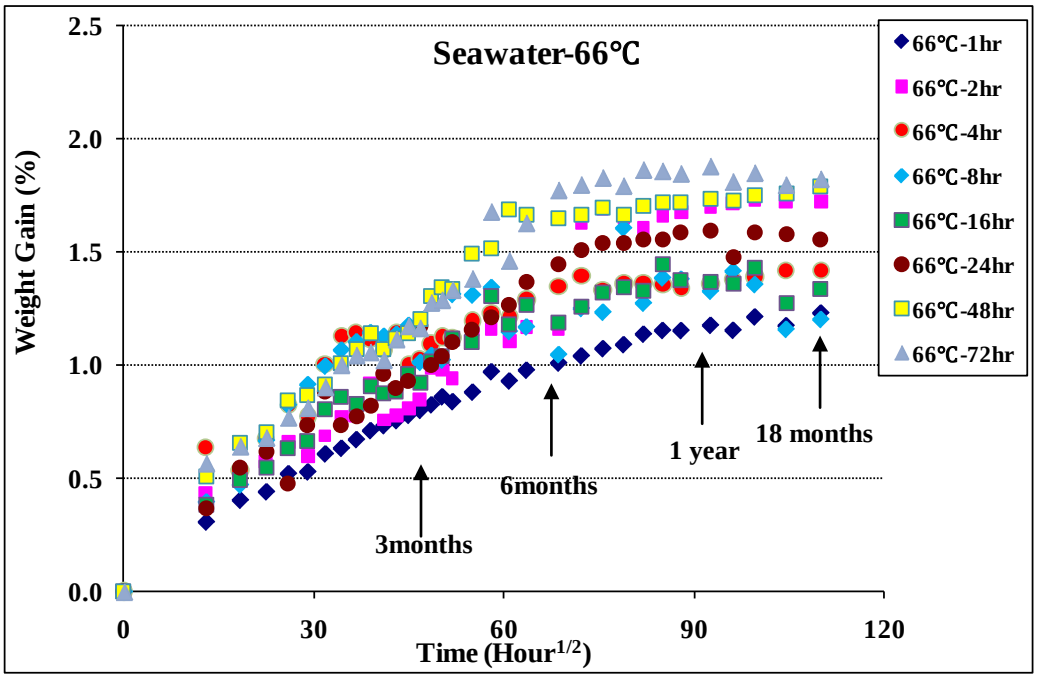

(b)

Figure 6-4: Weight Gain (%) on specimens immersed in seawater for 72 weeks after exposure to elevated temperatures, (a) ambient (b) 66℃ (c) 93℃ (d) 121℃ (e) 149℃ (f) 177℃ (g) 204℃ (h) 232℃ (i) 260℃

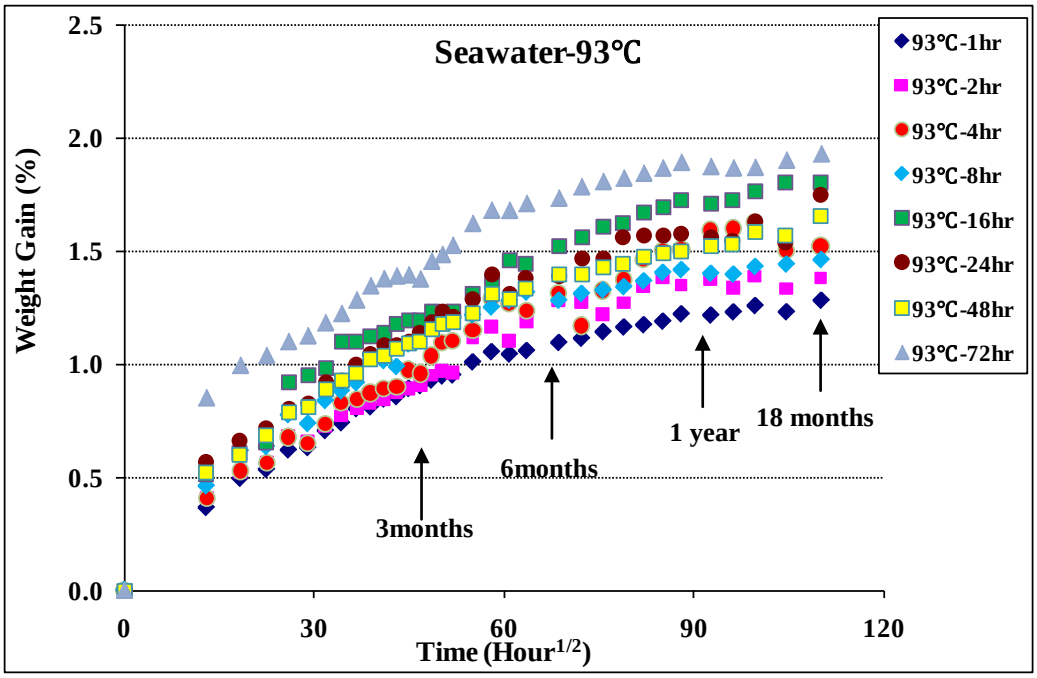

(c)

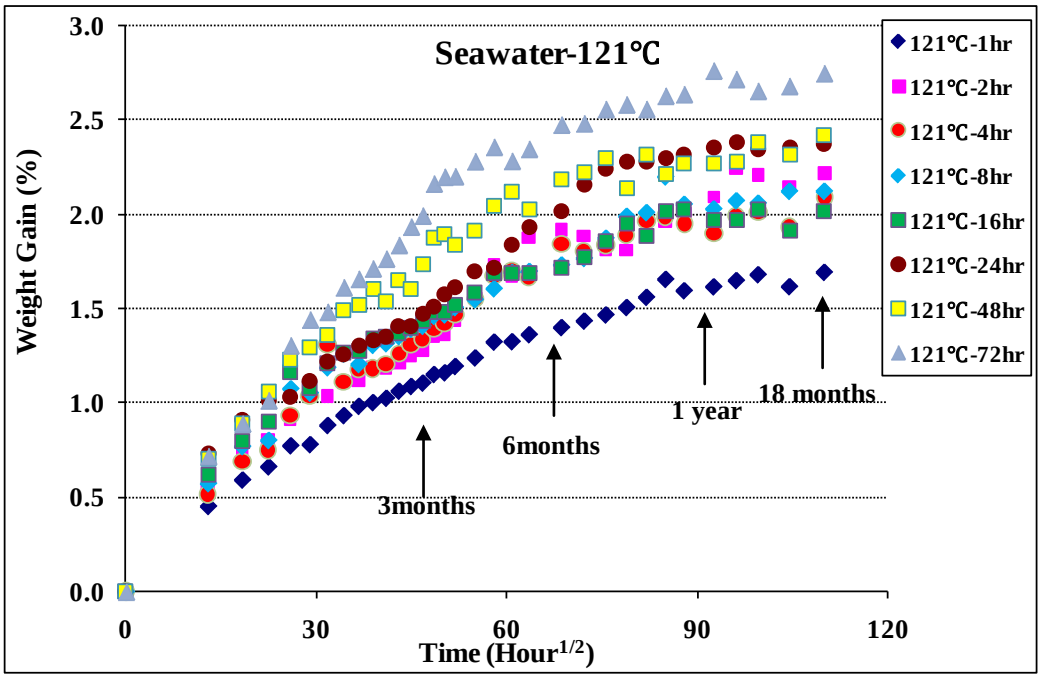

(d)

Figure 6-4: Continued

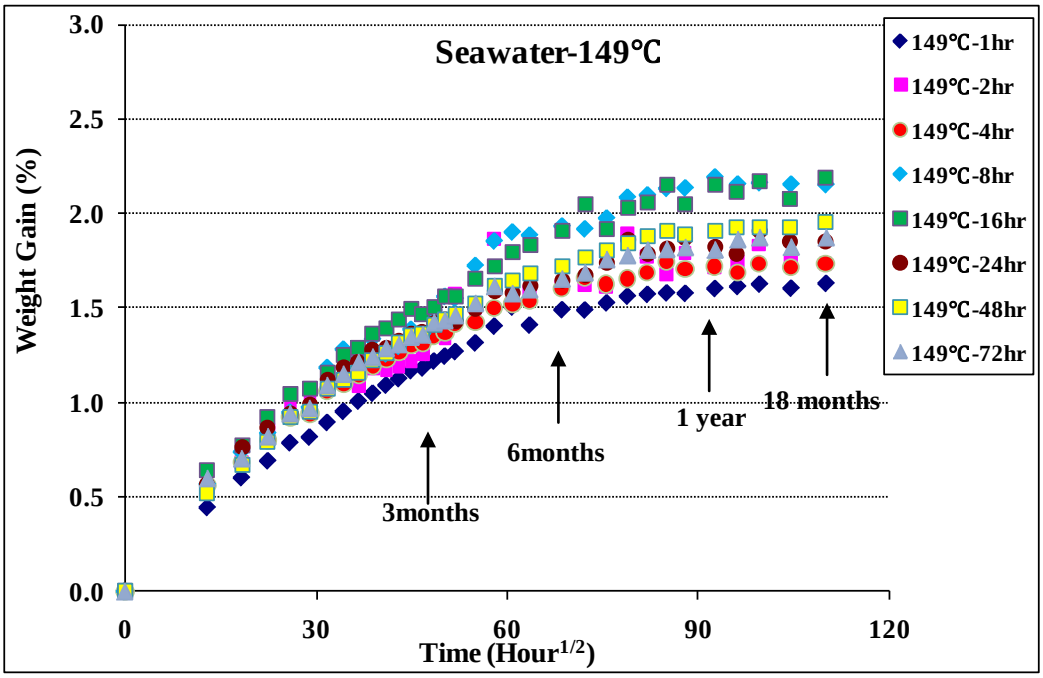

(e)

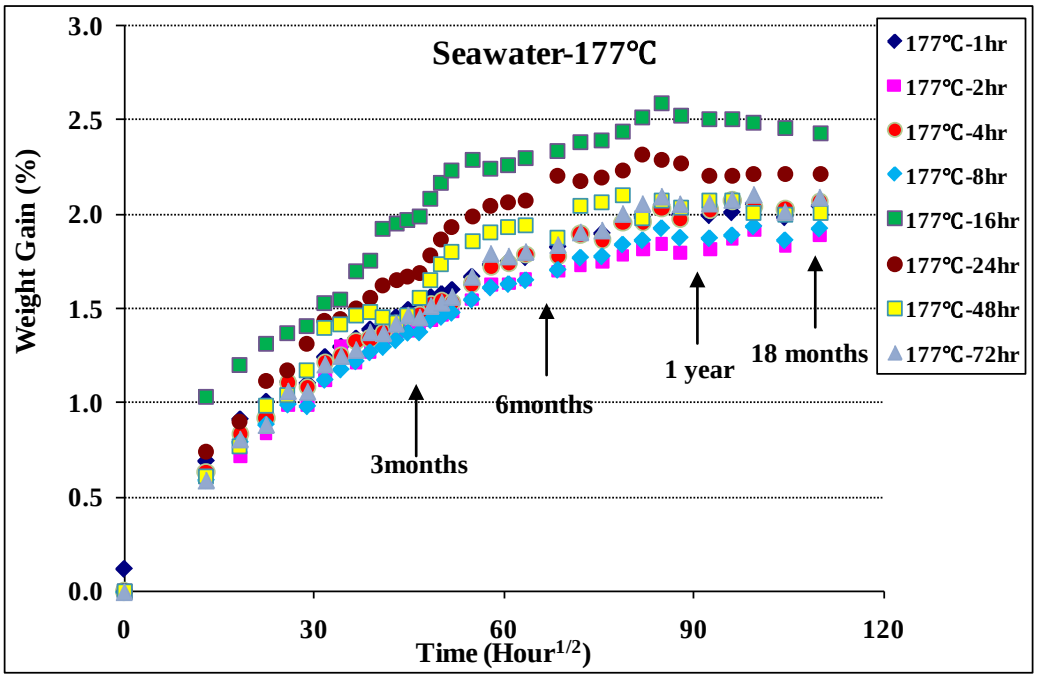

(f)

Figure 6-4: Continued

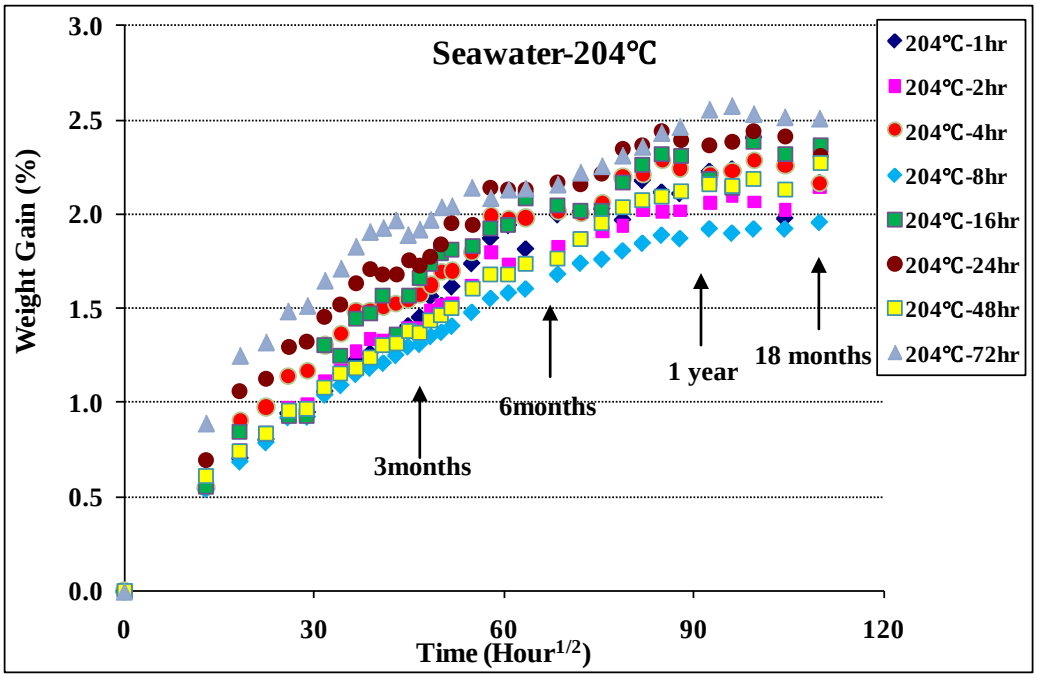

(g)

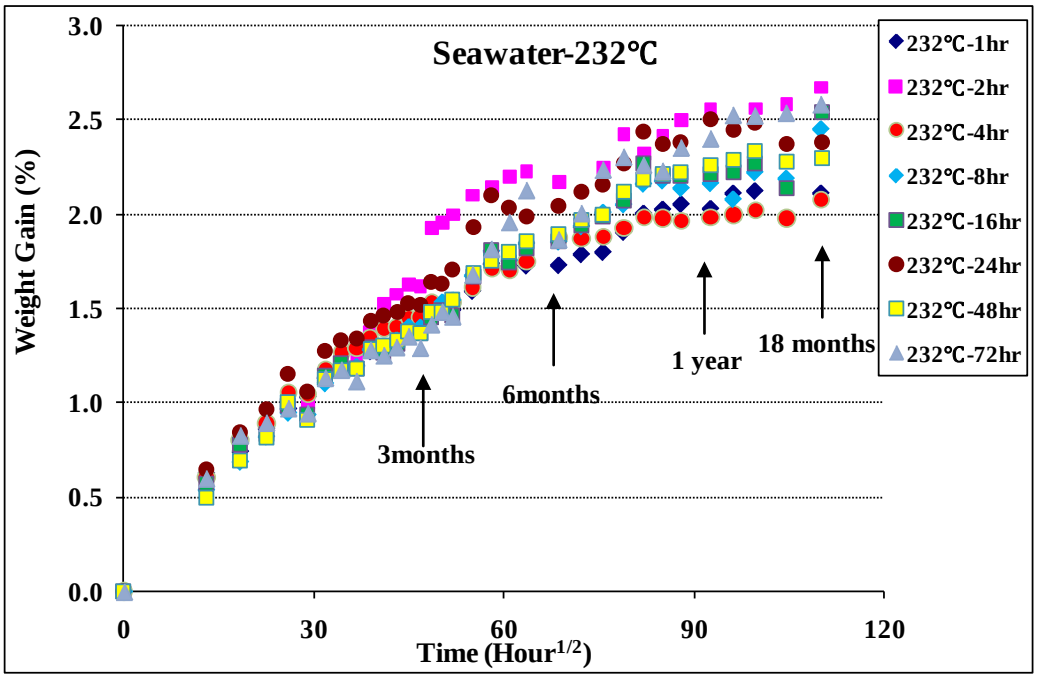

(h)

Figure 6-4: Continued

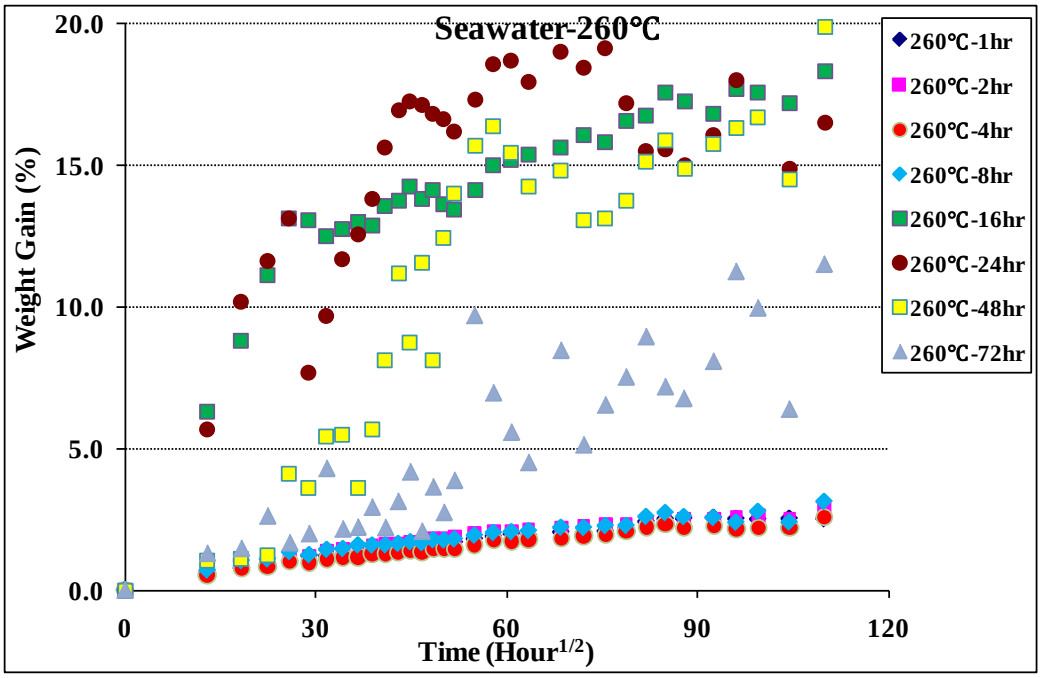

(i)

Figure 6-4: Continued

Table 6-2: Characteristics on specimens immersed in seawater for 72 weeks after exposure to elevated temperatures

Exposure Temperature	Time	seawater							
		width (mm)	length (mm)	thickness (mm)	Mass (g)	M_∞ (%)	$D\times10^8$ (mm^2/s)	$D_{corr}\times10^8$ (mm^2/s)	slope
Ambient (23℃)	0	25.91	25.78	2.98	2.385	1.826	9.677	0.0143	0.0191
	1	25.98	24.81	3.02	2.323	1.382	7.567	0.0121	0.0145
	2	25.91	25.26	3.05	2.165	1.826	6.503	0.0100	0.0153
	4	25.97	25.95	2.99	2.320	1.633	11.354	0.0166	0.0195
	8	25.8	25.92	3.1	2.362	1.360	11.942	0.0175	0.0176
	16	25.63	25.78	3.19	2.628	1.366	8.664	0.0128	0.0146
	24	25.91	25.86	3.07	2.516	1.433	8.071	0.0119	0.0150
	48	25.48	25.92	2.82	2.161	1.811	9.105	0.0133	0.0195
	72	24.86	25.53	3.24	2.355	1.779	13.393	0.0201	0.0204
66℃	1	25.91	25.71	3	2.367	1.178	9.754	0.0145	0.0153
	2	25.99	25.95	2.98	2.253	1.723	7.935	0.0116	0.0168
	4	26.05	25	2.9	2.199	1.420	10.584	0.0166	0.0181
	8	25.92	25.97	3.3	2.589	1.160	15.912	0.0377	0.0225
	16	25.69	25.59	3.15	2.411	1.278	15.941	0.0239	0.0194
	24	25.84	24.99	3.2	2.299	1.580	13.442	0.0211	0.0195
	48	25.83	25.56	3	2.111	1.762	15.646	0.0235	0.0237
	72	25.68	25.92	3.23	2.517	1.799	16.301	0.0238	0.0227
93℃	1	25.77	25.87	3.1	2.203	1.233	12.145	0.0178	0.0169
	2	25.73	24.95	3.05	2.314	1.334	10.993	0.0173	0.0170
	4	24.84	25.74	3.15	2.196	1.503	13.276	0.0197	0.0192
	8	25.84	24.86	3.23	2.402	1.443	17.561	0.0278	0.0211
	16	25.85	25.55	3.18	2.294	1.802	14.682	0.0221	0.0219
	24	25.56	25.8	2.82	2.381	1.534	13.072	0.0193	0.0215
	48	25.83	26.15	3.2	2.430	1.571	16.436	0.0236	0.0215
	72	26.02	25.68	3.15	2.385	1.904	19.960	0.0297	0.0265
121℃	1	25.83	25.57	2.9	2.430	1.620	12.729	0.0191	0.0212
	2	26.17	25.78	3	2.320	2.149	13.376	0.0198	0.0242
	4	26.15	25.11	3.02	2.340	1.932	16.744	0.0261	0.0255
	8	25.91	25.86	3.12	2.305	2.118	16.687	0.0245	0.0258
	16	25.95	25.53	3	2.186	1.911	16.702	0.0252	0.0255
	24	26.21	25.73	3.18	2.193	2.351	15.735	0.0233	0.0259
	48	25.81	25.67	3.15	2.306	2.317	24.516	0.0365	0.0324
	72	25.84	25.8	3.14	2.234	2.676	32.632	0.0481	0.0403
149℃	1	25.81	25.78	3.2	2.471	1.605	17.462	0.0258	0.0224
	2	24.56	26.01	3.1	2.338	1.745	17.879	0.0259	0.0244
	4	25.8	25.08	2.93	2.259	1.718	14.293	0.0223	0.0229
	8	25.81	25.74	2.88	2.316	2.152	16.598	0.0246	0.0281
	16	25.77	25.93	3.04	2.411	2.081	16.884	0.0247	0.0264
	24	25.9	25.7	2.74	2.201	1.853	12.517	0.0186	0.0238
	48	25.87	25.97	3.24	2.543	1.926	19.175	0.0279	0.0254
	72	25.56	25.66	3.2	2.240	1.857	17.759	0.0265	0.0243

Table 6-2: Continued

Exposure Temperature	Time	seawater							
		width (mm)	length (mm)	thickness (mm)	Mass (g)	M_∞ (%)	$D\times10^8$ (mm^2/s)	$D_{corr}\times10^8$ (mm^2/s)	slope
177℃	1	25.87	25.37	3.06	2.195	1.980	15.107	0.0230	0.0242
	2	25.93	25.87	2.9	2.330	1.866	15.115	0.0222	0.0248
	4	25.5	26.64	2.9	2.224	2.026	14.605	0.0202	0.0254
	8	26.05	24.86	2.98	2.242	1.860	15.126	0.0240	0.0241
	16	25.7	24.78	3.08	2.333	2.453	24.242	0.0387	0.0339
	24	25.79	25.84	3.04	2.358	2.213	22.032	0.0324	0.0311
	48	25.87	25.91	2.94	2.300	1.996	20.695	0.0303	0.0296
	72	25.73	25.82	3.12	2.259	2.012	18.670	0.0275	0.0266
204℃	1	25.86	25.8	3.12	2.411	1.975	23.552	0.0347	0.0296
	2	25.4	25.77	2.87	2.254	2.020	15.974	0.0236	0.0268
	4	25.33	25.73	3.07	2.297	2.258	19.815	0.0294	0.0295
	8	25.84	25.77	2.91	2.381	1.923	13.604	0.0201	0.0238
	16	25.93	25.83	2.89	2.367	2.313	19.912	0.0293	0.0318
	24	25.89	25.67	2.9	2.211	2.409	18.415	0.0275	0.0311
	48	25.89	25.82	3.2	2.540	2.127	16.809	0.0247	0.0253
	72	25.61	25.87	3.2	2.333	2.510	20.566	0.0301	0.0304
232℃	1	25.43	25.77	3.05	2.181	1.984	17.555	0.0260	0.0262
	2	25.65	25.95	3.18	2.430	2.584	22.964	0.0335	0.0328
	4	25.6	25.93	2.95	2.353	1.981	18.121	0.0265	0.0275
	8	26	25.74	3.21	2.594	2.187	20.291	0.0300	0.0281
	16	25.98	25.02	3.09	2.470	2.142	16.688	0.0261	0.0262
	24	25.66	25.82	3.13	2.383	2.370	19.616	0.0289	0.0295
	48	25.85	26.17	3	2.324	2.278	16.771	0.0241	0.0279
	72	25.89	25.76	2.96	2.532	2.542	11.751	0.0174	0.0250
260℃	1	25.86	26.02	3.13	2.327	2.519	16.397	0.0238	0.0278
	2	25.76	25.93	3.18	2.531	2.549	23.993	0.0350	0.0333
	4	25.89	25.03	2.94	2.201	2.189	15.011	0.0235	0.0264
	8	25.87	23.96	2.89	2.023	2.421	18.549	0.0317	0.0314

Figure 6-5 shows the maximum weight gain (%) on specimens immersed in deionized water and seawater at atmospheric temperature for 72 weeks. There is a little difference in the maximum weight gain. In particular, the maximum weight gain of all specimens which ageing time is less than 8 hrs in entire exposure temperatures was almost identical. All data of the maximum weight gain in these conditions existed between 1.2% and 2.8%. In both immersion conditions, the maximum weight gains were slightly increased in proportion to ageing time and exposure temperature. The difference among the maximum weight gains in lower (ambient, 66 and 93℃) and higher (121, 149, 177, 204, and 232℃) exposure temperatures existed on specimens immersed in deionized water. However, this gap was not shown on specimens immersed in seawater. This means that the unreacted chemical species in partially cured composite were released more rapidly into deionized water. In addition, it should be pointed out that the maximum weight gains in seawater were slightly lower than those in deionized water in overall environmental conditions. Apparently, the sorption of salts into the epoxy by diffusion and along fiber-matrix interface debonds and bulk material cracks by wicking can be resulted in the higher mass retention in seawater while the organic species leached from the specimens were separated from the salty residue by solvent extraction. The organic species were even found visually in seawater container. Consequently, mass loss by leaching of organic species than mass uptake by sorption of salts largely contributed to lower maximum weight gain in seawater compared to the values of deionized water.

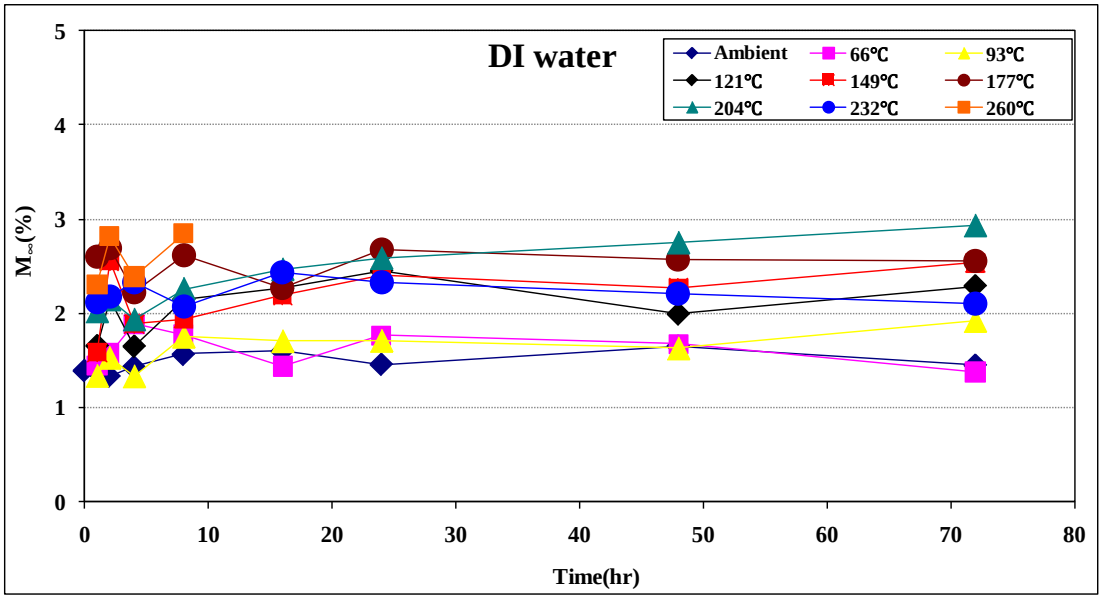

(a)

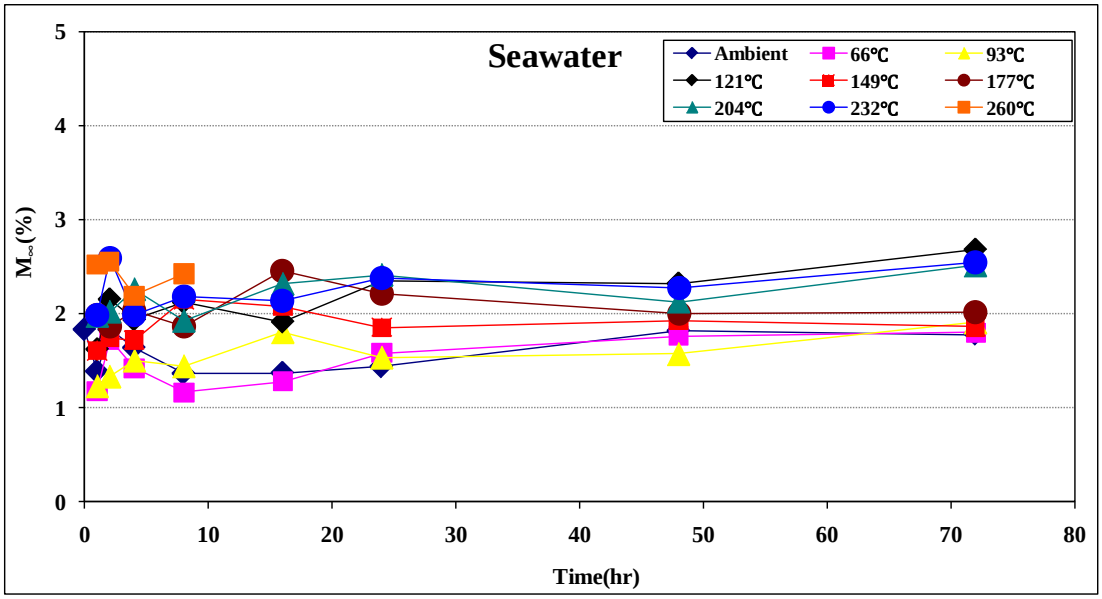

(b)

Figure 6-5: The maximum weight gain (%) on specimens immersed in (a) DI water and (b) seawater for 72 weeks

Figure 6-6 shows comparison of diffusion coefficients on specimens immersed in deionized water and seawater for 72 weeks. Overall diffusion coefficients calculated for deionized water immersion were higher than those for seawater immersion in all environmental conditions. Diffusion coefficients in deionized water were widely distributed with increase of ageing time and exposure temperatures. In other words, the degree of cure on specimens was strongly dependent on the diffusion coefficient. On the other hand, the variation of diffusion coefficients in immersion of seawater was less than that indeionized water. Lower diffusion coefficient in seawater seems to be attributed to mass loss by leaching out of organic species.

Epoxy resins have relatively high moisture absorption by the presence of hydroxyl groups in the epoxy chains attracting polar water molecules[90] whereas epoxy resins have superior chemical resistance compared to other resins. Therefore, although carbon/epoxy composites for this study showed higher maximum weight gain until saturation reach, this composite material showed the lowest diffusion coefficient compared to other composite materials.

It should be noted that both faces of the composite specimens were exposed to the deionized water and seawater. However, in real service conditions, only one face of a composite structure like naval vessel is exposed to water. Therefore, moisture uptake and diffusion coefficient were obtained by more severe conditions. In the case of naval vessel made of fiber reinforced polymer composites, pressure applied for composite materials by buoyancy must be considered when moisture uptake and diffusion will be analyzed.

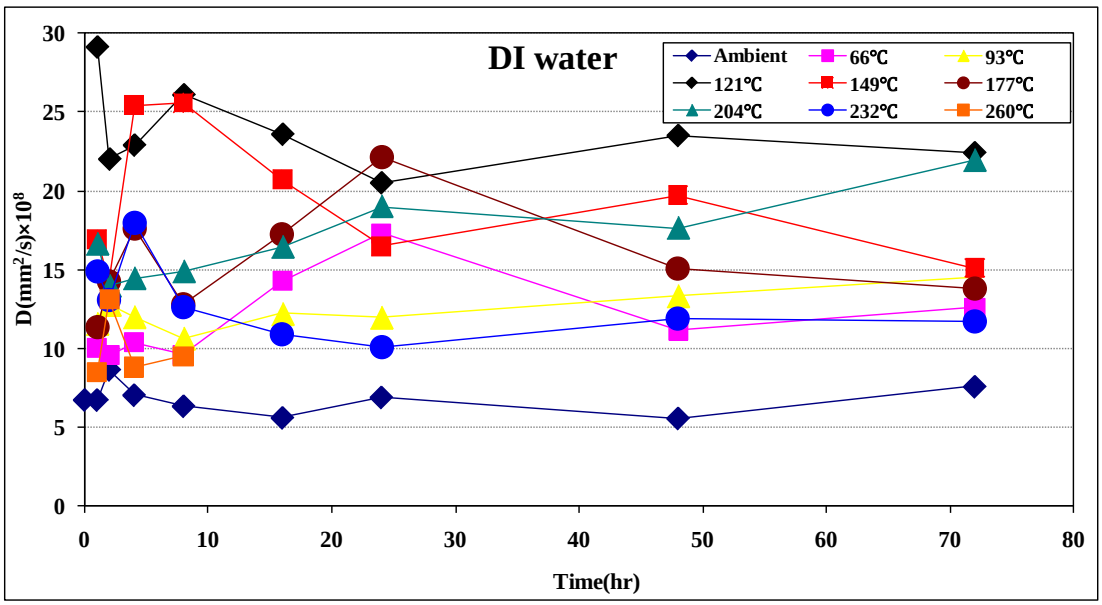

(a)

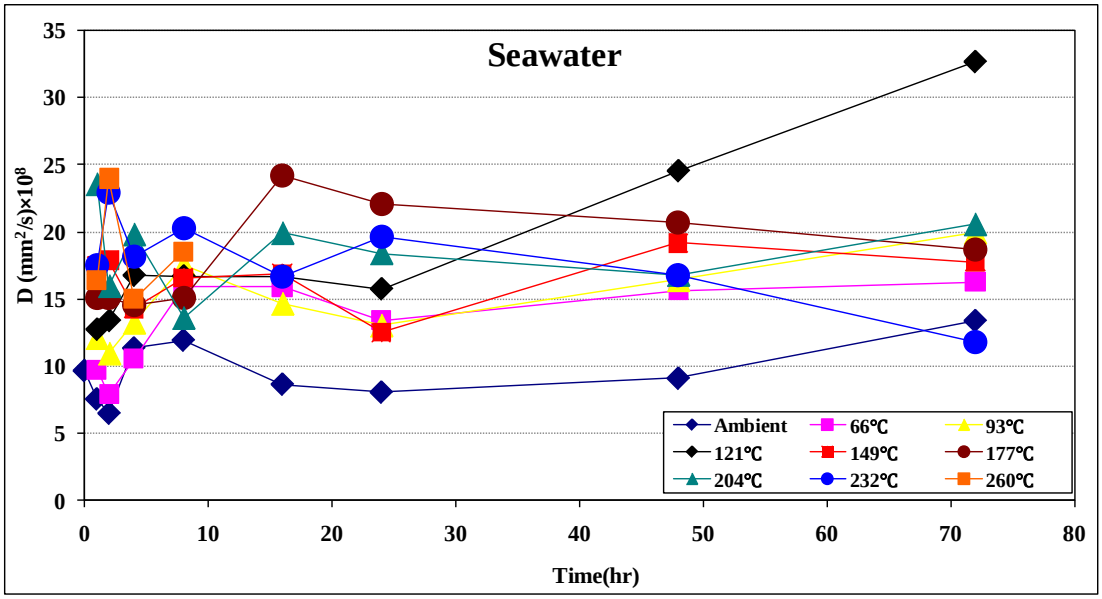

(b)

Figure 6-6: Diffusion coefficients on specimens immersed in (a) DI water and (b) seawater for 72 weeks

6.2.2 Morphological Analysis

Swelling of the carbon/epoxy laminate composite by water uptake is the following mechanisms such as the increase of the free volume between the molecules due to water penetration into small pores, interface between carbon fiber and the epoxy resin and the delamination interface between layers. By water uptake, the epoxy is plasticized and caused cracks by creating volume expansion and increased stress. These mechanisms can result in the degradations of the epoxy and interface.

Morphological analysis regarding degradations caused by water uptake was accomplished using SEM images on specimens immersed in deionized water and seawater. Figure 6-7 shows SEM images at 250× and 500× magnification fractured by short beam shear test on specimens immersed in seawater for 72 weeks after exposure to the various conditions. As shown in Figure 6-7 (a), specimens after exposure to 260℃ for 8 hrs showed severe fracture of the epoxy, pulling-out of the carbon fibers and smooth surface of the carbon fibers without resin particles in the section fractured by tension. In particular, the epoxy surrounding carbon fibers showed more severe cracks. Hydrolysis, swelling and plasticization by water uptake resulted in destruction of the epoxy and trail of carbon fibers in the section fractured by compression. Delamination between 2 layers was found on specimens exposed to 232℃ for 72 hrs as presented in Figure 6-7 (b). Beside delaimination, the evidences of degradation occurred on specimens exposed 260℃ for 8 hrs were also found by short beam shear test. Specimens exposed to 121℃ for 8 hrs showed relatively good fiber-matrix bonding and thus epoxy resin was closely adhered to carbon fibers as shown in Figure 6-7 (a).

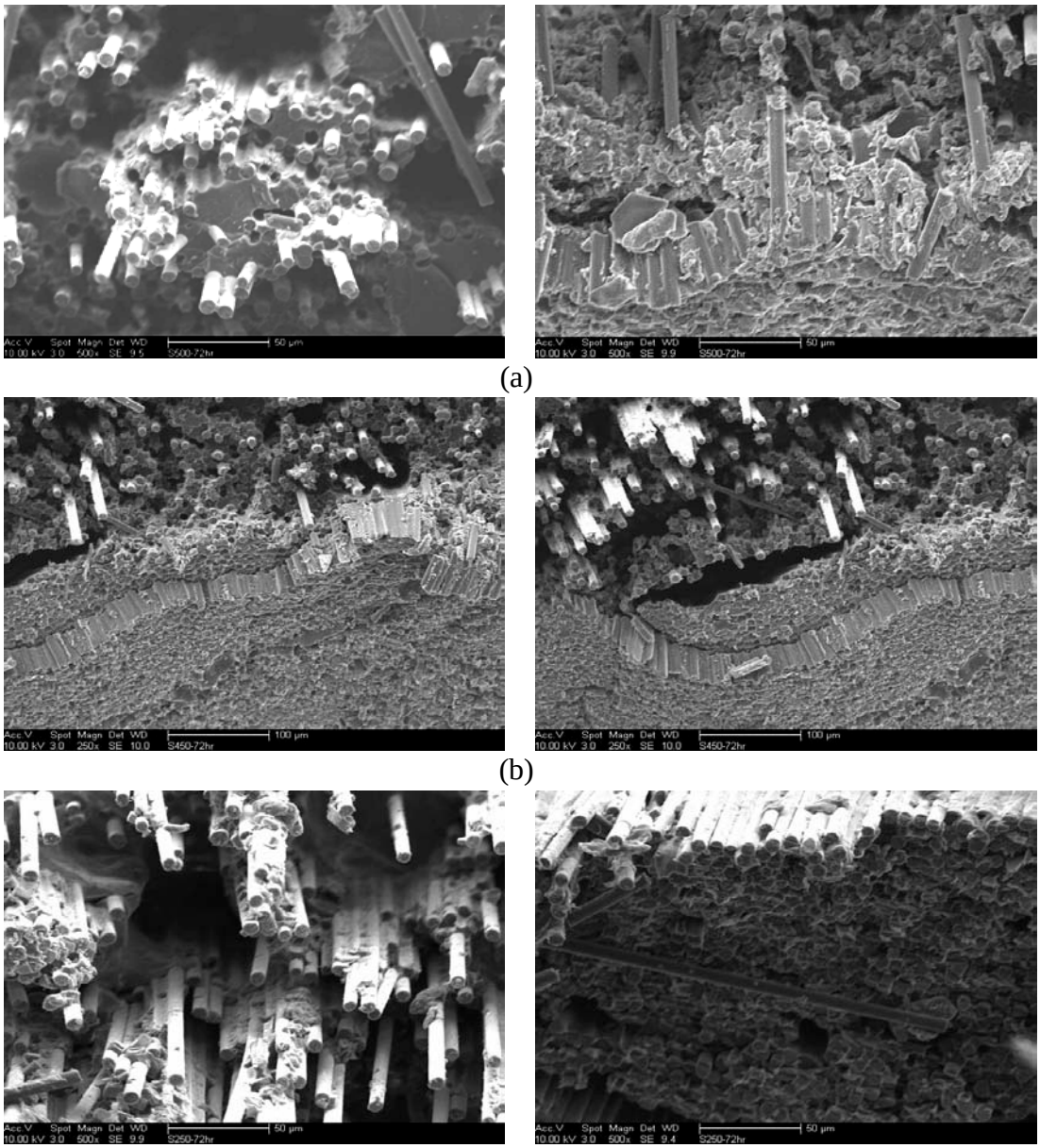

Figure 6-7: Scanning electron micrographs at 250× and 500× magnification fractured by short beam shear test on specimens immersed in seawater for 72 weeks after exposure to (a) 260℃ for 8 hrs (b) 232℃ for 72 hrs (c) 121℃ for 8 hrs

Compared to the morphological analysis on specimen immersed in seawater, the specimens fractured by short beam shear test after immersion in deionized water did not showed different degradation mechanisms. As depicted in Figure 6-8 (a), specimens immersed in deionized water for 72 weeks after exposure to 260℃ for 8 hrs showed catastrophic cracks in the epoxy and interface and the delamiations between 2 layers. Cracks and cavities created by thermooxidation when the specimens were heated to high temperature accelerated the severe degradations from rapid water uptake and hydrolysis within carbon/epoxy composite materials. Since specimens exposed to 121℃ for 8 hrs showed good mechanical properties by post-curing effect without degradation due to thermooxidation, bonding between the fibers and matrix was relatively superior to specimens exposed to high temperature as shown in Figure 6-8 (b) although immersion was progressed for 72 weeks.

Figure 6-9 shows SEM images of cross section delaminated between 2 layers on specimens immersed in seawater for 72 weeks after exposure to 260℃ for 8 hrs. Particles, cracks and cavities of the epoxy by water uptake and hydrolysis were founded in the cross section delaminated between 2 layers. No failure shape of 'hackles' as shown in Figure 4-38 (b), (c) and (f) were occurred on specimens immersed in deionized water for 72 weeks. This phenomenon is attributed to the deterioration of interfacial bonding between the carbon fibers and the epoxy resin.

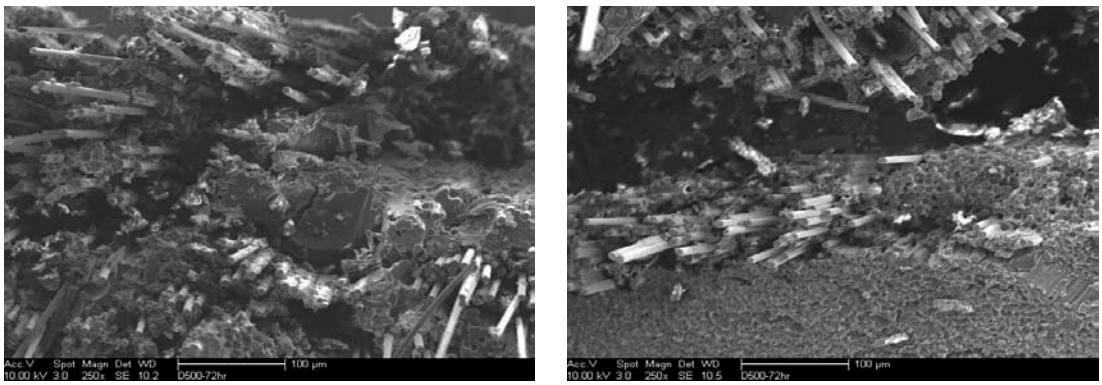

(a)

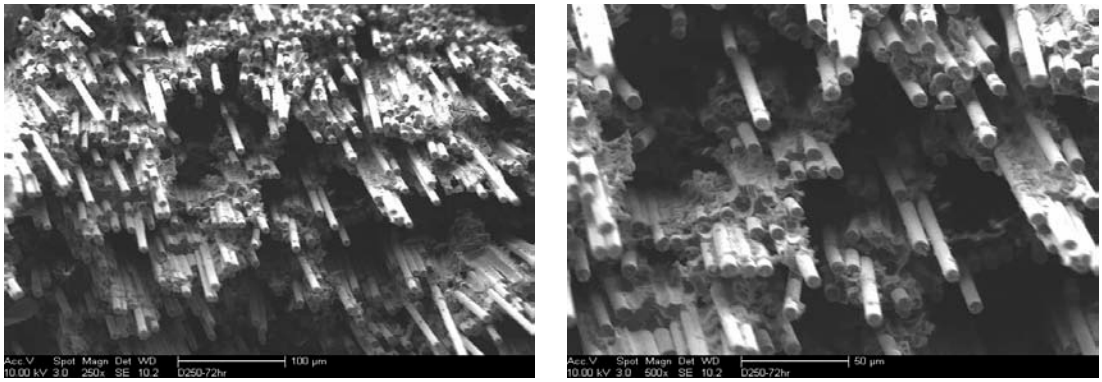

(b)

Figure 6-8: Scanning electron micrographs at 250× and 500× magnification fractured by short beam shear test on specimens immersed in deionized water for 72 weeks after exposure to (a) 260℃ for 8 hrs (b) 121℃ for 8 hrs

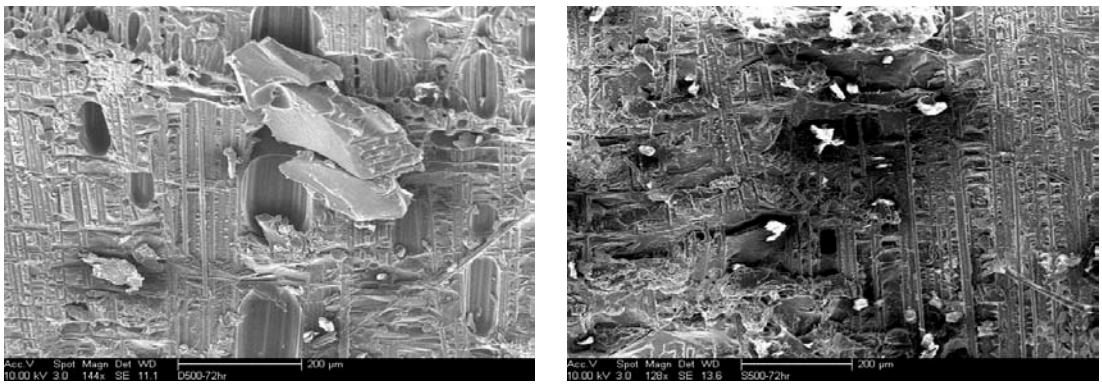

Figure 6-9: Scanning electron micrographs of cross section between 2 layers on specimens immersed in seawater for 72 weeks after exposure to 260℃ for 8 hrs

6.2.3 Short Beam Shear Testing

To investigate the mechanical property of specimens immersed in deionized water and seawater for 72 weeks after exposure to elevated temperatures for up to 72 hrs, short beam shear test was accomplished in accordance with ASTM D2344. In case the specimens of all conditions tested in chapter 4.4 are used to characterize the immersion effect, so many specimens and times are required for short beam shear test immersed in deionized water and seawater. Therefore, the specimens aged for 8 hrs at elevated temperatures were used to investigate the temperature-dependent characterization after immersion while, for time-dependent characterization, the specimens exposed to 232℃ for up to 72 hrs of ageing time were utilized. Total specimens used in short beam shear test for immersion effect were 1,280 since 5 specimens were tested in each of conditions such as 4, 8, 12, 16, 24, 36, 48 and 72 weeks in immersion period.

6.2.3.1 Temperature Dependence

Data and comparison of short beam shear strength on specimens immersed in deionized water for 72 weeks after exposure to elevated temperatures in 8 hrs of ageing time are presented in Table 6-3 and Figure 6-10. Except for the specimens immersed in deionized water after exposure to 260℃ for 8 hrs, all specimens showed similar characterizations which had initially decrease (~ 16 weeks), asymptotic trend or slightly increase (16 ~ 48 weeks) and rapidly decrease after 48 weeks in terms of short beam shear strengths. Initially rapid drop and asymptotic trend were corresponded to Fick's law which the mass of absorbed water increases linearly with the square root of time

and then gradually slows until equilibrium. The rate of decrease in short beam shear strengths after immersion from original state to 72 weeks in deionized water was 23.0, 28.1, 35.7, 38.7, 36.0, 33.7, 35.2, 35.9 and 30.7% on specimens exposed to ambient, 66, 93, 121, 149, 177, 204, 232 and 260℃, respectively. Post-cured specimens in intermediate exposure temperatures (121, 149, 177, 204, 232℃) had higher rate of decrease in short beam shear strengths compared to other conditions since, as investigated in chapter 6.2.1, specimens post-cured from the increase of ageing time and exposure temperature showed the rapid saturation and the higher maximum weight gain compared to un-cured specimens. Contrary to specimens in other conditions, specimens exposed to 260℃ for 8 hrs showed initially a little of increase in short beam shear strengths. However, after 48 weeks in immersion time, rapid decrease of short beam shear strengths occurred by delamination between 2 layers due to moisture uptake.

From many researches, it is well known that epoxy has the superior durability and the lowest diffusion coefficient compared to vinylester, polyester and phenolic resins in water environmental conditions. In addition, it is known that glass fibers chemically react with water while carbon fibers do not absorb moisture and are resistant to any corrosive effects of water. Therefore, intrinsic properties of epoxy and carbon fiber against water resulted in a slight decrease or asymptotic trend in terms of short beam shear strengths until 48 weeks in immersion period. However, it appears that catastrophic drop of short beam shear strengths after 48 weeks of immersion was derived from irreversible degradations such as hydrolysis, microcracking, microvoids and epoxy relaxation.

Table 6-3: Data of Short Beam Shear Strengths on specimens immersed in DI water for 72 weeks after exposure to elevated temperatures in 8 hrs of ageing time

	Strength (MPa) - DI water								
weeks	Ambi	66°C	93°C	121°C	149°C	177°C	204°C	232°C	260°C
0	42.43	45.45	46.94	47.93	50.69	46.03	48.08	46.71	27.34
4	38.79	41.61	41.55	40.15	42.35	41.98	39.99	42.73	31.74
8	39.45	42.47	41.08	38.35	39.12	40.90	40.95	40.75	30.63
12	39.51	40.82	40.48	40.42	38.54	38.37	37.45	41.85	30.48
16	36.25	41.50	40.88	39.89	38.67	38.99	36.16	40.81	31.57
24	36.97	39.72	41.23	38.89	38.47	40.31	39.11	41.05	30.66
36	39.13	40.21	39.46	38.65	39.28	39.68	38.11	39.39	30.65
48	39.37	41.47	39.23	38.27	40.20	42.00	37.29	38.92	27.60
72	31.69	32.68	30.17	29.39	32.44	30.51	31.15	29.95	18.94
	Standard deviation (MPa)								
weeks	Ambi	66°C	93°C	121°C	149°C	177°C	204°C	232°C	260°C
0	1.41	2.25	1.12	1.50	1.51	1.63	0.60	2.66	2.46
4	3.08	0.90	3.48	1.25	1.59	2.84	2.14	3.24	1.85
8	2.29	1.67	1.16	1.56	1.17	2.22	2.52	1.79	5.23
12	2.35	2.51	1.40	1.89	1.36	1.97	3.28	1.25	5.61
16	1.59	2.57	0.47	3.03	0.41	1.54	1.48	1.48	2.65
24	1.97	2.22	0.80	2.92	2.74	1.15	3.33	3.64	5.96
36	2.50	1.48	1.81	2.06	1.61	1.75	1.77	1.41	5.86
48	2.22	1.44	2.38	2.27	1.83	2.94	0.64	5.15	3.48
72	2.45	1.89	2.97	2.67	2.24	3.21	1.21	5.41	5.98

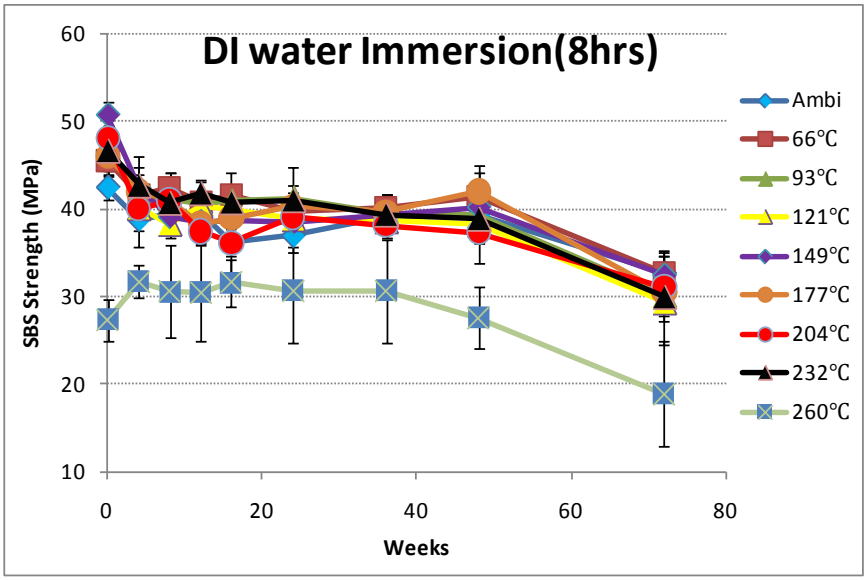

Figure 6-10: Comparison of Short Beam Shear Strengths on specimens immersed in DI water for 72 weeks after exposure to elevated temperatures in 8 hrs of ageing time

To compare of results of short beam shear test immersed in deionized water, short beam shear tests were conducted using specimens immersed in seawater under same environmental conditions. Data and comparison of short beam shear strength on specimens immersed in seawater for 72 weeks after exposure to elevated temperatures in 8 hrs of ageing time are shown in Table 6-4 and Figure 6-11. As demonstrated in chapter 6.2.1, although a little difference between specimens immersed in deionized water and seawater existed with regard to diffusion coefficient and the maximum water uptake, the results of short beam shear strengths on specimens immersed in seawater were in good agreement with the data immersed in deionized water as shown in Figure 6-10 and Figure 6-11. In addition, it seems that salt or salinity involving in seawater did not influence deterioration and degradation in short beam shear property.

The rate of decrease in short beam shear strengths after immersion from original state to 72 weeks in seawater was 22.7, 25.2, 32.8, 36.3, 40.7, 33.4, 31.0, 35.3 and 22.7% on specimens exposed to ambient, 66, 93, 121, 149, 177, 204, 232 and 260 °C, respectively. These rates of decrease in short beam shear strengths were slightly lower than the values after immersion in deionized water. However, the difference of rate of decrease was negligible.

Table 6-4: Data of Short Beam Shear Strengths on specimens immersed in Seawater for 72 weeks after exposure to elevated temperatures in 8 hrs of ageing time

	Strength (MPa) - seawater								
weeks	Ambi	66°C	93°C	121°C	149°C	177°C	204°C	232°C	260°C
0	42.43	45.45	46.94	47.93	50.69	46.03	48.08	46.71	27.34
4	39.59	41.56	39.39	40.15	39.48	40.18	36.40	41.57	32.52
8	39.18	39.22	40.99	39.22	41.56	39.71	39.49	40.58	31.10
12	39.84	41.79	40.31	38.63	40.54	39.52	40.40	41.70	32.70
16	37.24	42.31	41.12	38.95	39.43	38.62	40.10	39.06	31.06
24	41.84	41.73	40.64	41.22	38.46	39.19	42.22	38.13	32.19
36	38.18	40.37	39.96	38.86	38.36	38.64	39.27	39.50	31.85
48	40.87	43.89	39.68	38.30	38.76	39.61	42.40	37.29	30.87
72	32.79	34.01	31.54	30.55	30.07	30.65	33.17	30.22	21.12
	Standard deviation (MPa)								
weeks	Ambi	66°C	93°C	121°C	149°C	177°C	204°C	232°C	260°C
0	1.41	2.25	1.12	1.50	1.51	1.63	0.60	2.66	2.46
4	1.68	3.63	3.62	1.25	3.08	2.08	3.83	2.23	0.83
8	0.79	2.08	1.29	2.79	3.31	0.76	1.91	2.11	2.41
12	2.48	1.99	1.53	2.39	2.30	1.52	1.66	1.87	6.54
16	0.51	2.92	2.39	0.70	1.06	2.94	2.73	1.78	7.96
24	9.92	0.74	0.55	3.03	3.01	2.29	1.14	5.48	5.08
36	2.04	2.18	2.87	2.04	2.85	2.47	1.90	1.52	5.90
48	2.66	0.31	1.88	0.71	1.27	2.45	4.49	2.10	6.51
72	2.81	0.67	2.01	1.45	2.07	2.87	4.97	3.04	6.64

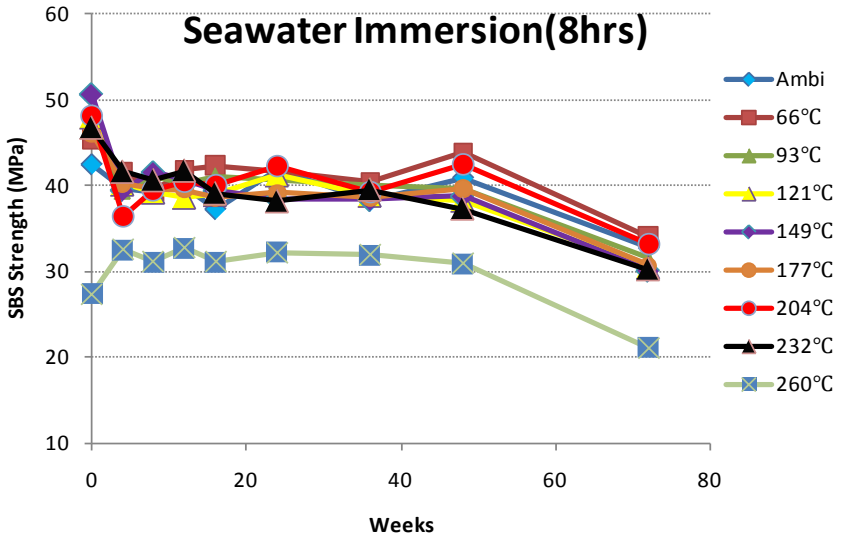

Figure 6-11: Comparison of Short Beam Shear Strengths on specimens immersed in sea- water for 72 weeks after exposure to elevated temperatures in 8 hrs of ageing time

6.2.3.2 Time Dependence

For time-dependent characterization on carbon/epoxy composite materials immersed in deionized water and seawater, specimens aged from 1 hr to 72 hrs under 232℃ of exposure temperature were immersed until 72 weeks in water bath at the atmospheric temperature. Table 6-5 and Figure 6-12 show data and comparison of short beam shear strengths on specimens immersed in deionized water for 72 weeks after exposure to 232℃ in various ageing times. Contrary to the results of tensile and flexural test, short beam shear strengths of specimens exposed to 232℃ were continuously and slightly increased without degradation caused by thermooxidation as ageing time was extended from 1 hr to 72 hrs as demonstrated in chapter 4.4.

The specimens exposed to 232℃ before immersion showed increasing short beam shear strengths with extended ageing time as shown in Table 6-5. The rate of decrease in short beam shear strengths after immersion until up to 72 weeks in deionized water was 26.1, 31.9, 35.5, 35.9, 34.5, 35.4, 37.5 and 38.7% on specimens exposed to 232℃ for 1, 2, 4, 8, 16, 24, 48, and 72 hrs, respectively. Namely, the increased short beam strengths by post-cure effect resulted in more degradation by water ingress. Consequently, the rapid drop of short beam shear strengths was attributed to water ingress and hydrolysis on fully post-cured specimens. Also, immersion effects and time-dependent characterization in terms of short beam shear strengths on specimens exposed to 232℃ were identical regardless of ageing times.

Table 6-5: Data of Short Beam Shear Strengths on specimens immersed in DI water for 72 weeks after exposure to 232℃ in various ageing times

	Strength (MPa) - DI water							
weeks	1hr	2hr	4hr	8hr	16hr	24hr	48hr	72hr
0	44.28	45.61	48.06	46.71	46.48	46.62	49.61	48.97
4	41.44	39.54	39.95	42.73	41.77	43.77	41.27	41.16
8	39.93	42.94	40.48	40.75	42.26	42.47	40.37	43.60
12	39.25	38.28	38.45	41.85	41.63	42.45	41.75	43.58
16	41.73	40.05	39.30	40.81	41.14	42.47	43.25	42.17
24	40.99	42.50	42.25	41.05	42.86	42.96	41.10	41.00
36	38.37	40.46	38.84	39.39	41.35	43.50	42.02	39.49
48	41.53	39.36	39.65	38.92	42.16	43.07	39.51	41.41
72	32.71	31.07	31.00	29.95	30.46	30.12	31.02	30.01
	Standard deviation (MPa)							
weeks	1hr	2hr	4hr	8hr	16hr	24hr	48hr	72hr
0	1.14	3.24	2.91	2.66	1.74	4.27	3.17	5.11
4	1.24	1.72	2.78	3.24	2.09	0.88	4.72	4.27
8	2.46	2.02	3.75	1.79	1.28	3.35	4.39	3.97
12	2.27	3.35	5.25	1.25	0.84	2.84	1.31	1.08
16	3.34	3.14	2.48	1.48	1.52	2.02	3.38	5.42
24	4.16	1.96	5.34	3.64	2.93	2.95	5.66	5.20
36	2.55	1.98	6.62	1.41	2.29	2.59	3.57	1.45
48	1.15	0.61	2.51	5.15	3.87	1.58	2.86	4.01
72	1.87	1.21	2.48	5.41	3.41	2.41	3.04	4.57

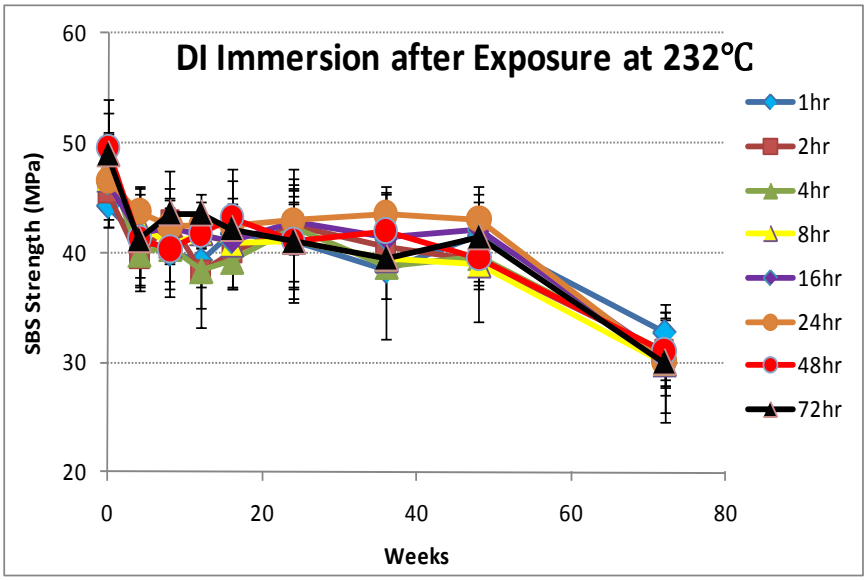

Figure 6-12: Comparison of Short Beam Shear Strengths on specimens immersed in DI water for 72 weeks after exposure to 232℃ in various ageing times

As shown in Table 6-6 and Figure 6-13, compared to the results of specimens immersed in deionized water, any specific characterization was not found on specimens immersed in seawater. Similar to temperature-dependent characterization, salt or sanity involving seawater did not affect additional decrease in terms of short beam shear strengths. The rate of decrease in short beam shear strengths after immersion until up to 72 weeks in seawater was 28.0, 27.6, 32.8, 35.3, 33.3, 35.0, 39.6 and 41.5% on specimens exposed to 232℃ for 1, 2, 4, 8, 16, 24, 48, and 72 hrs, respectively

Table 6-6: Data of Short Beam Shear Strengths on specimens immersed in seawater for 72 weeks after exposure to 232℃ in various ageing times

	Strength (MPa) - Seawater							
weeks	1hr	2hr	4hr	8hr	16hr	24hr	48hr	72hr
0	44.28	45.61	48.06	46.71	46.48	46.62	49.61	48.97
4	40.60	40.33	42.68	41.57	42.07	45.67	44.79	42.30
8	38.32	38.30	40.40	40.58	38.44	42.26	43.26	37.36
12	38.27	39.76	40.50	41.70	40.94	41.00	42.77	40.70
16	38.50	40.33	39.99	39.06	42.31	40.82	41.90	42.25
24	37.54	40.13	42.11	38.13	43.11	39.48	42.38	41.33
36	38.60	40.92	39.78	39.50	41.37	41.71	40.28	39.13
48	39.12	40.48	41.14	37.29	40.65	40.77	39.56	38.94
72	31.88	33.02	32.32	30.22	31.01	30.31	29.97	28.64
	Standard deviation (MPa)							
weeks	1hr	2hr	4hr	8hr	16hr	24hr	48hr	72hr
0	1.14	3.24	2.91	2.66	1.74	4.27	3.17	5.11
4	0.60	0.71	1.35	2.23	3.01	3.53	4.05	4.35
8	1.25	1.80	2.05	2.11	2.84	3.93	2.88	1.11
12	2.48	0.57	0.76	1.87	1.69	5.63	3.11	3.62
16	3.44	3.94	3.66	1.78	2.00	2.01	4.04	3.77
24	1.70	3.10	2.67	5.48	3.00	1.00	2.09	4.15
36	2.59	2.85	0.82	1.52	1.01	2.93	2.66	2.64
48	2.85	3.68	2.36	2.10	1.74	1.17	1.22	4.41
72	3.04	3.74	2.44	3.04	1.97	1.79	1.41	4.97

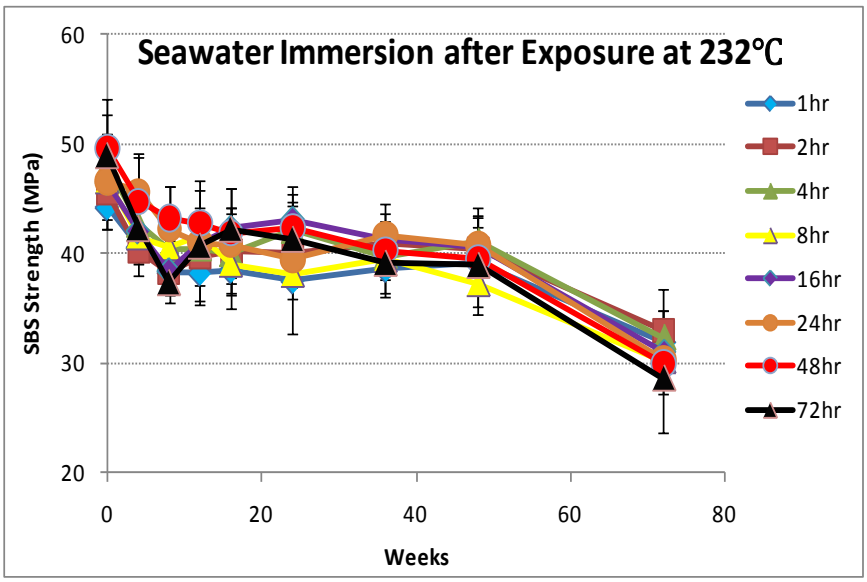

Figure 6-13: comparison of Short Beam Shear Strengths on specimens immersed in seawater for 72 weeks after exposure to 232℃ in various ageing times

7 Predictive Degradation Models

7.1 Introduction

A concern caused by using FRP composites in naval applications is their high flammability and poor fire resistance. As mentioned in chapter 4, the mechanical properties of FRP composites can be severely degraded by fire and elevated temperatures. Therefore, based on the data of mechanical properties determined in chapter 4 , it is very important that predictive degradation models must be performed to evaluate functions for desired periods of time without failure and severe degradation, in specified environments. For some period of exposure the strengths and the moduli may remain above their allowable limits. However, after some time, the mechanical properties may decrease that the composite materials cannot sustain the imposed loads or maintain the allowable desire. From this problem, a knowledge of long term strength retention under working conditions is required to estimate the accurate service life. Since the degradation caused by fire and elevated temperatures occurs rapidly and initial increase of mechanical properties due to post-cure effect must be considered, estimation of service life can be different with long term predictive degradation model applied for immersion which degradations continuously occurred.

Firstly, one of the earliest and most successful acceleration models, Arrhenius rate degradation model will be introduced. The Arrhenius rate model predicts how time-to-fail varies with temperature. Secondly, Time-Temperature Superposition (TTSP) will be used for analyzing of service life. This model is a well-known principle that works well for certain types of viscoelastic materials and related effects of time and

temperature, thereby allowing for an exchange between the effects of time and elevated temperature. Lastly, Weibull statistical strength model will be carried out to correlate between tension and flexure results.

7.2 Arrhenius Rate Degradation Model

The Arrhenius Rate degradation model is the most common model regarding life-stress relationships used in accelerated life estimation. The rate of a chemical reaction can be affected by several parameters, including temperature. The Arrhenius rate relationship is derived from the Arrhenius reaction rate equation suggested by Arrhenius in 1887[91]. The reaction rate can be expressed by

$$R(T) = A\exp\left(\frac{-E_a}{KT}\right) \tag{7.1}$$

where:

R = Speed of reaction

A= Non-thermal constant

E_a= activation energy (J/mol)

K = Boltzman's constant (1.38×10-23J/K)

T = Temperature (Kelvin)

In Equation 7.1, activation energy means the energy which molecules in composite materials shall possess to react. Therefore, the activation energy is a criterion of the effect that temperature has on the reaction.

Assuming that life is proportional to the inverse reaction rate of the process, the

Arrhenius life-stress relationship can be expressed as

$$L(T) = C\exp\left(\frac{B}{T}\right) \tag{7.2}$$

where:

L = a quantifiable life measure or material property

C = a model parameter to be determined (C>0)

B = another model parameter

T = Temperature (Kelvin)

A linear relationship can be obtained by taking the natural logarithm of both sides of Equation 7.2 as following.

$$\ln(L(T)) = \ln(C) + \frac{B}{T} \tag{7.3}$$

B is the slope of the line and ln(C) is the intercept of the line. The variable in this equation is the inverse of the temperature. Therefore, a quantifiable life measure is commonly drawn against the inverse temperature. The constant B and C can be identified from experimental data and relationships can be estimated for other temperatures than those used to determine these relationships.

7.2.1 Data Analysis Procedure

The analysis process (i.e., tensile strength) on Arrhenius rate model will be demonstrated in this section. The goal of the Arrhenius rate model is to determine the long-term degradation of the composites. Table 7-1 shows the tensile strength retentions (%) on specimens exposed to elevated temperatures up to 72 hrs.

Table 7-1: Data for tensile strength retentions (%) on specimens exposed to elevated temperatures up to 72 hrs

Time [hr]	Time [min]	Percent Strength Retention (%)								
		Ambient (23℃)	66℃	93℃	121℃	149℃	177℃	204℃	232℃	260℃
0	0	100.0	100.0	100.0	100.0	100.0	100.0	100.0	100.0	100.0
1	60	99.8	140.6	126.0	116.4	154.4	122.0	115.0	111.4	124.9
2	120	102.1	149.5	128.7	116.2	153.1	124.1	129.9	118.3	127.1
4	240	100.6	151.2	134.5	125.2	150.9	136.4	141.4	126.5	133.0
8	480	101.0	150.1	135.3	131.8	149.7	135.2	134.1	126.8	107.0
16	960	104.1	149.3	137.7	112.5	143.5	133.7	133.3	124.1	69.7
24	1440	102.5	120.3	121.7	104.4	137.6	124.3	124.5	121.7	60.4
48	2880	104.2	116.5	121.6	104.0	127.1	113.6	118.6	120.1	49.5
72	4320	103.4	115.2	119.9	104.8	136.4	112.3	116.0	112.5	37.6

More linear line can be plotted by taking natural logarithm of time versus the percent strength retentions as shown in Figure 7-1.

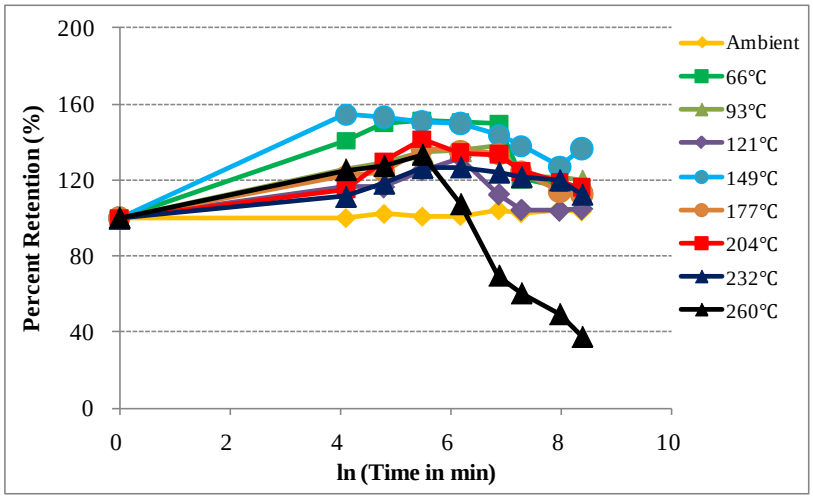

Time [min]	LN (Time[min])
0	0.000
60	4.094
120	4.787
240	5.481
480	6.174
960	6.867
1440	7.272
2880	7.966
4320	8.371

Figure 7-1: Percent tensile strength retentions (%) versus ln(time in minute)

In general, since degradation is more severe as time increase, linear line can be obtained from percent retention of property and logarithm of time. However, in this study, perfect linear line cannot be yielded due to initial increase of strengths by

residual post-cure effect. Therefore, using polynomial 2nd order curve-fit can bring higher R-squared values as demonstrated in Figure 7-2 and Table 7-2.

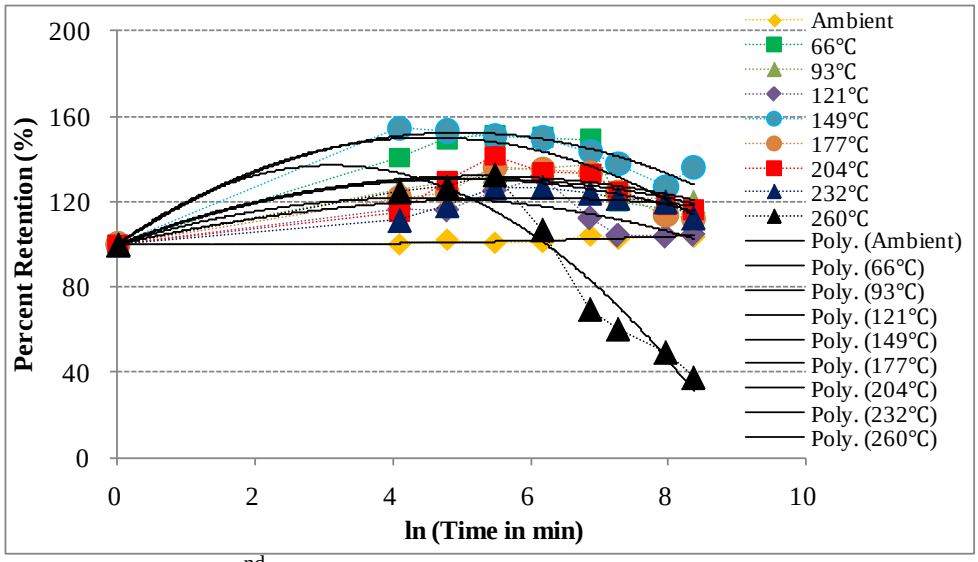

Figure 7-2: Polynomial 2nd order curve-fit on percent tensile strength retentions versus natural logarithm of time in minute

Table 7-2: Equation of polynomial 2nd order curve-fit on percent tensile strength retentions versus natural logarithm of time in minute

Exposure temperature	A	B	C	R^2
Ambient(23℃)	100	-0.239	0.0874	0.7081
66℃	100	22.206	-2.4564	0.8532
93℃	100	12.202	-1.1602	0.8420
121℃	100	10.075	-1.1651	0.6245
149℃	100	21.115	-2.1243	0.9412
177℃	100	12.547	-1.2788	0.7584
204℃	100	11.910	-1.1495	0.6876
232℃	100	7.3001	-0.6134	0.7249
260℃	100	23.811	-3.8236	0.9292
$\sigma(t) = \frac{\sigma_i}{100}\left(A+B\ln(t)+C\ln(t)^2\right)$				

Using equations in Table 7-2 , the tensile strength of the specimens for longer time at different temperatures can be yielded to predict the response of the composite materials.

Next step to get the Arrhenius rate analysis is to establish a relationship between percent tensile strength retention and temperature. Since the function between percent tensile strength retention and temperature is different for each time step and life is proportional to the inverse reaction rate of the process, a percent retention can be plotted against the inverse of temperature as Figure 7-3. Also, linear relationship between percent retention of tensile strength and inverse of temperature can be obtained from Figure 7-3. The reason why Figure 7-3 did not show perfect linear relationship is that post-curing effect was applied for specimens. However, the relationship and tendency in Table 7-3 can be used to determine the tensile strength of composite materials at different time steps for a particular temperature. From Table 7-4, the intercept of line was decreased and the slope of line was increased with increasing time. In particular, the slope of line showed minus values until ageing time reached 8 hrs. This means degradation of tensile strength did not occur in ranges of exposure temperatures (~ 260℃) in this study. Actually, test specimens did not lose the original property (100% in terms of percent tensile strength retention) in tensile test until ageing time reached 8 hrs in exposure temperature of 260℃.

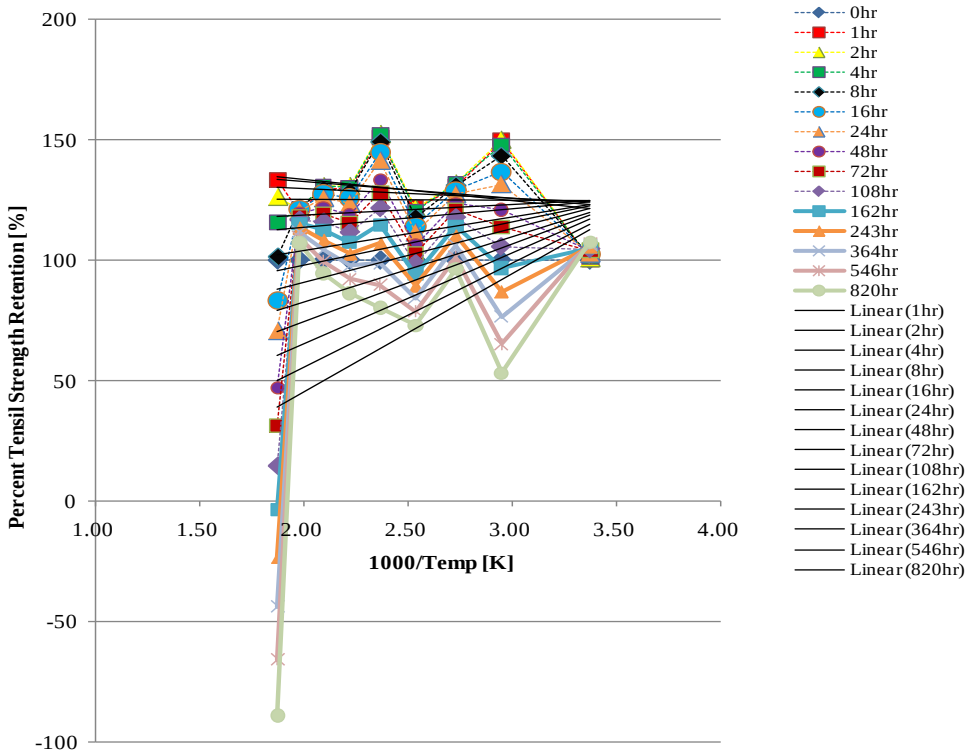

Figure 7-3: Percent retentions of tensile strength versus inverse of temperature

Table 7-3: Relationship between percent retentions of tensile strength and the inverse of temperature

Time [hr]	A	B
1	150.69	-8.61
2	146.13	-6.77
4	137.76	-3.98
8	125.58	-0.24
16	109.60	4.46
24	98.49	7.65
48	76.47	13.86
72	61.83	17.93
108	45.89	22.33
162	28.64	27.06
243	10.09	32.11
365	-9.76	37.49
547	-30.92	43.20
820	-53.38	49.23

$$\sigma(t) = \frac{\sigma_i}{100}\left(A + B\left(1000/T\right)\right)$$

Table 7-4: Comparison of experimental data and theoretical data by Arrhenius rate relationship for specimens exposed to elevated temperatures in tensile strength

Time[hr]	Ambient (23℃)		66℃		93℃	
	Experimental	Theoretical	Experimental	Theoretical	Experimental	Theoretical
0.0	100.0	100.0	100.0	100.0	100.0	100.0
1.0	99.8	121.6	140.6	125.3	126.0	127.2
2.0	102.1	123.3	149.5	126.2	128.7	127.6
4.0	100.6	124.3	151.2	126.0	134.5	126.9
8.0	101.0	124.8	150.1	124.9	135.3	124.9
16.0	104.1	124.7	149.3	122.8	137.7	121.8
24.0	102.5	124.3	120.3	121.0	121.7	119.4
48.0	104.2	123.3	116.5	117.3	121.6	114.3
72.0	103.4	122.4	115.2	114.7	119.9	110.8
108.0		121.3		111.7		106.9
162.0		120.0		108.4		102.5
243.0		118.5		104.8		97.8
364.5		116.8		100.8		92.6
546.8		114.9		96.4		87.1
820.1		112.9		91.8		81.1
Time[hr]	121℃		149℃		177℃	
0.0	100.0	100.0	100.0	100.0	100.0	100.0
1.0	116.4	128.9	154.4	130.3	122.0	131.6
2.0	116.2	129.0	153.1	130.1	124.1	131.1
4.0	125.2	127.7	150.9	128.3	136.4	128.9
8.0	131.8	125.0	149.7	125.0	135.2	125.1
16.0	112.5	120.9	143.5	120.2	133.7	119.5
24.0	104.4	117.9	137.7	116.6	124.3	115.5
48.0	104.0	111.6	127.1	109.3	113.6	107.3
72.0	104.8	107.3	136.4	104.3	112.3	101.7
108.0		102.5		98.8		95.5
162.0		97.3		92.7		88.8
243.0		91.6		86.2		81.4
364.5		85.4		79.0		73.5
546.8		78.7		71.4		65.0
820.1		71.5		63.2		56.0
Time[hr]	204℃		232℃		260℃	
0.0	100.0	100.0	100.0	100.0	100.0	100.0
1.0	115.0	132.7	111.4	133.7	124.9	134.5
2.0	129.9	131.9	118.3	132.7	127.1	133.4
4.0	141.4	129.4	126.5	129.9	133.0	130.3
8.0	134.1	125.1	126.8	125.1	107.1	125.1
16.0	133.3	118.9	124.1	118.4	69.7	118.0
24.0	124.5	114.5	121.7	113.6	60.4	112.8
48.0	118.7	105.5	120.1	103.9	49.5	102.5
72.0	116.0	99.4	112.6	97.3	37.6	95.5
108.0		92.7		90.1		87.8
162.0		85.3		82.2		79.4
243.0		77.4		73.7		70.3
364.5		68.8		64.5		60.6
546.8		59.6		54.6		50.1
820.1		49.8		44.1		39.0

Figure 7-4 shows comparison between the experimental values and predicted values of tensile strength determined by Arrhenius rate model for specimens exposed to elevated temperatures. Except for the conditions of exposure temperatures such as ambient, 66℃, and 260℃, predicted values of tensile strength were relatively in good agreement with experimental data. In other words, good relationships between theoretical and experimental data were shown in ranges of intermediate exposure temperatures. Tensile strengths in these exposure temperatures showed decrease or level-off after initial increase due to post-cure effect. Furthermore, since the rate of degradation by Arrhenius rate model in intermediate exposure temperatures showed higher rate compared to experimental data, it is possible to apply for design factor to predict the long-term service life in terms of tensile strength of carbon/epoxy composite materials.

The analysis procedure of Arrhenius rate model can be applied to experimental data from all tensile, off-axis shear, flexural and short beam shear tests and results are presented in the following section. From analysis in chapter 7.2.2, it can also be observed that Arrhenius rate model provides rather conservative estimates for all mechanical properties such as tension, off-axis shear, flexure and short beam shear in ranges of intermediate exposure temperatures.

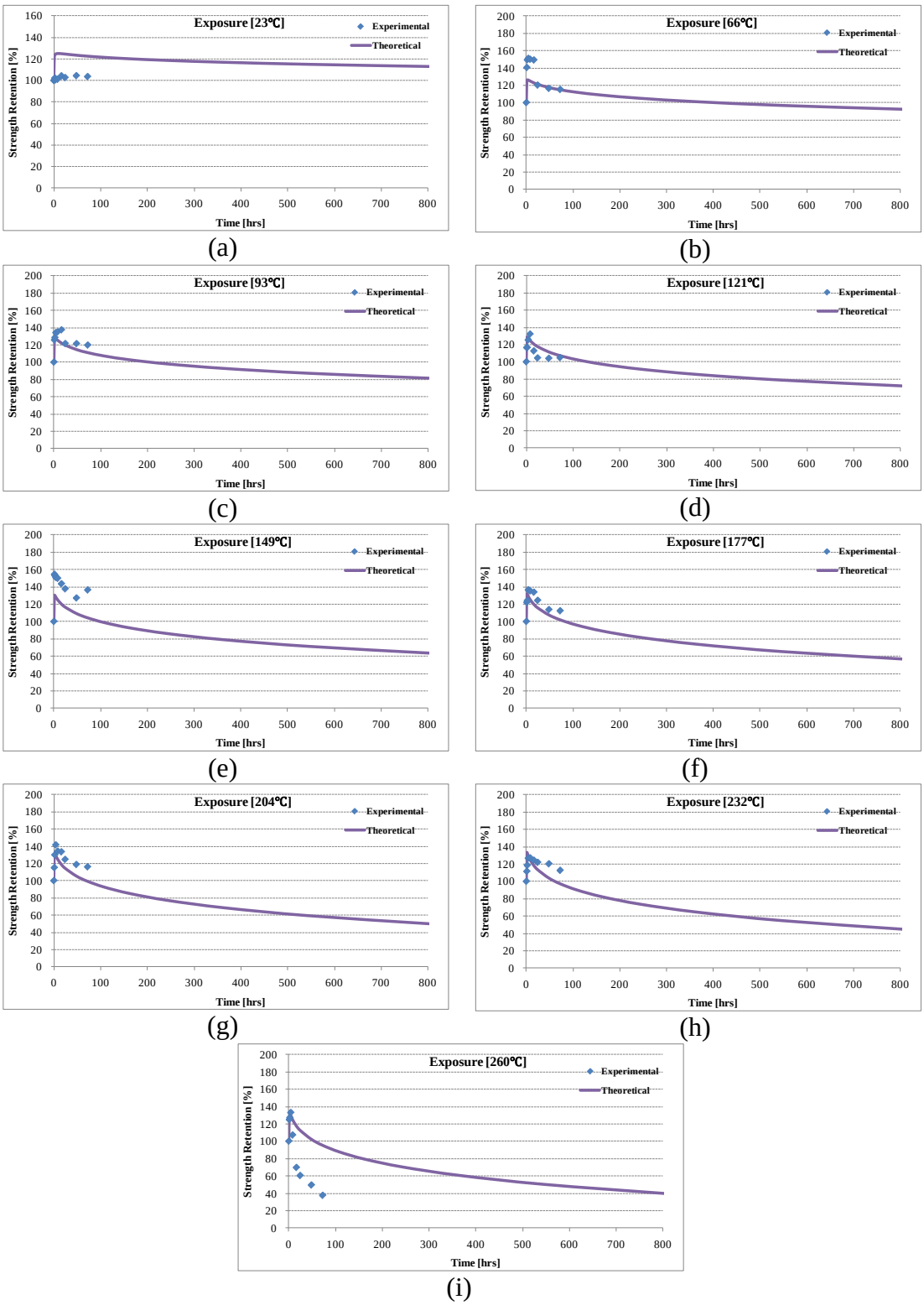

Figure 7-4: Comparison of the experimental values and predicted values of tensile strength by Arrhenius rate model on specimens exposed to elevated temperatures

7.2.2 Results

Predicted data related to strength and modulus on all mechanical tests determined by Arrhenius rate models will be presented in this section. Since predicted data are difficult to distinguish in same graph from experimental data, just predictive data will be introduced.

7.2.2.1 Tensile Testing

Tensile strengths based on Arrhenius rate model already were introduced in chapter 7.2.1. Predicted values of tensile modulus using Arrhenius rate model are presented in Figure 7-5. Similar to the results of predicted tensile strengths, until 72 hrs of ageing time which means the maximum time in this study, predicted values were corresponded well with experimental data except for the conditions of exposure temperatures (ambient and 260℃). Experimental data started to lose original properties of tensile modulus in conditions (exposure temperature: 260℃, ageing time: ~8 hrs) while predicted data showed decrease of original properties in lower environmental conditions.

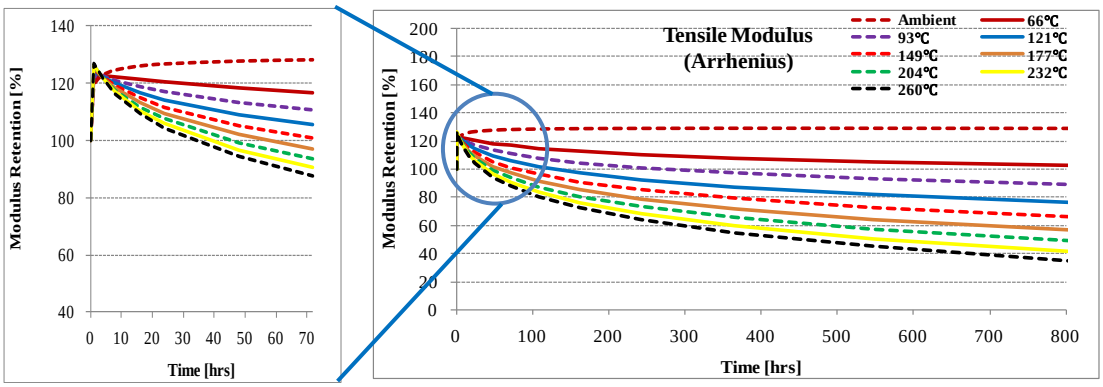

Figure 7-5: Predicted values of tensile modulus for specimens exposed to elevated temperatures using Arrhenius rate model

7.2.2.2 Off-Axis Shear Testing

Predicted values of off-axis shear modulus and strength using Arrhenius rate model are presented in Figure 7-6 and Figure 7-7. Predicted data were comparatively in good agreement with experimental data in both cases. Also, since post-cure effect was not applied to off-axis shear specimens, predicted data of off-axis shear test showed the best agreement with experimental data compared to other mechanical properties affected by post-cure effect.

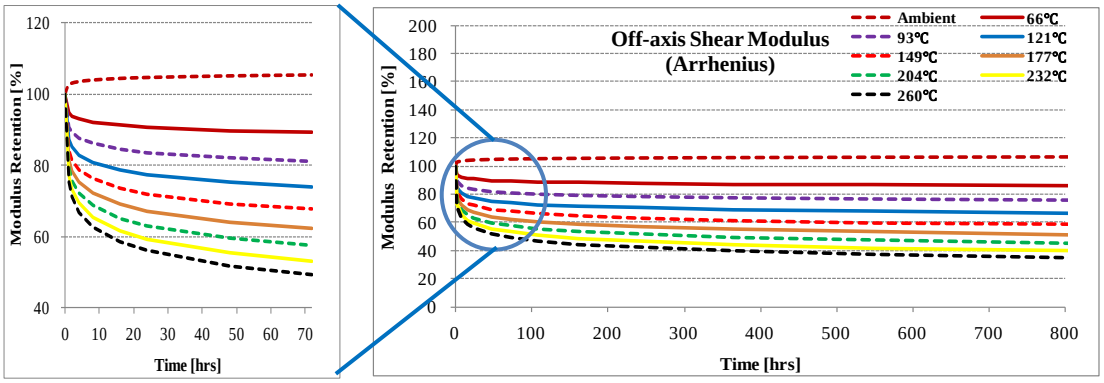

Figure 7-6: Predicted values of off-axis shear modulus for specimens exposed to elevated temperatures using Arrhenius rate model

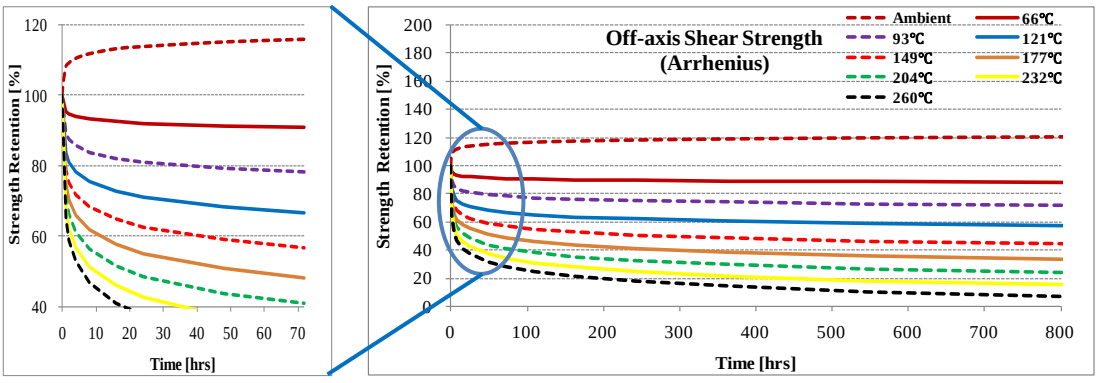

Figure 7-7: Predicted values of off-axis shear strength for specimens exposed to elevated temperatures using Arrhenius rate model

7.2.2.3 Flexural Testing

The Arrhenius predictions of flexural modulus and strength, for the specimens exposed to elevated temperatures are depicted in Figure 7-8 and Figure 7-9. Since the increase of mechanical properties by initial post-cure effect was not higher than the cases of tensile and short beam shear test, predicted data obtained by Arrhenius rate model showed rapid drop in terms of strength and modulus with extension of ageing time.

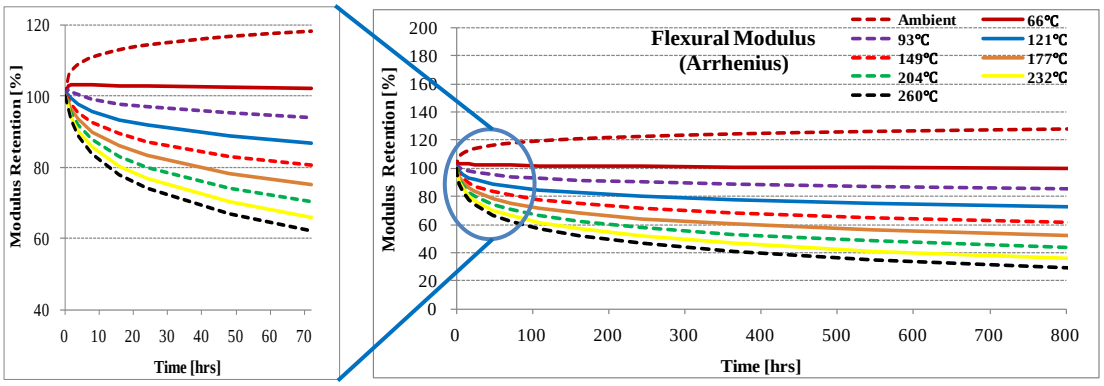

Figure 7-8: Predicted values of flexural modulus for specimens exposed to elevated temperatures using Arrhenius rate model

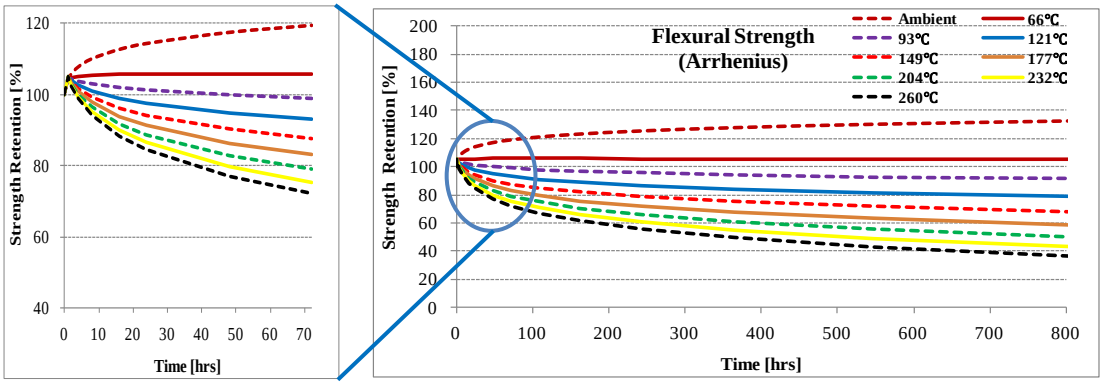

Figure 7-9: Predicted values of flexural strength for specimens exposed to elevated temperatures using Arrhenius rate model

7.2.2.4 Short Beam Shear Testing

The Arrhenius predictions of short beam shear strength, for the specimens exposed to elevated temperatures are presented in Figure 7-10. As seen from the Figure 7-10, predicted data for short beam shear strength showed the values between tensile and flexural strengths similar to experimental data.

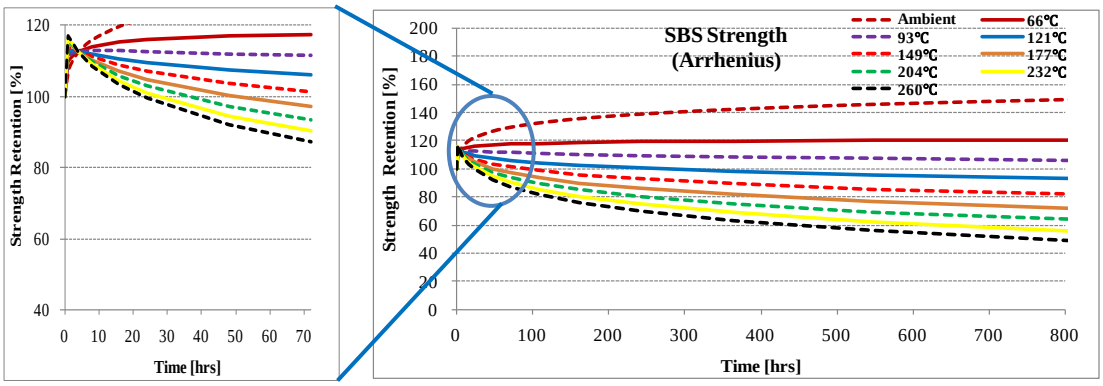

Figure 7-10: Predicted values of short beam shear strength for specimens exposed to elevated temperatures using Arrhenius rate model

7.3 Time Temperature Superposition Model

Time-Temperature Superposition (TTSP) principle comes from the concept that molecular relaxation occurs at faster rate in higher temperature and thus TTSP is a well-known methodology that frequently used to describe the mechanical and electrical relaxation behavior of polymer composites[92]. If the failure of composite materials occurs by one mechanism, TTSP provides a powerful tool for accurate prediction[93].

TTSP is based on the assumption that the effects of changing temperature on the time-dependent characteristic of a composite material are equivalent to the shift in the actual time scale of the measurement. If time-dependent data at a chosen temperature is selected as a reference curve, the shift on the time scale is dependent on the test temperature to obtain a master curve. A master curve can be generated by shifting the short term data on a logarithmic scale to the reference temperature. Therefore, master curve is the function of time and temperature. The horizontal shift is expressed as

$$f(T_0, t) = f(T_1, t / a_T) \tag{7.4}$$

where:

f = the property in the model

T_0 = the reference temperature (Kelvin)

t = time (hours)

T = the temperature that is being shifted (Kelvin)

a_T= shift factor

Based on the Williams-Landel-Ferry (WLF)[94], shifting for master curve can be derived from two criteria which the same shift factor should be capable of use in

superposition of all viscoelastic functions and the adjacent curves must match exactly over a reasonable distance. Beside the usual horizontal shift, reasonable master curve often needs vertical shift because of the inherent changes in the property of polymer composites. The vertical shift is based on the reference temperature whereas the horizontal shift is based on the Arrhenius relationship. All of shift factors are quantitatively in good agreement with two Arrhenius' equations with different activation energies ΔE[95]:

$$Log(a_T) = -\frac{\Delta E}{2.303R}\left(\frac{1}{T} - \frac{1}{T_{ref}}\right) \tag{7.5}$$

where:

$Log(a_T)$ = the shift factor using the logarithmic scale

ΔE = the activation energy (KJ/mol)

R = the gas constant (8.3143×10^{-3}[KJ/(K.mol)])

T = the temperature that is being shifted (Kelvin)

T_{ref} = the reference temperature (Kelvin)

7.3.1 Data Analysis Procedure

The analysis process (i.e., tensile strength) on TTSP model will be demonstrated in this section. Once the experimental data is shifted as Equation 7.5, the master curve can be generated in order to provide predicted data over long time. Table 7-5 and Figure 7-11 show the logarithm scale of tensile strength retentions (%) and time on specimens exposed to elevated temperatures up to 72 hrs for TTSP model.

Table 7-5: Data for logarithmic scale of tensile strength retentions (%) on specimens exposed to elevated temperatures up to 72 hrs

Time [hr]	Log(percent short beam shear strength retention)							
	66℃	93℃	121℃	149℃	177℃	204℃	232℃	260℃
0	2.000							
1	2.148	2.100	2.066	2.189	2.086	2.061	2.047	2.097
2	2.175	2.110	2.065	2.185	2.094	2.114	2.073	2.104
4	2.180	2.129	2.098	2.179	2.135	2.150	2.102	2.124
8	2.176	2.131	2.120	2.175	2.131	2.127	2.103	2.030
16	2.174	2.139	2.051	2.157	2.126	2.125	2.094	1.843
24	2.080	2.085	2.019	2.139	2.095	2.095	2.085	1.781
48	2.066	2.085	2.017	2.104	2.055	2.074	2.079	1.694
72	2.062	2.079	2.020	2.135	2.050	2.064	2.051	1.575

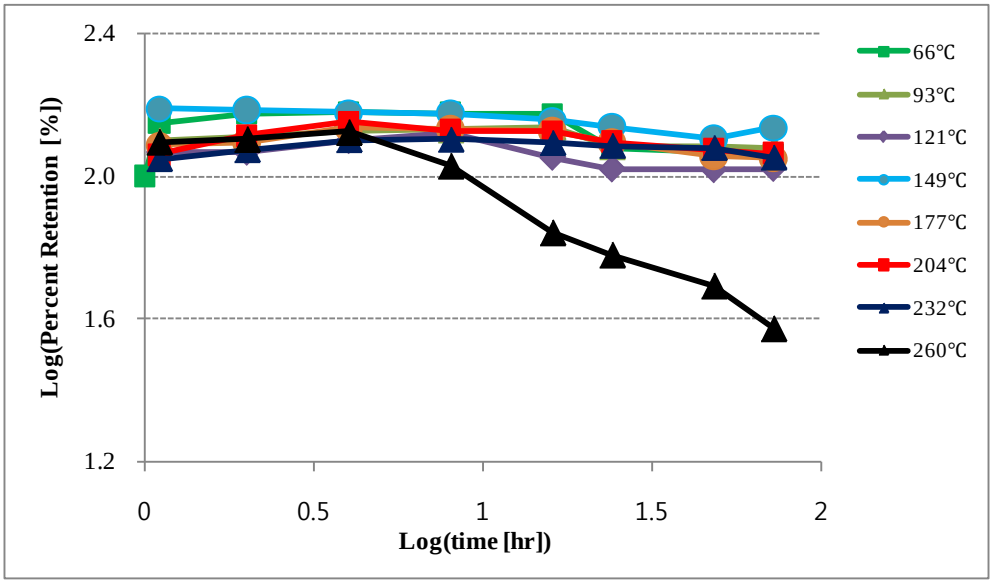

Figure 7-11: Logarithmic scale of percent tensile strength retention (%) versus time (hr)

According to Equation 7.5, the logarithmic horizontal shifts for the curves of Figure 7-11 are tabulated in Table 7-6. These shift factors were calculated by using activation energies obtained by Dynamic Mechanical Thermal Analysis. For accurate master curve, vertical shifts were slightly performed with curve of reference exposure temperature (66℃). Shifted curves to generate master curve for Time-Temperature Superposition model are shown in Figure 7-12. Based on Figure 7-12, master curve of good relationship (R^2 = 0.95745) using polynomial 3rd order curve fit was generated as shown in Figure 7-13. Using master curve, long-term service life in terms of tensile strength retentions can be estimated as shown in Figure 7-14.

Table 7-6: Horizontal shift factors from curve in exposure temperature (66℃) using the logarithmic scale on specimens exposed to elevated temperatures

ΔT	~93℃	~121℃	~149℃	~177℃	~204℃	~232℃	~260℃
log(a_T)	0.429	1.974	4.027	4.098	8.068	8.319	9.599

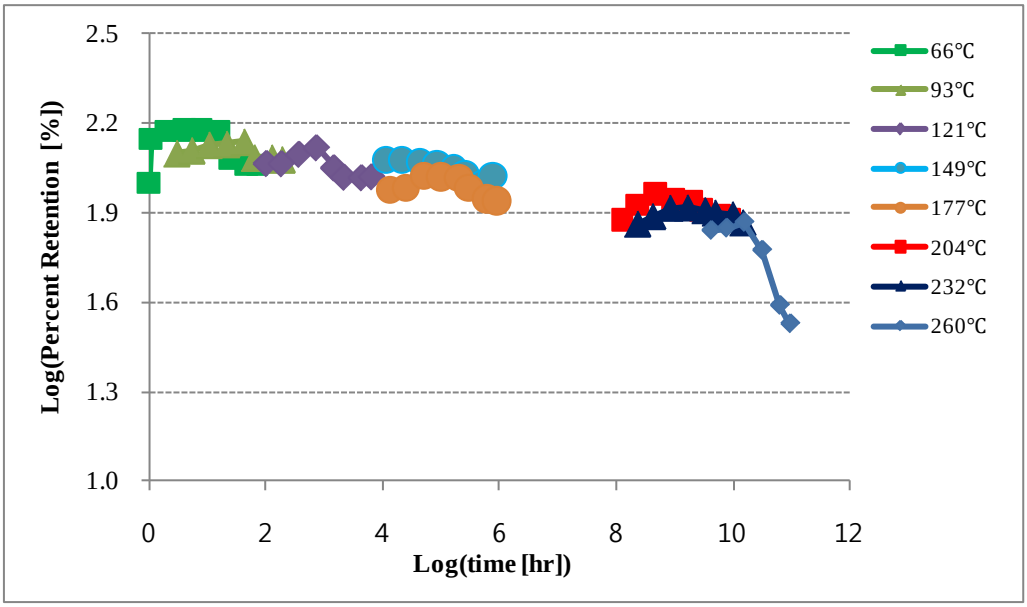

Figure 7-12: Shifted curves to yield master curve for Time-Temperature Superposition

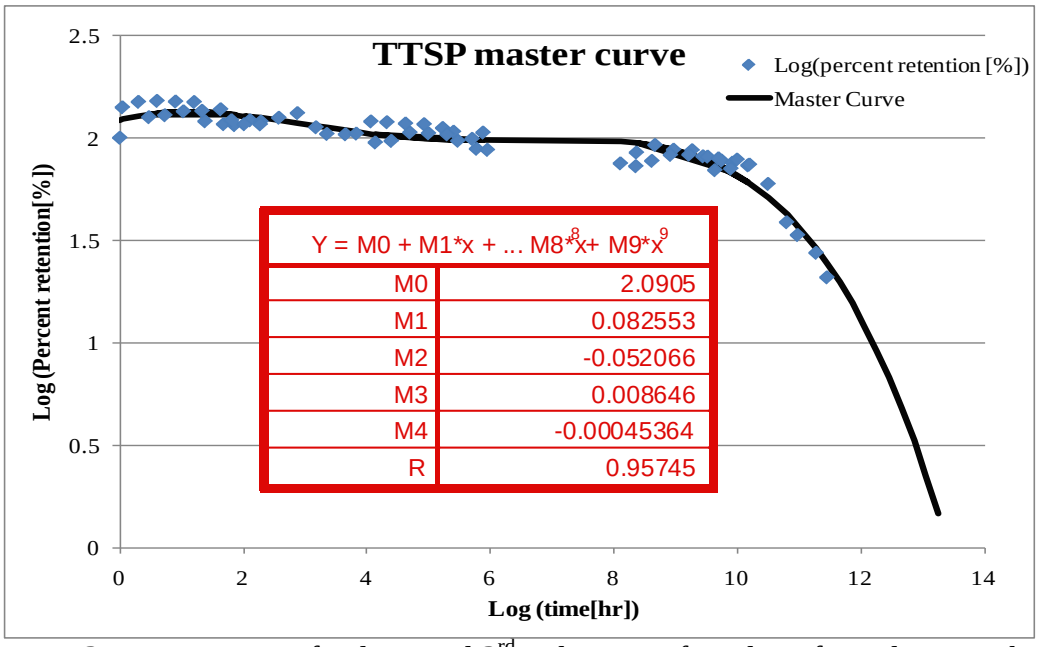

Figure 7-13: Master curve of polynomial 3rd order curve fit to log of tensile strength profile for Time-Temperature Superposition model

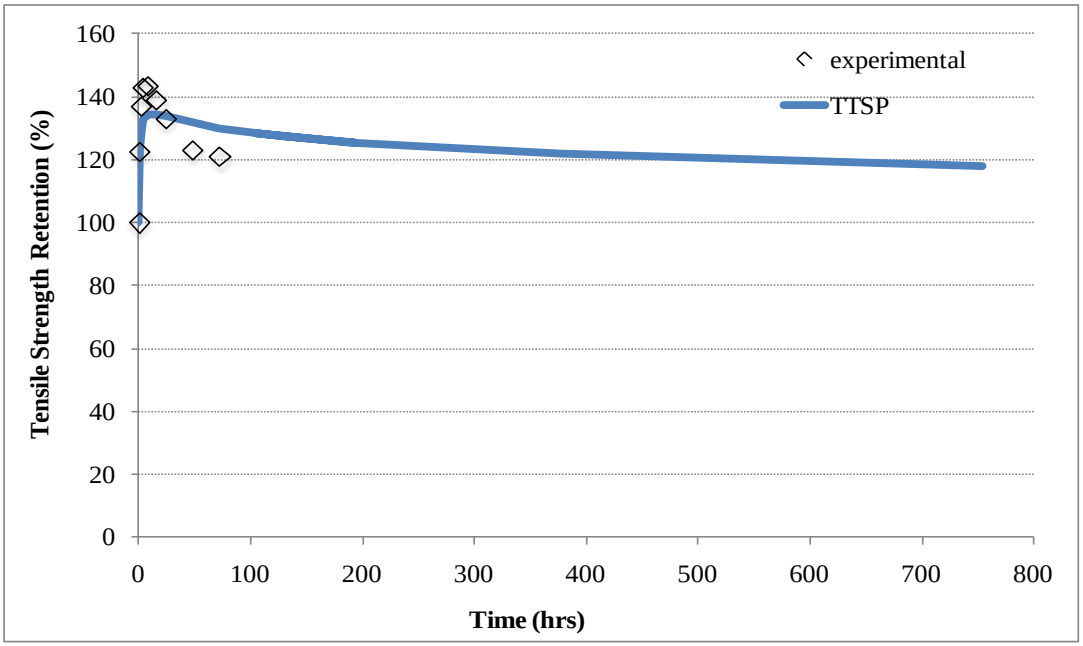

Figure 7-14: Comparison of predicted values and experimental values of tensile strength retention based on the Time-Temperature Superposition model

7.3.2 Results

Predicted data related to strength and modulus on all mechanical tests determined by Time-Temperature Superposition model will be presented in this section.

7.3.2.1 Other Mechanical properties

Results for the other mechanical properties as derived from Time-Temperature Superposition model are presented in Table 7-7, Figure 7-15 and Figure 7-16.

Table 7-7: Predicted data of additional mechanical properties based on Time-Temperature Superposition model - reference temperature (66°C)

Time (hr)	Strength Retention (%)				Modulus Retention (%)		
	Tension	Off-axis shear	Flexure	SBS	Tension	Off-axis shear	Flexure
0	100	100	100	100	100	100	100
1	124.12	82.87	87.76	92.18	112.50	83.95	87.19
2	129.08	90.22	96.68	103.83	121.62	89.42	95.20
4	132.79	95.93	104.49	114.57	129.26	93.36	101.95
8	134.48	98.62	109.47	121.92	133.70	94.87	105.93
16	134.45	98.62	111.76	125.88	135.17	94.32	107.35
24	133.76	97.58	112.00	126.76	134.83	93.22	107.17
48	131.70	94.44	110.89	126.21	132.56	90.35	105.47
72	130.08	92.02	109.53	124.89	130.43	88.25	103.84
103.7	128.43	89.58	107.97	123.21	128.13	86.19	102.08
128.9	127.38	88.05	106.92	122.03	126.62	84.90	100.93
188.6	125.45	85.28	104.91	119.72	123.79	82.60	98.78
193.4	125.32	85.09	104.78	119.56	123.60	82.45	98.63
377.1	121.75	80.11	100.93	114.96	118.22	78.35	94.62
754.3	117.99	75.07	96.82	109.91	112.45	74.26	90.43

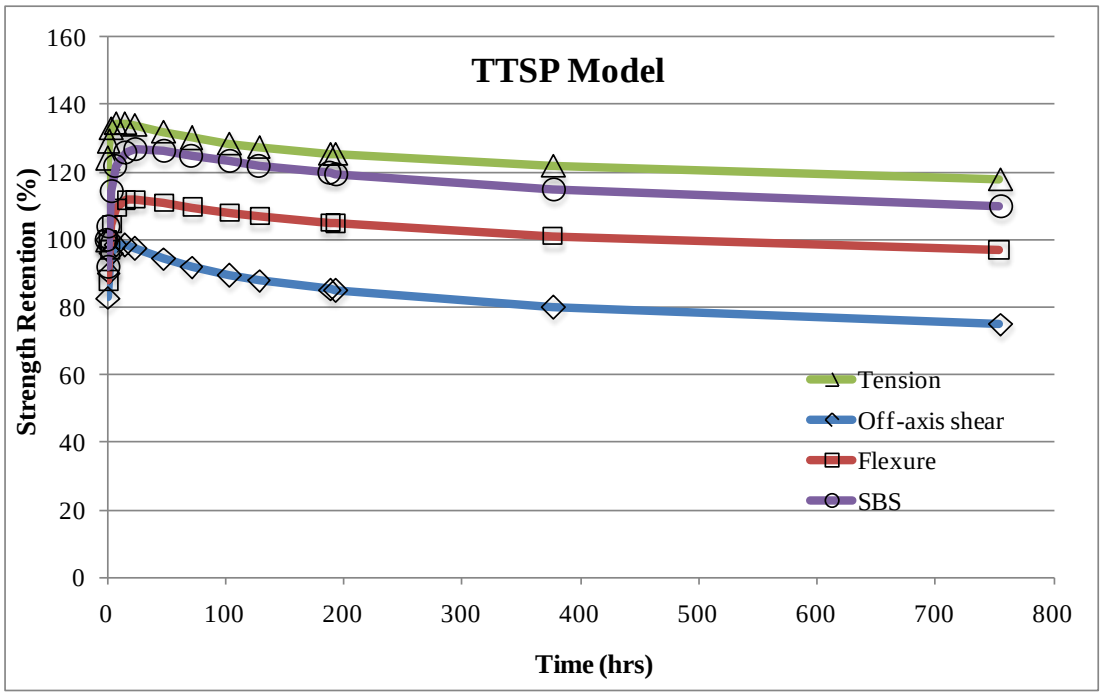

Figure 7-15: Predicted data of strengths based on Time-Temperature Superposition model - reference temperature (66°C)

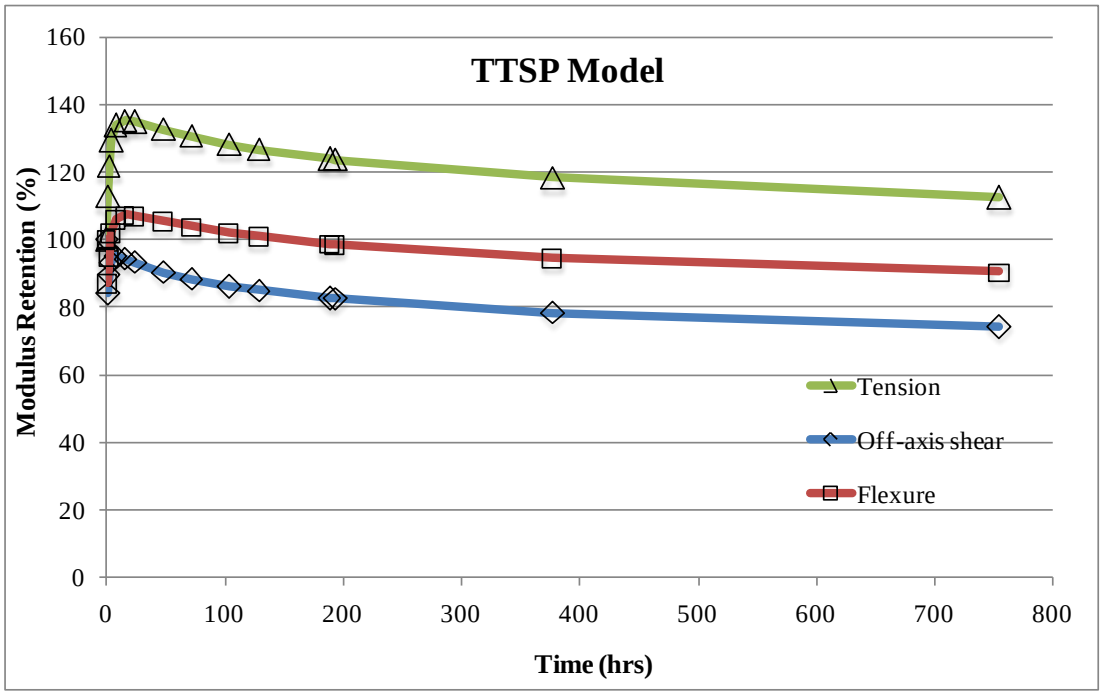

Figure 7-16: Predicted data of modulus based on Time-Temperature Superposition model - reference temperature (66°C)

7.3.2.2 Comparison with Arrhenius rate model

In this section, a direct comparison between Arrhenius rate model and Time-Temperature Superposition model will be accomplished to estimate which model is closer to experimental data. Since both models could not exactly reflect the increase of mechanical property due to residual post-cure effect, predicted data generated by two models were slightly different from experimental data. The difference between predictive model and experimental data is attributed to assumption to simply the process of analysis on predictive models. It is well known that the Arrhenius based prediction model assumes degradation processes to proceed in linear characteristic and hence can only be used in cased where self-consistent damage progression can be expected to occur. Also, in the case of TTSP model, it is assumed that the same mechanism of degradation occurs across all temperatures. Although some difference exists, two predictive models are useful for estimating the long-term service life because predicted data showed similar trend with experimental data and more conservative estimations in the majority of exposure temperatures compared to experimental results.

Figure 7-17, Figure 7-18, Figure 7-19 and Figure 7-20 illustrate comparison among prediction results of tension, off-axis shear, flexure and short beam shear retentions for Time-Temperature Superposition and Arrhenius rate model.

If looking at the results of tension retention, the modulus and strength retentions were almost identical at same model. However, the rate of degradation obtained by Arrhenius rate model was more conservative than that of TTSP model. The experimental data of tensile test on specimens exposed to 66°C were initially or largely affected by post-cure effect and were superior to other mechanical properties. Since

TTSP model was shifted from reference temperature (65°C) and initial increase was well reflected in predicted data, predicted data by TTSP model were similar with actual experimental data with minimal percent differences as shown in Figure 7-17.

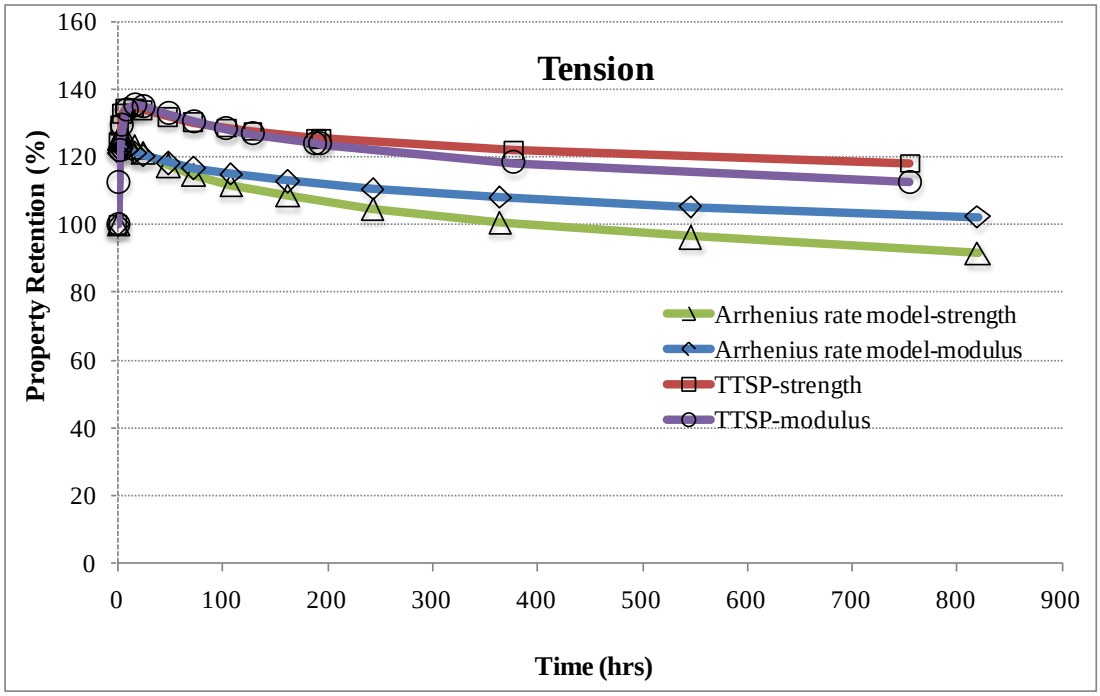

Figure 7-17: Comparison between prediction results of tensile retention for Time-Temperature Superposition and Arrhenius rate model

Since asymmetry on ± 45° specimens did not result in initial increase, as depicted in Figure 7-18, predicted data by two models were in good agreement with experimental data contrary to other mechanical properties because both models do not take into account effects of post-cure. Until ageing time (72 hrs) applied for this study, Arrhenius rate model showed higher rate of degradation than TTSP model while as ageing time is longer, TTSP model was reversely more conservative compared to Arrhenius rate model.

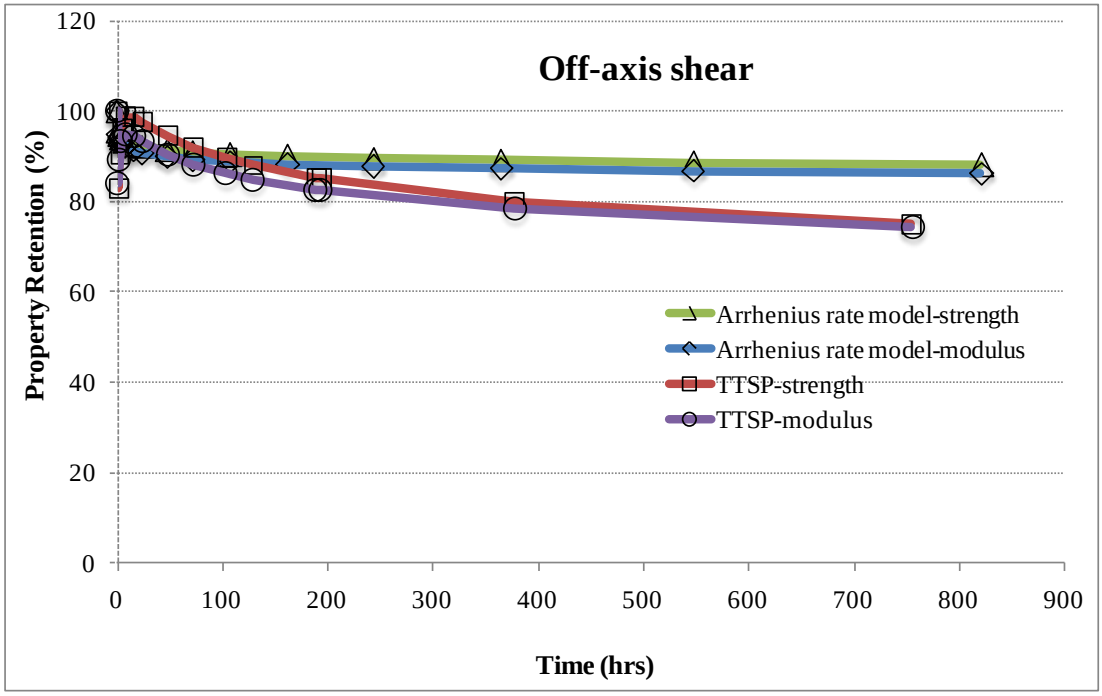

Figure 7-18: Comparison between prediction results of off-axis shear retention for Time-Temperature Superposition and Arrhenius rate model

As shown in Figure 7-19 and Figure 7-20, in the cases of flexural and short beam shear test on specimens exposed to temperature (66℃), initial increase of property retentions did not largely occur compared to the results of tension. In addition, continuous decrease like off-axis shear did not also take place. Therefore, predicted data generated by two models were almost identical regardless of extension of time. Two models can be equally applied for prediction of flexural and short beam shear retention on specimen exposed to 66℃.

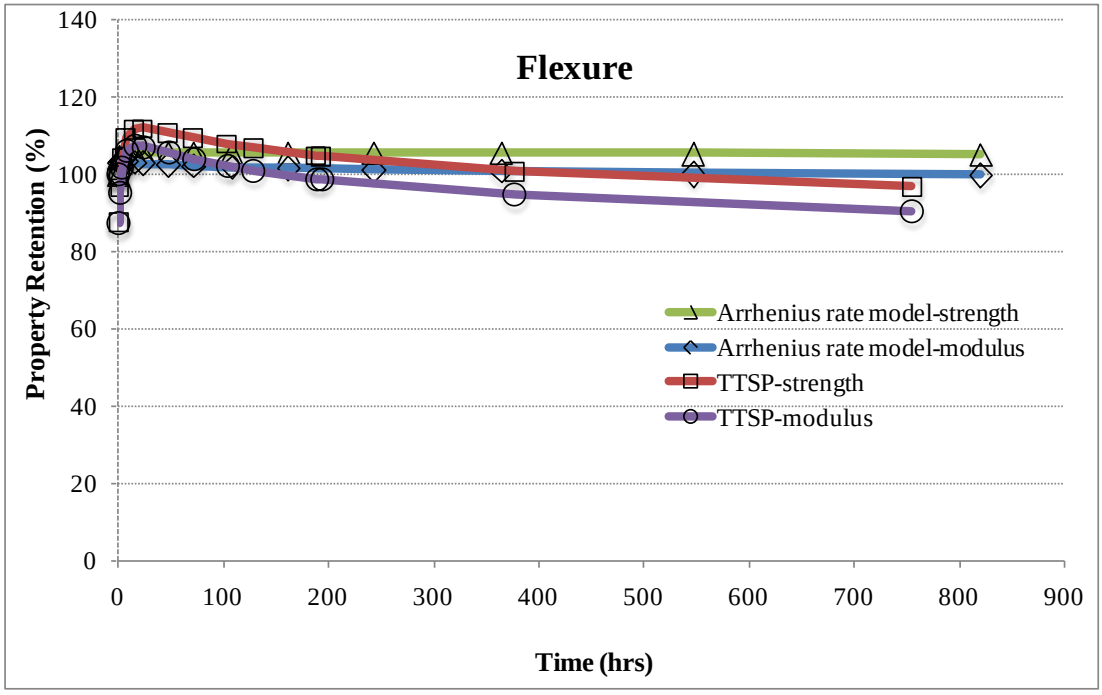

Figure 7-19: Comparison between prediction results of flexure retention for Time-Temperature Superposition and Arrhenius rate model

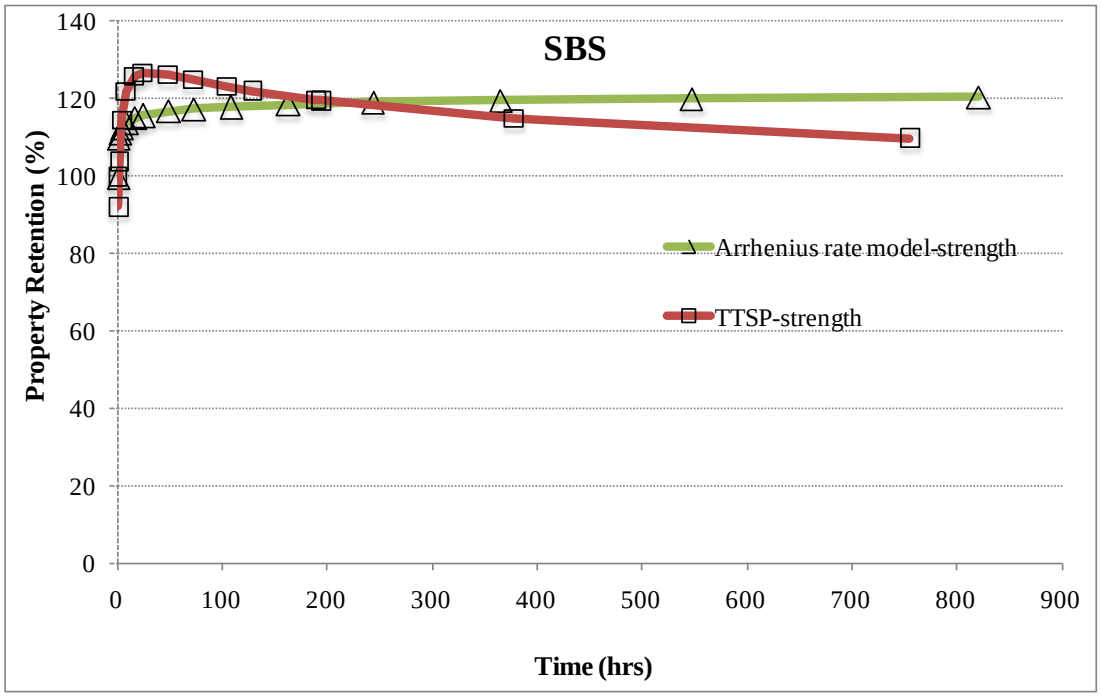

Figure 7-20: Comparison between prediction results of short beam shear retention for Time-Temperature Superposition and Arrhenius rate model

7.4 Weibull Statistical Strength Model

7.4.1 Introduction

If unidirectional composite materials are used in naval vessel applications, bending and tension are both major forms of loading. To characterize these properties, design practice relies strongly on testing which can be both expensive and time-consuming. For this problem, many researchers have been tried to develop unique tests that can provide multiple performance attributes or develop analytical approaches that would enable use of data from a series of other test results. Therefore, the ability to predict the strength of components subject to flexural, tensile or a combination of these types of loading is important practical interest[96].

Tensile data on unidirectional composite materials are usually used as design factor in composite materials selection and design of composite laminates. Flexural test is often accomplished in industry for material specification and quality control purpose. Even though flexural test is easier compared to tensile test, data generated from a unidirectional flexural test usually yield higher strength than data obtained from tensile test[97]. The tensile strength measured in flexural test is often 30% to 100% higher than the strength determined from unidirectional tensile test[98]. The presence of a stress gradient in the flexure-test results an increase in tensile strength compared to the tensile test under uniform stress. However, tensile strengths were higher than those measured by flexural test in this study. This phenomenon appears to be stemmed from good load-bearing of carbon fibers and superior interfacial bond between carbon fibers and epoxy resin.

In general, a statistical-strength theory based on a weibull distribution can be used to describe the difference between unidirectional-tensile data measured from a flexural test and a pure tensile specimen. In this chapter, the results of 3-point flexure test will be correlated with the data of a standard tensile coupon test for unidirectional carbon/epoxy composite materials. Also, theoretical results calculated by two parameter Weibull distribution model will be compared to the experimental data for tensile and flexural strength.

7.4.2 Theory

Ratios of flexural strengths to tensile strengths for wide varieties of brittle materials have been found to agree very well with Weibull's statistical strength theory.

Weibull theory defines the probability of survival of composite materials that a test specimen involving a distribution of flaws throughout its volume can survive the application of a stress distribution is expressed by[99],

$$P(S) = \exp\left\{-\int_V \left[\frac{\sigma(x,y,z)-\sigma_u}{S_0}\right]^{\alpha}\right\} dxdydz \tag{7.6}$$

where:

P(S) = the probability of survival

α = the flaw-density exponent that determines the scatter of strength for the materials (shape parameter)-this is related to the relative variance of the distribution

S_0 = the normalizing scale parameter that locates the strength distribution

σ_u = the threshold stress below which the material will never fail (usually taken

to be zero)

V = the volume of the specimen that is being stressed

For simpler form, taking σ_u as zero because tensile stress is uniform throughout the specimen, Equation 7.6 can be rewritten by,

$$P(S_t) = \exp\left[-V_t \left(\frac{\sigma_t}{S_0} \right)^{\alpha} \right] \tag{7.7}$$

where the subscript t denotes tension and V_t is the volume of the tensile coupon used in the tensile tests.

On the other hand, test specimen used in three-point bending flexural tests is subjected to non-uniform stress throughout the rectangular coupon. Therefore, Equation 7.8 including non-uniform factor can be made from Equation 7.6 as,

$$P(S_f) = \exp\left[-V_f \left(\frac{\sigma_f}{S_0} \right)^{\alpha} \left(\frac{1}{2(\alpha+1)^2} \right) \right] \tag{7.8}$$

where the subscript f denotes flexure and V_f is the volume of the specimen used in the flexural tests. $\frac{1}{2(\alpha+1)^2}$ means the non-uniform stress distribution.

The ratio of the median failure stress in three-point bending flexure to that in tension is obtained by setting $P(S_t)=P(S_f)$ as,

$$\frac{\sigma_f}{\sigma_t} = \left[2(\alpha+1)^2 \frac{V_t}{V_f} \right]^{\frac{1}{\alpha}} \tag{7.9}$$

The shape parameter (α) provides indications of scatter and in related to the relative variation of the distribution[100]. The shape parameter can be correlated to the

coefficient of variation (COV) as

$$COV = \left\{ \frac{\Gamma\left(1+\frac{2}{\alpha}\right)}{\Gamma^2\left(1+\frac{2}{\alpha}\right)} - 1 \right\}^{0.5} \tag{7.10}$$

where Γ means the gamma function. Two approximations are often used to explain this relationship with a high degree of accuracy, as follows,

$$COV = \alpha^{-0.926} \tag{7.11}$$

$$COV = \frac{1.2}{\alpha} \tag{7.12}$$

A relationship between the mean value, μ, the shape factor, α, and the scale parameter, β, can be described as[101]

$$\mu = \beta\Gamma\left(1+\frac{1}{\alpha}\right) \tag{7.13}$$

7.4.3 Results

According to Weibull statistical strength theory, predicted data for tensile and flexural test will be presented in this section.

7.4.3.1 Predictive Data of Flexural Strength from Tensile Tests

First of all, the Weibull shape parameter must be obtained in order to predict data of flexural strength from tensile test. Equation 7.12 and coefficient of variation (COV) are used to calculate the shape parameter in all environmental conditions. Shape

parameters obtained are tabulated in Table 7-8 and Figure 7-21 depicts the shape parameters as a function of ageing time from tensile test. If looking at the shape parameters obtained from tensile test, shape parameters showed very high values in under-cure conditions (ambient and low exposure temperature for short ageing time). Namely, coefficients of variation in under-cure conditions were lowered by the lowest standard deviation although mean values were lower compared to post-cure conditions. As post-cure effects are applied for specimens, shape parameters were getting lower. Since tensile failure mode can be largely affected by defects or voids in the process of hand layup fabrication, the standard deviation was getting higher in post-cure conditions. In high exposure temperature (260℃), lower mean values contributed to lower shape parameters.

Table 7-8: Values of shape parameters for the different exposure conditions and ageing time from tensile test

Time	Shape parameters for elevated exposure temperatures from tensile tests								
	Ambient (66℃)	66℃	93℃	121℃	149℃	177℃	204℃	232℃	260℃
0	37.8								
1	14.03	6.98	20.60	25.42	21.28	9.12	11.99	5.90	6.36
2	12.17	25.66	17.12	8.99	10.02	12.13	11.13	9.83	9.88
4	35.54	17.61	7.49	12.84	21.42	14.67	8.45	6.97	6.41
8	16.88	16.21	8.30	10.24	13.17	10.76	13.54	6.51	4.45
16	20.84	14.66	10.42	16.15	9.29	15.06	11.05	11.28	3.48
24	16.77	8.38	8.71	12.92	9.18	5.99	7.27	15.12	5.87
48	19.74	16.03	9.70	16.36	11.99	7.39	12.99	13.81	2.78
72	18.42	20.04	15.31	17.67	19.02	15.42	10.13	12.15	2.85

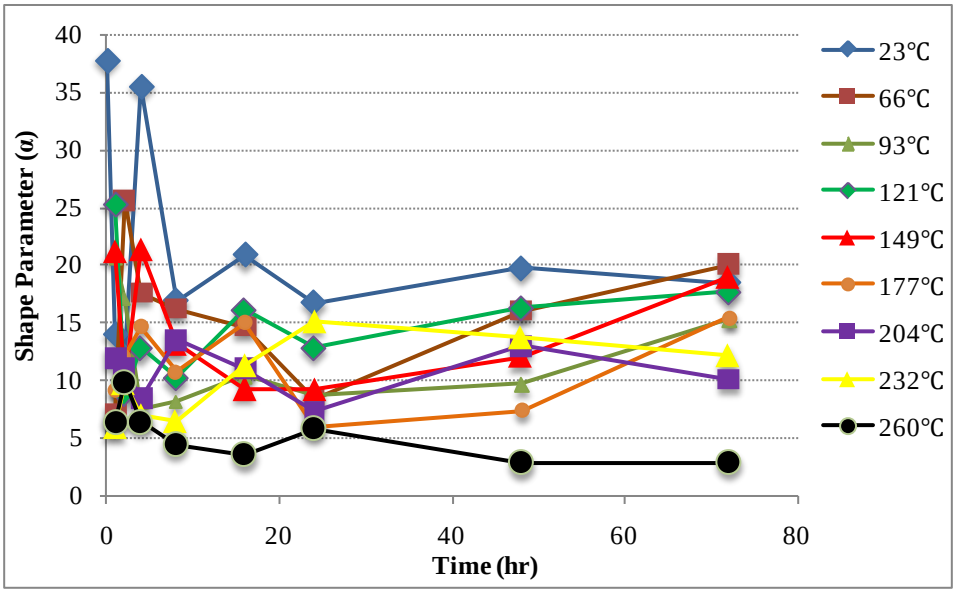

Figure 7-21: Shape parameters on specimens exposed to elevated temperatures as a function of time from tensile test

Table 7-9 and Figure 7-22 show values of flexural strength predicted from tensile test on specimens exposed to elevated temperatures for 72 hrs. It can be seen from Figure 7-22 that predictions of flexural strength are fairly close to the experimental values of flexural strength. In addition, predictive data of flexural strength were overall shifted to high values compared to the experimental data. Especially, predictive data for flexural strength were in good agreement with experimental data in the ranges showing high values of flexural strength due to post-cure effect. Also, predictive data were widely distributed compared to experimental data.

Table 7-9: Values of flexural strength predicted from tensile test on specimens exposed to elevated temperatures for 72 hrs

Time	Predicted Flexural Strength (MPa) : non-uniform term								
	Ambient (23℃)	66℃	93℃	121℃	149℃	177℃	204℃	232℃	260℃
0	493.69								
1	549.31	592.78	601.55	563.03	734.66	545.30	526.86	466.83	529.01
2	554.62	713.58	609.91	523.38	689.35	579.80	590.69	535.00	578.06
4	617.23	711.68	586.40	578.81	718.92	632.19	612.34	521.15	571.33
8	599.12	700.71	595.68	592.76	691.82	610.90	625.55	535.63	423.05
16	614.39	693.48	620.75	534.42	644.02	619.90	609.61	560.20	261.72
24	608.51	533.13	540.67	484.10	618.01	527.04	538.95	565.87	259.40
48	608.65	544.14	549.40	490.18	585.16	491.64	567.74	554.20	165.02
72	623.60	546.08	579.09	498.79	641.40	529.55	525.32	540.13	127.90
Time	Experimental Flexural Strength (MPa)								
	Ambient (23℃)	66℃	93℃	121℃	149℃	177℃	204℃	232℃	260℃
0	547.72								
1	543.11	525.82	512.19	535.95	498.76	540.21	530.27	549.63	494.27
2	585.72	520.14	540.10	554.82	574.78	586.62	562.61	516.77	534.28
4	527.26	558.61	512.58	529.80	505.41	529.97	492.13	528.36	575.69
8	532.05	544.49	483.48	523.24	594.22	548.39	526.03	540.63	295.26
16	527.11	513.13	518.38	543.61	576.04	530.45	545.35	538.35	122.17
24	515.97	543.15	495.93	555.62	553.59	527.56	526.99	557.54	104.44
48	523.90	495.65	540.55	523.16	542.36	549.98	548.88	534.48	76.88
72	514.70	511.71	545.66	553.06	461.98	602.56	600.62	356.95	51.66
Time	Percentage error (%)								
	Ambient (23℃)	66℃	93℃	121℃	149℃	177℃	204℃	232℃	260℃
0	-10.94								
1	1.13	11.30	14.85	4.81	32.11	0.93	-0.65	-17.74	6.57
2	-5.61	27.11	11.45	-6.01	16.62	-1.18	4.75	3.41	7.57
4	14.58	21.51	12.59	8.47	29.70	16.17	19.63	-1.38	-0.76
8	11.19	22.29	18.84	11.73	14.11	10.23	15.91	-0.93	30.21
16	14.21	26.01	16.49	-1.72	10.56	14.43	10.54	3.90	53.32
24	15.21	-1.88	8.28	-14.77	10.42	-0.10	2.22	1.47	59.74
48	13.92	8.91	1.61	-6.73	7.31	-11.87	3.32	3.56	53.41
72	17.46	6.29	5.77	-10.88	27.97	-13.79	-14.34	33.92	59.61

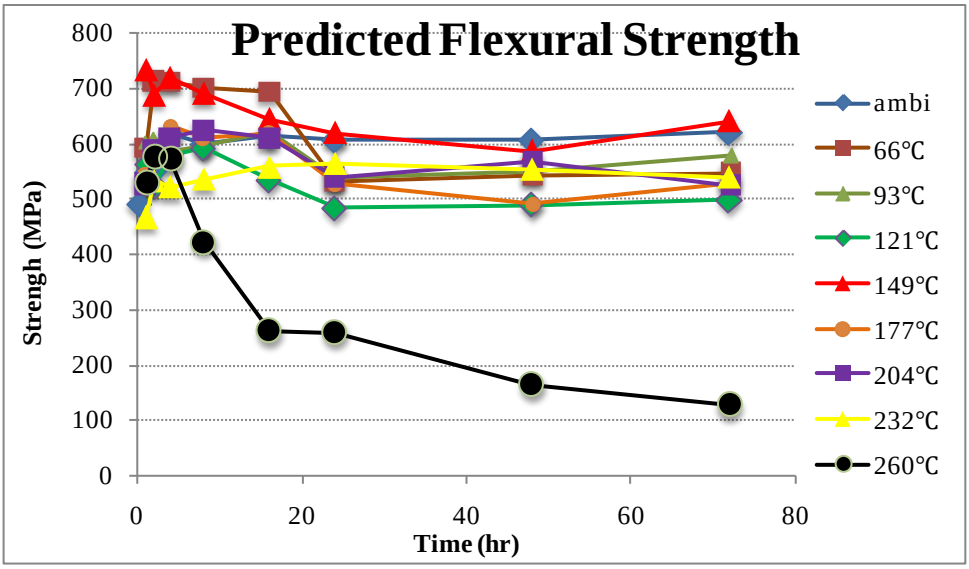

(a)

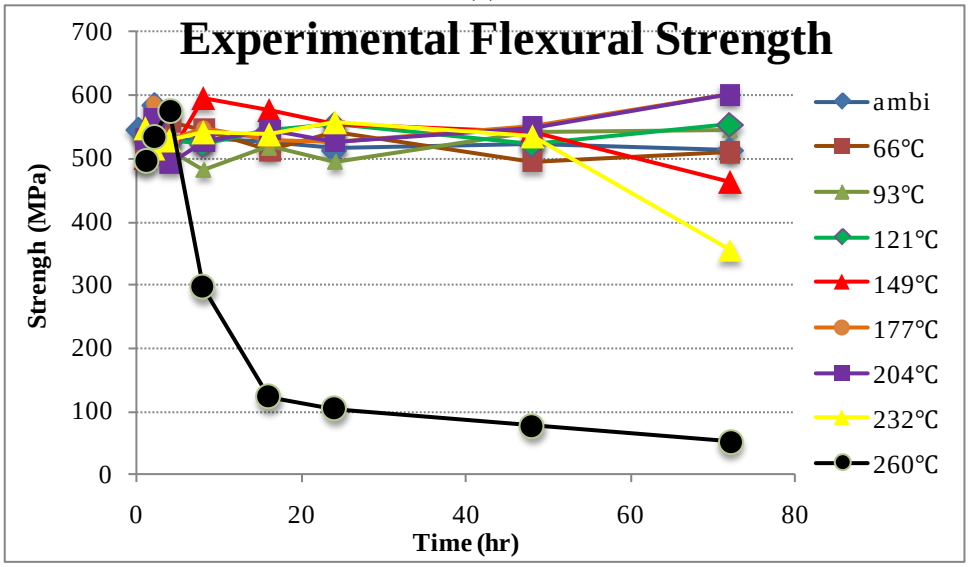

(b)

Figure 7-22: Comparison of (a) predicted flexural strength from tensile test and (b) experimental flexural strength

7.4.3.2 Predictive Data of Tensile Strength from Flexural Tests

As investigated in previous section, predicted data of flexural strength from tensile test showed good correlation with experimental data. On the contrary to this, if tensile strengths can be estimated from flexure test which has easier method compared to other mechanical tests, it can be more efficient prediction to avoid cost and time-consuming. The Weibull parameters for each of the flexural test data sets are evaluated as shown in Table 7-10 and Figure 7-23. Similar to shape parameters of tensile strength, shape parameters from flexure test showed high values in under-cure conditions and low values in high exposure temperatures (204, 232 and 260℃). In additions, the reasons why the high variation of shape parameters show compared to tensile strengths are that flexure test intrinsically has stress gradient in bending and failure mechanisms are very complicated.

Table 7-10: Values of shape parameters for the different exposure conditions and ageing time from flexural test

Time	Shape parameters for elevated exposure temperatures from flexural tests								
	Ambient (23℃)	66℃	93℃	121℃	149℃	177℃	204℃	232℃	260℃
0	29.11								
1	39.03	18.55	8.87	21.36	6.16	20.61	14.50	17.02	32.47
2	46.00	26.64	26.27	18.10	14.88	19.00	17.07	10.28	25.73
4	20.49	9.12	12.31	14.15	40.14	7.43	12.17	10.34	27.38
8	8.34	13.63	10.48	32.75	13.41	7.92	13.29	14.41	5.34
16	37.75	15.42	20.71	9.43	26.98	23.51	14.61	17.36	10.25
24	8.16	7.98	5.45	24.87	13.76	23.09	9.96	12.32	9.94
48	24.03	9.35	29.88	8.96	8.81	15.63	9.56	8.75	7.00
72	10.43	9.30	15.88	22.96	22.07	15.15	19.56	3.10	2.96

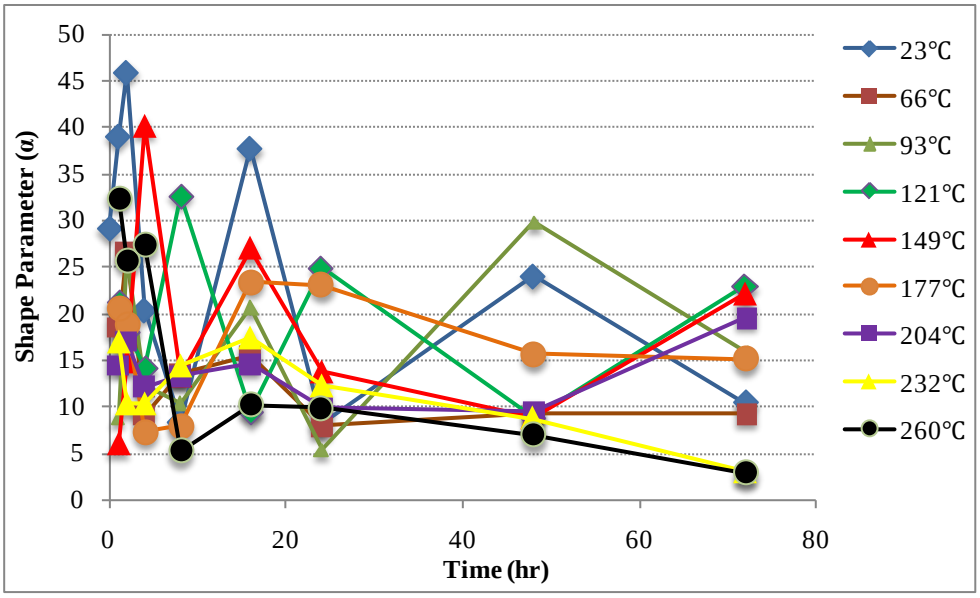

Figure 7-23: Shape parameters on specimens exposed to elevated temperatures as a function of time from flexural test

Table 7-11 and Figure 7-24 present values of tensile strength predicted from flexural test on specimens exposed to elevated temperatures for 72 hrs. As shown Figure 7-24, predicted data of tensile strength from flexural test showed a similar tendency with experimental tensile strengths. On the contrary to the predictive data of flexural strength, predictive data of tensile strength were overall shifted to lower values in intermediate exposure temperatures. In other words, the increase of strength due to post-cure effect was reduced by weibull statistical strength model. Except for severe condition (exposure temperature: 260℃), experimental data of tensile strength were scattered between 500 MPa and 800 MPa while predictive data were distributed between 500 MPa and 650 MPa.

Table 7-11: Values of tensile strength predicted from flexural test on specimens exposed to elevated temperatures for 72hrs

Time	Predicted Tension Strength (MPa)								
	Ambient (23℃)	66℃	93℃	121℃	149℃	177℃	204℃	232℃	260℃
0	575.20								
1	568.39	576.14	575.29	575.57	579.31	557.46	584.55	599.69	524.58
2	613.04	541.27	576.26	600.50	632.32	630.48	615.08	576.11	570.15
4	568.88	633.87	567.93	583.09	532.82	611.14	554.29	609.12	598.58
8	599.17	605.95	541.84	555.98	657.54	626.96	578.11	597.12	339.77
16	547.49	565.45	561.88	599.86	615.07	573.44	598.18	591.33	135.95
24	580.70	613.66	570.48	594.93	608.63	545.31	591.45	623.28	113.82
48	560.20	562.69	574.47	587.11	609.80	603.83	619.31	609.56	88.50
72	572.98	581.35	594.57	591.94	502.05	656.91	650.28	428.97	60.38
Time	Experimental Tension Strength (MPa)								
	Ambient (23℃)	66℃	93℃	121℃	149℃	177℃	204℃	232℃	260℃
0	502.26								
1	581.68	706.34	632.60	584.64	775.59	612.64	577.67	559.53	627.34
2	602.68	751.05	646.52	583.46	768.83	623.52	652.35	594.13	638.44
4	635.18	759.38	675.49	628.76	757.77	684.95	710.17	635.30	667.76
8	637.06	754.03	679.70	662.12	752.08	679.07	673.62	636.98	537.66
16	643.02	749.95	691.43	564.93	720.81	671.43	669.59	623.21	349.88
24	646.80	604.06	611.17	524.36	691.34	624.42	625.50	611.42	303.20
48	672.05	584.97	610.71	522.15	638.38	570.72	595.91	603.00	248.40
72	704.18	578.72	602.29	526.22	684.88	563.94	582.49	565.29	188.60
Time	Percentage error (%)								
	Ambient (23℃)	66℃	93℃	121℃	149℃	177℃	204℃	232℃	260℃
0	12.68								
1	-2.34	-22.60	-9.96	-1.58	-33.88	-9.90	1.18	6.70	-19.59
2	1.69	-38.76	-12.19	2.84	-21.59	1.10	-6.06	-3.13	-11.98
4	-11.65	-19.80	-18.94	-7.83	-42.22	-12.08	-28.12	-4.30	-11.56
8	-6.32	-24.44	-25.44	-19.09	-14.38	-8.31	-16.52	-6.67	-58.24
16	-17.45	-32.63	-23.06	5.82	-17.19	-17.09	-11.94	-5.39	-157.37
24	-11.38	1.56	-7.13	11.86	-13.59	-14.51	-5.76	1.90	-166.39
48	-19.97	-3.96	-6.31	11.06	-4.69	5.48	3.78	1.08	-180.67
72	-22.90	0.45	-1.30	11.10	-36.42	14.15	10.42	-31.78	-212.33

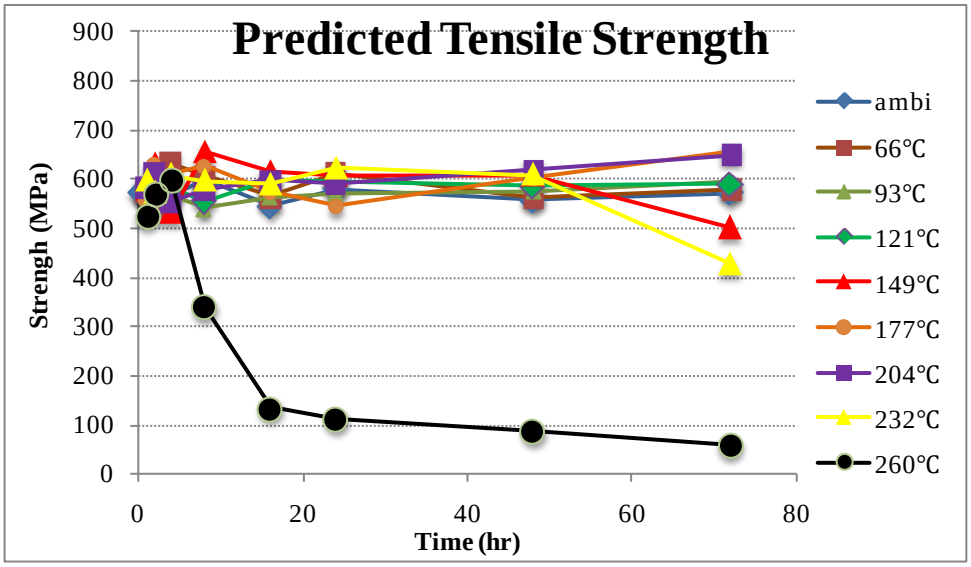

(a)

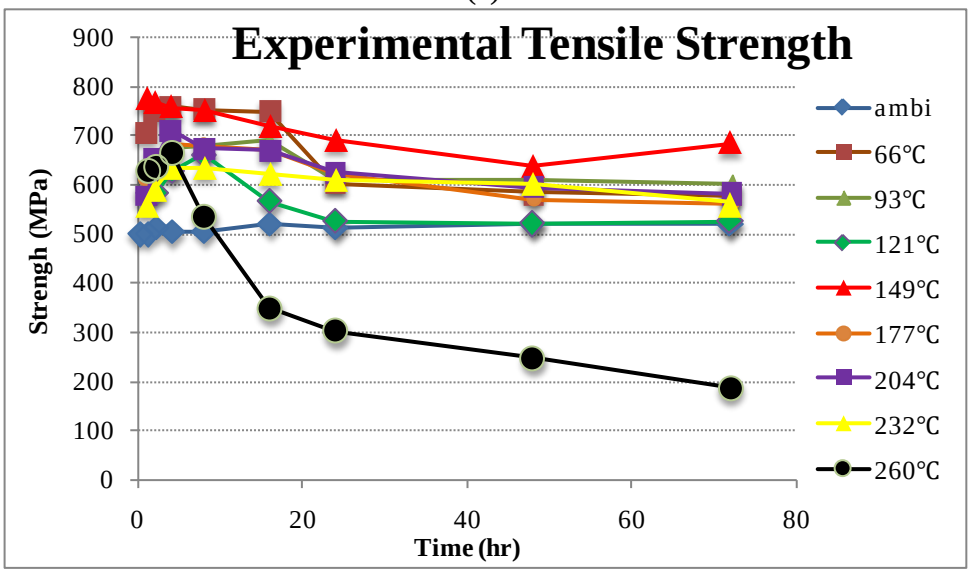

(b)

Figure 7-24: Comparison of (a) predicted tensile strength from flexural test and (b) experimental tensile strength

8 Conclusions

8.1.1 Summary

The various characterizations in conjunction with immersion effect were investigated for assessments of carbon/epoxy composite materials after exposure to elevated temperatures for navy vessel applications. This research can be summarized into mechanical characterization, thermal analysis, immersion analysis and predictive degradation model.

- *Mechanical characterizations*:

(1) As shown in Figure 8-1 and Figure 8-2, all tensile property retentions (%) within test conditions were more than 100% due to residual post-cure effect except for specimens exposed to temperature of 260℃ for 16 hrs of ageing time.

(2) The increase of tensile strength retentions by post-cure effect was superior to that of tensile modulus retention

(3) As expected, increase of tensile property occurred with extension of ageing time in the ranges of lower exposure temperatures whereas the enhancement of tensile property initially took place in the ranges of higher exposure temperatures and then tensile properties including strength and modulus were decreased due to degradation of thermooxidation.

(4) The color of the specimens exposed to elevated temperatures can be divided into five categories- no change, brown color with shiny surface, red color with shiny surface, dark color with shiny surface and char formation. Therefore, color of the

specimen exposed to temperature can be used in estimate the degree of curing and ageing as well as degradation in FRP composite materials.

(5) Specimens exposed to 260℃ for more than 16 hrs demonstrated a brooming mode of failure due to thermally perfect degradation of the matrix. Tensile strength and modulus were catastrophically dropped in these ranges.

(6) As shown in Figure 8-3 and Figure 8-4, the majority of the retentions (%) of off-axis shear property were less than 100% since test coupons were distorted by asymmetry when taken out from the oven and kept in atmosphere before off-axis shear test.

(7) Most retentions of flexural property existed between 80% and 120% as shown in Figure 8-5 and Figure 8-6. The residual post-cure effect did not largely lead to increase of flexural properties compared to tensile results. Since thermal oxidation caused catastrophic debonding between 2 layers in high exposure temperatures, the rate of drop of the flexural property was higher than that of the tensile property.

(8) Compared to the strength retentions of tensile and flexural test, the strength retentions of short beam shear test were initially increased in the amount of more than flexural strength retention and less than tensile strength retention by residual post-curing as shown in Figure 8-7. Therefore, the fractures of short beams shear test can be resulted in mixed failure mode. In particular, compared to experimental data of flexural test, the majority of failure modes of short beam shear test were occurred by not shear but flexural tension at outer surface.

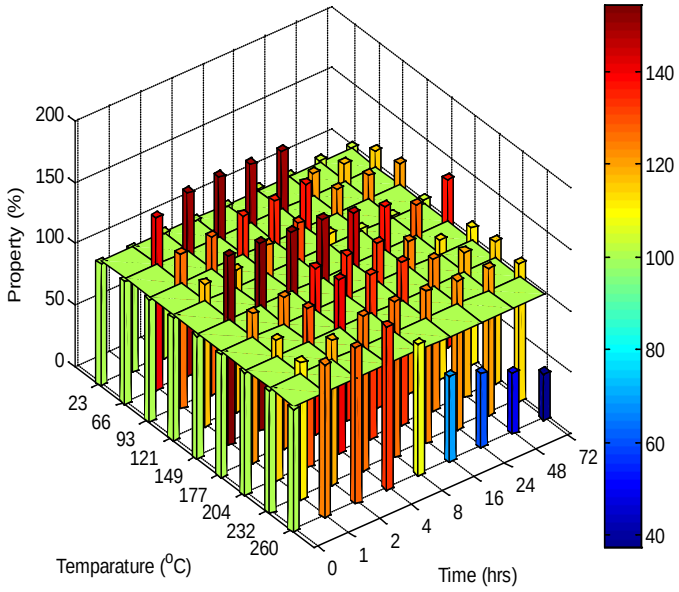

Retention (%) range	Tensile strength (count)
140~	11
120~140	31
100~120	26
80~100	1
60~80	2
~60	2
Total	73

Figure 8-1: The distribution of tensile strength retentions (%) on specimens exposed to elevated temperatures for up to72 hrs

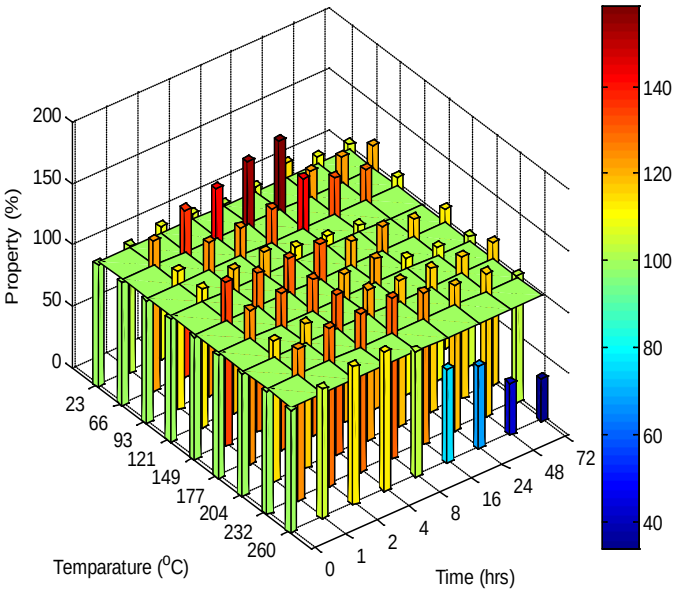

Retention (%) range	Tensile modulus (count)
140~	4
120~140	29
100~120	34
80~100	2
60~80	2
~60	2
Total	73

Figure 8-2: The distribution of tensile modulus retentions (%) on specimens exposed to elevated temperatures for up to72 hrs

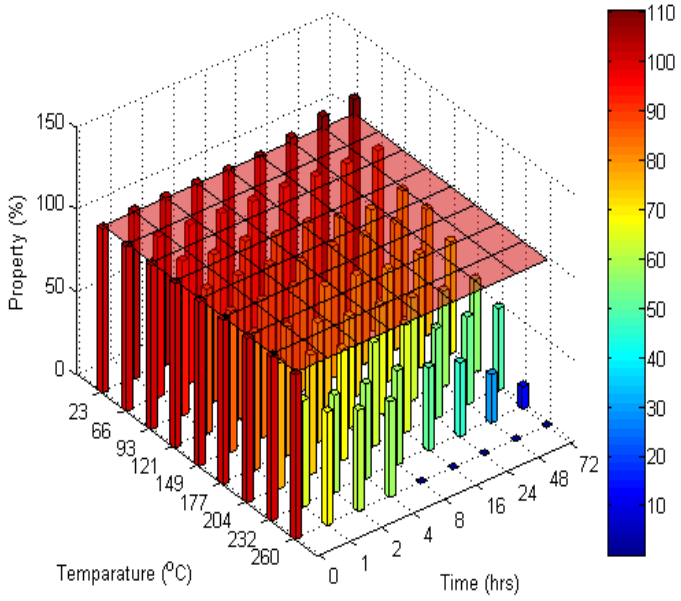

Retention (%) range	Off-axis shear strength (count)
140~	
120~140	
100~120	9
80~100	20
60~80	26
~60	18
Total	73

Figure 8-3: The distribution of off-axis shear strength retentions (%) on specimens exposed to the elevated temperatures for up to 72hrs

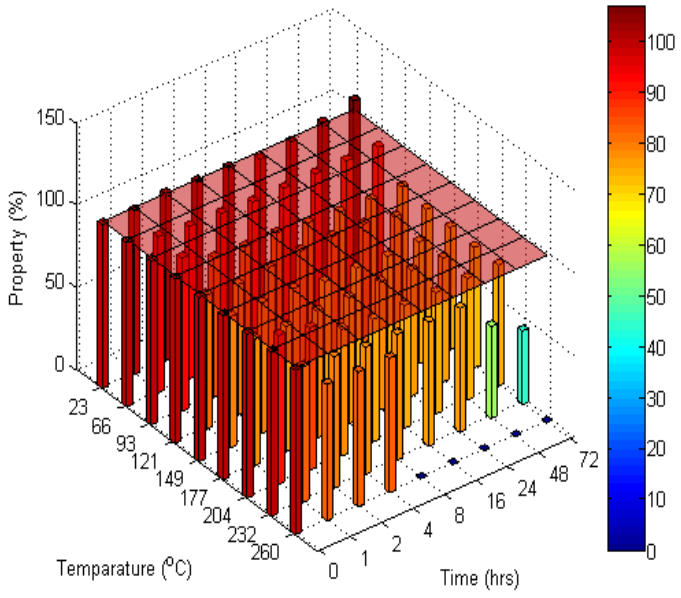

Retention (%) range	Off-axis shear modulus (count)
140~	
120~140	
100~120	6
80~100	28
60~80	32
~60	7
Total	73

Figure 8-4: The distribution of off-axis shear modulus retentions (%) on specimens exposed to the elevated temperatures for up to 72hrs

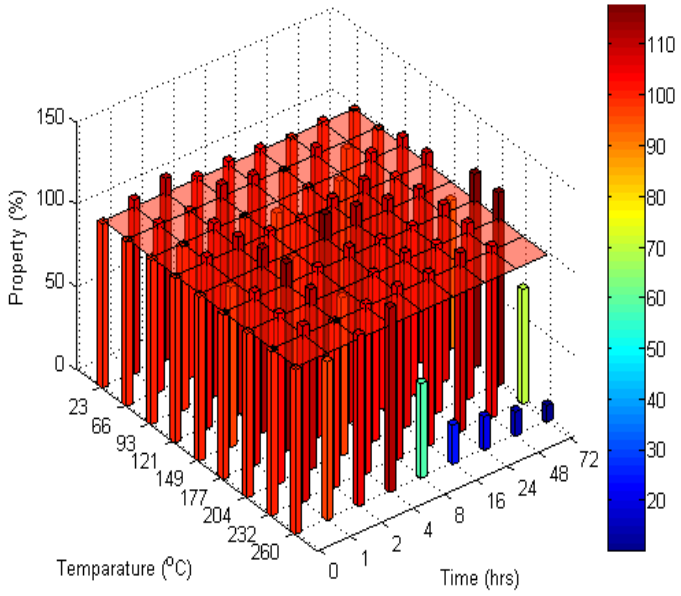

Retention (%) range	flexural strength (count)
140~	
120~140	
100~120	49
80~100	18
60~80	1
~60	5
Total	73

Figure 8-5: The distribution of flexural strength retentions (%) on specimens exposed to the elevated temperatures for up to 72hrs

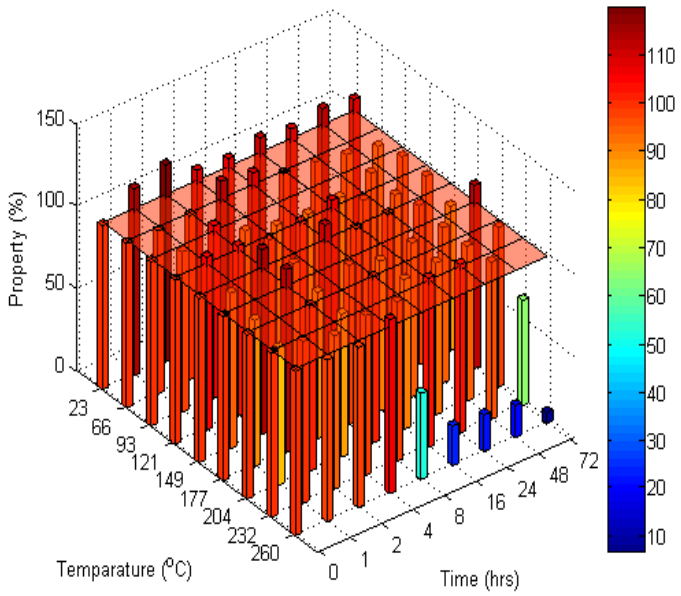

Retention (%) range	flexural modulus (count)
140~	
120~140	
100~120	28
80~100	39
60~80	1
~60	5
Total	73

Figure 8-6: The distribution of flexural modulus retentions (%) on specimens exposed to the elevated temperatures for up to 72hrs

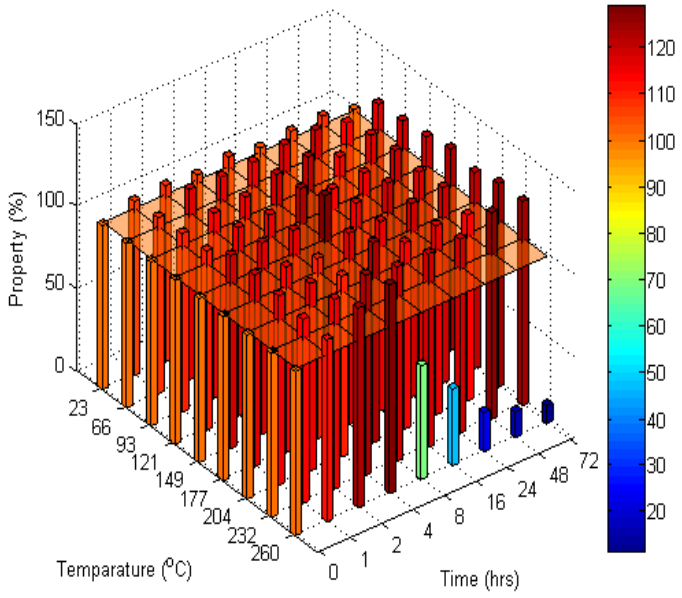

Retention (%) range	SBS strength (count)
140~	
120~140	11
100~120	57
80~100	
60~80	1
~60	4
Total	73

Figure 8-7: The distribution of Short Beam Shear strength retentions (%) on specimens exposed to the elevated temperatures for up to 72hrs

- *Thermal analysis*:

(1) Thermal ageing initially caused a significant increase of the glass transition temperature, which is attributed to the post-cure effect on ambient cured system.

(2) Glass transition temperatures determined from both fiber oriented test specimens using DMTA showed very similar data for all environmental conditions. However, because specimens were tested in bending with single cantilever fixture in longitudinal direction, glass transition temperatures of longitudinal specimen were slightly delayed compared to transverse test specimens.

(3) If the test frequency is increased, the relaxations corresponding to the glass transition is hard to reflect the mechanical strain input, and the polymer composites may have rigid property. Therefore, glass transition temperatures increase as the rate of frequency is increased.

(4) Since the tan δ is the ratio of the loss modulus to the storage modulus, the height of tan δ and glass transition temperatures shifted to higher levels with increase in test frequency. From increase of interfacial bonding by post-cure effect, broadened transition region and decreased tan δ value were observed due to the stiffness or rigid of test specimen.

(5) Activation energies were continuously increased up to 72 hrs of ageing time in the ranges of lower exposure temperatures (66, 93, 121 and 149℃). Continuous increases were attributed to residual post-cure effect, which led to an intense crosslinkage and the mobility of the polymer segment was constrained significantly. In ranges of intermediate temperatures (177, 204 and 232℃),

activation energies were leveled off after initially reaching to the maximum value.

(6) Except for the conditions of the severe exposure temperature (260℃), ambient temperature and off-axis shear test, the enhancement of mechanical properties were associated with increase of glass transition temperature.

(7) Glass transition temperatures determined by the analysis of DSC were overall higher than the results detected by the height of peak tan δ and storage modulus using DMTA in all environmental conditions.

(8) Since the epoxy resin used in this study was cured at room temperature and was not fully cured, weight loss of specimens was attributed to evaporating of uncured small molecules and spilt of the small molecular part from long polymer chain.

(9) The values of T_{ondset} initially increased due to the dominant increase of the crosslinkage with thermal treatment. For lower exposure temperatures (~149℃), the values of T_{ondset} continuously increased even though ageing time go up. In the exposure temperatures ranging from 177 to 260℃, the values of T_{ondset} continuously decreased with the extended ageing time. The higher exposure temperatures resulted in the more serious drop in the values of T_{ondset} by thermal decomposition of specimens.

- *Immersion analysis*:

(1) The results of the gravimetric measurements on specimens immersed in deionized water and seawater showed a Fickian response in all conditions.

(2) Specimens post-cured from the increase of ageing time and exposure temperature showed the rapid saturation and the higher maximum weight gain compared to un-cured specimens.

(3) The partially cured composite could be expected to have a greater concentration of unreacted chemical species with the epoxy resin and it appears that these species were released more rapidly into water resulting in a slower net mass gain.

(4) Mass loss by leaching of organic species than mass uptake by sorption of salts largely contributed to lower maximum weight gain in seawater compared to the values of deionized water.

(5) Overall diffusion coefficients calculated for deionized water immersion were higher than those for seawater immersion in all environmental conditions. Diffusion coefficients in deionized water were widely distributed with increase of ageing time and exposure temperatures.

(6) All specimens immersed in deionized water and seawater showed similar characterizations which had initially decrease (~ 16 weeks), asymptotic trend or slightly increase (16 ~ 48 weeks) and rapidly decrease after 48 weeks in terms of short beam shear strengths.

(7) Intrinsic properties of epoxy and carbon fiber against water resulted in a slight decrease or asymptotic trend in terms of short beam shear strengths until 48 weeks in immersion period. However, catastrophic drop of short beam shear strengths after 48 weeks of immersion was derived from irreversible degradations such as hydrolysis, microcracking, microvoids and epoxy relaxation.

(8) Specimens immersed in deionized water and seawater for 72 weeks after exposure to 260℃ for 8 hrs showed catastrophic cracks in the epoxy and interface and the delamiations between 2 layers by the increase of the free volume and water ingress into cracks and cavities created by thermooxidation when the specimens were heated to high temperature.

- *Predictive degradation models*:

(1) In tensile tests, the rate of degradation obtained by Arrhenius rate model was more conservative than that of TTSP model.

(2) Since asymmetry on $\pm 45^{o}$ specimens did not result in initial increase, predicted data by two models (Arrhenius rate model and TTSP model) were in good agreement with experimental data contrary to other mechanical properties.

(3) Predicted data of flexural and short beam shear test generated by two models (Arrhenius rate model and TTSP model) were almost identical regardless of extension of ageing time. Therefore, two models can be equally applied for prediction of flexural and short beam shear retention.

(4) Predictions of flexural strength generated by Weibull statistical strength model were fairly close to the experimental values of flexural strength. In addition, predictive data of flexural strength were overall shifted to high values compared to the experimental data.

(5) On the contrary to the predictive data of flexural strength, predictive data of tensile strength by Weibull statistical strength model were overall shifted to lower values in intermediate exposure temperatures.

8.1.2 Future Research

Even though this research provides insight to durability of wet layup carbon/epoxy composite systems exposed to the elevated temperatures and immersed in seawater, all the concerns with regard to these materials are not considered and resolved. In particular, since wet layup carbon/epoxy composite systems are used for naval vessels applications in marine environments, there are so many considerations to ensure these systems to safely use without degradation or deterioration. Therefore, Future researches must include such considerations as presented in followings.

1) *Radiation or UV light*:

Naval vessels operating in the sea can be strongly exposed by radiation or UV light from the sun compared to other environments. Especially, radiation or UV light reflected from the seawater is more intensive. Temperature effects by radiation or UV light in conjunction with the elevated temperatures from fire or heat source can be investigated in terms of durability.

2) *Thaw-freeze cycling*:

Composite materials used in the real field, in particular, marine conditions, are subjected to thaw-freeze cycling by a huge daily temperature range. Many researchers reported FRP composites showed the more severe degradation in thaw-freeze cycling condition compared to any other test conditions. In the process of thaw-freeze cycling, microcracking within composite systems by fatigue can be resulted in serious degradation. Therefore, this test condition must be considered to assure the use of

composite materials.

3) *Wet-dry cycling*:

Tides are the rise and fall of sea levels caused by the combined effects of the gravitational forces exerted by the Moon and the Sun, and the rotation of the Earth. The tides occur with a period of approximately 12 and a half hour and are influenced by the shape of the near-shore bottom. Composite systems of naval vessels in marine environmental condition are exposed to wet-dry cycling by tidal force. Contrary to immersion condition, moisture uptake can be differently applied for composite materials.

4) *Surface coating*:

Corrosion resistance is very important property to be attained to allow naval vessels to operate for long-term period. Furthermore, the functionality of naval vessels can be largely affected by attaching of barnacle, clam, oyster and so on in the bottom of naval vessels. These problems can be resolved by surface coating of composite systems. Therefore, the research regarding surface coating of the composite materials must be developed.

5) *EMI shielding*:

Metal film or materials having high conductivity are used for EMI shielding materials. However, metallic materials are prone to chemical corrosion and hard to manufacture for light-weight applications. To solve this problem, polymer composite with conducting fiber is possible alternative. Compared to glass fibers, carbon fibers are

attractive in electrical conductivity, which related to EMI shielding effectiveness[102]. Recently, it is well known that composites with carbon nanotubes are more effective materials for EMI shielding. To assure the stealth function for naval vessels, this research must be accomplished. In addition, this research can be broaden to the development of minecountermeasure vessels which not detected by acoustic and electromagnetic wave

6) *Impact property*:

Resistance to high velocity impact is an important requirement for high performance of naval vessels. Even though polymer matrix composites are characterized by high specific stiffness and high specific strength, they are susceptible to impact loading. For the effective use of composite materials on naval ships, their behavior under high velocity impact must be clearly understood.

7) *Immersion prediction*:

In this study, the durability of specimens immersed in seawater and deionized water for 72weeks was investigated using gravimetric analysis, SEM and short beam shear test. The extended time is necessary to estimate or predict the accurate service life for composite materials in the real seawater.

8) *Thickness effect*:

The carbon/epoxy composite materials comprised of 2 layers were used to assess the durability in this investigation. However, super structures such as naval

vessels are required to have thickness of more than 2 layers in order to withstand the higher loading. Since mechanical properties, immersion characteristics and failure mechanisms can be changed according to thickness of composite laminates, these investigations must be accompanied with other analyses.

REFERENCES

1. Caplan I, *Marine composites-First International Workshop on Composite Materials for Offshore Operation.* University of Houston, TX, 26-28, October 1993.

2. MIL-STD-2031, *Fire and Toxicity test methods and qualification procedure for composite materials systems used in Hull, Machinery, and Structural Application inside Naval Submarines.* 1991.

3. MeMarco RA, *36th International SAMPE Symposium.* 1991. 36.

4. Henderson, J.B., J.A. Wiebelt, and M.R. Tant, *A Model for the Thermal Response of Polymer Composite Materials with Experimental Verification.* Journal of Composite Materials, 1985. 19(6): p. 579-595.

5. Landrock, A.H., *Handbook of Plastics Flammability and Combustion Toxicology.* Noyes Publication, 1983. Park Ridge.

6. C.F.Cullis and M.M.Hirschler, *The Combustion of Organic Polymers.* Clarendon Press, 1981. Oxford.

7. Le Huy, H.M., Bellenger, V.,Verdu, J. and M. Paris, *Thermal oxidation of anhydride cured epoxies. I--mechanistic aspects.* Polymer Degradation and Stability, 1992. 35(1): p. 77-86.

8. Bruce, L.B., *The thermooxidative stability of cured epoxy resins. I.* Journal of Applied Polymer Science, 1993. 47(10): p. 1821-1837.

9. McMahon PE, *Oxidative resistance of carbon fibers and their composites. In: Advanced Composite Materials-Environmental Effects.* ASTM STP 658, 1978: p. 254-266.

10. Pering, G.A., P.V. Farrell, and G.S. Springer, *Degradation of tensile and shear properties of composites exposed to fire or high-temperature.* Journal of Composite Materials, 1980. 14(JAN): p. 54-68.

11. Grant, T.S. and W.L. Bradley, *In-Situ Observations in SEM of Degradation of Graphite/Epoxy Composite Materials due to Seawater Immersion.* Journal of Composite Materials, 1995. 29(7): p. 852-867.

12. Leif A. Carlsson, F.P., *Influence of sea water on transverse tensile properties of PMC, NIST Special Publication 887.* National Institute of Standards and Technology, 1995: p. 203-221.

13. Wood, C.A. and W.L. Bradley, *Determination of the effect of seawater on the interfacial strength of an interlayer E-glass/graphite/epoxy composite by in situ observation of transverse cracking in an environmental SEM.* Composites Science and Technology, 1997. 57(8): p. 1033-1043.

14. Lixin Wu. Karen Murphy. Vistap M. Karbhari and J.S. Zhang, *Short-term effects of sea water on E-glass/vinylester composites.* Journal of Applied Polymer Science, 2001. 84: p. 2760-2767.

15. Gellert, E.P. and D.M. Turley, *Seawater immersion ageing of glass-fibre reinforced polymer laminates for marine applications.* Composites Part A: Applied Science and Manufacturing, 1999. 30(11): p. 1259-1265.

16. Tucker, W.C. and R. Brown, *Moisture Absorption of Graphite/Polymer Composites Under 2000 Feet of Seawater.* Journal of Composite Materials, 1989. 23(8): p. 787-797.

17. Liao, K., C.R. Schultheisz, and D.L. Hunston, *Effects of environmental aging on the properties of pultruded GFRP.* Composites Part B: Engineering, 1999. 30(5): p. 485-493.

18. Strait, L.H., M.L. Karasek, and M.F. Amateau, *Effects of Seawater Immersion on the Impact Resistance of Glass Fiber Reinforced Epoxy Composites.* Journal of Composite Materials, 1992. 26(14): p. 2118-2133.

19. Kootsookos, A. and A.P. Mouritz, *Seawater durability of glass- and carbon-polymer composites.* Composites Science and Technology, 2004. 64(10-11): p. 1503-1511.

20. Rhee, K.Y.H., S. R. Park, S. J. Kim, H. J. and D.H. Jung, *Fracture behavior of seawater-absorbed carbon/epoxy laminated composites in the hydrostatic pressure condition.* Materials Science and Engineering: A, 2006. 419(1-2): p. 209-213.

21. McBagonluri, F.G., K. Hayes, M. Verghese, K. N. E. and J.J. Lesko, *Characterization of fatigue and combined environment on durability performance of glass/vinyl ester composite for infrastructure applications.* International Journal of Fatigue, 2000. 22(1): p. 53-64.

22. Roger M.Crane, J.W.G., Dirk Hieder, S. Yarlagadda, S. G. Advani, *Intelligent processing and inspection of Naval composites.* AMPTIAC Quarterly, 2003. 7, number 3(navy experts explain the newest materials & structural technologies).

23. Mouritz, A.P., Gellert, E. Burchill, P. and K. Challis, *Review of advanced composite structures for naval ships and submarines.* Composite Structures, 2001. 53(1): p. 21-42.

24. Smith J., *Novel submarine hulls.* naval composite news, 1999. 3:13-4.

25. Newan MR., *Development of non hull penetrating masts and perisopes. In: proceedings of Warship'99.* The International Symposium on Naval structures 6, 1999. June 14-16(paper No 6).

26. *MIL-HDBK-17-1F: composite Materials Handbook.* Polymer Matrix Composites Guidelines for Characterization of Structural Materials. 1.

27. ASTM D3039M, *Standard Test Method for Tensile Properties of Polymer Matrix Composite Materials.* Amercian Society of Testing Materials, 2003. Vol.15.03.

28. C.C. Chamis and J.H. Sinclair, *Ten-Degree Off-Axis Test for Shear Properties in Fiber Composites.* Experimental Mechanics, 1977. Vol.17: p. 339-346.

29. ASTM D5379, *Standard Test Method for Shear Properties of Composite Materials by the V-notch Beam Method.* Amercian Society of Testing Materials, 100 Barr Harbo Drive, West Conshohocken, PA 19428, 1997. Vol.15.03.

30. ASTM D5488, *Standard Test Method for In-plane Shear Properties of Hoop Wound Polymer Matrix Composite Cylinders.* Amercian Society of Testing Materials, 1998. Vol.04.10.

31. ASTM D4255, *Standard Test Method for Testing In-Plane Shear Properties of Composite Laminates.* Amercian Society of Testing Materials, 1997. Vol. 15.03.

32. ASTM D3518/D3518M-94, *Standard Test Method for In-Plane Shear Response of Polymer Matrix Composite Materials by Tensile Test of a $\pm 45^{o}$ Laminate.* Amercian Society of Testing Materials, 2001. Vol. 15.03.

33. Donald F. Adams, L.A.C., R. Byron Pipes,, *Experimental characterization of advanced composite materials.* CRC Press, 2003. Third edition.

34. ASTM D790M, *Standard Test Method for Flexural Properties of Unreinforced and Reinforced Plastics and Eletrical Insulated Materials.* Amercian Society of Testing Materials, 2003. Vol.08.01.

35. C.E. Browning, F.L.A., and J.M. Whitney, *A Four-Point Shear Test for Graphite/Epoxy Composites: Quality Assurance and Processing, STP 797.* Amercian Society of Testing Materials, Philadelphia, 1983(54-74).

36. ASTM D3846, *Standard Test Method for In-Plane Shear of Reinforced Plastics.* amercian Society of Testing Materials, 100 Barr Harbo Drive, West Conshohocken, PA 19428, 1998. Vol.08.02.

37. ASTM D5379, *Standar Test Method for Shear Properties of Composite Materials by the V-notch Beam Method.* Amercian Society of Testing Materials, 1997. Vol.15.03.

38. ASTM D2344/D2344M-00, *Standard Test Method for Short-Beam Strength of Polymer Matrix Composite Materials and Their Laminates.* Amercian Society of Testing Materials, 2006. Vol.15.03.

39. Karbhari, V.M. and Q. Wang, *Multi-frequency dynamic mechanical thermal analysis of moisture uptake in E-glass/vinylester composites.* Composites Part B: Engineering, 2004. 35(4): p. 299-304.

40. Chartoff RP, Weissman PT, and S. A., *Application of dynamic mechanical methods to Tg determination in polymers: an overview.* ASTM STP 1249, 1994: p. 88-107.

41. G. Li, P. Lee-Sullivan, and R.W. Thring, *Determination of Activation Energy for Glass Transition of an Epoxy Adhesive Using Dynamic Mechanical Analysis* Journal of Thermal Analysis and Calorimetry, 2000. Volume 60: p. 377-390.

42. Stephen, G.K. and S. Arun, *Dynamic mechanical analysis of fiber-reinforced phenolics.* Journal of Applied Polymer Science, 1999. 73(5): p. 649-658.

43. ASTM D5418-07, *Standard Test Method for Plastics: Dynamic Mechanical Properties: In Flexure.* Amercian Society of Testing Materials, 2001. Vol.08.03.

44. ASTM D3418-03, *Standard Test Method for Transition Temperatures of Polymers By Differential Scanning Calorimetry.* Amercian Society of Testing Materials, 2005. Vol.08.02.

45. Wu, C.S., Liu, Ying Ling, Chiu, Yie Chan and Y.S. Chiu, *Thermal stability of epoxy resins containing flame retardant components: an evaluation with thermogravimetric analysis.* Polymer Degradation and Stability, 2002. 78(1): p. 41-48.

46. H.H.Horovitz and Gershon.Metzger, *A New Analysis of Thermogravimetric Traces.* Anal. Chem, 1963. 35(10): p. 1464-1468.

47. ASTM E1131-03, *Standard Test Method for Compositional Analysis by Thermogravimetry.* Amercian Society of Testing Materials, 2003. Vol.14.02.

48. Abanilla, M.A., Y. Li, and V.M. Karbhari, *Durability characterization of wet layup graphite/epoxy composites used in external strengthening.* Composites Part B: Engineering, 2005. 37(2-3): p. 200-212.

49. Rochardjo, H.S.B., et al., *Effects of the fiber content on the longitudinal tensile fracture behavior of uni-directional carbon/epoxy composites.* Journal of Materials Processing Technology, 1997. 67(1-3): p. 89-93.

50. J.M.Hodgkinson, *Mechanical Testing of advanced Firber Composites.* Cambrige, Egland:CRC Press, 2000.

51. Abanilla, M.A., V.M. Karbhari, and Y. Li, *Interlaminar and intralaminar durability characterization of wet layup carbon/epoxy used in external strengthening.* Composites Part B: Engineering, 2006. 37(7-8): p. 650-661.

52. L.A. Carlsson and R.B. Pipes, *Experimental Characterization of Advanced Composite Materilas.* New Jersy:prentice-Hall, Inc., 1987.

53. W.W. Stinchcomb, E.G.H., and H.L.Price, *Use of the short-beam shear test for quality control of graphite-polymide laminates.* Reproducibility and Accuracy of Mechanical Tests, 1977. ASTM STP, 626:96.

54. Whitney, J.M. and C.E. Browing, *On short-beam shear tests for composite materials.* Experimental Mechanics, 1985. volume 25(3): p. page 294-300.

55. Daniels, B.K., N.K. Harakas, and R.C. Jackson, *Short beam shear tests of graphite fiber composites.* Fibre Science and Technology, 1971. 3(3): p. 187-208.

56. Richards-Frandsen, R. and Y. Naerheim, *Fracture Morphology of Graphite/ Epoxy Composites.* Journal of Composite Materials, 1983. 17(2): p. 105-113.

57. Drzal, L.T. and M. Madhukar, *Fiber matrix adhesion and its relationship to composite mechanical-properties.* Journal of Materials Science, 1993. 28(3): p. 569-610.

58. S.Timoshenko, *Strength of Materials, Part I.* Van Nostrand, Pronceton, 3rd edition, 1955: p. 95,118.

59. Akay, M., *Aspects of dynamic mechanical analysis in polymeric composites.* Composites Science and Technology, 1993. 47(4): p. 419-423.

60. Menard, K.P., *A Practical Introduction to Dynamic Mechanical Analysis.* Boc Raton, Florida, CRC Press, 1999.

61. Ward, I.M.H., D. W., *An Introduction to the mechanical Properties of Solid Polymer*. Wiley, New York, 1993.

62. Ferry, J.D., *Visocoelastic Properties of Polymers, 3rd edition.* Wiley, New York, 1980.

63. Joseph D. Menczel and R. Bruce Prime, *Thermal Analysis of Polymers.* Wiley, A John wiley & Sons, inc., Publication, 2008.

64. Pascault, J.P. and R.J.J. Williams, *Glass transition temperature versus conversion relationships for thermosetting polymers.* Journal of Polymer Science Part B: Polymer Physics, 1990. 28(1): p. 85-95.

65. Kennedy, J.M., et al., *Characterization of Interfacial Bond Strength by Dynamic Analysis.* Journal of Composite Materials, 1992. 26(6): p. 869-882.

66. Fraga, A.N., et al., *Relationship between Dynamic Mechanical Properties and Water Absorption of Unsaturated Polyester and Vinyl Ester Glass Fiber Composites.* Journal of Composite Materials, 2003. 37(17): p. 1553-1574.

67. Karbhari, V.M., *Dynamic Mechanical Analysis of the Effect of Water on E-glass-Vinylester Composites.* Journal of Reinforced Plastics and Composites, 2006. 25(6): p. 631-644.

68. Fox, T.G. and S. Loshaek, *Influence of molecular weight and degree of crosslinking on the specific volume and glass temperature of polymers.* Journal of Polymer Science, 1955. 15(80): p. 371-390.

69. De'Neve, B. and M.E.R. Shanahan, *Water absorption by an epoxy resin and its effect on the mechanical properties and infra-red spectra.* Polymer, 1993. 34(24): p. 5099-5105.

70. Bai, Y.U. and T. Keller, *Time Dependence of Material Properties of FRP Composites in Fire.* Journal of Composite Materials, 2009. 43(21): p. 2469-2484.

71. Remiro, P.M., et al., *The effect of crosslinking and miscibility on the thermal degradation of an uncured and an amine-cured epoxy resin blended with poly (epsilon-caprolactone).* Polymer Degradation and Stability, 2002. 78: p. 83-93.

72. Coats, A.W. and J.P. Redfern, *Kinetic parameters from thermogravimetric data.* nature 201:68, 1964.

73. Coats, A.W. and J.P. Redfern, *Kinetic parameters from thermogravimetric data. II.* Journal of Polymer Science Part B: Polymer Letters, 1965. 3(11): p. 917-920.

74. Lee, J.Y., M.J. Shim, and S.W. Kim, *Thermal decomposition kinetics of an epoxy resin with rubber-modified curing agent.* Journal of Applied Polymer Science, 2001. 81(2): p. 479-485.

75. Kissinger, H.E., *Reaction Kinetics in Differential Thermal Analysis.* Analytical Chemistry, 1957. 29(11): p. 1702-1706.

76. Collings, T.A. and S.M. Copley, *On the accelerated ageing of CFRP*. Composites, 1983. 14(3): p. 180-188.

77. Antoon, M.K. and J.L. Koenig, *The Structure and Moisture Stability of the Matrix Phase in Glass-Reinforced Epoxy Composites.* 1980. 19(1): p. 135 - 173.

78. Mijovic J, K.F.L., *The Effect of Hygrothermal Fatigue on Physical/Mechanical Properties and Morphology of Neat Epoxy Resin and Graphite/Epoxy Composite.* Journal of Applied Polymer Science, 1985. Vol.30, No.6: p. 2527-2549.

79. Fried, N., *Degradation of Composite Materials: The Effect of Water on Glass-Reinforced Plastics.* Proceedings of the Fifth Symposium on Naval Structural Mechanics, Philadelphia, 1967: p. 813-837.

80. Tsotsis, T.K. and S.M. Lee, *Long-Term Durability of Carbon and Glass-Epoxy Composite Materials in Wet Environments.* Journal of Reinforced Plastics and Composites, 1997. 16(17): p. 1609-1621.

81. Liao, K., Schultesiz, C. R., Hunston, D. L., Brinson, L. C, *Long-Term Durability of Fiber-Reinforced Polymer-Matrix Composite Materials for Infrastructure Applications: A Review.* Journal of Advanced materials, 1998. 30, No.4: p. 3-40.

82. Weitsman, Y.J., K. Anthony, and Z. Carl, *Effects of Fluids on Polymeric Composites--A Review*, in *Comprehensive Composite Materials*. 2000, Pergamon: Oxford. p. 369-401.

83. Marshall, J.M., G.P. Marshall, and R.F. Pinzelli, *The diffusion of liquids into resins and composites.* Polymer Composites, 1982. 3(3): p. 131-137.

84. Shen, C.-H. and G.S. Springer, *Moisture Absorption and Desorption of Composite Materials.* Journal of Composite Materials, 1976. 10(1): p. 2-20.

85. Mouritz, A.P., A. Kootsookos, and G. Mathys, *Stability of polyester- and vinyl ester-based composites in seawater.* Journal of Materials Science, 2004. 39(19): p. 6073-6077.

86. Bonniau, P. and A.R. Bunsell, *A Comparative Study of Water Absorption Theories Applied to Glass Epoxy Composites.* Journal of Composite Materials, 1981. 15(3): p. 272-293.

87. Joannie, W.C., N. Tinh, and A. Khaled, *Sorption and diffusion of water, salt water, and concrete pore solution in composite matrices.* Journal of Applied Polymer Science, 1999. 71(3): p. 483-492.

88. Prian, L. and A. Barkatt, *Degradation mechanism of fiber-reinforced plastics and its implications to prediction of long-term behavior.* Journal of Materials Science, 1999. 34(16): p. 3977-3989.

89. Apicella, A. and L. Nicolais, *Environmental aging of epoxy resins: synergistic effect of sorbed moisture, temperature, and applied stress.* Industrial & Engineering Chemistry Product Research and Development, 1981. 20(1): p. 138-144.

90. Tejraj, M.A., *Liquid diffusion into epoxy resin composites.* Journal of Applied Polymer Science, 1988. 35(5): p. 1251-1256.

91. Reliasoft(2000), *Reliasoft's Life Data Analysis Reference.* Reliasoft Publishing, Tucson, Arizona.

92. Ding, H.Z. and Z. Wang, *Time–temperature superposition method for predicting the permanence of paper by extrapolating accelerated ageing data to ambient conditions.* Cellulose, 2007. 14(3): p. 171-181.

93. A. Kuraishi, *Durability Analysis of Composite Structure Using the Accerlated Testing Methodolgy.* Ph.D disseration, Stanford University, 2001.

94. Wang, J.Z.P., H. Chang, T. Iyengar, N. Dillard, D. A. and K.L. Reifsnider, *Physical aging behavior of high-performance composites.* Composites Science and Technology, 1995. 54(4): p. 405-415.

95. Nakada, M.M., Yasushi Kinoshita, Masaya Koga, Ryuju Okuya, Tsuguyuki and R. Muki, *Time-Temperature Dependence of Tensile Strength of Unidirectional CFRP.* Journal of Composite Materials, 2002. 36(22): p. 2567-2581.

96. Wisnom, M.R., *The Relationship between Tensile and Flexural Strength of Unidirectional Composites.* Journal of Composite Materials, 1992. 26(8): p. 1173-1180.

97. Whitney, J. and M. Knight, *The relationship between tensile strength and flexure strength in fiber-reinforced composites.* Experimental Mechanics, 1980. 20(6): p. 211-216.

98. Holmberg, J.A., *On Flexural and Tensile Strength for Composites Manufactured by RTM.* Journal of Reinforced Plastics and Composites, 1992. 11(11): p. 1302-1320.

99. Bullock, R.E., *Strength Ratios of Composite Materials in Flexure and in Tension.* Journal of Composite Materials, 1974. 8(2): p. 200-206.

100. Karbhari, V.M. and M.A. Abanilla, *Design factors, reliability, and durability prediction of wet layup carbon/epoxy used in external strengthening.* Composites Part B: Engineering, 2007. 38(1): p. 10-23.

101. He, X. and S.O. Oyadiji, *Application of coefficient of variation in reliability-based mechanical design and manufacture.* Journal of Materials Processing Technology, 2001. 119(1-3): p. 374-378.

102. J. Wu and D.D.L. Chung, *Increasing the electromagnetic interference shielding effectiveness of carbon fiber polymer–matrix composite by using activated carbon fibers.* Carbon, 2002. 40: p. 445-467.